Dissolution mechanism of montmorillonite in synthetic lung fluids

Effect of organic ligands and biodurability

Tesis doctoral

Mª Elena Ramos Jareño

IACT
INSTITUTO ANDALUZ DE CIENCIAS DE LA TIERRA

Editor: Editorial de la Universidad de Granada
Autor: Mª Elena Ramos Jareño
D.L.: GR 1897-2013
ISBN: 978-84-9028-589-3

Instituto Andaluz de Ciencias
de la Tierra (CSIC-UGR)

Dissolution mechanism of montmorillonite in synthetic lung fluids: Effect of organic ligands and biodurability

Mecanismo de disolución de montmorillonita en fluidos pulmonares sintéticos: Efecto de los ligandos orgánicos y biodurabilidad

Memoria de Tesis presentada por la Licenciada en Química Dña. María Elena Ramos Jareño para optar al grado de Doctor por la Universidad de Granada.

Esta Tesis Doctoral ha sido dirigida por el Dr. F. Javier Huertas Puerta, Investigador Científico del CSIC, del Instituto Andaluz de Ciencias de la Tierra (CSIC-UGR)

Granada, Febrero 2013

V° B° del Director

F. Javier Huertas Puerta

La Doctoranda

M. Elena Ramos Jareño

Instituto Andaluz de Ciencias
de la Tierra (CSIC-UGR)

Tesis doctoral

Dissolution mechanism of montmorillonite in synthetic lung fluids: Effect of organic ligands and biodurability

Mecanismo de disolución de montmorillonita en fluidos pulmonares sintéticos: Efecto de los ligandos orgánicos y biodurabilidad

presentada por

María Elena Ramos Jareño

para optar al grado de Doctor, con mención de Doctorado Internacional

Granada, Febrero 2013

Evaluadores externos:

Dr. Ray E. Ferrell, Jr., Professor Emeritus
Geology & Geophysics, Louisiana State University, USA

Dr. Philippe Vieillard, Directeur de Recherches
Institut de Chime des Milieu et des Matériaux de Poitiers, CNRS-Université de Poitiers, France

Dr. Tsutomu Sato, Professor
Laboratory of Environmental Geology, Faculty of Engineering, Hokkaido University, Japan

Esta Tesis Doctoral ha sido financiada por los proyectos del Plan Nacional de I+D+i CGL2005-00618, CGL2008-01652 y CGL2011-22567 y el Grupo de Investigación RNM-264 de la Junta de Andalucía, con contribución de fondos FEDER y la beca del programa de Formación de Personal Investigador (MEC). El trabajo de investigación ha sido desarrollado en su mayor parte en la Estación Experimental del Zaidín (CSIC) y en el Instituto Andaluz de Ciencias de la Tierra (CSIC-Universidad de Granada).

A mis padres

TABLE OF CONTENTS

Ramos M.E., Cappelli C., Rozalen M., Fiore S. and Huertas F.J. (2011) *Effect of lactate, glycine and citrate on the kinetics of montmorillonite dissolution.* American Mineralogist 96, 768-780.

Acknowledgements
Agradecimientos

ACKNOWLEDGEMENTS/AGRADECIMIENTOS

Me gustaría expresar mi más profunda gratitud a todos aquellas personas que han contribuido de alguna forma a la elaboración de este trabajo, y sin los cuales no hubiera sido posible.

En primer lugar, a mi director de tesis el Dr. F. Javier Huertas. Gracias por su confianza y por brindarme la oportunidad de realizar este trabajo, así como su disponibilidad e inestimable ayuda durante estos años.

También quería dar las gracias al Instituto Andaluz de Ciencias de la Tierra y a la Estación Experimental del Zaidín por acogerme durante estos años, así como por el apoyo institucional recibido.

Al programa de doctorado de Ciencias de la Tierra, en especial al Prof. Antonio García Casco por su gran ayuda y dedicación a los estudiantes de doctorado.

I would like to thank to Prof. Cliff Johnston for open the door of his group at Purdue University. Cliff, I am very grateful for your guidance and your patience. I have learned so much from you during the two stays. I would also like to thank to Gail, Jess and Julie for making me feel at home and for being so sweet everyday.

In addition, I would like to thank to Dr. Gnanasiri Premachandra for the help with my lab work and instruments, his availability and friendship. I also would like to thank to Kiran and Eric for their kindness and for finding time to help me with the IC. Thanks to my friend Lara for the great company and all the funny moments shared in and out the lab. Thanks to Marika for the wonderful moments in the volleyball and basketball games, for the coffee breaks and her friendship. Muchas gracias a Juanfra por hacer que mi primera estancia en Purdue fuera mucho más llevadera.

Thanks to Prof. Ray Ferrell (Louisiana State University, USA), Prof. Philippe Vieillard (Hydrasa, CNRS-University of Poiters, France) and Prof. Tsutomu Sato (Hokkaido University, Japan) for the revision of the thesis manuscript.

Al Dr. Ignacio Sainz por sus discusiones y gran ayuda con el IR. También a David García de Amphos XXI, por su gran clase magistral con el FITEQL. Al Dr. Vicente Timón por su amabilidad y por darme la oportunidad de aportar mi granito de arena a la caracterización estructural de la basaluminita.

A todo el antiguo "departamento de Geoquímica Ambiental", gracias por su amabilidad, por los desayunos y por su sonrisa diaria.

A Rafael Bellver por aguantarme, por toda su inestimable ayuda y sus buenos consejos.

A todos mis compañeros de laboratorio y de "departamento": José, Paloma, Pepe, Edu y Elisa, por las risas, vuestra amistad e increíble compañía en el laboratorio. A Marisa y Chiara, por las discusiones con el trabajo y el gran apoyo moral. Mª Jesus por su sonrisa y los cambios de muestras en los puentes! Gracias a mis 'vecinos' de departamento. A Dani, por propagar la alegría en la casa roja con sus silbidos mañaneros. A Isa, Siham y Ana, con su sonrisita dibujada en el corazón. A José Antonio por estar siempre de buen humor, e intentar educarnos en Geología. Muchas gracias a todos por los buenos momentos compartidos durante estos años.

A la picnic/lolipandi, por la tertulias y los ratos de risas dentro y fuera del gym. A Jare, Julia y Elena por su sincera amistad y apoyo presencial-telefónico en estos años. A toda mi gente de Peal y de Jaén, por la buena compañía y las risas. A Robles y Manolo, por cuidar de mí, su amistad y por los viajecicos.

Gracias a mis hermanos, Loren y Eli y a mis padres Lorenzo y Julia, porque sin su esfuerzo, sacrificio y apoyo hubiera sido imposible llegar hasta aquí.

Y por último a la persona más especial en mi vida, Tillo, por caminar a mi lado durante todos estos años.

Acronyms and abbreviations

ACRONYMS AND ABBREVIATIONS

AAS	Atomic Adsorption Spectroscopy
ATR-FTIR	Attenuated Total Reflectance Fourier Transform Infrared
BET	Brunauer Emmett Teller
CEC	Cation Exchange Capacity
Cit	Citrate
d.l.	Detection limit
DLM	Diffuse Layer Model
DR-FTIR	Diffuse Reflectance Fourier Transform Infrared
ESA	Edge Surface Area
FEBEX	Full-scale Engineered Barriers EXperiments in crystalline host rocks
FTIR	Fourier-Transform Infrared
Gib	Gibbsite
Gly	Glycine
Gly^+	Glycinium ion
Gly^-	Glycinate ion
Gly(zw)	Zwitterionic form of glycine
IAP	Ion Activity Product
IARC	International Agency for Research of Cancer
IC	Ion Cromatography
ICP-MS	Inductively Coupled Plasma Mass Spectrometry
IR	Infrared
K_{eq}	Equilibrium constant
K-Mont	K-Montmorillonite
Kln	Kaolinite
Lac	Lactate
LMW	Low Molecular Weight
Ox	Oxalate
PTFE	Polytetrafluoroethylene
Qz	Quartz
R_{Al}	Al-derived dissolution rate
R_{Si}	Si-derived dissolution rate
SLF	Synthetic Lung Fluids

SiO_2(am)	Amorphous silica
TLM	Triple Layer Model
UV-Vis	Ultraviolet-Visible
V(Y)	Weighted sum of squares divided by degrees of freedom
WHO	World Health Organization
XRD	X-Ray Diffraction

Abstract
Resumen

ABSTRACT

Over the course of our lives we are exposed to airborne particulate matter in the workplace, home, and environment that results in the deposition of millions of particles in the lung. These exposures may result in disease if they are significant enough. The potential for harmful exposure depends in part on the inhalable particle's biodurability. In this study, geochemical methods have been used to characterize the behavior of inhaled particles in the body. As a case of study, we have used montmorillonite, since it constitutes an important part of the fine and ultrafine fraction in soils and sediments. Therefore, it is one of the main compounds present in natural dust.

Dissolution rates of a well-characterized sample of montmorillonite were measured in solutions that mimic fluids found in the human lung (synthetic lung fluids – SLF). Dissolution rates were measured at pH 4 (macrophages) and 7.5 (interstitial fluids) at 37°C in flow-though reactors. The effect of organic ligands was investigated through the addition of lactate, citrate, glycine and oxalate at variable concentrations. The addition of ligands markedly affects the measured dissolution rate and the data further indicate that the dissolution mechanism for montmorillonite in aqueous solutions is pH dependent. The effect of the addition of lactate or glycine is negligible, however, citrate enhances the dissolution rate by 0.5 orders of magnitude at pH 4 and more than one order of magnitude at pH 7.5. Oxalate enhances the dissolution rate from pH 4 to 8, reaching a maximum of 0.5 logarithmic units at pH 7.

Two mechanisms may contribute to the enhancement of the montmorillonite dissolution rate in citrate and oxalate solutions: the formation of surface complexes between the organic ligand and aluminol sites on the edge surface of the montmorillonite particles, and the decrease of the activity of Al^{3+} by formation of aqueous Al-ligand complexes. In order to understand the dissolution mechanism of montmorillonite particles, adsorption experiments of the organic ligands were measured in batch experiments at pH 2-11. It was found that lactate, citrate, glycine and oxalate absorb onto montmorillonite, but the adsorption mechanism was different depending on the organic ligand. FTIR spectroscopy was used to characterize the type of complexes formed at the smectite surface. However, FTIR results do not always provide definitive information on different coordination geometries for surface

complexes. In order to better understand the ligand-montmorillonite interactions, the experimental results obtained were integrated with a surface complexation model, which establishes the stoichiometry of the adsorption reactions and provides a thermodynamic characterization of the equilibria involved.

Adsorption edge and ATR-FTIR results indicate that lactate is likely adsorbed by electrostatic interactions. Nevertheless, ATR-FTIR results suggest that citrate is adsorbed in the >AlOH groups in an inner-sphere mode at low pH. The macroscopic adsorption behavior of citrate was successfully modeled as a function of pH by using the Triple Layer Model (TLM) and the single monodentate $>AlCit^{2-}$ species (logK=10.58). For oxalate, the monodentate complex >AlOxH (logK=14.39) dominated adsorption below pH 4, and the bidentate complex $>AlOx^{-}$ (logK = 10.39) was predominant at higher pH values. Both the proposed inner-sphere oxalate species were qualitatively consistent with DR-FTIR spectroscopic results.

Glycine adsorption is dominated by electrostatic interactions at the edges surface at low concentrations of glycine. When the edge surface is saturated, the adsorption occurs by cation exchange in the interlayer space. The measure of the desorbed interlayer cations showed that the 68% of the K^{+} was exchanged with glycine. The K^{+}-glycine exchange reaction produces a decrease of the smectite interlayer space from 14.5 to 12 Å and an arrangement of the smectite layers.

It can be concluded that lactate and glycine are adsorbed at the surface edges by electrostatic interactions, whereas citrate and oxalate are adsorbed in an inner-sphere mode. The fact that only citrate and oxalate catalyze the dissolution reaction of montmorillonite, allows to affirm that chemisorption is necessary for the detachment and release of the structural cations of smectite and promote the dissolution reaction.

A geometric shrinking particle model using the calculated dissolution rates predicts that a 500 nm smectite particle would be only reduced a 10% after 10 years under pulmonary conditions at pH 7.5. The addition of citrate at variable concentrations reduces this dissolution time. These data can be used to place constraints on the role of particle dissolution in the disease models associated with airborne respirable particulate matter. These results support the application of geochemical techniques to evaluate exposures to complex respirable materials.

RESUMEN

En el transcurso de nuestras vidas estamos expuestos a material aéreo particulado en el lugar de trabajo, en el hogar y en el medioambiente, que acaba con la deposición de millones de partículas en los pulmones. Esta exposición puede causar enfermedades si es suficientemente significantiva. El grado en que la exposición puede ser perjudicial depende, en parte, de la biodurabilidad de las partículas inhaladas. En este estudio se utilizan métodos geoquímicos para caracterizar el comportamiento de las partículas inhaladas en el cuerpo humano. Como material modelo se ha utilizado montmorillonita, ya que ésta constituye una parte importante de la fracción fina y ultrafina de suelos y sedimentos. Por lo tanto, es un componente principal del polvo natural.

Las velocidades de disolución de una muestra de montmorillonita previamente caracterizada se midieron en soluciones que simulan las encontradas en el pulmón humano (fluidos pulmonares sintéticos – SLF). Las velocidades de disolución se midieron a pH 4 (macrófagos) y 7.5 (fluidos intersticiales) a 37°C en reactores de flujo continuo. El efecto de los ligandos orgánicos se investigó a través de la adición de lactato, citrato, glicina y oxalato en concentraciones variables. La adición de ligandos afecta notablemente a las velocidades de disolución y además los datos indican que el mecanismo de disolución de la montmorillonita en soluciones acuosas depende del pH. El efecto de la adición de lactato y glicina es inapreciable, sin embargo, el citrato incrementa la velocidad de disolución 0.5 órdenes de magnitud a pH 4 y más un orden de magnitud a pH 7.5. El oxalato incrementa la velocidad de disolución desde pH 4 hasta 8, alcanzando un máximo de 0.5 órdenes de magnitud a pH 7.

El incremento de la velocidad de disolución de la montmorillonita se puede atribuir a 2 mecanismos: la formación de complejos solubles entre el ligando orgánico y los sitios aluminol de la superficie de borde de la montmorillonita, y la disminución de la actividad del Al^{3+} por formación de complejos acuosos Al-ligando. Para entender el mecanismo de disolución de las partículas de montmorillonita, se llevaron a cabo experimentos de adsorción tipo batch de los ligandos orgánicos a pH 2-11. Se ha encontrado que lactato, citrato, glicina y oxalato se adsorben en la montmorillonita, aunque el mecanismo de adsorción es diferente dependiendo de el ligando usado. Para caracterizar el tipo de complejos que se forman en la superficie de la esmectita se usó

la espectroscopía FTIR. Sin embargo, los resultados FTIR no siempre proporcionan una información definitiva de las diferentes geometrías de coordinación de los complejos superficiales. Para comprender mejor las interacciones montmorillonita-ligando, los resultados experimentales obtenidos fueron integrados con un modelo de complejación superficial, que establece la estequiometría de las reacciones de adsorción, así como una caracterización termodinámica del equilibrio que tiene lugar.

Tanto los resultados del borde de adsorción como los de ATR-FTIR indican que el lactato se adsorbe por interacciones electrostáticas. Sin embargo, los resultados de ATR-FTIR indican que el citrato se adsorbe en forma de esfera interna en los grupos >AlOH a pH bajo. Los datos de adsorción macroscópicos del citrato se modelizaron satisfactoriamente en función del pH usando el Modelo de la Triple Capa (TLM) y una única especie monodentada $>AlCit^{2-}$ (logK=10.58). Para el oxalato, el complejo monodentado >AlOxH (logK=14.39) domina la adsorción por debajo de pH 4, y el complejo bidentado $>AlOx^{-}$ (logK = 10.39) predomina a valores de pH más altos. Ambas especies de esfera interna son cualitativamente consistentes con los resultados de DR-FTIR.

La adsorción de glicina está dominada por las interacciones electrostáticas en la superficie de los bordes a bajas concentraciones de glicina. Cuando la superficie del borde se satura, la adsorción tiene lugar por intercambio catiónico en el espacio interlaminar. La medida de los cationes interlaminares desorbidos mostraron que un 68% de K^{+} era intercambiado por glicina. La reacción de intercambio K^{+}-glicina produce una disminución del espacio interlaminar de 14.5 a 12 Å y un ordenamiento de las láminas de esmectita.

Se puede concluir que el lactato y la glicina se adsorben en la superficie de los bordes por interacciones electrostáticas, mientras que el citrato y el oxalato se adsorben como complejos de esfera interna. El hecho de que sólo el citrato y el oxalato catalizan la reacción de disolución de la montmorillonita nos permite afirmar que es necesario que se produzca quimisorción para que los cationes estructurales de la esmecita se desprendan y liberen a la solución, y así promover la reacción de disolución.

Un modelo de reducción geométrica de partículas usando las velocidades de disolución calculadas, predice que una partícula de esmectita de 500 nm se puede

reducir un 10% después de 10 años en condiciones pulmonares a pH 7.5. La adición de citrato a varias concentraciones reduce este tiempo de disolución. Estos datos se pueden usar para limitar el papel de la disolución de partículas en los modelos de enfermedad asociados con el material aéreo particulado. Estos resultados apoyan la aplicación de técnicas geoquímicas para evaluar la exposición a materiales respirables complejos.

1. Introduction

1. INTRODUCTION

1.1. Earth materials linked to human health

After decades of research, earth sciences activities tied to health issues are growing and are commonly classified under the emerging discipline called *Medical Geology* (Selinus and Frank, 2000; Finkelman et al., 2001; Skinner and Berger, 2003). Medical Geology is the science that deals with the impacts of geologic materials and processes on animal and human health.

One of the environmental health problems that geologists and the medical community need to collaborate is exposure to natural dust. It is known that exposure to mineral dust can cause a wide range of respiratory problems. The dust can be generated by mining rocks or coal, sandblasting, and smoke plumes from fires (both natural and man-made) or simply from the wind dispersing fine-grained minerals from the Earth's surface. Of greatest concern for its affects on human health are the finer particles of respirable (inhalable) dusts. In this regard, considerable work is being conducted to identify dust particles derived from soils, sediment, and weathered rocks.

Particulate earth material can enter and interact with the organism via ingestion (gastrointestinal tract), percutaneous adsorption (skin) or inhalation (respiratory tract). This exposure is related with a variety of diseases and health problems. Harmful effects on human health of biodurable materials (insoluble or soluble with difficulty in biologic medium, so they can not be eliminated by chemical dissolution) mainly come from inhalation exposure of airborne dust.

The epidemiological studies developed since the 19th century have shown the relationship between dust inhalation and the development of lung diseases. The earth materials that are most commonly associated with adverse respiratory health effects include dusts of asbestos, erionite, crystalline silica and coal. For instance, exposures to airborne asbestos are known to cause mesothelioma, lung cancer and other lung diseases such as asbestosis. Similarly, exposure to elevated concentrations of quartz can produce silicosis. However, dusts from a wide variety of other biodurable earth materials (such as metal oxides, talc, kaolinite, feldspars, bentonite, 'fuller's earth' and micas) are also known to be associated with adverse health effects if exposures are of sufficient intensity and duration.

1.2. Factors influencing the health effects of biodurable minerals

Geochemical processes play an important role in health effects of biodurable minerals. The magnitude of the injuries depends on the type of dust and the organism response to the exposure. van Oss et al. (1999) show that potentially important factors in lung phatogenesis induced by minerals are, by importance order: particle morphology, solubility in intracellular conditions of macrophages or interstitial fluids, exposure duration and capacity to activate phagocytic cells.

1.2.1. Particle shape and size

Particle size and shape may determine the aerodynamic behavior of the particle in the conducting airways as well as their extent to deposit into the lung and retention rate after inhalation. The respiratory system contains structures that prevent most dust from reaching alveolar cavities, where only particles with equivalent diameters of approximately 1-2 μm can penetrate (Fig. 1.1). The largest inhaled particles (5 μm to somewhat greater than 10 μm) are deposited in the mucus lining of the nasopharyngeal tract. Progressively smaller particle sizes are deposited in successively deeper portions of the respiratory tract by entrapment in a layer of mucus lining the airways. The particle-laden mucus is cleared from the trachea and bronchi in part by coughing. In addition, the cells lining the trachea, bronchi, and bronchioles are ciliated. The cilia beat to transport the particle-laden mucous up and out of the respiratory tract. Particles cleared by coughing or mucociliary clearance are either expectorated or ingested.

It has to taken into account that the particle size is also important because the smaller a particle is, the larger surface area and greater chemical reactivity and higher biological activity it may exhibit. Thus, ultrafine particles have a higher potential risk due to their high specific surface and their capacity to go into interstitial spaces of the lung, where they can induce fibrotic reactions (Oberdörster et al., 1992).

The morphology has direct effects on the capacity of lungs to eliminate particles. The fiber toxicology paradigm in Figure 1.2a indicates the importance of particle length and their biopersistence in their potential toxicity and carcinogenicity. Whereas macrophages can engulf fibers with a low aspect ratio (ratio of length to width) before

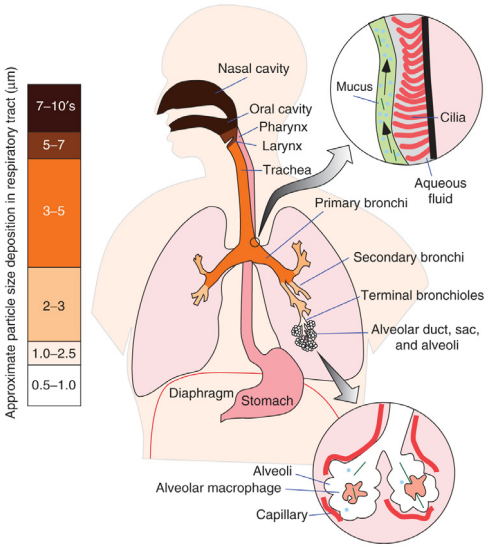

Figure 1.1. Fractionation of particle sizes that occurs with progressive depth in the respiratory system (Plumlee and Ziegler, 2007).

their clearance by draining lymph vessels, fibers with a high aspect ratio cannot be cleared and accumulate in tissues, where they promote carcinogenesis (Fig 1.2b.). Thus, macrophages (lung phagocyte cells with a diameter of 10 µm) are not capable of eliminating fibers longer than 10-12 µm (Churg, 1993) and the complete elimination of inhaled particles of approximately 1 µm can require more than 1 year (Singer et al., 1969).

Many different epidemiological and toxicological studies have shown that intense, generally prolonged inhalation exposure to asbestos and erionite dust is associated with elevated occurrences of diseases such as asbestosis, lung cancer and mesothelioma (Carbone et al., 2007). These fibrous minerals are considered as the group with greatest toxicity. However, there are other factors to take into account. For instance, chrysotile asbestos is less dangerous than amphibole and erionite asbestos and there are other fibrous minerals that do not induce cancer such as sepiolite and palygorskite (IARC, 1997).

Silica polymorphs are considered highly toxic even though their morphology is rather rounded. Barrenechea et al. (2002) found that lung cancer appear earlier among individuals with work-related exposure to silica, suggesting some carcinogenic effect of silica. Crystalline silica induces pulmonary fibrosis (silicosis) (WHO, 2000). However,

amorphous, non-crystalline silica has a lower toxicity, so it has been classified as non-carcinogenic (IARC, 1997).

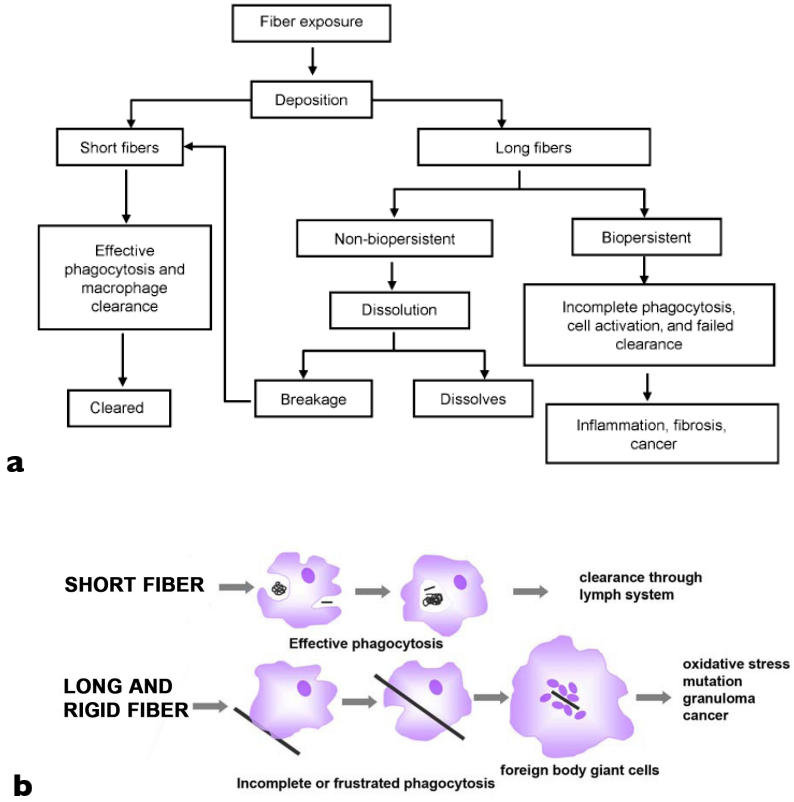

Figure 1.2. a. Paradigm for the role of long fibers and biopersistence in the pathogenic effects of fibers. b. Effect of fibers structure on phagocytosis by macrophages and clearing from tissues.

1.2.2. Particle solubility

As discussed above, the length and geometry are very important parameters to determine the pulmonary toxicity of the inhaled particles. Another factor controlling the tendency of a given particle to cause a disease is the residence time of the particle in the pulmonary environment. As summarized by Jurinski and Rimstidt (2001), two terms have been proposed to characterize substances that can persist in the body for many years after exposure. Biodurability is a measure of a substance's resistance to clearance by dissolution in body fluids. In contrast, biopersistence is a measure of a substance's resistance to all chemical, physical, and biological clearance mechanisms.

As shown in Figure 1.2b, following inhalation short fibers can be readily phagocyted by alveolar macrophage and cleared up the mucociliary escalator or via lymphatics to regional lymph nodes (Oberdorster et al, 2005). Non-biopersistent

particles will dissolve or break up into shorter ones and then cleared by macrophage phagocytosis, while long biopersistent fibers can not be completely phagocyted by macrophage and cause frustrated phagocytosis and then accumulate in the lung and may persist for decades, resulting in inflammation, fibrosis, and contribute to chronic lung diseases with long latency periods (Oberdorster, 2000).

The difficulty of an organism to eliminate a mineral grows with the mineral insolubility and its capacity to induce diseases is higher. To assess the biodurability and predict potential chronic effects, the dissolution rates of the particles in vivo and in vitro must be measured. The medium where the mineral is degraded corresponds to intrapulmonary fluid, with a pH around 7.4 (Plumlee and Ziegler, 2007), or intracellular fluid of the macrophages, with a pH around 4 (Nyberg et al., 1992), at a temperature of 37°C. The presence of certain biological compounds, including organic acids, aminoacids, polypeptides and proteins (Plumlee and Ziegler, 2007) may increase the dissolution rate of the particles.

1.2.3. Exposure dose

The exposure dose (intensity and duration) is an important factor that affects to the toxic level of each mineral. In general, some particles at low concentration can be cleared from the lungs by macrophages, but higher concentrations may cause frustrated phagocytosis and then result in inflammatory response. Very toxic minerals such as asbestos induce the development of diseases even if they are in trace levels. The intense and prolonged inhalation of minerals with moderate toxicity and high biodurability can cause the development of injuries if the organism capacity to expel and degrade the inhaled particles is exceeded. Depending on the dose of the exposure, silicotic diseases are classified into three classes: chronic, accelerated and acute.

1.2.4. Capacity of phagocyte response

The capacity of phagocyte response of the lungs is the result of a series of biochemical processes and it is important to show some aspects that help in the comprehension of this study and the responsible mechanisms of the pathogenesis (Lehnert, 1993). Once the particles reach the alveoli, the deepest portions of the lungs, alveoli macrophages cells try to phagocyte the particles to digest or clear by means of the secretion of digestive enzymes that create an oxidizing and acidic medium. Only particles with equivalent diameter of 10 μm or smaller can be completely phagocyted.

Macrophages that successfully engulf inhaled particulates are cleared upward in the airways, but the trachea clearance is inefficient if the inhalation is intense and prolonged. If the inhaled material is resistant to dissolution, it is liberated again by cellular death of the macrophage. Particles are phagocyted successively by the generation of other cells that try to eliminate them. The failure of this mechanism produces the reaction of the alveolar tissue against the liberated particles in two ways: oxidant segregation that is harmful for the cells, or transporting of the particles to the interstitial space, where tissues can suffer the attack of interstitial macrophages or can be eliminated by lymphatic via. If the tissue fails in the elimination process it is produced a response that generates a fibrosis to isolate the particle of the medium. This process could give rise to a cancer.

Moreover, the mineral dissolution products reach the blood stream to be metabolized and if one of them is toxic, can act on other organs before being eliminated. For instance, aluminum released from silicate degradation is considered neurotoxic and can be related with osteomalacy, Alzheimer's disease and other neurodegenerative diseases in humans (Oliver, 1997; Becaria et al., 2002; Rengel, 2004). However, there is continuous controversy regarding modes of aluminum toxicity to humans due to the difficulties found with detecting transport of Al across the plasma membrane of the cells, and other problems associated with the determination of speciation and location of Al in the medium (Rengel, 2004). On the other hand, silicon ameliorates aluminum toxicity to a range of organisms by means of a Si-specific intracellular mechanism, forming inert hydroxy-aluminosilicates (White et al., 2007). Moreover, the mineral incongruent dissolution produces silicon rich residues (Werner et al., 1995; Jurinski and Rimstidt, 2001) that have to be eliminated.

1.2.5. Particle surface features

Although the precise action mechanism of a mineral to induce disease in an organism has not yet been fully clarified, the initial contact between the organism and the mineral is produced through the mineral surface in an aqueous medium. The interaction of reactive surface groups (sites with acid-base properties, active sites for cation exchange, surface charge, hydrophilicity or hydrophobicity of the surface, production or adsorption of oxygen free radicals, etc.) with the biological medium originates the mineral toxicity (Fubini and Fenoglio, 2007). Furthermore, it has been

observed that the toxicity of quartz particles increase if they proceed from freshly ground rocks, due to a high reactivity of a fresh surface. Thus, it is very important the comprehension of how the surface interaction is produced to understand the pathogenesis mechanisms induced by minerals. It requires a mineralogical and geochemical surface characterization.

1.3. Medical geochemistry of biodurable earth materials: The case of smectite

The Earth materials that are most commonly associated with adverse respiratory health effects include dusts of asbestos, erionite, crystalline silica, and coal. However, dusts from a wide variety of other biodurable Earth materials (such as metal oxides, talc, kaolinite, feldspars, bentonite, fuller's earth, and micas) and non-Earth materials (such as wood dusts, wood fibers, glass fibers, and others) are also known to be associated with adverse health effects if exposures are of sufficient intensity and duration (i.e. occupational exposure). On the other hand, it has been found that numerous minerals are pathogenic in experiments *in vivo* and *in vitro* that include bioaccessibility, biodurability and toxicological tests. However, these conditions do not exactly correspond with the normal conditions of human activity and the implications for health cannot be extrapolated. It is very difficult to carry out epidemiologic studies due to the numerous factors than contribute and the high time that it takes to develop the disease induced by the inhalation of mineral dust (Guthrie, 1992).

Smectite is ubiquitous in soils and sediments, being an important part of the Earth's crust. In fact, there exists around 2.35 millions of km^2 of clayey soils with a high content in smectite in the Earth (Buol et al., 1980). Smectite is the most abundant clay mineral together with kaolinite and illite, and they constitute the main part of the fine and ultrafine fraction in soils and sediments. Therefore, they are one of the main compounds present in natural dust (Fig. 1.3). Mineral dust particles are transported into the atmosphere due to the suspension by turbulent diffusion of particles with diameter less than 70 mm. This process makes mineral dusts ubiquitous and therefore, there exists a general exposure of all the population that mainly depends on geographic factors (Fig. 1.4), as well as occupational exposure with variable intensity.

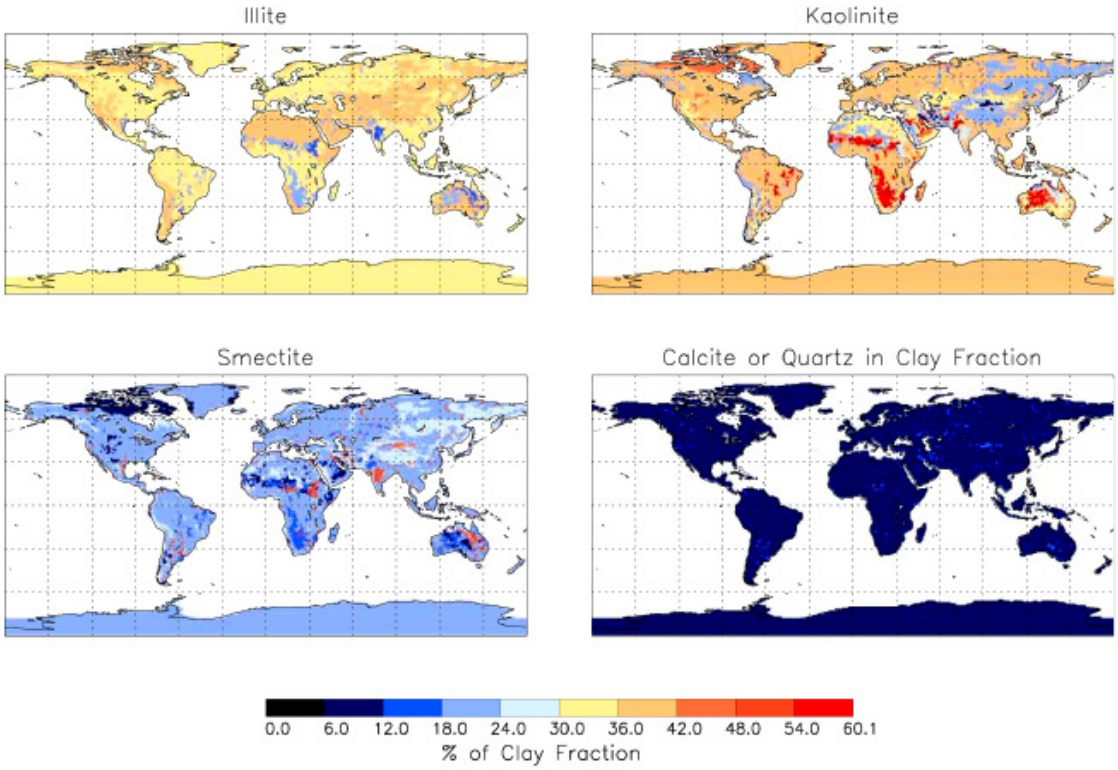

Figure 1.3. Distribution of the different mineralogical components in the soil (Hoose et al., 2008).

Guthrie (1992) indicated that smectite could induce moderate fibrosis in conditions of high exposure. However, there are very few studies about the toxicity of smectite. For this reason, the World Health Organization in its Environmental Health Criteria about Bentonites and Kaolins (WHO, 2005) indicated the urgency to tackle research in this matter.

1.4. Chemical conditions of the human body from a geochemical perspective

It is very important to see how the surface interaction between the mineral surface and the biological medium occurs to understand the pathogenesis of the minerals. Dissolution experiments can provide valuable information about the behavior of inhaled dust based on studies of the interaction of the dust particles and solvents chosen to simulate body fluids. Selection of appropriate physical and chemical parameters, such as particle size, solvent composition, and reaction temperature yields estimates of particle behavior in the body. There are very few studies on mineral

dissolution in a biologic medium, and they are mainly focused on asbestos and silica (Scholze and Conradt, 1987; Hume and Rimstidt, 1992; Werner et al., 1995; Gunter and Wood, 2000; Oze and Solt, 2010).

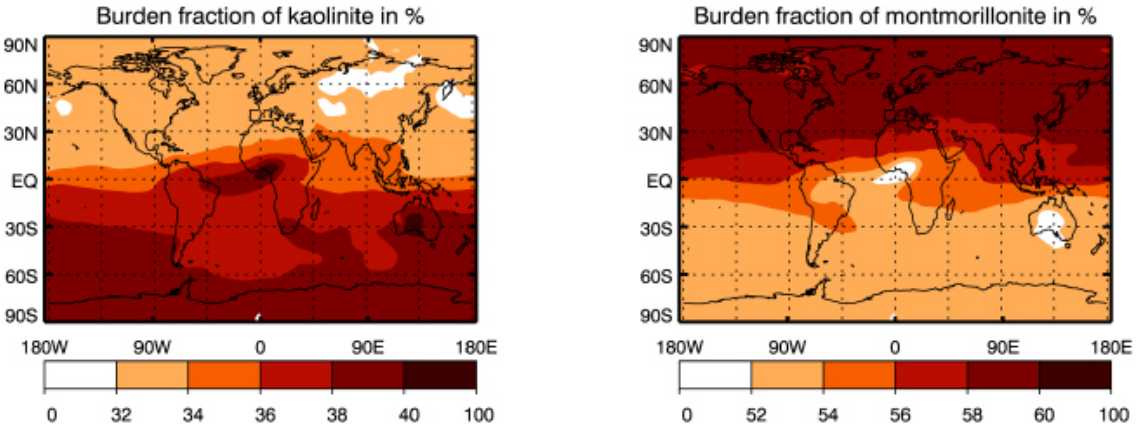

Figure 1.4. Annual mean kaolinite and montmorillonite fractions for the total atmospheric clay burden (Hoose et al., 2008).

The dissolution mechanism of a mineral comprises a group of elemental reactions that occur at the mineral/solution interface, where the ions and molecules dissolved in the solution interact with the surface cations, favoring the bonds breaking on the surface. This event produces mineral hydrolysis. The reaction is produced in specific active sites located on the crystal edge surface and it is controlled by several factors: temperature, pH, organics ligands and inhibitors. Thus, silicate dissolution is favored at acidic and basic pH by means of protonation/deprotonation of surface groups with acid/basic properties. Organic ligands can be adsorbed on the surface and form surface complexes that increase the dissolution rate. Moreover, organic ligands can complex cations released by dissolution, reducing the activity of the free cation and solution saturation respect to the mineral, accelerating the reaction. There are also cations and anions that can be adsorbed on the surface that prevent the dissolution reaction. Although corporal fluids are more complex than solutions present in the earth crust, the dissolution process is similar in both cases.

Interstitial fluid, with a temperature of 37°C, is basically a saline solution with calcium, sodium, potassium, chloride, sulfate, bicarbonate and phosphate as major constituents that keep the pH between 7.35-7.45 (Plumlee and Ziegler, 2007). It also contains aminoacids (glycine, alanine, lysine, etc.), low molecular weight organic acids

(lactate, citrate, salicylate, etc.) and proteins. The fluid in the macrophages is similar to interstitial fluid, but the pH is approximately 4 due to the presence of acids and complexing substances (Fig. 1.5).

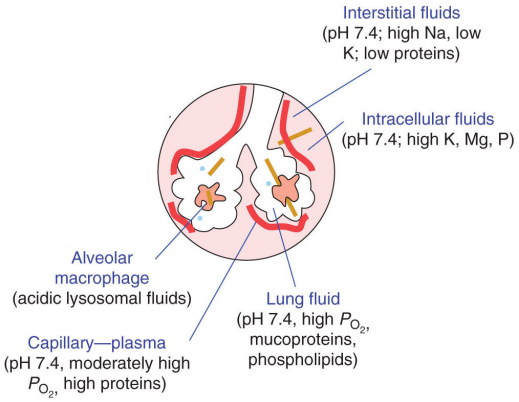

Figure 1.5. Compositions that would be encountered by particulate earth materials along the inhalation exposure pathway (modified from Plumlee and Ziegler, 2007).

The biodurability tests calculated under this conditions allow measuring the long-term solubility of smectite and understand its rates of chemical dissolution and alteration reactions under conditions that resemble those in the lung.

2. Scope and framework of the Thesis

2. SCOPE AND FRAMEWORK OF THE THESIS

2.1. Scope

This Thesis attempts to indentify how individual organic ligands (lactate, glycine, citrate and oxalate) affect to the dissolution rates of montmorillonite under conditions that may be similar to those found in the lung. In particular we investigate the reactions at the smectite/solution interface that contribute to smectite dissolution in synthetic lung fluid (SLF), including surface adsorption of organic ligands and the integration of the results with a surface complexation model.

Within this context, the specific objectives of the Thesis are:

1) Analysis of kinetics of smectite dissolution in saline and ligand solutions and to quantify the catalytic effect of organic molecules. This analysis includes the prediction of the saturation indices and the solubility of montmorillonite in equilibrium with solutions that mimic interstitial fluids.

2) Determination of the adsorption mechanism of ligands on smectite using the batch adsorption method.

3) Characterization of the ligand-montmorillonite complexes with FTIR spectroscopy.

4) Integration of the macroscopic adsorption data with the spectroscopic results to develop a surface complexation model.

5) To elucidate the dissolution mechanism of montmorillonite in presence of organic ligands.

6) Assessment of montmorillonite biodurability.

2.2. Framework of the thesis

Following these objectives, this Thesis is arranged in five chapters:

Chapter 3: This study is focused on the effect of lactate, glycine and citrate on the rate and mechanism of smectite dissolution under conditions that may be similar to those found in the lung. Moreover, it includes the study of surface adsorption of organic ligands (lactate, citrate and glycine) onto smectite and modeling of the speciation of released elements in the interstitial solution. An estimation of

biodurability of montmorillonite particles is derived from the kinetics results by using a geometric shrinking model.

Ramos M.E., Cappelli C., Rozalen M., Fiore S. and Huertas F.J. (2011) *Effect of lactate, glycine and citrate on the kinetics of montmorillonite dissolution.* American Mineralogist 96, 768-780. (doi: 10.2138/am.2011.3694)

Chapter 4: The objective of this chapter is to investigate the role of oxalate on the montmorillonite dissolution reaction. Dissolution rates are derived from flow-through dissolution experiments in buffered oxalate solutions. Moreover, the adsorption of the oxalate on montmorillonite was approached by batch adsorption experiments and through DR-FTIR spectroscopy.

Ramos M.E., Rozalen M., Johnston C.T. and Huertas F.J. *Effect of oxalate on the kinetics of montmorillonite dissolution.* (To be submitted).

Chapter 5: This chapter includes the study of the adsorption mechanism of lactate and citrate onto montmorillonite using the batch equilibrium adsorption method and attenuated total reflectance Fourier-transform infrared (ATR-FTIR) spectroscopy. The results of the complete adsorption study are used to develop a surface complexation model that explains the dependence of the adsorption of organic ligands onto the surface of montmorillonite.

Ramos M.E. and Huertas F.J. *Adsorption of lactate and citrate on montmorillonite.* Applied Clay Science (To be submitted).

Chapter 6: In this chapter, glycine adsorption on montmorillonite (adsorption edges and isotherms) is studied at different initial glycine concentrations and pHs, using the batch equilibrium adsorption method. ATR-FTIR spectroscopy and X-ray diffraction are also employed to elucidate the interaction between glycine and montmorillonite surface.

Ramos M.E. and Huertas F.J. *Adsorption of glycine on montmorillonite.* Applied Clay Science (under revision).

Chapter 7: The results of the oxalate adsorption on montmorillonite obtained in Chapter 4 are used to develop a surface complexation model that explains the dependence of the adsorption of oxalate onto the surface of montmorillonite. The manuscript also will include *ab initio* modeling of the montmorillonite-oxalate interaction, to unravel the geometry con the surface complex and the anchorage positions, as well as obtain infrared frequencies. However, this part is not included, as it was not performed by the dissertation's author.

Ramos M.E., Emiroglu C., García D., Sainz-Díaz C.I. and Huertas F.J. *Modeling the adsorption of oxalate onto montmorillonite*. (In preparation).

3. Effect of lactate, glycine and citrate on the kinetics of smectite dissolution

3. EFFECT OF LACTATE, GLYCINE AND CITRATE ON THE KINETICS OF SMECTITE DISSOLUTION.

Abstract.- The montmorillonite dissolution in saline solutions that mimic synthetic lung fluids (SLF) was investigated to gain knowledge on the clearance mechanisms of inhaled clay particles. Dissolution rates were measured at pH 4 (macrophages) and 7.5 (interstitial fluids) at 37 °C in flow-through reactors. The effect of organic acids was investigated through the addition of lactate, citrate, and glycine (0.15, 1.5, and 15 mmol/L). Lactate or glycine does not markedly affect the montmorillonite dissolution rates at pH 4, but at pH 7.5 there exists a slight inhibitory effect of lactate on the dissolution, probably due to a reduction in the number of reactive surface sites caused by lactate adsorption. Citrate enhances the dissolution rate by 0.5 order of magnitude at pH 4 and more than 1 order of magnitude at pH 7.5, thus indicating the prevalence of the ligand-promoted over the proton-promoted dissolution mechanism under these experimental conditions. The kinetic data were used to estimate the reduction in size of an inhaled clay particle. At pH 7.5, a particle 500 nm in diameter could be reduced 25% in the presence of citrate, whereas the reduction in saline solution would only be 10% after 10 years.

Ligand adsorption was measured in batch experiments at pH 2–11 and EQ3NR was used to model the capacity of the ligands to form soluble species of Al. Citrate, glycine, and lactate adsorb onto montmorillonite under acidic conditions, up to 23, 26, and 60 μmol/g, respectively. However, only citrate can complex the released aqueous Al at pH 4 and 7.5, which contributes to enhance dissolution rate and prevents precipitation of gibbsite at pH 7.5.

The enhancement of the dissolution rate in acidic citrate solution very likely comes from the formation of surface complexes between the ligand and the edge surface of montmorillonite. In neutral conditions the effect may be also due to the decrease of the activity of Al^{3+} by formation of aqueous Al-citrate complexes.

3.1. Introduction

After decades of research, a substantial and growing understanding of the important role played by geochemical processes on the health effects of biodurable

minerals has been gained. Although the precise mechanism to induce disease in an organism has not been fully clarified yet, the initial contact between the organism and the mineral is via the mineral surface in an aqueous medium. The interaction of surface reactive groups (sites with acid-base properties, active sites for cation exchange, surface charge, hydrophilicity or hydrophobicity of the surface, production or adsorption of oxygen-free radicals, etc.) with the biological medium may induce the mineral toxicity (Fubini and Fenoglio, 2007). Thus, it is important to see how the surface interaction occurs to understand the pathogenesis of minerals. This understanding requires a mineralogical and geochemical surface characterization. There are very few studies on mineral dissolution in a biologic medium and they are mainly focused on highly toxic asbestos and silica (Scholze and Conradt, 1987; Hume and Rimstidt, 1992; Werner et al., 1995; Gunter and Wood, 2000; Oze and Solt, 2010), as well as talc (Jurinski and Rimstidt, 2001).

Smectite, kaolin, and illite constitute the main part of the fine and ultrafine fraction in soils and sediments. Therefore, they are the main compounds of suspended dusts formed by mechanical and chemical weathering processes. Human beings are constantly exposed to mineral dust. However, very few studies exist on the toxicity of smectite and clays in general. The World Health Organization indicated the dire need to tackle research on this matter in its report "Environmental Health Criteria on Bentonites and Kaolins" (WHO, 2005).

Smectite dissolution has not been investigated using similar physical and chemical conditions to those found in the lung. However, this reaction has been extensively studied under Earth surface conditions for decades (Zysset and Schindler, 1996; Bauer and Berger, 1998; Cama et al., 2000; Huertas et al., 2001; Amram and Ganor, 2005; Metz et al., 2005a; Golubev et al., 2006; Rozalén et al., 2008, 2009b). The dissolution reaction is produced in specific active sites on the surface, and is controlled by several factors including temperature, pH, and the presence of organic ligands and inhibitors. Most studies agree that under the same pH conditions the dissolution rate is faster in the presence of organic ligands than that without organic ligand (Zutic and Stumm, 1984; Furrer and Stumm, 1986; Carroll-Webb and Walther, 1988; Chin and Mills, 1991; Wieland and Stumm, 1992; Ganor and Lasaga, 1994; Oelkers and Schott, 1998; Stillings et al., 1998), although the precise mechanisms are still being debated. The

dissolution process is a sequence of elementary reactions at the mineral/solution interface, where the ions and molecules dissolved in the solution interact with the surface cations, favoring the bonds breaking on the surface. This process is the result of several mechanisms acting simultaneously: proton-promoted dissolution (pH effect) and ligand-promoted dissolution due to the formation of metal-ligand surface complexes (Zutic and Stumm, 1984; Furrer and Stumm, 1986; Chin and Mills, 1991; Wieland and Stumm, 1992; Stillings et al., 1998) or the decrease in the solution saturation with respect to the mineral due to formation of soluble chelates.

This study is focused on the effect of lactate, glycine, and citrate on the rate and mechanism of smectite dissolution under conditions that may be similar to those in the lung. In particular, we investigate the reactions at the montmorillonite/solution interface that contribute to montmorillonite dissolution in synthetic lung fluid (SLF), including surface adsorption of organic ligands (lactate, citrate, and glycine) onto montmorillonite and the modeling of the speciation of released elements in the interstitial solution. Although the experimental conditions do not reproduce exactly the complexity of the human body, they provide a benchmark to evaluate the biological degradation of inhaled clay particles.

3.2. Materials and methods

3.2.1. Smectite characterization and pretreatment

The material used in this study was dioctahedral smectite extracted from the La Serrata–Cortijo de Archidona bentonite deposit located at Cabo de Gata (Almeria, SE Spain). For a detailed characterization of the sample and methods see Rozalén et al. (2008). This bentonite is ~92% montmorillonite and the rest consists of accessory minerals (quartz, feldspars, micas, calcite, and amphibole) plus volcanic glass. The experiments were performed on the <4 μm fraction saturated with K^+. The calculated structural formula of the K-smectite (based on a half-unit cell) corresponds to an Fe-rich montmorillonite (Newman and Brown, 1987):

$$K_{0.44}(Al_{1.27}Fe^{3+}_{0.22}Mg_{0.56})(Si_{3.95}Al_{0.05})O_{10}(OH)_2$$

The corresponding atomic ratio Al/Si is 0.334. Only 0.38 K^+ ions per half formula unit are exchangeable, which indicates the presence of a small proportion of non-swelling

layers.

X-ray diffraction (XRD) patterns recorded on powder specimens as well as on oriented and glycolated specimens showed that the sample is composed of a dioctahedral smectite with ~10–15% non-swelling layers, in agreement with the presence of non-exchangeable potassium determined by chemical analysis. No accessory phases were detected. The specific surface area after degassing the sample for two days at 110 °C under vacuum measured by BET (Brunauer et al., 1938), using 5-point N_2 adsorption isotherms, was 111 $m^2\ g^{-1}$ with an associated uncertainty of 10%. The edge surface area was estimated to be 6.5 $m^2\ g^{-1}$ (Rozalén et al., 2008).

3.2.2. Experimental setting

Dissolution experiments

Dissolution experiments were performed in single-pass, stirred, flow-through cells, which facilitated the measurement of the dissolution rate under fixed saturation state conditions by modifying the flow rate, initial sample mass, and input solution concentrations. The reactors were fully immersed in a thermostatic water-bath held at a constant temperature of 37 ± 1 °C. The flow rate was controlled with a peristaltic pump that injects the input solution into the bottom chamber of the cell (0.02 mL/min) where the solution is homogenized with a magnetic stirrer before reaching the upper chamber. The solid sample is confined within the upper chamber (reaction zone) by using two membrane filters: a 5 μm nylon mesh plus a 1.2 μm Durapore membrane at the bottom and a 0.45 μm Durapore membrane at the top. The total volume of the cell was 46 mL and the solid mass added to each cell was 0.1 g, to yield a solid solution ratio of ~2 g/L.

The composition of the input solutions mimics the fluids found in the human lung (synthetic lung fluids, SLF), the so-called Gamble's solution. They were prepared by using the formulation by Jurinski and Rimstidt (2001) with additional modifications. Saline solutions have the same molar composition, but all the salts were potassium salts to keep montmorillonite saturated in K^+: KCl 112.3 mmol/L, K_2SO_4 0.556 mmol/L, and the appropriate amount of HCl or $KHCO_3$ to adjust to the initial pH. Phosphate salts were avoided, because phosphate interferes in the Si analysis. Sodium azide

(NaN_3, 2 ppm) was added as bactericide. Several runs with ligand-free saline solutions were carried out as control and background experiments covering the pH range between 3 and 8, to have the complete dissolution profile under our experimental conditions.

The effects of three different organic ligands, lactate, citrate, and glycine on the dissolution rate were investigated. Lactate and citrate are contained in interstitial fluids. Glycine was used as a proxy for the amino acids and proteins found in these fluids. The concentration of each organic anion in the interstitial fluid is not well documented. However, lactate has been reported to be the most abundant organic acid in the interstitial fluids, having a concentration of 164 ppm, followed by citrate with 23 ppm (Plumlee and Ziegler, 2003).

To assess the ligand effect on the dissolution rate the input solutions were prepared by adding glycine, lactate, or citrate in three different concentrations (0.15, 1.5, and 15 mmol/L for each ligand) to the saline solution. The pH was adjusted with HCl or $KHCO_3$ solutions to ~4 or 7.5. No montmorillonite structural cations (Si, Al, Mg, Fe) were added to the input solutions. The compositions of the input solution in every dissolution experiment are reported in Table 3.1.

In each run, the flow rate and the input pH were held constant until steady-state conditions were achieved. The steady state was assumed to prevail when the Si output concentration remained fairly constant, differing by <6% between consecutive samples (Rozalén et al., 2008). Reaction times were from 1200 to 1800 h depending on the experimental conditions (pH, temperature, and ligand concentration). At steady state, dissolution is expected to proceed under far-from-equilibrium conditions. All the experiments consisted of a single stage; the cell was dismantled after the steady state was achieved.

After sampling every 24 h, the pHs of the output solutions were immediately measured at room temperature by using Crison combination electrodes standardized with pH 4.01 and 7.00 buffer solutions. The reported accuracy was ±0.02 pH units. To evaluate whether any temperature correction between room and experimental temperature was necessary, the pH of input and standard solutions covering a pH range from 4 to 9 was measured both at 20 and 37°C. The difference in the pH value between both temperatures was less than the accuracy of the measurement, thus no

Table 3.1. Experimental conditions and results of flow-through dissolution experiments. Dissolution rates were normalized to mass.

Run	Duration (h)	Flow rate (mL/min)	Initial mass (g)	Ligand (mmol/L)	pH in	pH out	C Si,out (μmol L^{-1})	C Al,out (μmol L^{-1})	C Mg,out* (μmol L^{-1})	C Fe,out* (μmol L^{-1})	Al/Si	log R Si (mol $g^{-1}s^{-1}$)	log R Al (mol $g^{-1}s^{-1}$)	ΔR Si %	ΔR Al %
Ligand free															
Sm-SE-3	1334	0.0239	0.1005	-	3.21	3.06	8.09	3.60	*0.89*	*0.11*	0.446	-11.38	-11.26	5.0	5.0
Sm-SE-4	1334	0.0221	0.1013	-	4.24	4.10	3.49	1.30	*1.26*	*1.83*	0.374	-11.79	-11.74	5.1	5.1
Sm-SE-5	1191	0.0226	0.1008	-	5.52	5.19	1.38	0.060	*0.81*	*0.12*	0.043	-12.18	-13.07	5.1	5.1
Sm-SE-6	1191	0.0227	0.0999	-	6.17	5.83	1.37	0.039	*0.81*	*0.12*	0.029	-12.18	-13.24	5.1	5.1
Sm-SE-7	1533	0.0230	0.0990	-	6.91	7.02	1.55	0.131	*0.54*	*1.15*	0.084	-12.12	-12.71	5.1	5.1
Sm-SE-8	1538	0.0229	0.0993	-	7.92	7.58	1.61	0.23	*0.56*	*1.19*	0.141	-12.10	-12.47	5.0	5.0
Lactate															
Sm-SEL0.15-4	914	0.0198	0.0991	0.15	3.90	3.92	6.17	2.32	*2.22*	*3.24*	0.376	-11.58	-11.53	5.0	5.0
Sm-SEL0.15-4b	1676	0.0217	0.0998	0.15	3.95	3.93	3.83	1.54	*1.38*	*2.01*	0.401	-11.75	-11.66	5.0	5.0
Sm-SEL1.5-4	1030	0.0193	0.0994	1.5	4.51	4.52	2.82	1.07	*1.02*	*1.48*	0.379	-11.94	-11.88	5.1	5.1
Sm-SEL1.5-4b	1555	0.0215	0.0999	1.5	3.96	3.94	3.76	1.87	*1.35*	*1.97*	0.424	-11.76	-11.59	5.0	5.0
Sm-SEL15-4	1150	0.0193	0.0998	15	4.39	4.30	4.98	1.74	*1.79*	*2.61*	0.349	-11.69	-11.67	5.1	5.1
Sm-SEL15-4b	979	0.0220	0.1000	15	3.92	3.89	6.68	2.55	*2.40*	*3.51*	0.381	-11.50	-11.44	5.0	5.0
Sm-SEL0.15-7	1440	0.0223	0.0996	0.15	6.98	7.09	0.894	0.103	*0.31*	*0.66*	0.116	-12.37	-12.83	5.1	5.1
Sm-SEL0.15-7b	1744	0.0231	0.1001	0.15	7.05	7.50	1.52	0.12	*0.53*	*1.12*	0.080	-12.14	-12.77	5.2	5.3
Sm-SEL1.5-7	1440	0.0235	0.0997	1.5	7.22	7.28	0.774	0.135	*0.27*	*0.57*	0.179	-12.41	-12.69	5.1	5.1
Sm-SEL1.5-7b	1747	0.0221	0.0997	1.5	7.12	7.46	1.74	0.18	*0.61*	*1.29*	0.102	-12.09	-12.60	5.1	5.1
Sm-SEL15-7	1584	0.0229	0.1000	15	7.20	7.79	1.93	0.22	*0.68*	*1.43*	0.115	-12.03	-12.50	5.1	5.1
Sm-SEL15-7b	1604	0.0220	0.1006	15	7.07	7.46	1.37	0.34	*0.48*	*1.01*	0.248	-12.20	-12.33	5.1	5.1
Citrate															
Sm-SEC0.15-4	1119	0.0231	0.0999	0.15	4.00	3.99	7.44	2.87	*2.68*	*3.91*	0.386	-11.43	-11.37	5.0	5.0
Sm-SEC1.5-4	1119	0.0244	0.0999	1.5	4.14	4.13	8.71	2.98	*3.14*	*4.57*	0.344	-11.34	-11.26	5.0	4.3

Sm-SEC15-4	1168	0.0227	0.1006	15	4.04	4.03	12.09	4.65	*4.35*	*6.35*	0.385	-11.23	-11.17	5.0	5.0
Sm-SEC0.15-5a	1071	0.0217	0.1000	0.15	5.56	6.81	2.66	0.60	*0.93*	*1.97*	0.222	-11.91	-12.08	5.0	5.0
Sm-SEC0.15-5b	1197	0.0204	0.1018	0.15	5.36	5.65	3.93	1.48	*2.32*	*0.35*	0.375	-11.77	-11.72	5.0	5.0
Sm-SEC1.5-5	1149	0.0204	01005	1.5	5.57	5.61	5.82	1.94	*3.43*	*0.52*	0.333	-11.58	-11.58	4.8	4.8
Sm-SEC15-5	1027	0.0210	0.1003	15	5.47	5.50	8.05	2.50	*4.75*	*0.72*	0.340	-11.44	-11.27	5.0	3.1
Sm-SEC0.15-7	1151	0.0230	0.0999	0.15	7.16	7.34	3.55	0.46	*1.24*	*2.63*	0.131	-11.76	-12.16	5.0	5.0
Sm-SEC1.5-7	1118	0.0200	0.1001	1.5	6.98	7.19	9.64	1.97	*3.37*	*7.13*	0.207	-11.39	-11.59	5.0	5.0
Sm-SEC15-7	1094	0.0229	0.1007	15	6.98	7.02	13.24	2.47	*4.63*	*9.80*	0.192	-11.20	-11.44	5.1	4.9
Glycine															
Sm-SEG0.15-4	1461	0.0235	0.0992	0.15	4.37	4.44	1.91	0.80	*0.69*	*1.00*	0.420	-12.02	-11.92	5.0	5.0
Sm-SEG1.5-4	1748	0.0233	0.0995	1.5	4.34	4.37	1.94	0.80	*0.70*	*1.02*	0.413	-12.02	-11.93	5.1	5.1
Sm-SEG15-4	1604	0.0217	0.1003	15	4.30	4.42	1.80	0.75	*0.65*	*0.95*	0.417	-12.09	-11.99	5.1	5.1
Sm-SEG15-4b	1917	0.0235	0.1001	15	4.34	4.33	1.74	0.66	*0.63*	*0.91*	0.381	-12.06	-12.00	5.0	5.0
Sm-SEG0.15-7	1384	0.0224	0.1002	0.15	7.26	7.40	1.57	0.14	*0.55*	*1.16*	0.092	-12.13	-12.69	5.0	5.0
Sm-SEG1.5-7	1290	0.0235	0.1001	1.5	7.24	7.34	2.31	0.10	*0.81*	*1.71*	0.043	-11.94	-12.82	5.1	5.1
Sm-SEG15-7	1056	0.0218	0.1000	15	7.32	7.87	1.53	-	*0.54*	*1.13*	-	-12.19	-	5.5	-
Sm-SEG15-7b	1317	0.0243	0.0993	15	7.29	7.49	1.35	0.11	*0.47*	*1.00*	0.084	-12.16	-12.75	5.1	5.0

* Estimated concentrations (see text for details) to be used exclusively as proxy in EQ3NR calculations

temperature correction was applied. An aliquot of 3 mL was separated for organic ligand analysis. Then the output solutions were acidified to pH 3 with HCl to prevent the precipitation of Al- or Fe-bearing phases during storage for Si and Al analyses.

The Si concentration in the samples was determined by colorimetry by using the molybdate blue method (Grasshoff et al., 1983). Total Al concentration in the solutions was determined by atomic adsorption spectroscopy (AAS), inductively coupled plasma mass spectrometry (ICP-MS), and fluorimetry using lumogallion as a complexing agent at pH 4.86 (Howard et al. 1986). High salt concentration (~8 g L^{-1}) produced a high-matrix effect with AAS and ICP-MS which gives rise to a low reproducibility and a detection limit above the Al concentration in the samples (ppb). The presence of citrate affected the measurement of Al by fluorimetry at its highest concentration (15 mmol/L), since citrate can compete with lumogallion for Al, leading to a negative interference. A correction was carried out by adding the same concentration of ligand to the Al standards. Such an effect was not observed for lactate and glycine.

The concentration of lactate and citrate was measured by ion chromatography using a Metrohm 761 Compact Ion Chromatograph with a Metrosep Organic Acids column. The eluent was prepared with 0.5 mmol/L sulfuric acid/15% acetone. Glycine was analyzed colorimetrically with a UV-visible spectrometer, using the ninhydrin method (Sun et al., 2006). The detection limits are 5 ppb for Si, 0.5 ppb for Al, 0.9 ppm for lactate, 9 ppm for citrate, and 0.7 ppm for glycine. The associated errors were 5% for Si and Al, 3% for lactate and citrate, and 4% for glycine.

Adsorption experiments

Adsorption experiments were performed as a complement to dissolution results to assess whether ligands were adsorbed onto the montmorillonite surface as a function of pH and interpret the dissolution mechanism.

Adsorption experiments of lactate, citrate, and glycine onto montmorillonite were carried out at room temperature. Potassium chloride was added to the solutions as a background electrolyte. For lactate and glycine, individual suspensions were prepared for every point of the adsorption series. For lactate adsorption, a quantity of 0.023 g of

montmorillonite was added to 20 mL of 10 mmol/L KCl in a polyethylene bottle. For glycine experiments the amount of montmorillonite in each suspension was 0.058 g. The suspensions were stirred for 3–4 min and left to equilibrate for 24 h. A volume of lactic acid or glycine stock solution was added to reach a total ligand concentration of 0.15 mmol/L. The pH was adjusted in each sample with an appropriate amount of HCl or KOH solution to cover a pH range from 2 to 10. After 5 h the pH was measured in each bottle and an aliquot of 10 mL was withdrawn and filtered through a 0.22 μm Durapore membrane. The solutions were analyzed for lactate or glycine.

For citrate adsorption 0.58 g of montmorillonite were suspended in 100 mL of 10 mmol/L KCl solution. The suspension was stirred for 3–4 min and equilibrated for 24 h. Then a volume of citrate stock solution was added to reach a total ligand concentration of 0.15 mmol/L and the pH was adjusted to 2 by adding 1 mol/L HCl solution. Every 20 min the pH was measured and a 5 mL aliquot was withdrawn while stirring. The pH was then increased in steps of ~1 unit using an appropriate amount of KOH solution. The 5 mL aliquot was immediately filtered through a 0.22 μm Durapore membrane and the solution was analyzed for citrate.

The anion exclusion volume of the montmorillonite was determined by measuring the concentration of chloride in montmorillonite slurries at increasing ionic strength (Polubesova and Borisover, 2009). Chloride concentration in the extract was measured by ion chromatography using a Metrosep A Supp–250 column and a solution of 1.7 mmol/L $NaHCO_3$/1.8 mmol/L Na_2CO_3 as eluent. Under our experimental conditions (10 mmol/L KCl) the anion exclusion volume was estimated of 0.39 $cm^3\ g^{-1}$ of clay.

3.2.3. Kinetic calculations

In a well-mixed, flow-through reactor the dissolution rate, *Rate* (mol $g^{-1}\ s^{-1}$), can be calculated based on the mass balance of a given mineral component *j*. Under steady-state conditions this is given by the following equation (e.g., Cama et al., 2000; Rozalén et al., 2008):

$$Rate(mol g^{-1} s^{-1}) = -\frac{1}{\nu_j}\frac{q}{M}(C_{j,out} - C_{j,in}) \qquad (3.1)$$

where ν_j is the stoichiometric coefficient of component *j* in the dissolution reaction, *q* stands for the volumetric fluid flow through the system, *M* is the mass of montmorillonite, and $C_{j,out}$ and $C_{j,in}$ correspond to the concentrations of component *j* in the output and input solutions, respectively. The rate is defined as negative for dissolution and positive for precipitation. The error in the calculated rate is estimated by using the Gaussian error propagation method and is <5% in all cases, which corresponds to ~0.05 logarithmic units. In this study the dissolution rate is calculated from the Si and Al concentrations (R_{Si} and R_{Al}) in the output solutions. All dissolution rates were normalized to the initial mass of montmorillonite (Rozalén et al., 2008).

Montmorillonite dissolves according to the following reaction:

$$K_{0.44}(Al_{1.27}Fe^{3+}_{0.22}Mg_{0.56})(Si_{3.95}Al_{0.05})O_{10}(OH)_2 + 6.18\ H^+ \longrightarrow$$

$$\longrightarrow 0.44\ K^+ + 1.32\ Al^{3+} + 0.22\ Fe^{3+} + 0.56\ Mg^{2+} + 3.95\ SiO_2 + 4.09\ H_2O \quad (3.2)$$

The estimated equilibrium constant for the K-montmorillonite dissolution reaction at 37 °C was log K_{eq}(K–Sm) = 4.94 (Rozalén et al., 2009b). The saturation state of the solution with respect to solid phases is calculated in terms of the free energy of reaction, ΔG_r:

$$\Delta G_r = RT \ln\left(\frac{IAP}{K_{eq}}\right) \quad (3.3)$$

where IAP and K_{eq}, respectively, stand for the ion activity product and the equilibrium constant for the dissolution reaction. Aqueous activities and chemical affinities are calculated here by using the EQ3NR geochemical code (Wolery, 1992).

The IAP was calculated from pH, Si and Al concentration in the output solutions at steady-state conditions. The Mg concentration was estimated according to the Mg/Si ratio observed by Rozalén et al. (2009b) in ligand-free solutions. The same procedure was used to estimate the Fe concentration in ligand-free acidic solutions (pH 2–3). At pH 4–9, the Fe^{3+} concentration was assumed to be in equilibrium with amorphous $Fe(OH)_3$ (Rozalén et al., 2009b). Such concentrations were used as proxies for the estimation of the solution saturation in K montmorillonite. Additional tests were conducted to assess the variation of montmorillonite saturation with Mg and Fe concentration. The change in ΔG_r was negligible when Mg or Fe contents were diluted or concentrated by a factor of 10.

EQ3NR was used to model the capacity of the ligands to form soluble species of Al. To attain this aim, the Lawrence Livermore National Laboratory thermodynamic database (cmp) (Wolery, 1992) was modified to include the ligands species and the complexation reactions of aqueous Al (Table 3.2). Although the dissolution experiments were performed at 37°C, the most complete set of complexation constant was obtained at 25°C. Several tests were run to assess the effect of the temperature, concluding that the variation of the species distribution due to the increase in temperature was negligible, if compared with the analytical errors and the scattering of the complexation constant in the literature.

Table 3.2. Stability constants of Al^{3+} with the organic ligands.

Reaction	Constant	Reference
Lactate		
$HLac = Lac^- + H^+$	$pK_a = 3.86$	(1)
$Al^{3+} + Lac^- = Al(Lac)^{2+}$	$logK_1 = 2.36$	(2)
$Al^{3+} + 2Lac^- = Al(Lac)_2^+$	$log\beta_2 = 4.42$	(2)
$Al^{3+} + 3Lac^- = Al(Lac)_3$	$log\beta_3 = 5.79$	(2)
Citrate		
$H_3Cit = H_2Cit^- + H^+$	$pK_{a1} = 3.10$	(1)
$H_2Cit^- = HCit^{2-} + H^+$	$pK_{a2} = 4.80$	(1)
$HCit^{2-} = Cit^{3-} + H^+$	$pK_{a3} = 6.40$	(1)
$Al^{3+} + Cit^{3-} = Al(Cit)$	$logK_1 = 7.98$	(3)
$Al(Cit) + H^+ = AlH(Cit)^+$	$logK = 2.94$	(3)
$Al(Cit) = AlH_{-1}Cit + H^+$	$logK = -3.31$	(3)
$AlH_{-1}Cit = Al(H_{-1}Cit)(OH) + H^+$	$logK = -6.23$	(3)
Glycine		
$HOOC\text{-}CH_2\text{-}NH_3^+ = {}^-OOC\text{-}CH_2\text{-}NH_3^+ + H^+$	$pK_{a1} = 2.35$	(4)
${}^-OOC\text{-}CH_2\text{-}NH_3^+ = {}^-OOC\text{-}CH_2\text{-}NH_2 + H^+$	$pK_{a2} = 9.78$	(4)
$Al^{3+} + 3({}^-OOC\text{-}CH_2\text{-}NH_2) = Al(OOC\text{-}CH_2\text{-}NH_2)_3$	$log\beta_3 = 19.40$	(5)

(1) Filius et al., (1997), (2) Marklund et al., (1986), (3) Martell et al., (1990), (4) Martell and Smith, (1974), (5) Yadava et al., (1984)

3.3. Results

3.3.1. Dissolution experiments

The variation with time of the output solution composition of several

representative flow-through experiments is shown in Figure 3.1. The concentrations of Si and Al and the pH were monitored throughout the duration of all the experiments. The experimental conditions of all the series, the average pH and the concentrations of Si and Al at steady state are reported in Table 3.1. The nomenclature of the dissolution experiments follows the pattern: Sm-SEL0.15-4b, where *Sm-SE* is smectite in electrolyte solution that can be followed by *L*, *C*, or *G* that is the ligand used (lactate, citrate, or glycine), with its concentration in mmol/L (0.15, 1.5, or 15). The last number is the initial pH in the experiment (4 or 7.5) and finally, the *b* corresponds to a replicate.

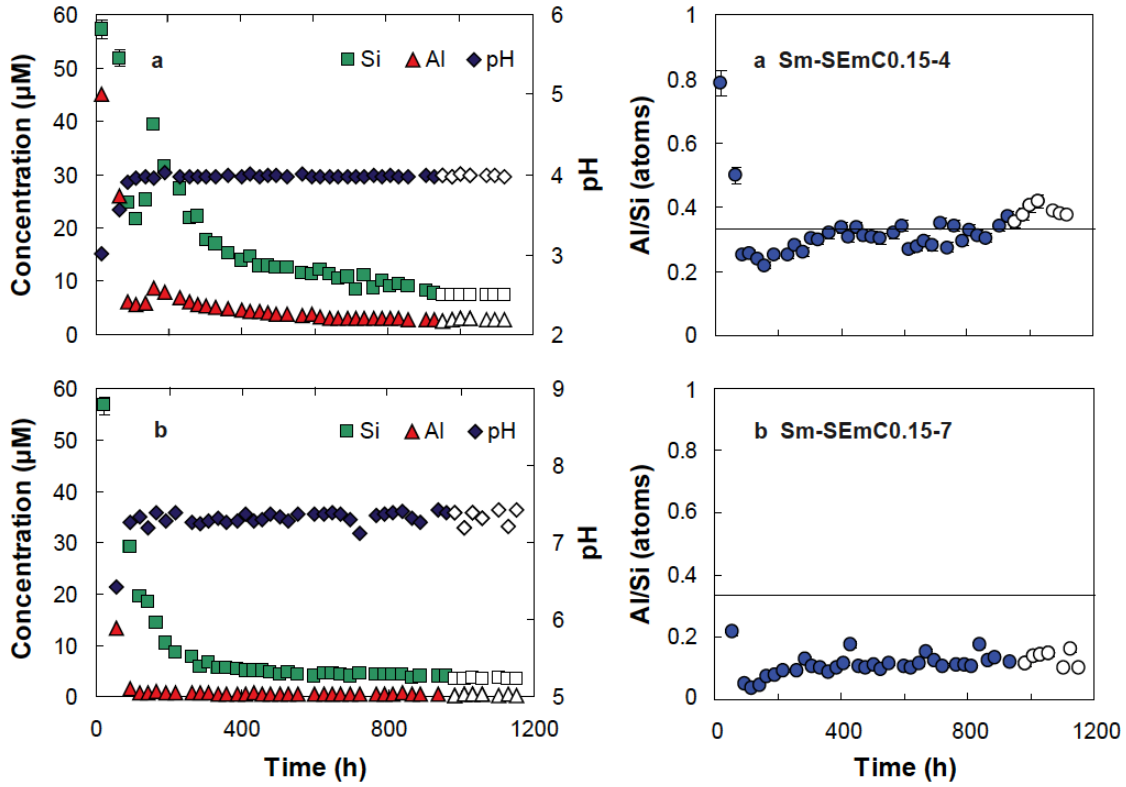

Figure 3.1. Evolution of the pH, Si and Al concentrations, and Al/Si atomic ratio in the output solutions of a selected group of dissolution experiments conducted in flow-through cells. Output solutions used to calculate the average steady state are denoted by open symbols. Horizontal line at Al/Si = 0.334 represents the stoichiometric ratio in the solid sample.

Experiments without organic ligands

In the experiments without an organic ligand cation-release rates tend to decrease significantly with elapsed time until steady-state conditions are attained. The solution pH remains constant with elapsed time in all the experiments. High Al and Si

concentrations were observed at the onset of most experiments. Afterward, Al and Si concentrations decrease asymptotically until a steady state is approached. The Al/Si release ratio increases up to a constant value at the steady state in all the experiments. Figure 3.2 shows the Al/Si ratio in solution at steady state as a function of the solution pH. The Al/Si release ratio at pH 4–4.5 is very close to stoichiometric, and the dissolution rates derived from Si and Al concentrations are consistent with each other. In circumneutral pH solutions (pH 4.5–8) the stoichiometric ratio decreases involving a deficit in aqueous aluminum.

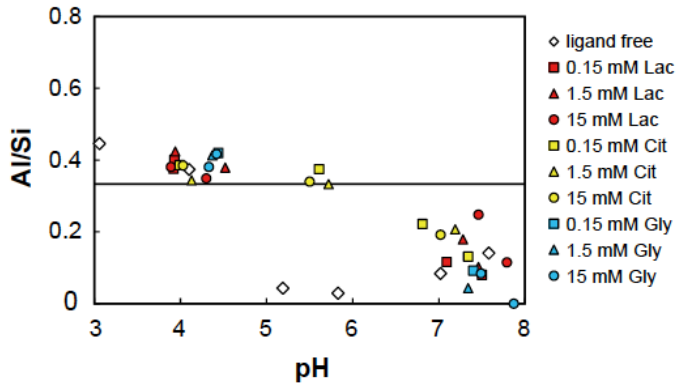

Figure 3.2. Variation in the Al/Si ratio with the pH in dissolution experiments. The line corresponds to stoichiometric ratio in the solid sample.

Experiments with organic ligands

The evolution of pH and concentrations of Si, Al, and organic ligand with elapsed time in a representative experiment is illustrated in Figure 3.1. The tendency observed for Si and Al is the same as in experiments without an organic ligand: an initial fast release of montmorillonite structural cations to the solution and an asymptotical decrease until steady state is approached.

The pH remained constant in the experiments at pH 4 (Fig. 3.1). However, it was necessary to readjust the pH in the same series at pH 7, because of a drift to higher values during the first days of reaction.

The behavior of the Al/Si ratio with elapsed time is also similar to that found in organic ligand-free solutions (Fig. 3.1), which reach a constant value when steady state is approached. At pH 4 and 5.5, montmorillonite dissolution is stoichiometric irrespective of the ligand and its concentration. The dissolution reaction at pH 7–8 is

incongruent in solutions with lactate, citrate, or glycine, regardless of their concentrations. Lactate, citrate, and glycine concentrations remain constant with elapsed time in all the experiments.

3.3.2. Adsorption experiments

Adsorption experiments were performed as a complement to dissolution series to assess whether ligands were adsorbed onto the montmorillonite surface as a function of pH and interpret the dissolution mechanism. The pH dependence of the adsorption of lactate, citrate, and glycine onto montmorillonite (adsorption edges) is shown in Figure 3.3. The amount of ligand adsorbed is small, but all three of these produced different adsorption patterns. In the case of lactate adsorption, three pH intervals exist. Up to pH ~6, the amount of adsorbed lactate is approximately constant, with a maximum adsorption of 60 μmol/g at pH 5.5–6. From pH 6 to 9, the adsorbed lactate is progressively lower. Finally, at pH > 9, lactate does not adsorb onto the montmorillonite surface. The glycine adsorption pattern is very similar to that found for lactate, with a maximum of 26 μmol/g, but the decrease in adsorption occurs at pH 5. Citrate adsorption is very close to zero at a low pH, increasing up to a maximum of 23 μmol/g at approximately pH 6 and decreasing over pH 6.

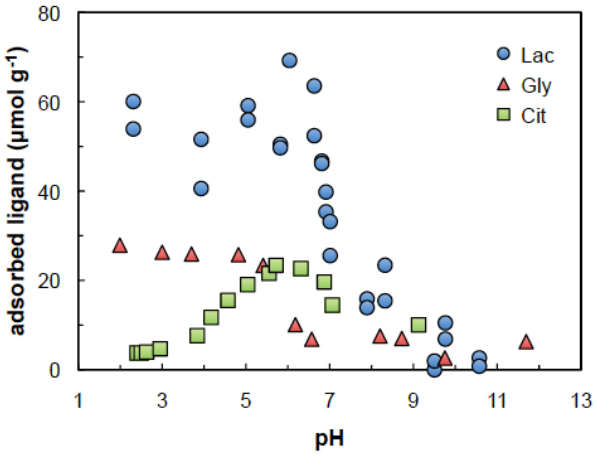

Figure 3.3. Dependence on solution pH (adsorption edge), lactate, citrate and glycine adsorption onto montmorillonite.

3.3.3. Saturation and aqueous speciation

To assess the contribution of Al speciation, the steady-state composition of the

output solutions of the dissolution experiments with no ligand, lactate, citrate and glycine (Table 3.1) was modeled with EQ3NR. The saturation of the output solutions with respect to montmorillonite and secondary minerals is given in Table 3.3.

Table 3.3. Saturation state (kcal mol^{-1}) of output solutions at steady-state conditions computed according to Eq. 3 for flow-through montmorillonite dissolution experiments at 37°C. Shadowed values indicate saturation or oversaturation.

Run	pH_{out}	K-Mont	SiO_2(am)	Qz	Gib	Kln
Sm-SE-3	3.06	-29.14	-3.25	-1.49	-6.61	-15.24
Sm-SE-4	4.10	-22.50	-3.74	-1.99	-2.99	-9.00
Sm-SE-5	5.19	-19.49	-4.29	-2.54	-0.708	-5.53
Sm-SE-6	5.83	-16.20	-4.30	-2.54	0.776	-2.57
Sm-SE-7	7.02	-12.69	-4.23	-2.47	1.40	-1.19
Sm-SE-8	7.58	-11.85	-4.21	-2.45	1.06	-1.82
Lactate series						
Sm-SEL0.15-4	3.92	-22.19	-3.41	-1.65	-3.38	-9.09
Sm-SEL0.15-4b	3.93	-23.82	-3.69	-1.93	-3.58	-10.06
Sm-SEL1.5-4	4.52	-23.27	-3.87	-2.12	-1.49	-6.26
Sm-SEL1.5-4b	3.94	-24.80	-3.70	-1.95	-3.46	-9.85
Sm-SEL15-4	4.30	-22.35	-3.53	-1.78	-2.51	-7.62
Sm-SEL15-4b	3.89	-20.54	-3.36	-1.61	-3.83	-9.90
Sm-SEL0.15-7	7.09	-14.74	-4.55	-2.80	1.18	-2.27
Sm-SEL0.15-7b	7.50	-12.55	-4.24	-2.48	0.771	-2.47
Sm-SEL1.5-7	7.28	-14.37	-4.64	-2.88	1.11	-2.58
Sm-SEL1.5-7b	7.46	-11.88	-4.16	-2.40	1.07	-1.70
Sm-SEL15-7	7.79	-12.02	-4.10	-2.35	0.758	-2.22
Sm-SEL15-7b	7.46	-11.33	-4.30	-2.55	1.45	-1.24
Citrate series						
Sm-SEC0.15-4	3.99	-22.06	-3.30	-1.54	-4.01	-10.14
Sm-SEC1.5-4	4.13	-22.89	-3.20	-1.45	-5.19	-12.30
Sm-SEC15-4	4.03	-23.13	-3.01	-1.25	-6.33	-14.20
Sm-SEC0.15-5a	6.81	-15.73	-3.91	-2.15	-1.65	-6.65
Sm-SEC0.15-5b	5.65	-18.31	-3.67	-1.92	-2.71	-8.30
Sm-SEC1.5-5	5.61	-18.63	-3.44	-1.69	-3.82	-10.06
Sm-SEC15-5	5.50	-20.17	-3.25	-1.49	-5.28	-12.59
Sm-SEC0.15-7	7.34	-13.06	-3.74	-1.98	-1.08	-5.15
Sm-SEC1.5-7	7.19	-11.64	-3.15	-1.40	-1.77	-5.36
Sm-SEC15-7	7.02	-12.95	-2.95	-1.20	-3.12	-7.68
Glycine series						
Sm-SEG0.15-4	4.44	-24.62	-4.55	-2.80	-1.93	-8.49
Sm-SEG1.5-4	4.37	-24.80	-4.54	-2.79	-2.20	-9.02
Sm-SEG15-4	4.42	-25.25	-4.59	-2.83	-2.36	-9.41
Sm-SEG15-4b	4.33	-25.93	-4.61	-2.85	-2.68	-10.09
Sm-SEG0.15-7	7.40	-13.83	-4.67	-2.92	0.963	-2.94
Sm-SEG1.5-7	7.34	-13.09	-4.44	-2.69	0.843	-2.72
Sm-SEG15-7	7.87	-13.57	-4.69	-2.93	-0.007	-4.92
Sm-SEG15-7b	7.49	-14.78	-4.76	-3.01	0.400	-4.25

*K-Mont: K-montmorillonite; SiO_2(am); amorphous silica; Qz; quartz; Gib: gibbsite; Kln: kaolinite

All the solutions are undersaturated in montmorillonite, amorphous silica, quartz and kaolinite. Ligand free solutions are saturated in gibbsite at pH > 5.8. Solutions from the experiments at pH 7.5 with lactate or glycine are saturated in gibbsite. However, citrate solutions are undersaturated in gibbsite irrespective of the solution pH.

The aqueous speciation of the lactate, citrate, and glycine was derived from their acidity constants (Table 3.2) by using EQ3NR. The results are shown in Figure 3.4. Si-ligand speciation was not taken into account as Si forms very weak organic complexes in solution (Pokrovski and Schott, 1998). The capacity of lactate, citrate, and glycine to form soluble complexes with aqueous Al^{3+} was also investigated with EQ3NR, using the corresponding constants values listed in Table 3.2. The concentrations of aqueous Al (0.1 to 4.7 μmol/L) and ligands (0.15, 1.5, and 15 mmol/L) in the output solutions cover a wide range of conditions. The modeling with EQ3NR reveals no substantial differences in the distribution of Al species. Thus, to facilitate the comparison the speciation results in Figure 3.5 were modeled for a total Al concentration of 1 μmol/L.

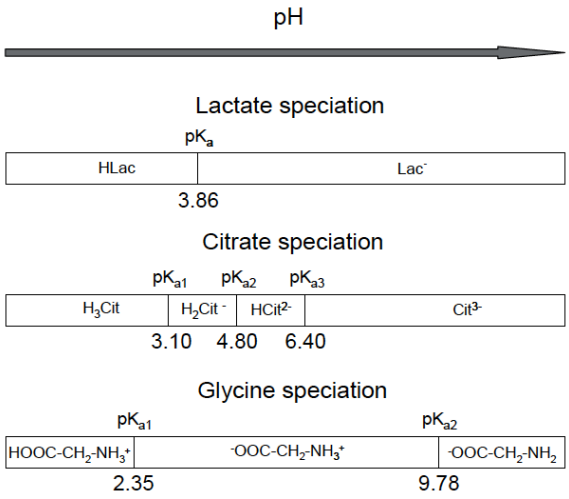

Figure 3.4. Sketch of the speciation of the lactate, citrate and glycine with the pH.

The Al speciation diagram was different for each ligand (Fig. 3.5). In the case of lactate, only the complex $Al(Lac)_3^{2+}$ is relevant in the range of pH between 4 and 5, representing only 10% of the total aqueous Al. For citrate, the speciation is more complex. In the pH range 3–4, three species coexist: around 10% of $AlH(Cit)^+$, 20% of Al(Cit), and increasing values from 1 to 80% of $Al(Cit)^-$. This last species reaches a maximum of 90% between pH 4 and 5, where it starts to coexist with $Al(OH)(Cit)^{2-}$.

At pH 6, it exists 50% of $Al(Cit)^-$ and 50% of $Al(OH)(Cit)^{2-}$. Above pH 6, the concentration of $Al(OH)(Cit)^{2-}$ increases up to 100% at 7–8.5. Finally, for glycine no relevant amounts of Al-Gly complexes are observed under our experimental conditions. The capacity of the three ligands investigated to complex Al ions follows the trend citrate >> lactate > glycine, from strong to very weak complexants.

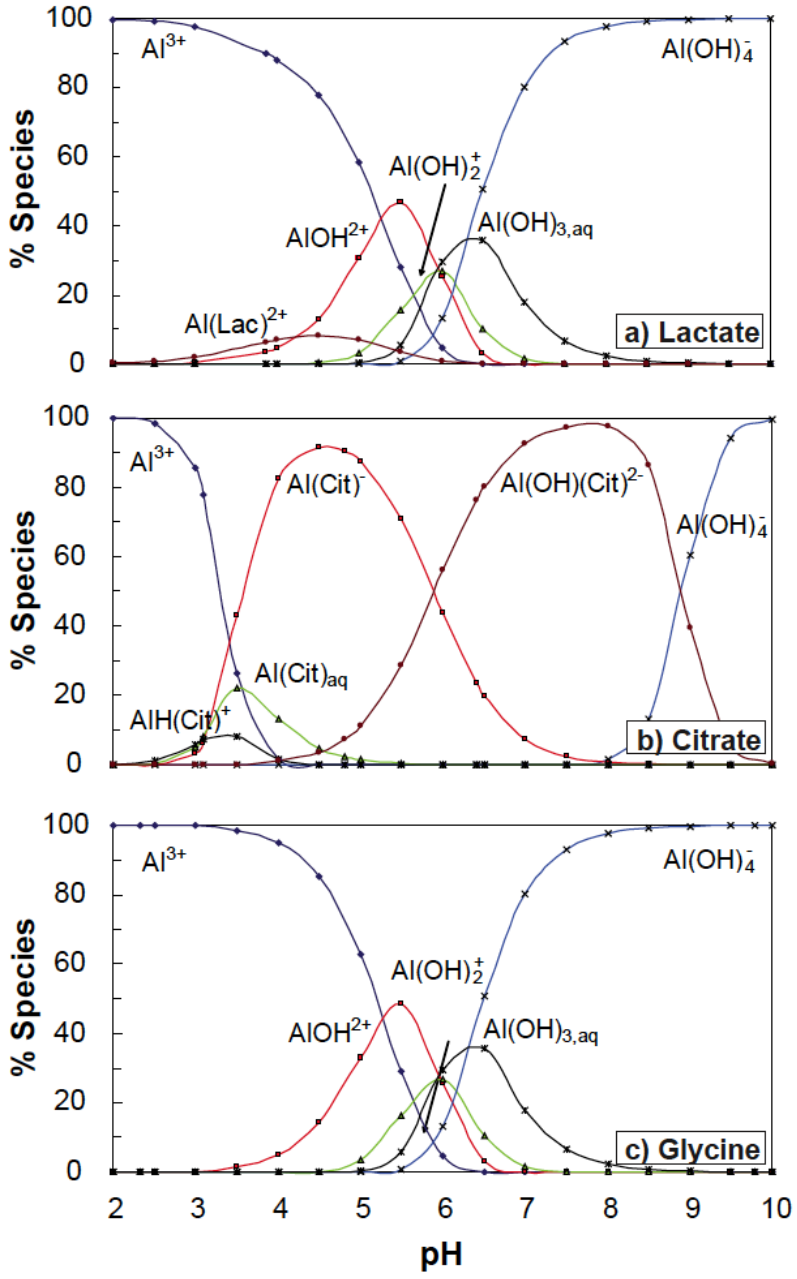

Figure 3.5. Aluminum (1 μmol L^{-1}) speciation in solutions with 1.5 mmol L^{-1} of a) lactate , b) citrate and c) glycine as a function of the solution pH.

3.4. Discussion

3.4.1. Dissolution experiments

Montmorillonite dissolution rates at steady state are plotted in Figure 3.6 as a function of the solution pH. In ligand-free solutions, the rates show the typical variation in the dissolution rate with the pH observed for Al-silicates and complex oxides: the rates decrease with increasing pH in acidic conditions, they reach a minimum at near neutral pH and increase with increasing pH at more basic conditions.

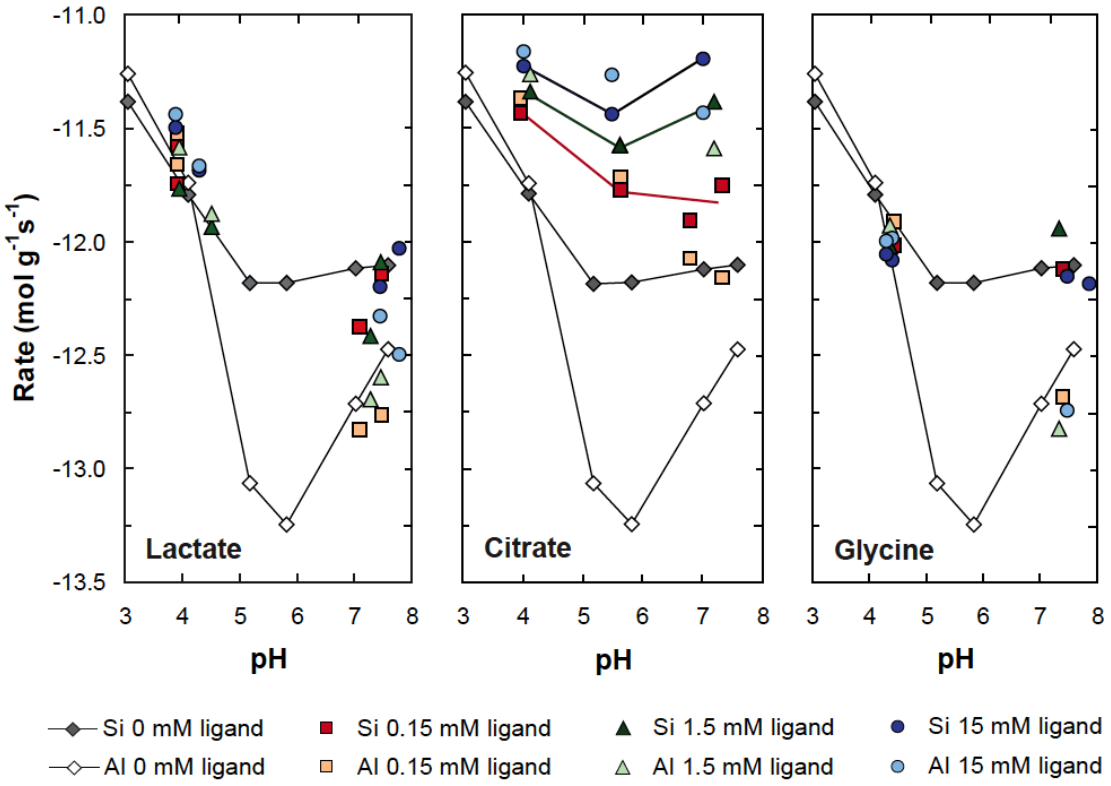

Figure 3.6. Experimental dissolution rates derived from Si and Al concentrations in outlet solution calculated with lactate, citrate and glycine solutions. Dissolution rates in ligand-free solutions were included for comparison.

The dissolution rates derived from Si and Al concentrations are consistent with each other, indicating a stoichiometric dissolution at steady-state conditions for pH $\leq$ 4.5. Incongruent dissolution under circumneutral pH conditions is produced by a back-precipitation or sorption of Al and caused a decrease in the dissolution rates derived from Al concentration (Metz et al., 2005a; Rozalén et al., 2008). As a consequence, the dissolution rates derived from Al under these conditions should be considered as apparent dissolution rates.

In the absence of organic ligands, the species that attack the silicate are mainly protons, water molecules, and hydroxyls, which can form surface complexes with cations at surface sites. Thus, the variation in the dissolution rate with pH can be described as the sum of the contribution of the three components associated with the concentration of protons, hydroxyls, and water molecules (Huertas et al., 1999). For acidic conditions, dissolution rate is proportional to the proton activity powers to the proton reaction order

$$Rate(mol \cdot g^{-1}s^{-1}) = 10^{-10.24} a_{H^+}^{0.37} \quad (3.4)$$

The reaction order (n_H = 0.37) is consistent with the value n_H = 0.40 obtained at 25°C for diluted solutions of electrolytes (0.01 mol/L) (Rozalén et al., 2009b), as well as close to those from Amram and Ganor (2005) (n_H = 0.57) and Golubev et al. (2006) (n_H = 0.21) at 25°C. Nevertheless, a similar equation cannot be derived around neutral conditions and there are not enough data on the basic branch.

Lactate and glycine solutions

The increase in the ligand concentration from 0.1 to 15 mmol/L, both at pH 4 and 7.5, does apparently not produce any relevant change in the dissolution rate (Fig. 3.6; Table 3.1). At pH ~4, the dissolution reaction is congruent with and without the lactate or glycine, since the Si- and Al-based rates are very similar in both cases. There is a slight increase in the dissolution rates by adding lactate, but the difference is within the error associated with the dissolution rate.

At pH ~7.5, the dissolution reaction is incongruent with lactate or glycine as was also observed in ligand-free solutions in this pH interval. The Si-derived dissolution rates in solution with lactate are 0.2–0.3 logarithmic units lower than those in pure electrolyte solutions except for the series with lactate 15 mmol/L, which have similar values of dissolution rate. This difference in Si-derived dissolution rates was not found in glycine experiments. The Al-based dissolution rates with lactate and glycine at pH 7.5 follow a parallel trend to the rates measured in experiments without ligands. Furthermore, Al-derived dissolution rates in lactate solutions are slightly lower than the corresponding rates in ligand-free solutions, but the differences are not significant.

Citrate

The citrate enhances the montmorillonite dissolution rate significantly at all the pH values studied and this effect strongly depends on the citrate concentration added (Figs. 3.6 and 3.7). To gain a more complete understanding of the effect of this ligand an additional set of experiments was performed at pH 5.5. The variation in the Si-derived dissolution rates (R_{Si}) with the pH is similar to that obtained in ligand-free solutions. However, a strong catalytic effect can be observed when citrate is added even at the lowest concentration. In the presence of a high concentration of citrate (15 mmol/L) the Si-release based rate is increased by 0.5 logarithmic units at pH 4 with respect to the rate calculated without organic ligand at the same pH. This increase is greater at near neutral pH, so that the rate obtained in 15 mmol/L citrate is one order of magnitude faster than that without citrate. Montmorillonite dissolution in citrate solution is stoichiometric at pH 4 and 5.5, but incongruent at pH 7.5. Nevertheless, the Al/Si ratio at the steady state increases in the experiments with citrate when compared with ligand-free solutions (Fig. 3.2).

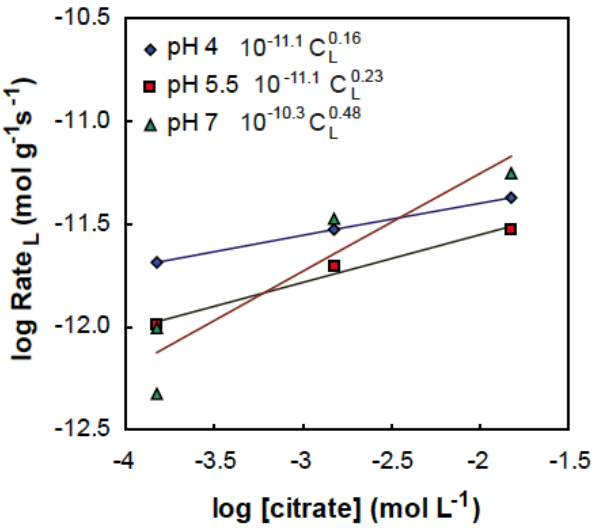

Figure 3.7. Effect of citrate on Si-derived dissolution rates. Ligand promoted dissolution rate for each pH conditions, R_L, derived from Eq. 3.6a-c, are included.

The dissolution rates obtained by Golubev et al. (2006) at pH 6.7 also showed the catalytic effect of citrate, although their values were one order of magnitude lower than those obtained in the present study.

Montmorillonite biodurability

Dissolution rates are a complex function of the chemical solubility of particles in the body fluids that determine the rate at which particles dissolve (Plumlee and Ziegler, 2003). The resistance to chemical dissolution in the body (particle's biodurability) controls the residence time of a particle in the lungs and it is related with the tendency to cause a disease (Jurinski and Rimstidt, 2001). An estimation of biodurability of clay particles can be derived from our kinetics results by using a simple model: a disk was used as a proxy for particles shape and dissolution reaction occurs from the edge inward (Rozalén et al., 2008). Biodurability is estimated as the reduction in the diameter as time progress. Although the experimental conditions do not reproduce exactly the complexity of the human body, they provide a benchmark to evaluate the biological degradation of inhaled clay particles. The parameters used in the calculation are the following:

• Particle morphology: disks of 0.5 μm in diameter and 5 nm in thickness that correspond to 4 layers of smectite (Verburg and Baveye, 1994) with a monolayer of interlayered water.

• Molar weight: 767.89 g/mol, according to the structural formula.

• Molar volume: 372.33 cm^3/mol (Robie and Hemingway, 1995).

• Specific weight: 2.06.

The calculated rates allow us to estimate the dimensions of the particle as time progress, assuming that reactive surface area corresponds to the particle edges (see discussion in Rozalén et al. 2008). The evolution of the particle radius (*r*) with time can be obtained by the following equation:

$$r^2 = r_0^2 - \frac{Rate_v}{\pi h} t \qquad (3.5)$$

where r_0 is the initial radius, $Rate_v$ the volumetric dissolution rate expressed in $cm^3\ s^{-1}$, *h* particle thickness, and *t* the elapsed time.

Simulations were performed with a concentration of 1.5 mmol/L lactate, 0.15 mmol/L glycine, and 0.15 mmol/L citrate (Fig. 3.8), which corresponds to the conditions most similar to biological fluids (Plumlee and Ziegler, 2003). Clay particles dissolved faster at pH 4 (lysosomes) than at pH 7.5 (interstitial fluids). Considering the

three ligands investigated, only citrate enhances substantially the montmorillonite dissolution. The effect of citrate is stronger at pH 4 than at pH 7.5. At pH 7.5, a particle 500 nm in diameter could be reduced 25% in the presence of citrate, whereas the reduction in saline solution would only be 10% after 10 yr. However, under both conditions, acidic and neutral, it takes several years to halve the particle diameter.

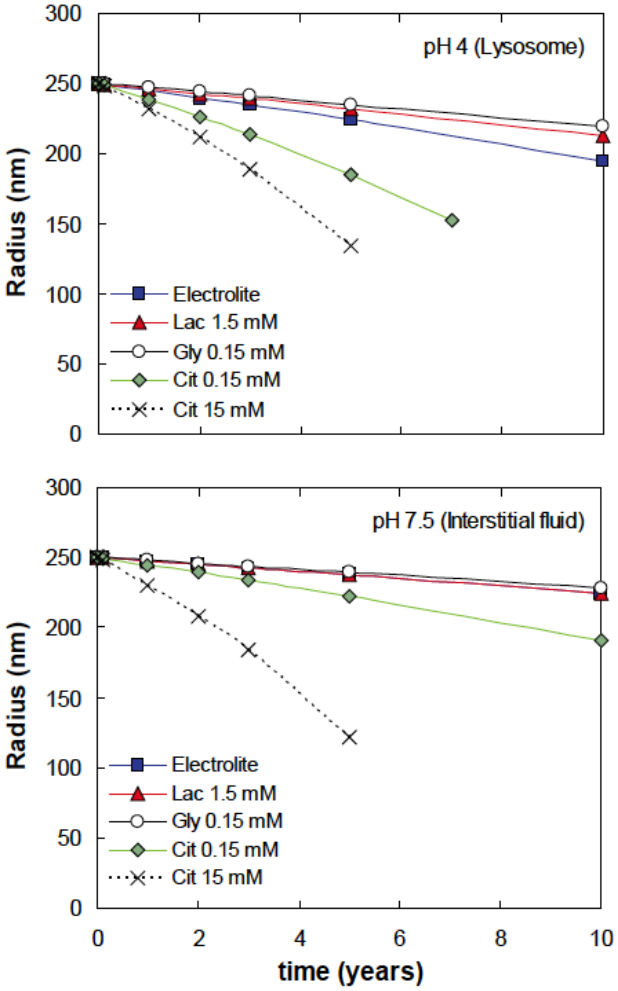

Figure 3.8. Decrease in the diameter of a montmorillonite particle during the dissolution in lung fluids. Ligand concentrations were of 1.5 mmol L^{-1} lactate, 0.15 mmol L^{-1} glycine and 0.15 mmol L^{-1} citrate. The curve for 15 mmol L^{-1} citrate concentration was included for comparison.

Extending the conclusions on montmorillonite to other 2:1 phyllosilicates (Rozalén et al., 2008), the chemical degradation efficiency of clayey particles inhaled (smectites, illites, micas) elements such as Si or Al may have additional consequences for human health. Strong complexants as citrate contribute to the transport of released elements such as Al. The application of geochemical methods may help health science in the

understanding of the hazard of toxic minerals as well as those considered as inert such as clay minerals.

3.4.2. Adsorption experiments

Ligand adsorption is the result of the interaction between ligand and montmorillonite at the mineral/solution interface. As the ligand deprotonation and montmorillonite edge surface charge are both pH dependent the adsorption reactions depend on the solution pH. The pH-dependent surface charge at the montmorillonite edge surface was modeled on the basis of three types of adsorption sites: amphoteric sites on Al cations, basic silanol sites and cation exchange sites (>ZEX) associated with the montmorillonite cation exchange capacity (Fig. 3.9) (Rozalén et al., 2009a). The aqueous speciation of the lactate, citrate, and glycine was derived from their acidity constant (Table 3.2) by using EQ3NR (Fig. 3.4).

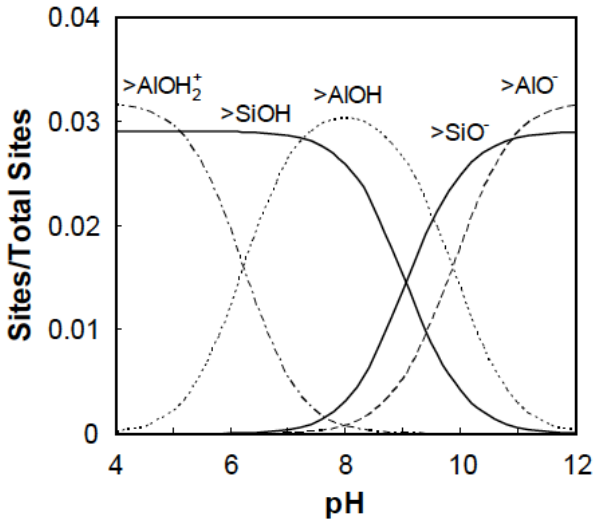

Figure 3.9. Predicted distribution of the surface species of montmorillonite as a function of pH at 0.1 M ionic strength at 25°C according to the constant capacity model, modified from Rozalén et al. (2009a). Site density is expressed in terms of the molar fraction of the total surface density for edges sites and basal plane sites (not shown).

Lactate

At pH values over ~7.5, both the montmorillonite edge surface and lactate are negatively charged. There may be no interaction between the montmorillonite edge surface and lactate anion, and no lactate adsorption can be observed under alkaline

conditions. Below pH 7.5, the montmorillonite edge surface is positively charged due to the relative abundance of $>AlOH_2^+$ and the positive charge increases as the solution becomes more acidic (to approximately pH <5). Negatively charged lactate adsorbs onto the montmorillonite edge surface increasing adsorption as the pH decreases from 9 to 7. Below pH 7, the amount of lactate adsorbed is approximately constant in all the experiments. This behavior indicates an electrostatic interaction between the anion and the positively charged surface, as observed for the lactate-goethite interaction (Filius et al., 1997). According to Figures 3.3 and 3.9 that correspond to the adsorption edges and the edge surface speciation of the montmorillonite, respectively, lactate adsorbed onto the montmorillonite (Lac^- or HLac) is probably bound to positively charged Al sites.

The lactate molecules in solution are predominantly uncharged below pH 3.86, while the montmorillonite edge surface is positively charged. The protonation of lactate below pH 3.86 should reduce the amount of the ligand adsorbed onto the montmorillonite edge surface. However, this behavior, found for other solids (Filius et al., 1997), is not observed in our experiments.

Citrate

The adsorption behavior of citrate also points to electrostatic binding. At approximately pH < 3.2 a very weak interaction is expected between the fully protonated citrate and positively charged montmorillonite. No clear evidence of adsorption was found. The interaction between the citrate and the montmorillonite edge surface increases from pH 3.2 up to 7 due to the partial deprotonation of citric acid. The most abundant species are H_2Cit^- (pH 3.1–4.8) and $HCit^{2-}$ (pH 4.8–6.4), which can interact with the positively charged montmorillonite edge surface, producing the adsorption maximum at pH 6. Above pH 7, the electrostatic repulsion between the fully deprotonated citrate and the negatively charged montmorillonite edge surface (both $>SiO^-$ and $>AlO^-$ sites) makes ligand adsorption difficult. This decreases progressively as the negative charge develops at the montmorillonite edge surface with an increasing pH.

Lackovic et al. (2003) found that a small amount of citric acid can be adsorbed onto kaolinite and illite, modeling the adsorption with outer-sphere complexation to

the variable-charge edge groups. Their adsorption maximum (~3 μmol/g illite) is approximately one order of magnitude lower than in the present study, although the citrate solutions were also more diluted.

Glycine

The glycine molecule contains carboxylic and amino functional groups that show differential acid-base behavior with the formation of a zwitterion as a main species between pH 2.3 and 9.8 (Fig. 3.4). The zwitterion dominates the pH interval studied. Thus, glycine could adsorb onto smectite at the edges through carboxylate group or at the negatively charged basal plane through amino group. Due to the existence of an anion exclusion volume around the basal planes, we assume that glycine adsorption is only plausible at the montmorillonite edge surface.

The adsorption edge of glycine is very similar to that found for lactate, although shifted to more acidic conditions. The adsorption shows a plateau up to pH 5 and then a smooth decrease toward alkaline conditions, as the positive charge on montmorillonite reduces and basic sites deprotonate. A slight amount of glycine is still adsorbed above pH 7, probably through the interaction between negatively charged edge surface sites and protonated amino groups.

Hedges and Hare (1987) studied the adsorption of amino acids onto montmorillonite and kaolinite and interpreted the adsorption patterns as a result of the electrostatic interactions between the clay surface and the amino acid. These results were also found for lysine adsorbed on montmorillonite (Kitadai et al., 2009b).

3.4.3. Dissolution mechanism

Montmorillonite dissolution in acidic and neutral solutions containing ligands may occur through contributions of protonand ligand-promoted reactions. The effect of pH on montmorillonite dissolution (proton-promoted dissolution) has previously been studied (Rozalén et al., 2008, 2009b and references therein). The mechanism of ligand-promoted dissolution may occur through the formation of surface complexes or a reduction in the ion activity product by complexation of the released cations, in particular Al in the present case.

In the case of the formation of surface complexes, the adsorption experiments show that lactate, citrate, and glycine are adsorbed under acidic conditions (Fig. 3.3). The amount of ligand adsorbed onto the montmorillonite can be converted into surface density, assuming that the adsorption mainly occurs on the edge surface with an estimated edge surface area (ESA) of 6.5 $m^2\ g^{-1}$. The maximum amount of ligand adsorbed per nm^2 of ESA is of 5.6 lactate, 2.4 glycine, and 2.2 citrate. These surface concentrations are in the same order of magnitude as the edge surface density of amphoteric >AlOH sites (3.55 sites nm^{-2}) and basic >SiOH sites (3.16 sites nm^{-2}) (Rozalén et al., 2009a). Nevertheless, we cannot assess if adsorption occurs by formation of inner- or outer-sphere surface complexes. However, there are some studies about the adsorption of organic ligands onto mineral surfaces by ATR-FTIR. Kubicki et al. (1999) did not observe a strong surface complexation of citrate on montmorillonite. However, Kang and Xing (2007) suggested that organic acids prefer to adsorb onto montmorillonite by outer-sphere complexation in aqueous environments, but inner-sphere complexation is favored under dry conditions.

Lactate and glycine

Soluble Al-Lac and Al-Gly complexes are not relevant at pH 4 nor pH 7.5 based on EQ3NR calculations (Fig. 3.5). Thus, the role of lactate or glycine in enhancing the dissolution rate through the formation of soluble Al complexes and by diminishing the activity of Al^{3+} ions is negligible. Possible effects of lactate and glycine on montmorillonite dissolution are supposed to be found in their interaction with the clay surface.

At pH ~4, there is a slight increase in the dissolution rates by adding lactate, but the difference is within the error associated with the dissolution rate. Thus, this increase is not significant enough to confirm a possible catalytic effect due to lactate. Although lactate and glycine are adsorbed onto montmorillonite (Fig. 3.3) at pH 4, they do not promote or inhibit the dissolution reaction. For lactate and glycine under the experimental conditions, the contribution of ligand-promoted dissolution mechanism is much less relevant than the proton-promoted mechanism.

The Al-based dissolution rates with lactate and glycine at pH 7.5 follow a parallel

trend to the rates measured in experiments without ligand. Under these pH conditions and in the absence of Al ligands, montmorillonite dissolution is stoichiometric but followed by the precipitation of Al hydroxides (Rozalén et al., 2008, 2009b). Moreover, the EQ3NR calculations reveal that output solutions are almost in equilibrium with Al hydroxides (boehmite and gibbsite). Al-derived dissolution rates at pH 7.5 represent the balance between montmorillonite dissolution and Al hydroxide precipitation.

The Si-based dissolution rates indicate a slight inhibitory effect due to the addition of lactate to the solutions. Figure 3.3 shows that at pH 7.5 the lactate is partially adsorbed onto Al surface sites at the clay edges. At this pH value, the dissolution reaction is mainly controlled by the attack of water molecules to the reactive sites on the surface followed by the hydrolysis of the network and the release of Al and Si cations. The lactate adsorbed onto the surface at pH 7.5 could reduce the number of the reactive sites available to be attacked by water molecules, which may slightly induce a diminishing in the dissolution rate. Consequently, lactate adsorption at pH 7.5 may inhibit the dissolution reaction. This inhibitory effect was not found for glycine experiments, probably due to the small amount of glycine adsorbed at pH 7.5.

The different behavior of lactate observed at pH 4 and 7.5 is due to the effectiveness of protons and water molecules to attack the surface. The proton-promoted mechanism at pH 4 is much more efficient than the water-promoted mechanism at pH 7.5 and overwhelms the potential inhibition due to lactate adsorption in acidic solution. In neutral conditions the inhibition produced by adsorption is probably due to a reduction in available reactive sites on the montmorillonite edges.

Citrate

Comparing the dissolution rates obtained at the same concentration of citrate and at different pH (Fig. 3.6), a similar V-shaped trend can be observed. By increasing the citrate concentration the trend becomes smoother. At 0.15 mmol/L citrate, the trend of the dissolution rates is similar to that found for ligand-free experiments with the Si-based dissolution rate higher at pH 4 than that found at pH 7.5 due to the efficiency of the proton-promoted mechanism at acidic pH. As citrate concentration increases up to 1.5 mmol/L the rates at pH 4 approach those at pH 7.5. At 15 mmol/L the effect of

the citrate on the dissolution is so high that similar Si-derived dissolution rates were obtained for the three pH conditions, which indicates that under these conditions the ligand-promoted dissolution mechanism is much more important than the proton-promoted one. Thus, the effect of citrate is completely different from that of lactate or glycine, although citrate adsorption is more limited when compared with the other two ligands.

For a ligand there exists a rough correlation between the stability constants of aqueous and surface complexes (Kummert and Stumm, 1980; Stumm et al., 1980; Sigg and Stumm, 1981). Citrate forms stabler aqueous complexes with Al than lactate and glycine (Table 3.2). Therefore, we may suppose that citrate surface complexes are also stabler than those with lactate and glycine. Strong citrate adsorption would contribute in more extension to the detachment of Al to solution. This behavior enhances dissolution rates in citrate solutions.

The overall rate of montmorillonite dissolution can be expressed as the contribution of proton- and ligand-promoted dissolution mechanisms (e.g., Golubev and Pokrovsky, 2006; Golubev et al., 2006; Olsen and Rimstidt, 2008)

$$Rate_{Tot} = Rate_H + Rate_{Ligand} = k_H \cdot a_{H^+}^{n_H} + k_L \cdot a_L^{n_L} \quad (3.6)$$

The first term in this equation corresponds with the proton-promoted dissolution following Equation 3.4 and the second term corresponds with the ligand-promoted dissolution. At each specific pH, the ligand-promoted dissolution can be estimated by subtracting the dissolution rate of ligand-free solutions from the overall dissolution rate, $R_{Tot} - R_H$ (Fig. 3.7), obtaining these empirical laws:

pH 4 $\quad Rate_L = 10^{-11.1} C_L^{0.16}$ (3.7a)

pH 5.5 $\quad Rate_L = 10^{-11.1} C_L^{0.23}$ (3.7b)

pH 7 $\quad Rate_L = 10^{-10.3} C_L^{0.48}$ (3.7c)

Ligand-promoted dissolution rates increase with increasing citrate concentration. This effect is steeper from pH 4 to 7.5, as reveals the increase in the reaction order n_L with the solution pH, from 0.16 to 0.48. This indicates that the effect of citrate is stronger at pH 7.5 that in acidic conditions. The effect of citrate in enhancing dissolution reactions at various pH should be derived from the citrate surface adsorption and formation of aqueous Al complexes.

The stoichiometry of the reaction changes with solution pH and citrate concentration (Fig. 3.2). At pH 4 and 5.5, the dissolution is stoichiometric irrespective of citrate concentration, but at pH 7.5 the dissolution is incongruent even in 15 mmol/L citrate, although citrate can form stable complexes with aluminum in solution (Venturini and Berthon, 1989).

Strong chelating ligands such as citrate also inhibit the hydrolytic reactions of aluminum in solution, thus retarding the crystallization of aluminum hydroxides (Jardine and Zelazny, 1996). The effectiveness to hinder the hydrolysis and polymerization of aluminum increases with the affinity of organic ligands for aluminum and the concentrations of these ligands in solution. These effects may contribute to reduce saturation with respect to Al-bearing phases, including montmorillonite. EQ3NR results revealed that the aluminum in the output solutions should be completely complexed by citrate regardless of pH and citrate concentrations (Fig. 3.5). That is the case in the experiments with citrate at pH 4 and 5.5. Furthermore, citrate concentration should complex the total aluminum released if dissolution were stoichiometric. It is necessary to answer where the difference between stoichiometric and steady-state Al is, and why so strong a ligand as citrate cannot chelate the total Al released at pH 7 producing a stoichiometric dissolution process.

The deficit in Al may be due to precipitation of gibbsite particles (Nagy et al., 1999) or Al-citrate complexes (Cambier and Sposito, 1991). Nagy et al. (1999) demonstrated that gibbsite can grow on phyllosilicate basal planes. Thus, the Al deficit can be converted into surficial gibbsite deposits. For example, the Al deficit in the experiment with 15 mmol/L citrate at pH 7.5 is 1.5 μmol. Assuming for gibbsite deposits a thickness of 4 layers (Nagy et al., 1999), a molar volume of 31.83 $cm^3\ mol^{-1}$ (Robie and Hemingway, 1995), and c^* of 9.75 Å (Gaines et al., 1997), the surface covered by gibbsite is only of 0.01 m^2. That value contrasts with the total montmorillonite surface area in the experiment, which can be approximated in the following way

$$m(g)\cdot SA_{total}(m^2/g)\cdot\frac{1}{n}=0.1\cdot 750\cdot\frac{1}{4}=18.75m^2 \qquad (3.8)$$

where m is the montmorillonite mass, SA_{total} stands for the total surface area (Meunier, 2003), and n corresponds to the average number of layers in smectite tactoids, which

for K-montmorillonite is 4 (Verburg and Baveye, 1994).

Alternative explanations consider Al adsorption at Al surface hydroxyl groups located on the broken edges of the particle surfaces at higher pH values or at permanently charged surface sites by cation exchange up to pH 3 (Charlet et al., 1993). Nevertheless, no decrease in montmorillonite swelling capacity after solvation with ethylene-glycol was observed (Moore and Reynolds, 1989). An estimation of the interlayer space occupied by Al hydroxides (0.04 m^2) when compared with the total interlayer surface indicates that this effect should be difficult to detect by X-ray diffraction.

Our experimental results do not allow us to decide if one mechanism is predominant over the others. All of these could contribute to Al uptake from solution in different proportions. However, how the released Al can escape from complexation with citrate is still unclear.

One feasible hypothesis to justify the absence of Al-Cit complexation is the presence of an exclusion volume due to the high-negative surface charge of the montmorillonite. The overall surface of montmorillonite is dominated by basal planes with a permanent negative charge that develops an anion exclusion volume of 0.39 cm^3 g^{-1}. The thickness of the anion exclusion volume (36 Å) can be obtained by dividing the anion exclusion volume by the external surface area, assuming that the BET surface area may be a proxy of the external surface area. Thus, a layer of solution can be found around clay particles, where the concentration of citrate is considerably lower than the bulk concentration. Although the results of EQ3NR calculations indicate that the bulk solutions are undersaturated in gibbsite and presumably in aluminum hydroxides due to the complexation with citrate, we may hypothesize that a fraction of the detached Al precipitates or re-sorbs before diffusing through the exclusion volume and gives rise to the non-stoichiometric reaction.

3.5. Concluding remarks

The results of the present investigation may contribute to the understanding of the clearance mechanisms of inhaled particle in the lung. The effect of lactate, citrate and glycine on the K-montmorillonite dissolution rate was investigated at 37°C at pH 4

and 7.5. The adsorption of lactate, citrate and glycine onto the montmorillonite surface in the pH range between 2 and 10 was also studied. Lactate is the most abundant organic acid in interstitial solutions and lung fluids, having a concentration of 164 ppm (Plumlee and Ziegler, 2003), followed by citrate with 22 ppm. Glycine was used as a proxy of amino acids and proteins, whose content is important in body fluids. EQ3NR was used to model aqueous speciation of Al and ligands in the output solutions.

Citrate is the only ligand that enhances montmorillonite dissolution rate, approximately 3 times (half order of magnitude) at pH 4 and 10 times at pH 7.5 for 15 mmol L^{-1} citrate. Lactate and glycine do not show a significant effect on the dissolution rate.

The three ligands adsorbed onto montmorillonite in acidic conditions, although the adsorption patterns were different each other. Maximum adsorption was measured for lactate and minimum for citrate. At pH 7.5 the amount of ligand adsorbed is close to zero. Surface complexes form by electrostatic interaction between positively charged montmorillonite surface and deprotonated ligands. On the other hand, only citrate can complex the aqueous Al between pH 3 and 9, whereas glycine complexation is irrelevant and lactate can complex approximately 10% of the total aqueous Al at pH 4.5.

A tentative reaction mechanism can be derived from dissolution rates, surface adsorption and aqueous speciation. Dissolution rates results from proton- and ligand-promoted dissolution reactions. Only for citrate ligand-promoted reaction is relevant. Although the adsorption of the ligands on montmorillonite is very reduced, we can conclude that the enhancement of the dissolution rate of montmorillonite in acidic conditions likely comes from the formation of surface complexes between the ligand and the edge surface of montmorillonite. In neutral conditions the effect is also due to the decrease of the activity of Al^{+3} by formation of aqueous Al-Cit complexes. The application of geochemical methods may help health science in the understanding of the hazard of toxic minerals as well as those considered as inert such as clay minerals.

4. Effect of oxalate on the kinetics of montmorillonite dissolution

4. EFFECT OF OXALATE ON THE KINETICS OF MONTMORILLONITE DISSOLUTION.

Abstract.- The dissolution rate of montmorillonite was measured in buffered oxalate solutions over a pH range from 3 to 8 and total oxalate concentration of 0.1, 0.3 and 1.0 mmol L^{-1} at 25°C in stirred flow-through reactors. Dissolution rates were obtained based on the release of Si at steady state under far from equilibrium conditions. Oxalate enhanced the montmorillonite dissolution rate from pH 4 to 8, reaching a maximum of 0.5 logarithmic units at pH 7. In order to understand the dissolution mechanism, oxalate adsorption was measured in batch experiments at pH 2-11 and EQ3NR was used to check the oxalate capacity to form soluble species of Al. Oxalate adsorbs onto montmorillonite at pH < 8 up to 18 μmol g^{-1} at the highest concentration studied. DR-FTIR spectroscopy was used to model the adsorption by means of two surface complexes: >AlOH$\cdots Ox^{-2}$ and >Al-Ox^{-}, outer- and inner-sphere respectively. Based in these results, two mechanisms may contribute to the enhancement of the montmorillonite dissolution rate in oxalate solutions: the formation of surface complexes between oxalate and aluminol sites on the surface of the montmorillonite edges, and the decrease of the activity of Al^{3+} by formation of aqueous Al-oxalate complexes.

4.1. Introduction

Low molecular weight organic acids are ubiquitous in soils and sediments, where vegetation and microbes introduce them. They can react with minerals in the Earth crust playing an important role in the alteration and weathering reactions. In particular, they are implicated in the enhancement of clay mineral dissolution because of their ability as organic ligands to form aqueous and surface complexes, and increase the acidity of soils (e.g. Zutic and Stumm, 1984; Furrer and Stumm, 1986).

Recent evidence indicates that the dissolution reactions of phyllosilicates occur mainly on broken edge sites and are controlled by several factors including temperature, pH and presence of organic ligands and inhibitors. The dissolution reaction of phyllosilicates is produced in specific active sites located at the crystal edge surface, and it is controlled by several factors including temperature, pH and presence

of organic ligands and inhibitors. Most studies agree that under the same pH conditions the dissolution rate is faster in the presence of organic ligands than that without (e.g. Zutic and Stumm, 1984; Furrer and Stumm, 1986; Carroll-Webb and Walther, 1988; Chin and Mills, 1991; Wieland and Stumm, 1992; Ganor and Lasaga, 1994; Oelkers and Schott, 1998; Stillings et al., 1998). There is general agreement in prior dissolution studies that dissolution process results from a sequence of elementary reactions at the mineral/solution interface, including the formation of surface complexes between surface cations and aqueous ligands. The formation of stable metal-ligand complexes facilitates the release of the structural cations (e.g., Al^{3+} and Si^{4+}) to the aqueous solution. This process is the result of several mechanisms that act simultaneously: proton-promoted (pH effect) and ligand-promoted (surface complexation) dissolution (Zutic and Stumm, 1984; Furrer and Stumm, 1986; Chin and Mills, 1991; Wieland and Stumm, 1992; Stillings et al., 1998) as well as the decrease of ion activity product with respect to the mineral due to formation of aqueous chelates as the activity of the 'free' metal ions in aqueous solution are attenuated due to complexation by metal ligands. Which mechanism prevails in the presence of organic ligands is still under debate.

Montmorillonite was chosen in this study because its dissolution mechanism and reactivity have been widely investigated in previous work (Furrer et al., 1993; Zysset and Schindler, 1996; Bauer and Berger, 1998; Cama et al., 2000; Huertas et al., 2001; Amram and Ganor, 2005; Metz et al., 2005a,b; Rozalén et al., 2008; Rozalén et al., 2009a,b; Ramos et al., 2011). Furthermore oxalate, the organic ligand of interest in this study, is an abundant anion in surface environments, as a result of its exudation by plant roots and fungi (Gadd, 1999; Ryan et al., 2001). Oxalate exhibits a strong capacity to significantly enhance the dissolution rate of silicates and aluminum oxides (Zutic and Stumm, 1984; Furrer and Stumm, 1986; Chin and Mills, 1991; Wieland and Stumm, 1992; Welch and Ullman, 1993; Pokrovsky et al., 2005; Wang et al., 2005; Cama and Ganor, 2006; Golubev and Pokrovsky, 2006; Golubev et al., 2006; Olsen and Rimstidt, 2008).

The adsorption and clay-induced dissolution promoted by organic ligands in phyllosilicates has been investigated by batch adsorption experiments (Ward and Brady, 1998; Lackovic et al., 2003; Kang and Xing, 2007; Kitadai et al., 2009b). Batch equilibrium and adsorption edge studies provide useful information about the role of

organic ligands in clay dissolution studies. These macroscopic methods are incapable, however, of providing mechanistic insight of the organic ligand-clay interactions (Johnston and Sposito, 1987). In the study of organic ligands and their interaction with clay minerals, vibrational spectroscopy has been applied successfully. Attenuated total reflectance (ATR) and diffuse reflectance (DR) FTIR methods, in particular, have been extensively used to investigate the bonding mechanism of organic ligands to clays as well as to oxides to examine surface complexation (inner-sphere or outer-sphere complexation), and the stoichiometry of the surface interaction (monodentate or polydentate, mononuclear or polynuclear) (Biber and Stumm, 1994; Kubicki et al., 1997; Nordin et al., 1997; Nordin et al., 1998; Kubicki et al., 1999; Specht and Frimmel, 2001; Lackovic et al., 2003; Johnson et al., 2004b; Yoon et al., 2004; Kang and Xing, 2007; Noren and Persson, 2007; Ha et al., 2008; Noren et al., 2008; Kitadai et al., 2009a,b; Jonsson et al., 2010).

The objective of this study is to investigate the role of oxalate on the montmorillonite dissolution reaction. Dissolution rates are derived from flow-through dissolution experiments in buffered oxalate solutions. Moreover, the adsorption of the oxalate on montmorillonite was approached by batch adsorption experiments and through DR-FTIR spectroscopy.

4.2. Materials and methods

4.2.1. Materials

The clay material used in this study was a bentonite from the La Serrata – Cortijo de Archidona deposit located at Cabo de Gata (Almeria, SE Spain). This bentonite is approximately 92% montmorillonite; the rest consist of accessory/companying minerals (quartz, feldspars, micas, calcite, amphibole) and volcanic glass (for a detailed characterization of the sample and methods see Rozalén et al., 2008). The experiments were performed on the <4 μm fraction, collected by repeated sedimentation-suspension cycles in deionized water, and then exchanged with K^+ ions.

The calculated structural formula of the K-smectite (based on half unit cell) corresponds to a montmorillonite:

$$K_{0.44}(Al_{1.27}Fe^{3+}_{0.22}Mg_{0.56})(Si_{3.95}Al_{0.05})O_{10}(OH)_2$$

Only 0.38 K^+ ions per half formula unit are exchangeable which indicates the presence of a small proportion of non-swelling layers. X-ray diffraction (XRD) patterns recorded on powder specimens and on oriented and glycolated mounts indicate that the sample is composed of a dioctahedral smectite with approximately 10-15% non-swelling layers. No accessory phases were detected. The specific surface area was measured by BET (Brunauer et al., 1938), using 5-point N_2 adsorption isotherms, after degassing the sample for two days at 110°C under vacuum. The specific surface area was 111 $m^2 g^{-1}$, with an associated uncertainty of 10%.

4.2.2. Flow through dissolution experiments

Dissolution experiments were performed in single-pass, stirred, flow-through cells which facilitated the measurement of the dissolution rate under fixed saturation state conditions by modifying flow rate, initial sample mass and input solution concentrations. The reactors were fully immersed in a thermostatic water-bath held at a constant temperature of 25±1°C. The flow rate was controlled with a peristaltic pump that injects the input solution into the bottom chamber of the cell (0.02 mL min^{-1}) where the solution is homogenized with a magnetic stirrer before reaching the upper chamber. The solid sample is confined within the upper chamber (reaction zone) by using two membrane filters: a 5 µm nylon mesh plus a 1.2 µm Durapore membrane at the bottom and a 0.45 µm Durapore membrane at the top. The total volume of the cell was 46 mL and the solid mass added to each cell was approximately 0.1 g, to yield a solid solution ratio of approximately 2 g L^{-1}.

Buffer solutions were prepared using sodium oxalate in concentrations of 0.03, 0.1 and 1.0 mmol L^{-1}. In the experiments, 10 mmol L^{-1} KNO_3 was used as background electrolyte concentration. The pH was adjusted from 3 to 8 by adding HNO_3 or KOH solutions. Sodium azide (NaN_3, 2 ppm) was added as bactericide. No smectite structural cations (Si, Al, Mg, Fe) were added to the input solutions.

In each run, the flow rate and the input pH were held constant until steady-state conditions were achieved. The steady state was assumed to prevail when the Si output concentration remained fairly constant, differing by less than 6% between consecutive samples (Rozalén et al., 2008). Reaction times were from 800 to 1200 h depending on the pH and oxalate concentration. At steady state, dissolution is expected to proceed

under far-from-equilibrium conditions. All the experiments consisted of a single stage; the cell was dismantled after the steady state was achieved.

After sampling every 24 h, the pH of the output solutions were immediately measured at room temperature by using a Crison combination electrode standardized with pH 4.01 and 7.00 buffer solutions. The reported accuracy was ± 0.02 pH units. An aliquot was separated for oxalate analysis. Then the output solutions were acidified to pH 3 with HNO_3 to prevent the precipitation of Al- or Fe-bearing phases during storage for Si and Al analyses.

The Si concentration in the samples was determined by colorimetry by using the molybdate blue method (Grasshoff et al., 1983). Total Al, Fe and Mg concentration in the solutions at steady-state conditions was determined by inductively coupled plasma mass spectrometry (ICP-MS) in a Hewlett Packard 4500 series spectrometer. The concentration of oxalate was measured by ion chromatography (IC) using a Metrohm 761 Compact Ion Chromatograph with a Metrosep A Supp 4-250 column with chemical suppression. The eluent was prepared with 1.7 mmol L^{-1} $NaHCO_3$ and 1.8 mmol L^{-1} $NaCO_3$. The detection limits are 5 ppb for Si, 0.3 ppb for Al, 0.3 ppb for Mg, 3 ppb for Fe and 0.9 ppm for oxalate. The associated errors were 5% for Si and Al, 3% for Mg and Fe, and 5% for oxalate.

In a well-mixed, flow-through reactor the dissolution rate, *Rate* (mol g^{-1} s^{-1}), can be calculated based on the mass balance of a given mineral component *j*. Under steady-state conditions this is given by the following equation (e.g. Cama et al., 2000; Rozalén et al., 2008):

$$Rate(molg^{-1}s^{-1}) = -\frac{1}{\nu_j}\frac{q}{M}(C_{j,out} - C_{j,in}) \qquad (4.1)$$

where ν_j is the stoichiometric coefficient of component *j* in the dissolution reaction, *q* stands for the volumetric fluid flow through the system, *M* is the mass of smectite and $C_{j,out}$ and $C_{j,in}$ correspond to the concentrations of component *j* in the output and input solutions, respectively. The rate is defined as negative for dissolution and positive for precipitation. In this study the dissolution rate is calculated from the Si and Al concentrations (R_{Si} and R_{Al}) in the output solutions. All dissolution rates were normalized to initial mass of smectite. The error in the calculated rate is estimated by

using the Gaussian error propagation method and is less than 6% in all cases, which corresponds to approximately 0.1 logarithmic units.

Montmorillonite dissolves according to the following reaction:

$$K_{0.44}(Al_{1.27}Fe^{3+}_{0.22}Mg_{0.56})(Si_{3.95}Al_{0.05})O_{10}(OH)_2 + 6.18\ H^+ \rightarrow$$
$$\rightarrow 0.44K^+ + 1.32\ Al^{3+} + 0.22\ Fe^{3+} + 0.56\ Mg^{2+} + 3.95\ SiO_{2,aq} + 4.09\ H_2O \quad (4.2)$$

The estimated equilibrium constant for the K-montmorillonite dissolution reaction at 25°C was log K_{eq}(K–Sm) = 5.76 (Vieillard, 2000; Rozalén et al., 2008). The saturation state of the solution with respect to solid phases is calculated in terms of the free energy of reaction, ΔG_r:

$$\Delta G_r = RT \ln\left(\frac{IAP}{K_{eq}}\right) \quad (4.3)$$

where *IAP* and K_{eq}, respectively, stand for the ion activity product and the equilibrium constant for the dissolution reaction. Aqueous activities and chemical affinities are calculated here by using the EQ3NR geochemical speciation code (Wolery, 1992). The *IAP* was calculated from pH, Si, Al, Mg and Fe concentration in the output solutions at steady-state conditions. EQ3NR was also used to model the capacity of oxalate to form aqueous Al species. The aqueous Al-oxalate complexes were implemented in the Lawrence Livermore National Laboratory thermodynamic database (data0.cmp in EQ3/6 package) using reactions of aqueous Al and oxalate at 25°C (Table 4.1).

Table 4.1. Oxalic acid dissociation constants and Al^{3+} - oxalate stability constants.

Reaction	Constant	Reference
$H_2Ox = HOx^- + H^+$	$pK_{a1} = 1.25$	(1)
$HOx^- = Ox^{2-} + H^+$	$pK_{a2} = 4.27$	(1)
$Al^{3+} + Ox^{2-} = Al(Ox)^+$	$\log K_1 = 7.3$	(2)
$Al^{3+} + 2Ox^{2-} = Al(Ox)_2^-$	$\log\beta_2 = 13.3$	(2)
$Al^{3+} + 3Ox^{2-} = Al(Ox)_3^{3-}$	$\log\beta_3 = 17.2$	(2)

[1] Filius et al. (1997), [2] Jaber et al. (1977).

4.2.3. Adsorption experiments

Oxalate adsorption edges were carried out using the batch equilibrium method. A quantity of 0.2 g of initial smectite was placed in 30 mL Corex centrifuge tubes with

polytetrafluoroethylene (PTFE) caps. Twenty mL of 0.1, 0.3, 1.0 or 1.5 mmol L^{-1} oxalate solution were added to each tube, using 10 mmol L^{-1} KCl as background electrolyte. KCl was used for sorption and FTIR experiments instead KNO_3 to avoid the strong absorbance introduced by the nitrate anion in the spectral region of interest. Control samples containing 0.1, 0.3, 1.0 or 1.5 mmol L^{-1} oxalate without clay were prepared to quantify the potential loss of oxalate due to other processes. The pH was adjusted in each sample with an appropriate amount of HCl or KOH solution to cover a pH range from 2 to 8. Every suspension had a replicate at the same pH without oxalate, for comparison purposes. All the suspensions were vortexed for 30 s and let equilibrate for 5 h in a horizontally shaker at room temperature. A 5 h equilibration time was chosen for adsorption as previous kinetic experiments showed that the adsorption reached a steady state within 4 h under these experimental conditions. The suspensions were centrifuged at 5000 rpm during 20 minutes to separate the solution and the clay and 5 mL of supernatant were filtered to measure the oxalate remaining in the solution. Samples were diluted and analyzed for oxalate using a Dionex ion chromatograph equipped with an AS50 autosampler, a GP50 gradient pump, an AS50 thermal compartment, EG40 eluent generator and ES50 electrochemical detector. A Dionex OmniPac PAX-100 4X250 mm analytical column and an ASRS ULTRA II 4 mm self-regenerating suppressor were used for all measurements. The detection limit is 0.01 ppm for oxalate and the associated error was 3%. The amount of oxalate adsorbed was calculated from the difference between the concentration in the control sample and that remaining in samples solution.

The concentrations of the smectite structural cations were determined in the filtered supernatants after the 1.5 mmol L^{-1} oxalate adsorption experiments and compared with a control suspension without oxalate. Al, Mg and Fe were measured by inductively coupled plasma mass (ICP-MS) spectrometry using a PerkinElmer ELAN DRC-e spectrometer, equipped with an AS93 Plus Autosampler. The detection limits are 0.01 ppb for Al, 0.05 ppb for Mg and 0.6 ppb for Fe. The associated error was 2%.

After sampling 5 mL of supernatant for the IC and ICP-MS analysis, the smectite left in the tubes of the 1.5 mmol L^{-1} oxalate experiments was re-suspended in the remaining supernatant and was measured with DRIFT spectroscopy. The smectite suspension was passed through a membrane filter on a Millipore holder under vacuum.

The resulting clay powder was allowed to air-dry overnight and was removed with a spatula. The solid collected (5 mg) was ground and mixed during 20 s with 95 mg of KBr (background) in a Wig-L-Bug© mixer. Diffuse reflectance spectra were obtained using a PerkinElmer GX2000 Fourier Transform Infrared (FTIR) spectrometer with a MCT detector. The wavenumber resolution for the spectra was 4.0 cm^{-1} and a total of 64 scans were collected for each spectrum.

A PerkinElmer Spectrum One Fourier Transform Infrared (FTIR) spectrometer equipped with a lithium tantalate ($LiTaO_3$) detector was used to collect ATR-FTIR spectra of oxalate solutions. The samples were recorded in absorbance mode in the 4000-400 cm^{-1} range with a wavenumber resolution of 4.0 cm^{-1}. A total of 100 scans were collected for each spectrum at a scan speed of 0.2 cm/s. Spectra of oxalate aqueous solutions were measured by placing 1 mL of ligand solution in the ATR cell. The concentration of oxalate solutions was 25 mmol L^{-1} and the solution spectra were collected at pH 3 and 6. The transmission spectra of the crystalline oxalate was obtained with KBr pressed pellet by diluting 1 mg of sample in 100 mg of dried KBr.

Grams/32 (ThermoFisher Scientific Inc., 2011) program was used to plot and analyze the spectra, and make the conversion to the Kubelka-Munk function. The ATR-FTIR spectrum of a 10 mmol L^{-1} KCl solution was collected and subtracted from every sample spectra to remove the strong contributions from water bands. In the spectra the absorbance was normalized against the Si-O stretching vibration band at 1027 cm^{-1} so that the relative intensities reflect the amount of oxalate adsorbed at each pH. The DRIFT spectra of the oxalate/montmorillonite complexes were obtained from the subtraction of the reference mineral spectrum treated with a solution at the same pH and ionic strength without any adsorbed oxalate.

4.3. Results

4.3.1. Dissolution experiments

The experimental conditions of all the dissolution experiments, the average pH and Si and Al concentrations at steady state are reported in Table 4.2. The nomenclature of the dissolution experiments follows the pattern: *Sm-Ox0.1-4b*, where *Sm* is smectite followed by *Ox* that is oxalate, with its concentration in mmol L^{-1} (0.03,

Table 4.2. Experimental conditions and results of flow-through dissolution experiments. Dissolution rates were normalized to initial mass.

Run	Duration (h)	Flow rate (mL/min)	Initial mass (g)	C Oxalate (mmol L^{-1})	pH out	C Si,out (μmol L^{-1})	C Al,out (μmol L^{-1})	C Mg,out (μmol L^{-1})	C Fe,out (μmol L^{-1})	log R Si (mol $g^{-1}s^{-1}$)	log R Al (mol $g^{-1}s^{-1}$)	ΔR Si %	ΔR Al %
Sm-Ox0.03-3	910	0.0216	0.0914	27.8	2.68	11.34	6.33	2.11	0.67	-11.24	-11.06	5.1	5.6
Sm-Ox0.03-3.5	1173	0.0240	0.0902	25.6	3.57	1.76	4.76	3.09	0.43	-11.82	-11.13	3.4	5.6
Sm-Ox0.03-4.5a	1052	0.0224	0.0909	31.1	4.40	4.25	1.52	1.40	0.16	-11.65	-11.67	5.1	5.7
Sm-Ox0.03-4.5b	912	0.0231	0.0910	30.1	4.51	2.83	1.18	0.89	0.10	-11.81	-11.76	5.0	5.6
Sm-Ox0.03-7	980	0.0229	0.0903	25.1	6.77	1.85	n.d.	n.d.	n.d.	-12.00	-	5.1	-
Sm-Ox0.1-3.5a	1120	0.0190	0.0914	96.1	3.50	7.46	2.03	1.25	0.46	-11.48	-11.62	5.1	5.7
Sm-Ox0.1-3.5b	1125	0. 0182	0.0924	95.4	3.51	6.89	2.05	0.27	0.21	-11.54	-11.64	5.1	5.6
Sm-Ox0.1-4a	1028	0.0210	0.0906	95.6	3.81	6.42	2.10	1.23	0.45	-11.49	-11.57	5.0	5.8
Sm-Ox0.1-4b	1006	0.0216	0.0914	101.0	4.35	4.70	1.50	3.43	0.46	-11.63	-11.69	5.1	5.6
Sm-Ox0.1-4c	932	0.0203	0.0907	105.8	4.36	5.75	1.55	1.09	0.39	-11.56	-11.70	5.1	5.7
Sm-Ox0.1-5	934	0.0218	0.0904	92.4	5.03	4.29	1.12	n.d.	n.d.	-11.66	-11.70	5.0	4.4
Sm-Ox0.1-6a	772	0.0226	0.0913	98.7	5.99	3.91	1.31	1.10	n.d.	-11.69	-11.74	5.1	5.7
Sm-Ox0.1-6b	790	0.0180	0.0902	95.7	6.33	4.86	1.94	0.92	0.10	-11.68	-11.65	4.9	5.5
Sm-Ox0.1-6.5a	927	0.0224	0.0912	97.6	6.42	2.70	2.01	0.95	0.40	-11.85	-11.55	5.1	5.7
Sm-Ox0.1-6.5b	1004	0.0220	0.0900	98.3	6.41	2.08	1.74	1.70	0.10	-11.97	-11.61	5.0	5.7
Sm-Ox0.1-7a	836	0.0217	0.0908	99.6	6.81	2.85	1.20	0.85	0.01	-11.84	-11.79	5.1	5.7
Sm-Ox0.1-7b	956	0.0189	0.0918	99.6	6.72	3.11	1.13	1.11	0.16	-11.88	-11.82	5.3	5.0
Sm-Ox0.1-8	785	0.0210	0.0910	99.1	7.80	2.59	1.09	2.24	n.d.	-11.90	-11.85	5.1	5.8
Sm-Ox1-3a	1051	0.0207	0.0900	912	3.07	10.37	6.19	n.d.	n.d.	-11.30	-11.09	5.1	5.7
Sm-Ox1-3b	956	0.0209	0.0912	980	3.06	11.89	3.98	n.d.	n.d.	-11.24	-11.28	5.1	5.7
Sm-Ox1-4a	1005	0.0234	0.0934	911	4.03	4.68	n.d.	n.d.	n.d.	-11.60	-	5.1	-

Sm-Ox1-4b	978	0.0203	0.0909	916	4.05	4.33	5.45	2.40	n.d.	-11.69	-11.16	5.1	5.7
Sm-Ox1-5a	1004	0.0228	0.0905	917	5.17	4.10	1.15	1.18	n.d.	-11.65	-11.78	5.0	5.7
Sm-Ox1-5b	1059	0.0236	0.0913	902	5.18	3.31	8.31	4.19	1.02	-11.74	-10.91	5.1	5.7
Sm-Ox1-5c	1148	0.0228	0.0909	904	5.25	2.91	28.60	10.69	2.56	-11.80	-10.38	5.0	5.6
Sm-Ox1-6	861	0.0233	0.0912	806	5.68	3.22	n.d.	n.d.	n.d.	-11.75	-	5.0	-
Sm-Ox1-7a	979	0.0222	0.0904	907	7.26	2.53	0.64	n.d.	n.d.	-11.88	-12.05	5.1	5.8
Sm-Ox1-7b	1053	0.0221	0.0915	892	6.84	3.74	1.98	1.16	0.10	-11.71	-11.56	5.0	5.7

0.1 or 1). The last number is the initial pH in the experiment (3-8) and finally, *b* corresponds to a replicate.

The variation with time of the output solution composition of a representative flow-through experiment is shown in Figure 4.1. The general trend for all the experiments shows that the solution pH remains constant with elapsed time. High Si concentrations were observed at the onset of most experiments. Afterwards, Si concentrations decrease asymptotically until a steady state is approached (Fig. 4.1a). Measured values of Al concentration at steady state remain constant. Oxalate concentration was measured in the input and output solutions (Fig. 4.1b) in order to assess its potential degradation along time, obtaining in all cases concentrations around the initial value and scattered within the experimental error interval.

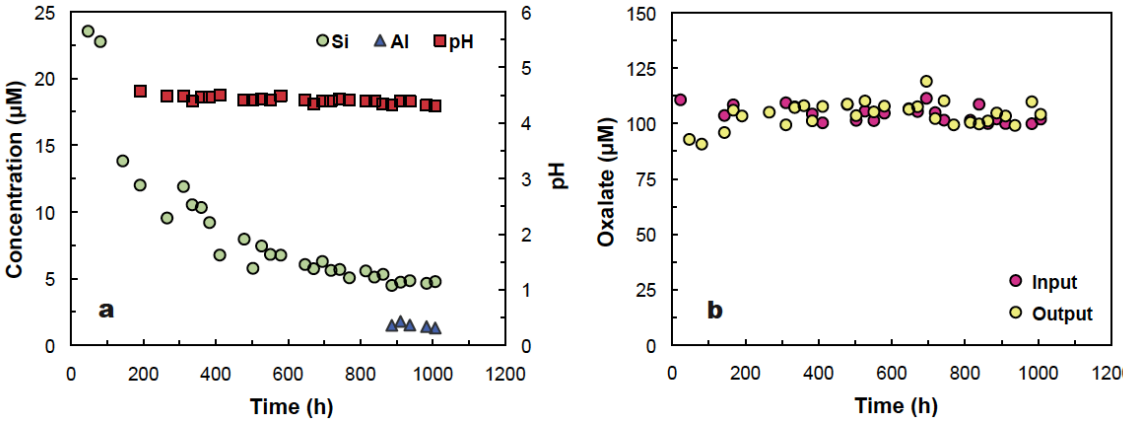

Figure 4.1. Evolution of a) pH and Si and Al concentrations at steady state in the output solution of the flow-through cell, and b) oxalate concentration in the input and output solutions along time (dashed lines represent the selected concentration for the cell (0.1 mmol L^{-1}) and error interval) for run Sm-Ox0.1-4b.

Montmorillonite dissolution rates at steady state are plotted in Figure 4.2 as a function of pH. The solid line corresponds to montmorillonite dissolution rates in ligand-free solutions obtained by Rozalén et al. (2008). Our results show that oxalate does not modify the dissolution rates in the range from pH 2.5 to 4. Nevertheless, at pH > 4 oxalate enhances the dissolution rates depending on the pH and the oxalate concentration. This effect is stronger when pH increases from 4 to 7, where the enhancement reaches a maximum of 0.5 logarithm units respect to the ligand-free dissolution rate at the same pH, and then it decreases from pH > 7. The oxalate catalytic effect has been observed for smectite (Golubev et al., 2006), kaolinite (Wang

et al., 2005; Cama and Ganor, 2006), forsterite (Olsen and Rimstidt, 2008), plagioclase (Stillings et al., 1998) and K-feldspars (Drever and Vance, 1994). A minimal concentration of 0.1 mmol L^{-1} oxalate is necessary to catalyze the dissolution reaction. Golubev et al. (2006) reported a minimal concentration of 1 mmol L^{-1} oxalate to observe any enhancement of smectite dissolution at pH 6.08. This target concentration is also found in the case of dissolution of K-feldspars (Drever and Stillings, 1997).

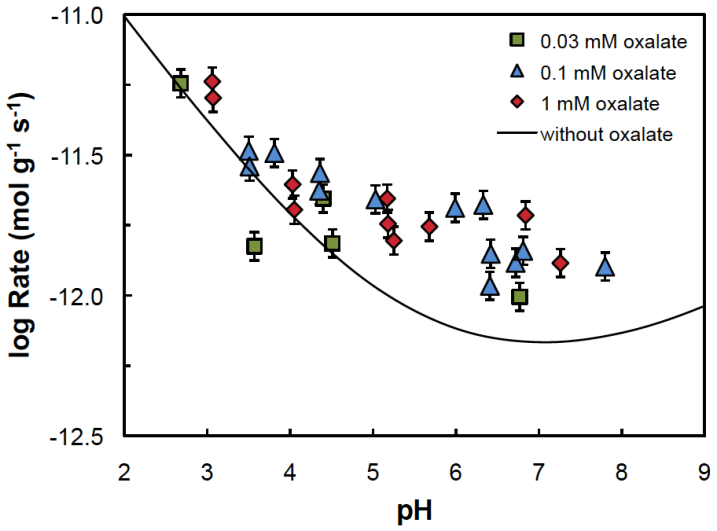

Figure 4.2. Experimental dissolution rates derivated from Si concentrations in the output solutions. Solid line corresponds to montmorillonite dissolution rates in ligand-free solutions (Rozalén et al., 2008).

The composition of the output solutions of the dissolution experiments at steady-state conditions was modeled with the geochemical code EQ3NR in order to calculate the saturation of the solution with respect to montmorillonite and other secondary minerals (Table 4.3). Results show that all the solutions are undersaturated respect to montmorillonite, amorphous silica, quartz, gibbsite and kaolinite. According to Amram and Ganor (2005), our dissolution experiments proceed under far from equilibrium conditions.

Oxalate is well known as a strong complexant of aluminum. The aluminum-oxalate speciation was calculated with EQ3NR for the output solutions concentrations at steady state of several dissolution experiments. The speciation diagram between pH 2-8 corresponding to the experiment Sm-Ox0.03-3, which consists of 6 μmol L^{-1} Al^{3+} and 30 μmol L^{-1} oxalate (maximum Al/oxalate ratio) is depicted in Fig. 4.3. Si-ligand

speciation was not taken into account as Si forms very weak organic complexes in solution (Pokrovsky and Schott, 1998).

Table 4.3. Saturation state (kcal mol^{-1}) of the output solutions at steady-state conditions computed according to Equation 4.3 for flow-through montmorillonite dissolution experiments at 25°C.

Run	pH_{out}	K-Mont	SiO_2(am)	Qtz	Gib	Kln
Sm-Ox0.03-3	2.68	-26.26	-3.04	-1.29	-8.41	-18.45
Sm-Ox0.03-3.5	3.57	-25.91	-4.15	-2.39	-6.33	-16.48
Sm-Ox0.03-4.5a	4.40	-21.20	-3.63	-1.87	-5.33	-13.45
Sm-Ox0.03-4.5b	4.51	-21.74	-3.87	-2.11	-5.12	-13.50
Sm-Ox0.03-7	6.77	-7.24	-4.20	-2.36	2.49	1.20
Sm-Ox0.1-3.5a	3.50	-27.03	-3.30	-1.54	-8.85	-19.82
Sm-Ox0.1-3.5b	3.51	-27.45	-3.34	-1.58	-8.82	-19.85
Sm-Ox0.1-4a	3.81	-25.91	-3.38	-1.63	-8.21	-18.72
Sm-Ox0.1-4b	4.35	-23.89	-3.57	-1.81	-7.12	-16.90
Sm-Ox0.1-4c	4.36	-24.45	-3.45	-1.69	-7.13	-16.69
Sm-Ox0.1-5	5.03	-19.67	-3.62	-1.87	-4.81	-12.40
Sm-Ox0.1-6a	5.99	-12.12	-3.68	-1.92	-1.00	-4.88
Sm-Ox0.1-6b	6.33	-8.36	-3.55	-1.79	0.68	-1.26
Sm-Ox0.1-6.5a	6.42	-9.03	-3.90	-2.14	1.04	-1.24
Sm-Ox0.1-6.5b	6.41	-9.80	-4.05	-2.30	0.89	-1.84
Sm-Ox0.1-7a	6.81	-6.64	-3.86	-2.11	2.09	0.94
Sm-Ox0.1-7b	6.72	-7.04	-3.81	-2.06	1.77	0.40
Sm-Ox0.1-8	7.80	-6.05	-3.94	-2.18	1.71	0.02
Sm-Ox1-3a	3.07	-33.03	-3.09	-1.34	-12.50	-26.72
Sm-Ox1-3b	3.06	-33.41	-3.02	-1.26	-12.93	-26.41
Sm-Ox1-4a	4.03	-32.45	-3.57	-1.81	-11.71	-26.08
Sm-Ox1-4b	4.05	-31.00	-3.61	-1.86	-10.90	-24.55
Sm-Ox1-5a	5.17	-24.74	-3.65	-1.89	-7.89	-18.61
Sm-Ox1-5b	5.18	-22.85	-3.77	-2.02	-6.61	-16.30
Sm-Ox1-5c	5.25	-25.26	-3.85	-2.09	-7.65	-18.54
Sm-Ox1-6	5.68	-21.11	-3.79	-2.03	-5.68	-14.47
Sm-Ox1-7a	7.26	-9.85	-3.96	-2.21	0.23	-2.99
Sm-Ox1-7b	6.84	-10.82	-3.71	-1.96	-0.75	-4.45

K-Mont = K-montmorillonite; SiO_2(am) = amorphous silica; Qtz = quartz; Gib = gibbsite; Kln = kaolinite

The Al speciation diagram shows that aqueous Al-oxalate complexes are the predominant Al species in the pH range from approximately 2 to 7. Between pH 2-3 three species coexist: Al^{3+} decreases from 40 to 5%, $Al(Ox)_2^-$ increases from 8 to 50% and $Al(Ox)^+$ increases from 50 to a maximum of 65% at pH 2.5 and decrease until 45% at pH 3. Between pH 3-4.5 a new specie, $Al(Ox)_3^{3-}$, increases progressively until attaining a 10% while $Al(Ox)^+$ decreases until 10% and the main complex (85%) is $Al(Ox)_2^-$. In the pH range 4.5-6 the prevailing specie corresponds with an 85% of $Al(Ox)_2^-$, coexisting with a 10% of $Al(Ox)_3^{3-}$ and a 5% of $Al(OH)_2^+$. From pH 6 and above the amount of $Al(Ox)_2^-$ decreases drastically until it disappear at pH 7.5 where soluble Al-hydroxyl species, $Al(OH)_{3,aq}$ and $Al(OH)_4^-$, dominate the speciation. In conclusion, at pH < 7 most of dissolved Al^{3+} remains in solution forming stable aqueous complexes with oxalate, whereas at pH > 7 Al hydrolysis products dominates the speciation.

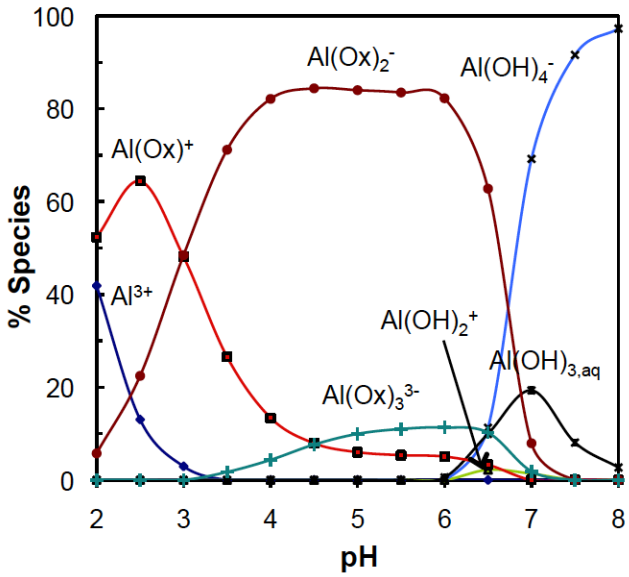

Figure 4.3. Aluminium (6 μmol L^{-1}) speciation in solutions with 0.03 mmol L^{-1} of oxalate as a function of the solution pH (Sm-Ox0.03-3).

4.3.2. Adsorption

The pH dependence of the adsorption of oxalate onto smectite is shown in Figure 4.4, for several oxalate concentrations. The trend of the curve is similar for the several concentrations used, although it is less scattered for the lowest oxalate concentration (0.1 mmol L^{-1}), where a maximum of adsorption occurs at pH 2.7 (5.4 μmol g^{-1}). From

pH 2.7 to 3 the adsorbed oxalate decreases until attaining a plateau from pH 3 to 5.2 (3 μmol g^{-1}). At pH > 5.2 the adsorption decreases progressively approaching zero at pH > 6.5. Increasing the oxalate concentration the adsorbed oxalate also increases, as well as the data scattering. The trend is less clear, as higher the oxalate concentration is.

The analysis of the IR spectra of oxalate in solution and adsorbed at the smectite surface gives useful information about the nature of the oxalate-smectite surface complexes. In this study, it has not been possible to measure oxalic acid (H_2Ox) (pK_{a1} = 1.25) in solution because the ATR cell crystal has a working range from pH 3 to 9. The spectra of oxalate solutions in Johnson et al. (2004b) and Yoon et al. (2004) were used for comparison purposes.

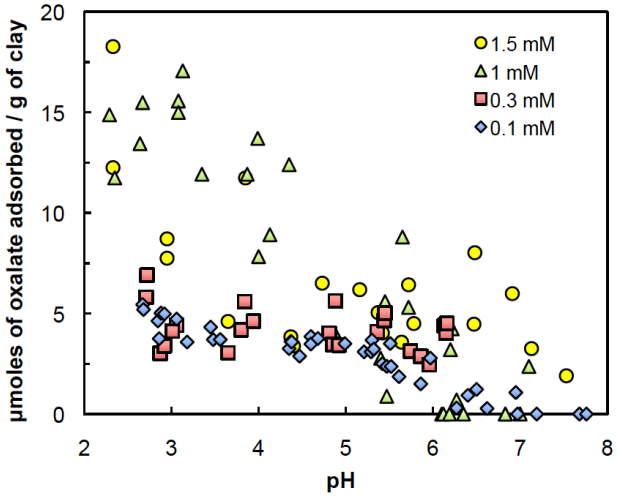

Figure 4.4. Dependence of oxalate adsorption onto montmorillonite vs. solution pH (adsorption edge).

In Fig. 4.5 the ATR-FTIR spectra of oxalic acid in aqueous solution (a) and the transmission spectra of crystalline oxalic acid in KBr pellet (b) are depicted. The characteristic peaks of oxalic acid fall within expected ranges. In the spectrum of oxalic acid in aqueous solution at pH 6.4, where the dominating specie is oxalate (Ox^{2-}), two strong bands can be observed: the antisymmetric (1570 cm^{-1}) and symmetric (1307 cm^{-1}) stretching vibration of the carboxylate group (υ^{a}_{CO} and υ^{s}_{CO}, respectively) (Nakamoto, 1997). In contrast, the ATR-FTIR spectrum of the hydrogen oxalate (HOx^{-}) at pH 3.8 shows more complex features (additional adsorption bands at 1238, 1625 and 1722 cm^{-1}) due to the breakdown of molecular symmetry of oxalate as a

result of protonation. The band at 1238 cm^{-1} can be attributed to the stretching vibration of the C-OH group ($\upsilon_{C\text{-}OH}$) and the band at 1722 cm^{-1} to the stretching vibration of the carbonyl group ($\upsilon_{C=O}$) (Socrates, 1994). The band at 1625 cm^{-1} has been assigned to the stretching vibration of the weakened carbonyl group due to the partial deprotonation at pH < pK_{a2} (Specht and Frimmel, 2001).

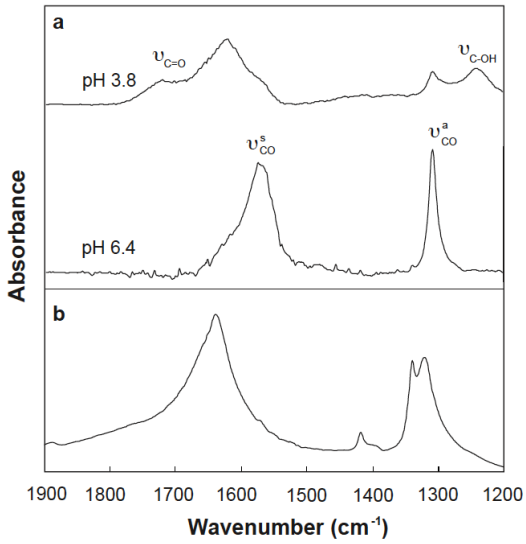

Figure 4.5. ATR-FTIR spectra of oxalic acid in aqueous solution at pH 3.8 and 6.4 (a) and transmission spectra of crystalline oxalic acid in KBr pellet (b).

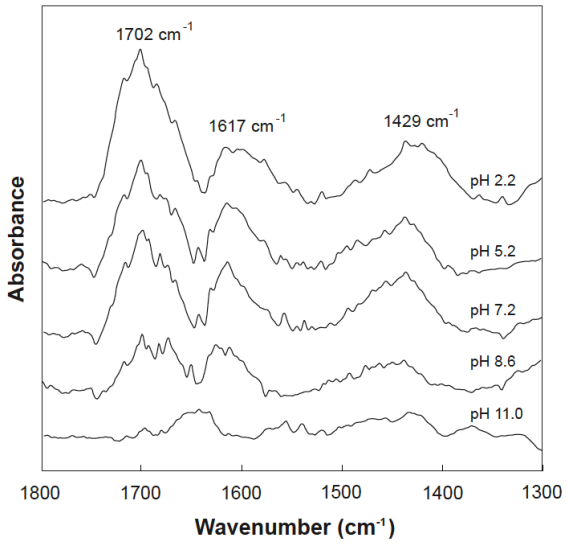

Figure 4.6. DRIFT spectra of oxalate adsorbed to montmorillonite at pH 2.2, 5.2, 7.2, 8.6 and 11.0.

The spectra of oxalate adsorbed on montmorillonite measured by DRIFT at some representative pHs are shown in Figure 4.6. They were normalized against the Si-O stretching vibration band at 1027 cm^{-1}, thus the relative intensities reflect the amount of oxalate adsorbed at each pH. However, the low intensities of the observed bands do not allow us a quantitative estimation of the amount of oxalate adsorbed. The spectra contain three mayor peaks that correspond to the adsorbed oxalate species on montmorillonite, positioned at 1702, 1618 and 1420 cm^{-1}, whose intensity and precise position depends on the pH. The spectra between pH 2.2 and 7.2 present similar intensities in the three peaks observed. Nevertheless at pH > 7.2 all the peak intensities decreases until disappear at pH 11. The peak at 1420 cm^{-1} slightly shifts to higher wavenumber when pH increases. Johnson et al. (2004b) observed a similar spectral change for the adsorption of oxalate on corundum when oxalate concentration was increased. They concluded that the peak shift was due to the slight

alterations in the average environment of inner-spherically adsorbed oxalate, which arise as a function of increasing surface coverage.

4.4. Discussion

The oxalate anion interacts with the montmorillonite surface in aqueous solutions, forming surface complexes. Moreover, oxalate can form aqueous complexes with Al or Fe released during montmorillonite dissolution process.

The dissolution rates of montmorillonite at steady state (Fig. 4.2) show that between pH 4 and 8 oxalate enhances montmorillonite dissolution rate. Increasing oxalate concentration from 0.03 to 1 mmol L^{-1} enhances dissolution rate of montmorillonite. The effect of oxalate on the dissolution reaction is very rapid as can be derived from the concentration of structural cations in short-time dissolution tests. Figure 4.7 shows the concentration of Al, Mg and Fe in the adsorption batch after 5 hours of reaction. Oxalate increases total aqueous Al and Fe concentration in solution at pH < 7. For example, in 1.5 mmol L^{-1} oxalate solution at pH 2, Al released to solution is 30 times higher than that in the blank sample. However, Mg^{2+} concentrations do not differ from those measured without oxalate at pH < 5. At pH > 5, Mg^{2+} released to the solution increases when oxalate is present, probably due to the aqueous complexation of free Mg^{2+} with oxalate (Visual Minteq tests indicate that oxalate complexes Mg^{2+} in solution from pH 4 to pH 10).

The potential formation of surface complexes was examined with the adsorption edge experiments. Isomorphic substitutions on the montmorillonite basal planes produce an excess of negative charge that develop an anion exclusion volume on the basal surface of montmorillonite (Ramos et al., 2011). Moreover, oxalate is a small molecule (~ 8 $Å^3$) with two negatives charges and a high charge density (Materials Studio 5.0, 2009). The electrostatic repulsion between the oxalate molecule and the negative charged surface limits or even prevent oxalate adsorption at the basal surface. Thus only adsorption at the crystal edges is expected.

The comprehension of the oxalate adsorption should be constraint by a surface model that provides the reactive surface area and the surface sites density. Oxalate adsorbed on the lateral surface of the montmorillonite crystals, occupied by aluminol

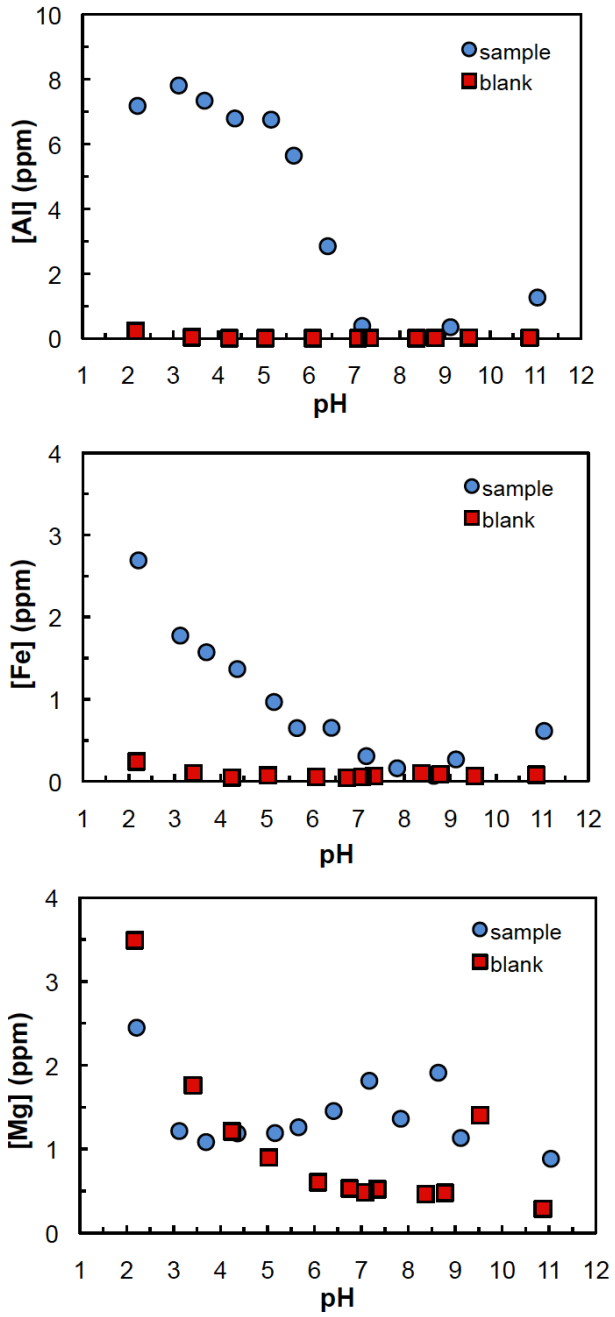

Figure 4.7. Dissolved Al, Mg and Fe measured at the end of the batch adsorption experiments.

and silanol surface sites (Rozalén et al., 2009a). There exist similarities between aqueous and surface complexes, what would allow us to limit oxalate adsorption to aluminol sites and exclude silanol. We may assume an edge surface area of 6.5 $m^2\ g^{-1}$ (Rozalén at al., 2008) and an aluminol surface density of [>AlOH] = 3.55 sites nm^{-2} (Rozalén et al., 2009a). The edge surface maximum coverage of oxalate derived from

adsorption experiments is given in Table 4.4. Coverage increases with oxalate concentration in solution and tends to reach saturation above 1 mmol L^{-1} concentration, which corresponds approximately to half of the aluminol sites reacted with oxalate.

Table 4.4. Maximum amount of oxalate adsorbed on the lateral surface of montmorillonite crystals. The values were calculated for an edge surface area of 6.5 $m^2 g^{-1}$ (Rozalén et al., 2008) and aluminol site density of 3.55 sites nm^{-2} (Rozalén et al., 2009a).

Aqueous oxalate (mmol L^{-1})	Maximum adsorbed oxalate		
	µmol g^{-1}	Sites nm^{-2}	% occupied >AlOH sites
0.1	5.4	0.5	14
0.3	6.91	0.64	18
1.0	17.06	1.58	44
1.5	18.27	1.69	48

The adsorption versus pH pattern (Fig. 4.4) is consistent with the surface charge distribution at the active surface sites (Rozalén et al., 2009a). The extent of oxalate adsorption approaches zero at pH > 7, when the overall charge at the smectite edges is negative. Under these conditions, a net repulsive electrostatic interaction exists between the negatively charged montmorillonite surface and oxalate anions and adsorption does not occur. The increase in adsorption of oxalate on montmorillonite surface at low pH and the decrease in adsorption at high pH can be explained by considering the electrostatic interactions between the oxalate and the edge surface sites (Ward and Brady, 1998). As the pH decreases, the aluminum sites at the edge surface are protonated and form >AlOH and $>AlOH_2^+$. The development of a positively charged surface allows oxalate anions to be electrostatically adsorbed at the montmorillonite edges. Furthermore, protonation of aluminol sites weakened the Al-O bond due to a decreased electron density of the bond (Evanko and Dzombak, 1998), what permits the reaction between oxalate and aluminol sites by ligand exchange and the formation of inner-sphere complexes. Consequently, the oxalate adsorption on montmorillonite can be satisfactorily accounted for inner and outer-sphere complexes in the acidic range and only outer-sphere in the near neutral pH range.

Little is known about the molecular mechanisms of oxalate interactions with montmorillonite. The potential interactions for anionic oxalate species to interact with

montmorillonite are restricted to metal-ligand complexation in the interlayer region of the clay and to complexation on edge sites involving aluminol sites. The metal-ligand complexation constant for potassium-oxalate is low, thus, interlayer complexation of oxalate by potassium ions occupying isomorphic substitution sites on the basal surface of the clay would be negligible. Thus, complexation of oxalate on broken-edge aluminol sites are the only plausible sorption sites. The amount of oxalate sorbed is consistent with the site density of aluminol groups, however, the overall amount of oxalate sorbed is small, ranging from 5 to 18 mmol/g. From the perspective of surface spectroscopy, this is low surface coverage of oxalate, ranging from 0.5 to 1.6 mg of oxalate/g (0.05 to 0.16 wt %). These results are consistent with those found for the adsorption of oxalate onto a spodic horizon soil (Bhatti et al., 1998).

The nature and geometry of these oxalate surface complexes was consistent with the analysis of the DRIFT spectra. However, the low surface concentration of oxalate makes definitive spectral assignments difficult of the sorbed species, and reinforces the need for the macroscopic adsorption and adsorption edge data.

DRIFT spectrum of oxalate adsorbed onto smectite at the lowest pH (maximum surface coverage) contains two major peaks at 1702 and 1420 cm^{-1} (Fig. 4.6). These peaks are similar to those found by Johnson et al. (2004b) for the adsorption of oxalate on corundum and correspond with oxalate binding in a side-on, mononuclear, bidentate, inner-sphere complex. On the other hand, the peak at 1618 cm^{-1} can be attributed to oxalate adsorbed via an outer-sphere mechanism as has been found for boehmite and corundum surfaces (Axe and Persson, 2001; Johnson et al., 2004b; Yoon et al., 2004). One possibility for the outer-sphere adsorption is the complexation through hydrogen bonding interactions involving surface >AlOH or $>AlOH_2^+$ groups. These findings are consistent with Kang and Xing (2007) results for montmorillonite. They found that outer-sphere complexation was dominant at the interface at pH 4, 7 and 9 and inner-sphere coordination increases as the pH is lowered. Other studies use the differing separations between the carboxylate asymmetric and symmetric stretching adsorption bands to distinguish the nature of the carboxylic acid/mineral surface complexes (Kang and Xing, 2007). However, in the present study the band shifts were too small to make any statements regarding possible surface complexes. Both types of complexes have been found in montmorillonite for the adsorption of

other dicarboxylic acids (Kang and Xing, 2007). ATR-FTIR studies (Kubicki et al., 1999) did not suggest a strong complexation of oxalate on montmorillonite surface.

Based on the DRIFT results, together with the adsorption edge data, two surface complexation reactions are proposed to explain oxalate adsorption at the montmorillonite surface. The aluminol sites are assumed to be the locus for oxalate adsorption at the edges:

$$>AlOH + Ox^{2-} = >AlOH\cdots Ox^{2-} \quad (4.4)$$

$$>AlOH + H^{+} + Ox^{2-} = >Al\text{-}Ox^{-} + H_2O \quad (4.5)$$

The first reaction corresponds with the formation of an outer-sphere complex in the whole pH range where oxalate sorption occurs (Ward and Brady, 1998). The second one represents the formation of an inner-sphere complex favored at low pH (Fein and Brady, 1995). According to the spectroscopic analysis, the last complex involves one surface Al atom to form a mononuclear, bidentate, 5-member ring. Additional surface complexes could be suggested to justify the adsorption behavior, as one oxalate bound to the surface through one inner-sphere complex and the other end of carboxylate molecule sees the proton-rich environment of the aluminol group and becomes protonated (Bhatti et al., 1998). Additional studies should be carried out to determine what specific complex are formed.

Dissolution mechanism

Montmorillonite dissolution in acidic and neutral solutions containing ligands may occur thought contributions of proton- and ligand-promoted reactions (Zutic and Stumm, 1984; Furrer and Stumm, 1986; Chin and Mills, 1991; Wieland and Stumm, 1992; Stillings et al., 1998). The latter mechanism may occur thought the formation of surface complexes or a reduction in the ion activity product by complexation of the released cations, particularly Al. The existence of oxalate surface complexes was assessed by macroscopic adsorption experiments and infrared spectroscopy. It has been demonstrated that oxalate anions interact with both surficial and aqueous Al cations and that surface and aqueous complexation reactions coexist in a similar range of pH values. The calculated ΔG_r (Fig. 4.8) shows that dissolution experiments take place under far-form-equilibrium conditions ($\Delta G < -20$ kcal mol^{-1}). Comparing these

values with those without oxalate at equivalent pH values (Rozalén et al., 2008), an increase of the equilibrium distance is observed as the oxalate concentration increases. Thus, the role of oxalate in enhancing the dissolution rate through the formation of soluble Al complexes and by diminishing the activity of Al^{3+} can be important as is supported by other studies (e.g. Ganor and Lasaga, 1994; Oelkers and Schott, 1998).

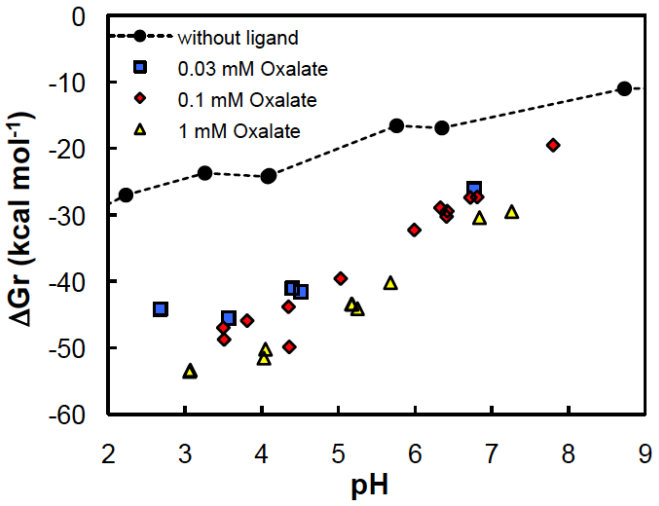

Figure 4.8. pH-dependent values of the saturation function, ΔGr, for montmorillonite with and without oxalate (from Rozalen et al., 2008).

The oxalate enhances montmorillonite dissolution depending on pH. At pH 3-4, the dissolution rate is similar to that calculated without oxalate and does not catalyze the reaction. Although oxalate forms aqueous Al complexes at these pHs and the formation of surface complexes occurs, it seems that the dissolution reaction takes place throught the attack of protons (H^+) to the surface. In these conditions, ligand-promoted dissolution mechanism is much less relevant than the proton-promoted one.

When pH increases from 4 to 7.5, the dissolution rate is enhanced with respect to that calculated without oxalate. In this pH range, Al is fully complexed by oxalate in solution (Fig. 4.3). Moreover, oxalate is adsorbed onto the aluminol edges in an inner/outer-sphere mode (>Al-Ox^- and >AlOH$\cdots Ox^{2-}$, respectively). In this case, ligand-promoted mechanism predominates with respect to the proton-promoted one, and both, formation of soluble and surface complexes contribute to the overall rate law. Although the prevalence of these two has been focus of a debate for many years these results together with those obtained for citrate (Ramos et al., 2011) support the

idea previously suggested by Stillings et al. (1998) that both hypothesis are not mutually exclusive and can coexist.

Consequently, the overall rate of montmorillonite dissolution can be expressed as the contribution of proton- and ligand-promoted dissolution mechanisms (e.g. Golubev and Pokrovsky, 2006; Golubev et al., 2006; Olsen and Rimstidt, 2008, Ramos et al., 2011):

$$Rate_{Tot} = Rate_H + Rate_{Ligand} = k_H \cdot a_{H^+}^{n_H} + k_L \cdot a_L^{n_L} \quad (4.6)$$

The first term in this equation corresponds with the proton-promoted dissolution and the second term corresponds with the ligand-promoted dissolution. As an example, at pH 7 the ligand-promoted dissolution can be estimated by subtracting the dissolution rate of ligand-free solutions from the overall dissolution rate, $R_{Tot} - R_H$, obtaining this empirical law at pH 7:

$$Rate_{Ox} = 10^{-10.68} C_{Ox}^{0.40} \quad (4.7)$$

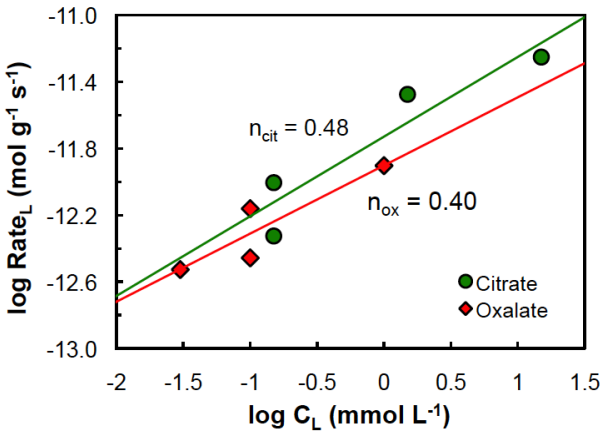

Figure 4.9. Effect of oxalate and citrate on Si-derived dissolution rates. Ligand-promoted dissolution rates for pH 7, R_L, derived from equation 4.8 is included.

As for others organic ligands studied, oxalate has the ability to enhance dissolution rate of montmorillonite. However, this effect is lower than for others like citrate, as observed in the empirical law obtained by Ramos et al. (2011) with a reaction order of 0.48 (Fig. 4.9). This difference is consistent with the stability constants of the aqueous of Al^{3+}-Ligand complexes, stronger for citrate than for oxalate (log K 7.98 and 7.3 respectively).

4.5. Conclusions

In the present study the effect of oxalate on the montmorillonite dissolution rate was investigated a 25°C, using stirred flow-through cells, adsorption batch experiments and FTIR spectroscopy. The following conclusions concerning the dissolution mechanism can be withdrawn:

1) Oxalate enhances the montmorillonite dissolution reaction from pH 4 to 8, reaching a maximum of 0.5 logarithmic units with respect to ligand-free conditions at pH 7.

2) Oxalate adsorbs onto montmorillonite from pH 2 to 8. We hypothesize that interaction between oxalate and montmorillonite surface occurs at the aluminol edges.

3) Based on DRIFT results we have described the oxalate adsorption assuming the formation of two complexes. In the first one, $>AlOH\cdots Ox^{-2}$, oxalate is bound to the aluminol group in an outer-sphere mode and exists from pH 2 to 8. At low pH, the formation of an inner-sphere complex $>Al\text{-}Ox^{-}$ is favored.

Combined results of dissolution, adsorption and DRIFT experiments let us to conclude that the formation of oxalate surface complexes and soluble chelates contribute to the overall dissolution mechanism. Additional studies using complexation models (e.g., extended constant capacitance or triple layer) are necessary to better understand and assess the interaction of low molecular weight organic acids with montmorillonite.

5. Adsorption of lactate and citrate on montmorillonite

5. ADSORPTION OF LACTATE AND CITRATE ON MONTMORILLONITE.

Abstract.- Lactate and citrate were adsorbed on montmorillonite surface from aqueous solutions from pH 2 to 12 in the presence of 10 mmol L^{-1} KCl. The adsorbed molecules were characterized using Attenuated Total Reflectance Fourier transform infrared (ATR-FTIR) spectroscopy at pH 4, 6 and 8. Macroscopic adsorption measurements indicate that the adsorption of both ligands is highly pH dependent. ATR-FTIR results indicate that lactate is likely adsorbed by nonspecific electrostatic interactions, since no changes were found in peak positions and shapes of carboxyl group stretches. Nevertheless, ATR-FTIR results suggest that citrate is adsorbed in the >AlOH groups as an inner-sphere surface complex at low pH. The macroscopic adsorption behavior of the ligands was modeled as a function of pH by using the Diffuse Layer Model (DLM) for lactate and the Triple Layer Model (TLM) for citrate. Surface complexation of lactate and citrate was described with the complex >AlLac (logK = 11.25) and the complex >$AlCit^{2-}$ (logK = 10.58) respectively.

These findings are of relevance for the evaluation of the catalytic effect that takes place during the dissolution of clay minerals in presence of low-molecular-weight organic ligands.

5.1. Introduction

The nature of bonding between organic species and mineral surfaces may play a role in catalyzing the reaction of mineral dissolution as surface-organic complex formation and increases the solubility of the structural cations (Johnson et al., 2004a,b; Yoon et al., 2004). However, the catalytic mechanism is still under debate (Drever and Vance, 1994; Drever and Stillings, 1997; Oelkers and Schott, 1998; Stillings et al., 1998; Cama and Ganor, 2006; Golubev and Pokrovsky, 2006; Li et al., 2006; Pokrovsky et al., 2009).

Low-molecular-weight (LMW) organic acids can absorb onto mineral surfaces either by specific chemical interactions (chemisorption) to form inner-sphere complexes or by nonspecific interactions (physisorption) via hydrogen bonding and/or electrostatic interactions to form outer-sphere complexes (Filius et al., 1997; Axe and

Persson, 2001). Among the LMW organic acids, lactate and citrate play a significant environmental role because of its prevalence in soil, sediments and aerosols resulting from its exudation by plant roots, production by fungi, and discharge by microorganisms (Gadd, 1999; Ryan et al., 2001). Extensive works have been done to characterize the type and structure of surface complexes of simple organic acids with minerals (Cornell and Schindler, 1980; Filius et al., 1997; Evanko and Dzombak, 1999; Kubicki et al., 1999; Axe and Persson, 2001; Johnson et al., 2004a,b; Yoon et al., 2004; Jonsson et al., 2010). However, the adsorption mode of lactate has been only studied in metal oxides. Cornell and Schindler (1980) suggested that lactate was adsorbed as monodentate inner-sphere complexes, whereas Fillius et al. (1997) found that lactate adsorbs predominantly as outer-sphere complexes. Awatani et al. (1998) examined the adsorption of lactate on titanium oxide and concluded that lactate adsorbs in a bidentate fashion involving hydroxyl and carboxyl groups. These results may suggest that the structures and binding modes of lactate at mineral/water interfaces vary depending on the type of absorbent. On the other hand, citrate adsorption has been studied before in clays, but the adsorption mode is still unclear. Kubicki et al. (1999) found that citrate was adsorbed on montmorillonite by outer-sphere complexation. Lackovic et al. (2003) modeled citrate adsorption on illite with two bidentate outer-sphere complexes, but they did not provided spectroscopic information.

Spectroscopy methods are a well suite for probing the structure and binding in metal-carboxylate complexes in aqueous solutions and at interfaces. Carboxylate groups of organic ligands have characteristic infrared-active vibrational bands that are sensitive to changes in proton and metal coordination. ATR-FTIR spectroscopy is one of the most direct methods used to distinguish different structures of organic adsorbents at mineral/water interfaces under *in-situ* conditions. It has been widely used to investigate organic ligand/clay surface complexation (Kubicki et al., 1997; Kubicki et al., 1999; Specht and Frimmel, 2001; Lackovic et al., 2003; Kang and Xing, 2007). Wet samples obtained in the adsorption reactions can be directly mounted on the ATR cell without any preparation that may affect the surfaces or adsorbed complexes. Thus, ATR-FTIR is able to provide information about the binding mode of ligands usually by comparing the IR spectra from adsorbed species with corresponding solution species. However, ATR-FTIR results do not always provide definitive information on different

coordination geometries for surface complexes. In order to better understand the ligand-montmorillonite interactions, the experimental results obtained must be integrated with a surface complexation model, which establishes the stoichiometry of the adsorption reactions and provides a thermodynamic characterization of the equilibria involved.

We focused on montmorillonite in the present study because its prevalence in soils and sediments. Moreover, montmorillonite dissolution mechanism and reactivity have been widely investigated in previous work (Furrer et al., 1993; Zysset and Schindler, 1996; Baeyens and Bradbury, 1997; Bauer and Berger, 1998; Cama et al., 2000; Huertas et al., 2001; Amram and Ganor, 2005; Metz et al., 2005a,b; Rozalén et al., 2008; Rozalén et al., 2009a,b; Ramos et al., 2011).

In this work we study the adsorption mechanism of lactate and citrate onto montmorillonite using the batch equilibrium adsorption method and attenuated total reflectance Fourier-transform infrared (ATR-FTIR) spectroscopy. The results of the complete adsorption study are used to develop a surface complexation model that explains the dependence of the adsorption of organic ligands onto the surface of montmorillonite. The results of this study allow making quantitative predictions that can facilitate evaluation of the potential role of mineral surface chemistry in several geochemical processes involving the interactions of organic molecules and mineral surfaces.

5.2. Materials and methods

5.2.1. Materials

The clay material used in all experiments was a bentonite from the La Serrata – Cortijo de Archidona deposit located at Cabo de Gata (Almeria, SE Spain). This bentonite is approximately 92% montmorillonite; the remainder consists of accessory/companying minerals (quartz, feldspars, micas, calcite, amphibole) and volcanic glass (for a detailed characterization of the sample and methods see Rozalén et al., 2008). The adsorption experiments were performed on the <4 μm fraction, collected by repeated sedimentation-suspension cycles in deionized water, and then exchanged with K^+.

The calculated structural formula of the K-smectite (based on half unit cell) corresponds to a montmorillonite (Newman and Brown, 1987):

$K_{0.95}Mg_{0.02}Ca_{0.01}(Al_{2.79}Fe^{3+}_{0.35}Mg_{0.86})(Si_{7.84}Al_{0.16})O_{20}(OH)_4$

Only 0.34 K^+ ions per half formula unit are exchangeable which indicates the presence of a small proportion of non-swelling layers. X-ray diffraction (XRD) patterns recorded on powder specimens and on oriented and glycolated mounts indicate that the sample is composed of a dioctahedral smectite with approximately 10-15% non-swelling layers. No accessory phases were detected. The specific surface area was measured by BET (Brunauer et al., 1938), using 5-point N_2 adsorption isotherms, after degassing the sample for two days at 110°C under vacuum. The specific surface area was 111 $m^2 g^{-1}$, with an associated uncertainty of 10%.

The organic carbon content determined by the wet oxidation method (Mingorance et al., 2007) yielded 2.57 ± 0.27 g C kg^{-1} (0.26 ± 0.03%), which is consistent with the value 0.35 ± 0.05% obtained for bulk FEBEX bentonite (Fernandez et al., 2004). Although the presence of organic carbon could affect to the adsorption results, the clay was used as adsorbent without any pretreatment. Previous works suggest that the process of removal of organic carbon may affect the mineral surface more than the presence of organic carbon (Brown and Brindley, 1980).

5.2.2. Batch adsorption experiments

Adsorption edges of lactate and citrate were carried out at room temperature using the batch equilibrium method at room temperature. Potassium chloride was added to the solutions as background electrolyte. For lactate individual suspensions were prepared for every point of the adsorption series. For lactate adsorption, a quantity of 0.023 g of montmorillonite was added to 20 mL of 10 mmol L^{-1} KCl in a polyethylene bottle. The suspensions were stirred for 3-4 minutes and left to equilibrate for 24 h. A volume of 0.3 mol L^{-1} lactic acid stock solution was added to reach a total ligand concentration of 0.15 and 1.5 mmol L^{-1}. A control sample without clay was prepared to quantify the potential loss of lactate due to other processes. The pH was adjusted in each sample with an appropriate amount of 1 mol L^{-1} HCl or KOH solution to cover a pH range from 2 to 11. After 5 h the pH was measured in each

bottle and an aliquot of 10 mL was withdrawn and filtered through a 0.22 µm Durapore membrane to analyze the lactate remaining in the solution.

For citrate adsorption 0.58 g of montmorillonite were suspended in 100 mL of 10 mmol L^{-1} KCl solution. The suspension was stirred for 3-4 minutes and equilibrated for 24 h. Then a volume of citrate stock solution was added to reach a total ligand concentration of 0.15 and 1.5 mmol L^{-1} and the pH was adjusted to 2 by adding 1 mol L^{-1} HCl solution. Every 20 minutes the pH was measured and a 5 mL aliquot was withdrawn while stirring. The pH was then increased in steps of approximately 1 unit using an appropriate amount of 1 mol L^{-1} KOH solution. The 5 mL aliquot was immediately filtered through a 0.22 µm Durapore membrane and the solution was analyzed for citrate.

Lactate and citrate concentrations in the supernatants were measured by ion chromatography using a Metrohm 761 Compact Ion Chromatograph with a Metrosep Organic Acids column. The eluent was prepared with 0.5 mmol L^{-1} sulfuric acid/15% acetone. The detection limits are 0.9 ppm for lactate and 9 ppm for citrate. The associated errors were 3% for lactate and citrate.

There was no indication of decreasing of lactate or citrate concentration over time in the control solutions, indicating that no bacterial degradation took place in the clay suspensions during the experiments. The adsorption of lactate and citrate from solutions 0.15 mmol L^{-1} were reported in Ramos et al. (2011) only to show qualitatively the amount and pH of ligands adsorption. The analysis and modeling of theses results is an objective of the present study.

5.2.3. Infrared spectroscopy

All reactions of lactate and citrate with montmorillonite were conducted in acid-washed 30 mL glass vials with polytetrafluoroethylene (PTFE) caps. A volume of 10 mL of 10 mmol L^{-1} KCl (background electrolyte) at desired pH (4, 6 or 8) was added to each vial with 0.625 g of smectite. The IR adsorption experiments were performed a three different pH conditions, acid, near neutral and basic conditions, which according to the results of the adsorption edges corresponds to ligand adsorbed, partially adsorbed and desorbed, respectively. The suspensions were stirred for 3-4 minutes

and let to equilibrate for 24 h. After equilibration, 2.5 mL of 125 mmol L^{-1} ligand solution was added to each vial to reach a total ligand concentration of 25 mmol L^{-1} and a total solid/solution ratio of 50 g L^{-1}. Every suspension had a replicate at the same pH without ligand to use it as a reference in the spectral analysis. All the suspensions were stirred and let equilibrate for 5 h at room temperature. To separate the supernatant and the wet paste of the montmorillonite-ligand complex, the suspensions were filtered through a 0.22 μm Durapore membrane. A part of the precipitated complex was washed with a background solution containing 10 mmol L^{-1} of KCl. Every paste of the montmorillonite-ligand complex (with and without washing) was removed from the filter with a spatula and placed in a horizontal flat ATR cell. The sample holding region was sealed with a lid to prevent evaporation during the measurements. ATR-FTIR spectra were collected with a PerkinElmer Spectrum One Fourier Transform Infrared (FTIR) spectrometer equipped with a lithium tantalate ($LiTaO_3$) detector and a horizontal ATR sampling accessory. The experiments were carried out in a horizontal flat ATR cell containing a ZnSe crystal with an angle of incidence of 45°. Every spectrum was obtained by collecting 100 scans with a wavenumber resolution of 4 cm^{-1} between 4000-400 cm^{-1} range and a scan speed of 0.2 cm/s. Grams/32 (Thermo Fisher Scientific Inc., 2011) program was used to plot and analyze the spectra. To isolate the spectrum of the ligand at the water/mineral interface, a subtraction procedure was necessary. The ATR-FTIR spectrum of a 10 mmol L^{-1} KCl solution was collected and subtracted from every sample spectra to remove the strong contributions from water bands. In the spectra the absorbance was normalized against the Si—O stretching vibration band at 1027 cm^{-1} so that the relative intensities reflect the amount of ligand adsorbed at each pH. The ATR-FTIR spectra of the montmorillonite-ligand complexes were obtained from the subtraction of the reference mineral spectrum treated with a solution at the same pH and ionic strength without any adsorbed ligand.

Spectra of ligands in aqueous solutions were measured by placing 1 mL of 25 mmol L^{-1} ligand solution in a ZnSe HATR trough cell with a volumen of 2 mL. The spectra were collected at pH 4, 6 and 8, recorded in absorbance mode in the 4000-400 cm^{-1} range with a wavenumber resolution of 4.0 cm^{-1}. A total of 100 scans were collected for each spectrum at a scan speed of 0.2 cm/s.

5.2.4. Surface model

The macroscopic adsorption edge data can be tentatively linked with the ATR-FTIR data results using a suitable surface complexation model. Montmorillonite edge surface contains functional groups with oxygen atoms, which are coordinated by different numbers of protons and silicon and aluminum. These groups can accept and release protons and also take part in complexation reactions with metal ions and ligands. Because the low ability of Si to form complexes in solution (Pokrovsky and Schott, 1998), complexation reactions of silanol groups of the surface have not been considered in our conceptual model. In addition, silanol groups become as neutral sites under acidic conditions as they protonates under very acidic conditions (Huertas et al., 1998). Furthermore, the absence of adsorption of organic ligands on quartz indicates that there is no interaction between organic ligands and silanol groups (Ward and Brady, 1998). The reactive surface at the particle edges can be described as a homogeneous surface with only one type of reactive hydroxyl groups (aluminol, >AlOH), which is responsible for all the surface complexation reactions. This relatively simple model of surface groups is often satisfactory for modeling of adsorption data (Nordin et al., 1998; Ward and Brady, 1998).

The surface site density and protolysis constants for aluminol edge sites optimized by Rozalen et al. (2009a) were adopted. Protonation and deprotonation reactions are assumed to occur on the inner plane, and are described by the reactions:

$$>AlOH_2^+ = >AlOH + H^+$$

$$>AlOH = >AlO^- + H^+$$

The experimental data were evaluated using the program FITEQL 4.0 (Herbelin and Westall, 1999). Since lactate was present in the solution as HLac and Lac^- (Fig. 5.1), and citrate as H_3Cit, H_2Cit^-, $HCit^{2-}$ and Cit^{3-} (Fig 5.1); and Lac^- and Cit^{3-} are used as main component in the definition of the equilibrium model for the surface complexation, it is convenient to represent the measured aqueous ligand concentration by a parameter that is independent of the aqueous speciation. Therefore, the input of data into FITEQL was done as described in Westall and Herbelin (1992) using the dummy components Lac(ads) and Cit(ads), which represent the total concentration of

adsorbed lactate and citrate respectively. Lac(ads) and Cit(ads) were calculated for each data point as the difference between the total concentration of ligand added and the analyzed total concentration in solution (see section 2.2.).

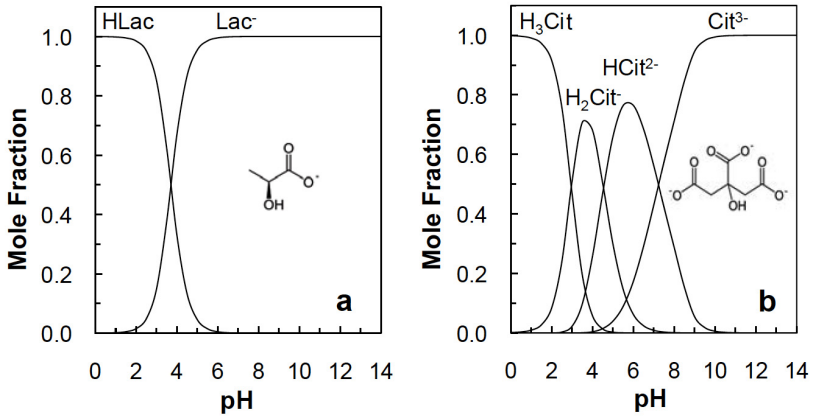

Figure 5.1. Chemical structures of the ligands used in the adsorption experiments and the relative abundances of the species in aqueous solution as a function of pH (a: lactate, b: citrate). Visual MINTEQ (Gustafsson, 2010) was used to calculate the fraction of every species in aqueous solution using the pKa values included in the NIST database (NIST, 2001).

The evaluation of the experimental data in the system H^+ - >AlOH - ligand consisted of a systematic test of combinations of complexes with different compositions and an optimization of the corresponding equilibrium constants. The combination of complexes giving the lowest average WSOS/DF (V(Y)) was considered the best fitting model. Moreover, special attention was focused on making sure that the final model was in good semiquantitative agreement with ATR-FTIR spectroscopic measurements.

5.3. Results and discussion

5.3.1. ATR-FTIR analysis of ligand sorption on montmorillonite

The comparison and analysis of the ATR-FTIR spectra of the ligands in solution and on montmorillonite surface gives useful information about the nature of the complexes formed.

Spectroscopic analysis of aqueous ligands

Figure 5.2 shows the ATR-FTIR spectra of lactate and citrate at pH 4, 6 and 8 in the region 1800 to 1200 cm^{-1}, which covers most of the main vibrational signature of LMW organic acids (Cabaniss and McVey, 1995) and excludes infrared peaks due to montmorillonite vibrations (Farmer, 1974). The characteristic bands of the ligands in aqueous solutions fall within the expected ranges.

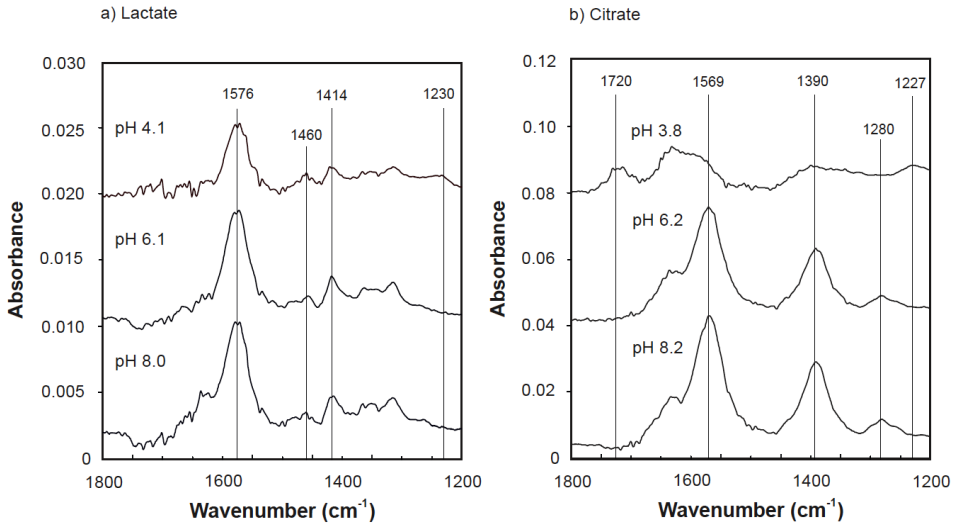

Figure 5.2. ATR-FTIR spectra of of lactate (a) and citrate (b) at pH 4, 6 and 8.

Lactate occurs in aqueous solutions as fully deprotonated or singly protonated species, depending on pH. Each of these species is expected to give rise to a distinctively different infrared spectrum as a function of pH value (pKa = 3.86). In Figure 5.2a the ATR-FTIR spectra of lactate in aqueous solution is depicted. The most abundant specie at the three pHs studied (4, 6 and 8) is Lac^- (Fig 5.1), although at pH 4 the protonated specie HLac is also present in small amount. The ATR-FTIR spectra agree with those reported earlier (Strathmann and Myneni, 2004; Ha et al., 2008) (Table 5.1).

Figure 5.2b shows the spectra of citrate in aqueous solution. The main aqueous citrate species are (Fig. 5.1): fully deprotonated at pH 8 (70% of Cit^{3-}), monoprotonated at pH 6 (80% of $HCit^{2-}$) and doubly protonated at pH 4 (70% of H_2Cit^-). The main peaks in the IR spectra at the three pHs studied were assigned based on literature data (Lackovic et al., 2003; Strathmann and Myneni, 2004) (Table 5.1).

The weak band at 1280 cm^{-1} likely results from skeletal vibrations according to Lackovic et al. (2003).

Spectroscopic analysis of surface complexes

Lactate-montmorillonite: In Figure 5.3a the ATR-FTIR the spectra of lactate adsorbed onto montmorillonite at pH 4, 6 and 8 are shown. The spectra of adsorbed lactate are very similar to that found for lactate in aqueous solution. For the three pHs studied, the bands appear in the same position that the free ligand spectra at every pH. The comparison between the spectra of lactate adsorbed and in solution suggests that lactate structure does not change substantially when it is adsorbed. Furthermore, because the spectra are very similar at the three pHs, the structure of the complex of lactate adsorbed with the surface does not likely change with the pH.

Table 5.1. Assignments of main lactate and citrate bands in the 1800-1200 cm^{-1} region.

Assignment	Wavenumber (cm^{-1})
Lactate	
$\upsilon_{as}COO$	1576
$\upsilon_{s}COO + \upsilon C\text{-}C + \delta CCH$	1460
$\upsilon_{s}COO + \upsilon C\text{-}C$	1414
$\upsilon C\text{-}OH$	1230
Citrate	
$\upsilon C{=}O$	1720
$\upsilon_{as}COO$	1569
$\upsilon_{s}COO$	1390
$\upsilon C\text{-}OH + \delta C\text{-}O\text{-}H$	1227

In this case, it is possible to suggest the presence of an outer-sphere complex since the ATR-FTIR spectrum of an outer-sphere complex resembles that of the corresponding aqueous specie (Ha et a., 2008). Outer-sphere complexes are expected to retain its hydration shell and form no direct chemical bonds with the mineral surface. Moreover, lactate bands disappear from the spectra after rinsing with a solution of 10 mmol L^{-1} KCl (spectra not shown). The fact that rinsing the sample removes lactate from

montmorillonite confirms the weak adsorption interpretation. Therefore, lactate is probably bound as an outer-sphere complex to the montmorillonite edge surface.

Citrate-montmorillonite: At first sight the spectra appear similar to the corresponding ones in aqueous solution at every pH. However, at pH 4 the C—O asymmetric band shifts from 1569 to 1589 cm^{-1}, while the position of other bands remain invariable. At pH 6 and 8, the spectra are very similar to those of the free citrate at the same pHs, suggesting that the ligand interacts with the surface by formation of outer-sphere complexes.

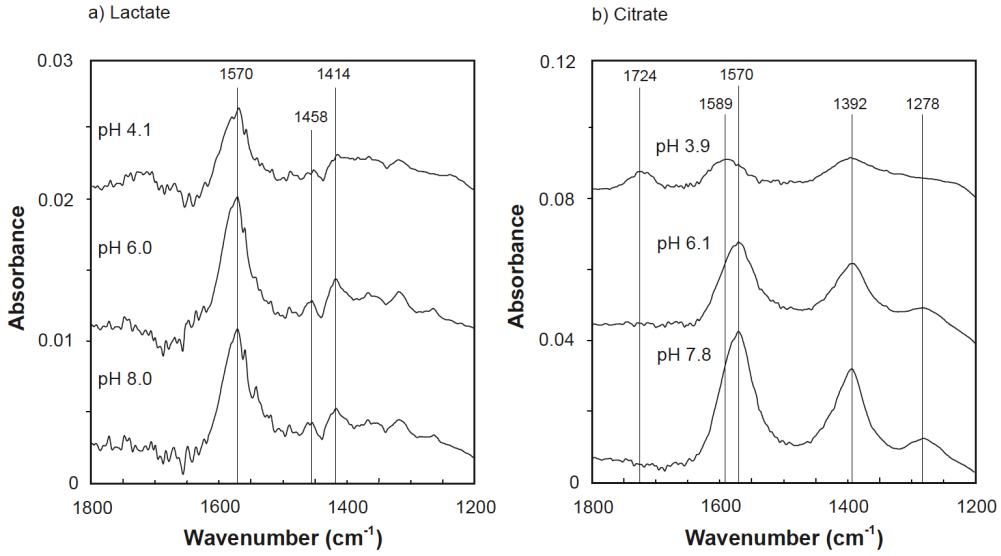

Figure 5.3. ATR-FTIR spectra of lactate (a) and citrate (b) adsorbed onto montmorillonite at pH 4, 6 and 8.

Peak shifts are a result of specific carboxylate-metal ion interaction when an inner-sphere complex forms. Thus, the shift of the C-O asymmetric band from 1569 to 1589 cm^{-1} observed at pH 4 suggests that adsorbed citrate molecules are strongly affected by the adsorption reaction. Hay et al. (2007) reported that the coordination of one oxygen of the carboxylate (monodentate coordination) causes an increase in the υ^{as} in an extent that depends on the nature of the complex formed. Kang and Xing (2007) suggested that this shift was due to the formation of an inner-sphere complex.

As a summary, according to the ATR-FTIR results, citrate is adsorbed in an inner-sphere mode at low pH and outer-sphere mode is favored at near neutral pHs. Acidic

pH provides better environmental conditions for inner-sphere complexation of dicarboxylic acids on clays than alkaline pH (Kang and Xing, 2007).

5.3.2. Quantitative analysis of ligands adsorption on montmorillonite

Indications on the mechanism of adsorption and the affinity between a particular ligand and a surface can be obtained by study the dependence the amount of ligand sorbed as a function of pH. Figure 5.4 illustrates that adsorption of lactate and citrate on montmorillonite was strongly pH-dependent. For lactate adsorption, the amount adsorbed is approximately constant below pH 6 where maximum occurs (60 μmol g^{-1} for 0.15 mmol L^{-1} and 140 μmol g^{-1} for 1.5 mmol L^{-1} lactate sorption edge). From pH 6 to 9 the adsorbed lactate decreases progressively until pH 9 where the lactate does not absorb onto the montmorillonite surface. Citrate adsorption is very close to zero at a low pH, increasing up to a maximum at approximately pH 6 (23 μmol g^{-1} for 0.15 mmol L^{-1} and 34 μmol g^{-1} for 1.5 mmol L^{-1} citrate sorption edge) and decreasing over pH 6. The shape of the adsorption edge is similar to that found for the adsorption of citrate on illite (Lackovic et al., 2003).

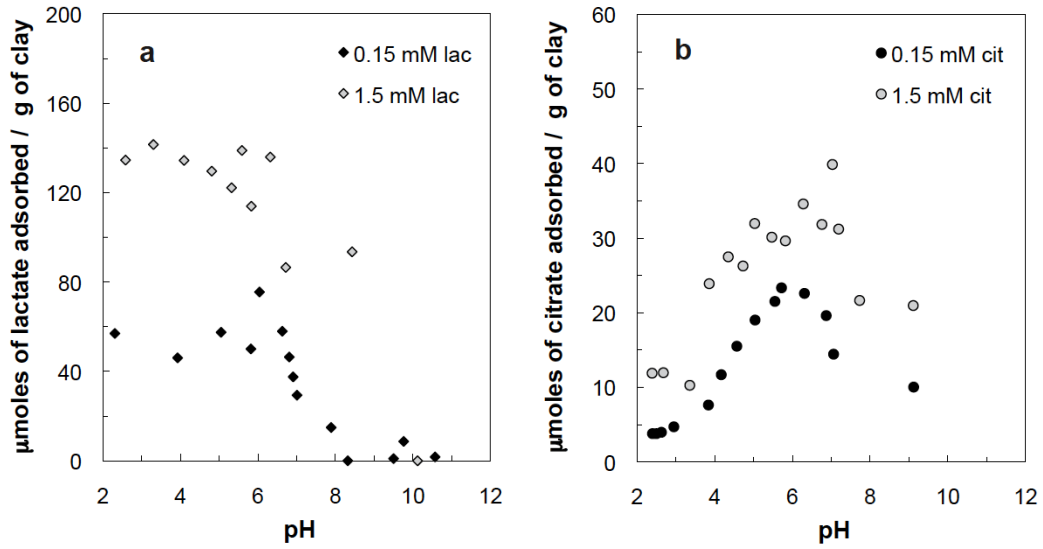

Figure 5.4. Experimental data of adsorption of lactate (a) and citrate (b) on montmorillonite as a function of pH at varying ligand concentrations.

Both lactate and citrate adsorption by montmorillonite is influenced by pH (Fig. 5.4), since the ligand protonation state (Fig. 5.1) and smectite surface charge (Rozalen

et al., 2009a) are both pH dependent. In general, the increase in adsorption at low pH and the decrease in adsorption at high pH can be explained by considering the electrostatic interactions between the carboxylic acid species and the charged surface sites (Ward and Brady, 1998).

Lactate: At pH values over ~7.5, both the montmorillonite surface and lactate are negatively charged. There may be no interaction between the montmorillonite surface and lactate anion, and no lactate adsorption can be observed under alkaline conditions. Below pH 7.5 the montmorillonite surface is positively charged due to the relative abundance of $>AlOH_2^+$ and the positive charge increases as the solution becomes more acidic (to approximately pH <5). Negatively charged lactate adsorbs onto the montmorillonite surface increasing adsorption as the pH decreases from 9 to 7. Below pH 7 the amount of lactate adsorbed is approximately constant in all the experiments. This behavior indicates an electrostatic interaction between the anion and the positively charged surface, as observed for the lactate-goethite interaction (Filius et al. 1997). This is in agreement with the discussed spectroscopic evidence.

Citrate: The adsorption behavior of citrate also points to electrostatic binding. At approximately pH < 3.2 a very weak interaction is expected between the fully protonated citrate and positively charged montmorillonite, as it is confirmed in Figure 5.4. No clear evidence of adsorption was found. The interaction between citrate and montmorillonite surface increases from pH 3.2 up to 7 due to the partial deprotonation of citric acid. The most abundant species are H_2Cit^- (pH 3.1-4.8) and $HCit^{2-}$ (pH 4.8-6.4), which can interact with the positively charged montmorillonite edge surface, producing the adsorption maximum at pH 6. Above pH 7 the electrostatic repulsion between the fully deprotonated citrate and the negatively charged montmorillonite surface (both $>SiO^-$ and $>AlO^-$ sites) makes ligand adsorption difficult. This decreases progressively as the negative charge develops at montmorillonite surface with an increasing pH.

Lackovic et al. (2003) found that a small amount of citric acid can be adsorbed on kaolinite and illite, modeling the adsorption with outer-sphere complexation to the variable-charge edge groups. Their adsorption maximum (~3 μmol g^{-1} illite) is approximately one order of magnitude lower that in the present study, although the citrate solutions were also more diluted.

5.3.3. Modeling the adsorption edge data

Special attention was focused on making sure that the surface complexation model for both ligands was consistent with ATR-FTIR measurements in all cases. In the case of lactate adsorption, only outer-sphere complexation at the montmorillonite surface may be considered according to the experimental ATR-FTIR results. The Triple Layer Model (TLM) accounts for the formation of outer-sphere complexation; nevertheless, the use of the TLM to fit lactate adsorption data do not converge and it was necessary the use of a simpler model. In our case, the use of the Diffuse Layer Model (DLM) was satisfactory. The DLM is often limited to lower ionic strength conditions, and thus, it can be applied in our experiments with a background electrolyte concentration of 10 mmol L^{-1}. In the DLM, the mineral/water interface is considered to comprise two layers of charge: a surface layer and a diffuse layer of counterions in solution (Hayes et al., 1991). All specifically sorbed ions are assigned to one surface layer, and all non-specifically sorbed counterions are assigned to the diffuse layer. Therefore, the adsorption of lactate should occur by ligand exchange reaction between hydroxyl surface groups and lactate.

The adsorption of lactate can be described with one surface species (>AlLac) since lactate is a monoprotic acid. The equilibrium constants for the lactate acid/base reactions and the montmorillonite surface protonation/deprotonation were considered as known parameters (Table 5.2). In the 0.15 mmol L^{-1} adsorption edge experiment, the lactate:aluminol edge sites ratio was 3.37 (assuming 3.55 >AlOH sites nm^{-2}), which indicates a possible saturation of the available adsorption sites. However, the increase of lactate adsorption with lactate concentration (Fig. 5.4) indicates that the aluminol sites available for lactate adsorption are likely underestimated. For this reason, fitting was accomplished by letting FITEQL optimize the formation constant for the complex >AlLac to obtain the lowest average WSOS/DF for a given value of aluminol sites. The best fitting (V(Y)=40.49) was achieved by considering 5.38 sites nm^{-2}. Thus, the reaction that represents the lactate adsorption is:

$>AlOH + Lac^- + H^+ = >AlLac + H_2O \qquad logK = 11.25$

Speciation diagram for 0.15 mmol L^{-1} lactate adsorbed onto montmorillonite, calculated from the model parameters given in Table 5.2, is shown in Figure 5.5.

At first, the infrared data do not agree with the proposed model, since the spectra suggested the formation of outer-sphere complexes at all the pHs values studied. This can be due to a weak nature of the proposed complex >AlLac, which formation does not alter the IR bands position of absorbed lactate with respect to those found for aqueous free lactate.

Table 5.2. Parameters of the surface complexation model

	log K	Reference
Protonation of lactate		
$Lac^- + H^+ = HLac$	3.86	(1)
Protonation of citrate		
$Cit^{3-} + H^+ = HCit^{2-}$	6.40	(1)
$Cit^{3-} + 2H^+ = H_2Cit^-$	11.20	(1)
$Cit^{3-} + 3H^+ = H_3Cit$	14.30	(1)
Surface reactions (I=0.01 mol L^{-1})		
$>AlOH_2^+ = >AlOH + H^+$	6.44	(2)
$>AlOH = >AlO^- + H^+$	-9.94	(2)
$>AlOH + H^+ + NO_3^- = >AlOH_2^+\text{-}NO_3^-$	8.30	(3)
$>AlOH - H^+ + K^+ = >AlO^-\text{-}K^+$	-9.20	(4)
$>AlOH + Lac^- + H^+ = >AlLac + H_2O$	11.25	(5)
$>AlOH + Cit^{3-} + H^+ = >AlCit^{2-} + H_2O$	10.58	(5)
Other parameters		
Site density for >AlOH (sites nm^{-2})	3.55	(2)
S_{edges} ($m^2\ g^{-1}$)	6.5	(2)
Inner capacitance (F m^{-2})	7.0	(6)
Outer capacitance (F m^{-2})	3.0	(6)

[1] NIST (2001), [2] Rozalen et al. (2009a), [3] Reich et al. (2011), [4] Kulik et al. (2000), [5] This study, [6] Ikhsan et al. (2005)

According to the experimental ATR-FTIR results for citrate adsorption, both inner- (at acidic pH) and outer-sphere (near neutral pHs) complexation may be considered. The ATR-FTIR results also indicated that citrate adsorbs in a mononuclear manner and therefore, binuclear complexes have not been considered in our conceptual model. The TLM can distinguish inner- and outer-sphere complexes: sorbates forming inner-sphere complexes are typically placed on the 0 plane, whereas those forming outer-sphere complexes are placed on the b plane. The inner layer

(between the surface plane and the b-plane) and the outer layer (between the b-plane and the bulk solution) have their own constant capacitance values, C_1 and C_2, respectively.

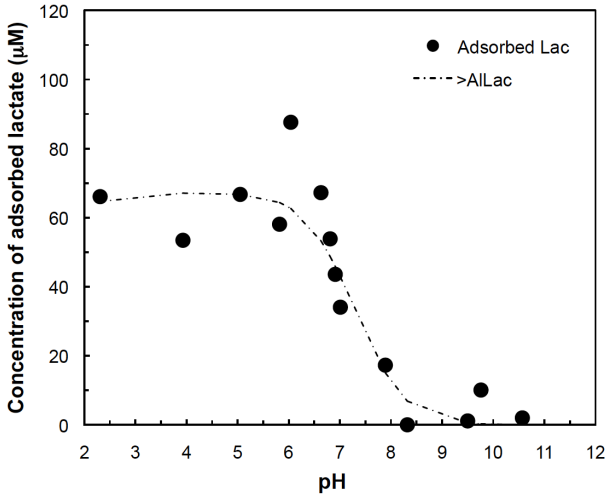

Figure 5.5. Speciation diagram of lactate adsorption at 25°C from 0.15 mmol L^{-1} solution onto montmorillonite, calculated from the surface complexation model. Model parameters are detailed in Table 5.2. Filled circles: experimental adsorption edge data; Dashed black line: overall model fit to experimental data for lactate sorption.

The free concentration of the background electrolyte ions (K^+, NO_3^-) 0.01 mol L^{-1} is assumed to remain constant in the experiments. The equilibrium constants for the citrate acid/base reactions and the montmorillonite surface protonation/deprotonation, as well as the density of surface aluminol groups and the outer and inner capacitance for the electrostatic double layer were considered as known parameters and used without modifications (Table 5.2).

The equilibrium constants for the outer-sphere complexes $>AlOH_2^+$-NO_3^- and $>AlO^-$-K^+ published previously for γ-Al_2O_3 (Reich et al., 2011) and illite (Kulik et al., 2000), respectively, were used to complete the set of constants required to implement the TLM. Unfortunately, the assumption that electrolyte ions are bounded in the outer layer plane led to poor fit of the data. Therefore, the formation reactions of $>AlOH_2^+$-NO_3^- and $>AlO^-$-K^+ were modeled by placing the electrolyte ions in the inner plane. The effect of this change is not expected to be relevant according to the low

background electrolyte concentration (0.01 mol L^{-1}) used in the macroscopic adsorption experiments (Johnson et al., 2004b).

The TLM fit for citrate sorption to montmorillonite is satisfactory (V(Y)=22.7), and it was achieved when citrate sorption is represented by a single reaction:

$>AlOH + Cit^{3-} + H^{+} = >AlCit^{2-} + H_2O$ logK = 10.58

This reaction support the hypothesis that citrate sorption to montmorillonite is dominated by specific sorption to amphoteric aluminol edge sites in the whole pH range studied (2-9). The ATR-FTIR data agree with the proposed model in acidic conditions, since the spectra suggested that the formation of an inner-sphere monodentate complex is favored at low pH. However, modeling results indicate that this complex exist in the whole pH range studied, with a maximum concentration at pH 5.5. This complex involves one surface Al atom to form a mononuclear, monodentate complex. The infrared spectra also suggested the formation of an outer-sphere complex at near neutral pHs. However, the introduction of outer-sphere complexes in the model led to poor convergence. Speciation diagram for 0.15 mmol L^{-1} citrate adsorbed onto montmorillonite, calculated from the model parameters given in Table 5.2, is shown in Figure 5.6.

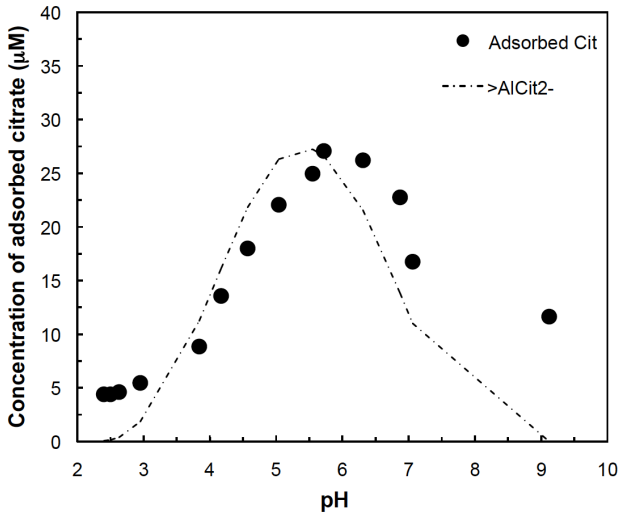

Figure 5.6. Speciation diagram of citrate adsorption at 25°C from 0.15 mmol L^{-1} solution onto montmorillonite, calculated from the surface complexation model. Model parameters are detailed in Table 5.2. Filled circles: experimental adsorption edge data; Dashed black line: overall model fit to experimental data for citrate sorption.

The model fit for 1.5 mol L^{-1} adsorption edges is also satisfactory and the general trend for the model fit is in good agreement with the experimental observations, taking into account the data dispersion.

Although FTIR results indicated that the inner-sphere citrate complexes were favored at low pH and outer-sphere complexes were favored at near-neutral pHs, the model indicates that only one inner-sphere complex is formed in the pH range studied.

5.4. Conclusions

The present study has shown that lactate and citrate adsorb to montmorillonite edge surface from pH 2 to 7. ATR-FTIR spectroscopic data suggest that lactate is weakly adsorbed at the positively charged edge surface sites. The DLM was used to model lactate adsorption with the specie >AlLac. Moreover, ATR-FTIR results indicate that citrate is adsorbed in an inner-sphere manner at acidic pHs. Macroscopic data for citrate adsorption on montmorillonite can be generally well fit using the TLM model with the single monodentate, inner-sphere complex >$AlCit^{2-}$. These results have implications for the study of the mineral dissolution catalyzed by LMW organic acids.

6. Adsorption of glycine on montmorillonite

6. ADSORPTION OF GLYCINE ON MONTMORILLONITE

Abstract.- Glycine was adsorbed on the surface of montmorillonite from aqueous solutions of variable glycine concentrations (0.001 – 0.3 mol L^{-1}) and pHs (2 – 12) at room temperature. The reaction products were characterized using X-ray diffraction and Attenuated Total Reflectance Fourier transform infrared (ATR-FTIR) spectroscopy. The results indicate that adsorption is highly pH dependent, increasing at acidic pHs. Glycine adsorption is dominated by complexation of the carboxylate group of zwitterionic glycine onto the edges surface at low concentrations of glycine. When the edge surface is saturated, the adsorption occurs by cation exchange in the interlayer space. ATR-FTIR results point to an adsorption by hydrogen bonding between the $-NH_3^+$ group and the basal oxygens of the interlayer surface. The dependence of glycine adsorption with its aqueous concentration fits for a Freundlich equation. The measure of the desorbed interlayer cations shows that the 68% of the K^+ was exchanged with glycine. The K^+-glycine exchange reaction produces a decrease of the smectite interlayer space from 14.5 to 12 Å and an arrangement of the smectite layers. Intercalated glycine is present as both glycinium and zwitterionic forms. Since only glycinium contribute to structural charge balance, total adsorbed glycine can exceed K^+ released. These findings are of relevance for the evaluation of distribution and reactions of free amino acids in natural environments.

6.1. Introduction

Dissolved free amino acids have been found at measurable concentrations in natural waters and sediments (Hedges and Hare, 1987). Adsorption is a potentially important process in natural environments because it can lead to preferential removal of some amino acids from the natural solutions, and so sorption may affect amino acid transport processes in soils and sediments.

The interaction of proteins with mineral surfaces has also a very significant impact on several aspects of natural or anthropogenic processes occurring in soils. The study of the mechanism of amino acid bond formation on clays contributes to a better understanding of prebiotic chemical evolution (Parbhakar et al., 2007). Clays and other oxides were present in large amounts on the prebiotic earth crust after the formation

of the hydrosphere and may have played an important role in the process of chemical evolution. For the study of these systems glycine, a neutral non-polar amino acid and the simplest protein structural unit (see Fig. 6.1), it is often regarded as a model.

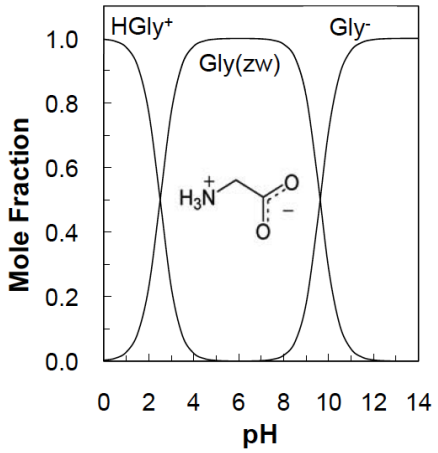

Figure 6.1. Chemical structure of glycine and relative abundance of species in aqueous solution as a function of pH. Visual MINTEQ (Gustafsson, 2010) was used to calculate the fraction of every species in aqueous solution using the pK_a values included in the NIST database (NIST, 2001).

Adsorption studies with well-characterized particulate clays allow interpreting the mechanism involved in the adsorption reaction. The potential of clay minerals for amino acid adsorption in natural environments has been studied in controlled laboratory experiments at several pH conditions (Theng, 1974; Dashman and Stotzky, 1982, 1985; Lahav, 2002). In general, positively charged basic amino acids such as lysine are more strongly adsorbed than neutral or acidic amino acids, due to ion-exchange reactions onto negatively charged clay surfaces (Theng, 1974; Dashman and Stotzky, 1982; Parbhakar et al., 2007; Cuadros et al., 2009; Kitadai et al., 2009). Montmorillonite-type clays, due to their high cation-exchange capacities and surface area, have particularly a great adsorption capacity for basic amino acids which at high loadings can cause swelling by adsorption within the interlayer space (Weiss, 1969; Theng, 1974; Dashman and Stotzky, 1985). However, there are other processes that may control amino acid adsorption on clays as amino acid dipole interaction with the interlayer cation and the charged surface, hydrogen bonding and physical forces (Mortland, 1970).

Attenuated total reflectance Fourier-transform infrared spectroscopy (ATR-FTIR) has been widely used to investigate organic ligand/clay surface interactions (Kubicki et al., 1997; Kubicki et al., 1999; Specht and Frimmel, 2001; Lackovic et al., 2003; Kang and Xing, 2007). Wet samples obtained in the adsorption experiments can be directly mounted on an ATR cell without any additional preparation that may affect the surfaces or adsorbed complexes. Thus, ATR-FTIR is able to provide information about the binding mode of ligands usually by comparing the IR spectra from adsorbed species with the corresponding species in solution. Infrared analysis also is useful to determine the protonation state of the amino acid functional groups and to assess the interaction among interlayered water, cations and amino acid molecules.

The present study is focused on montmorillonite because its prevalence in soils and sediments, where may control the ion exchange and surface properties. Moreover, the dissolution mechanism and reactivity of montmorillonite have been widely investigated in previous work in inert electrolyte and ligand solutions (e.g., Zysset and Schindler, 1996; Cama et al., 2000; Rozalén et al., 2008; Ramos et al., 2011, and references therein). In the present work we performed a series of experiments of glycine adsorption on montmorillonite (adsorption edges and isotherms) at different initial glycine concentrations and pHs, using the batch equilibrium adsorption method. ATR-FTIR spectroscopy and X-ray diffraction (XRD) were employed to elucidate the interaction between glycine and montmorillonite surface. The results of this study will contribute to a better understanding of the mechanism of amino acid uptake by clay particles in natural environments.

6.2. Materials and methods

6.2.1. Materials

The montmorillonite sample used in the present study was obtained from bentonite (FEBEX project, Huertas et al., 2000) and corresponds to an aliquot of the same batch previously characterized by Ramos et al. (2011). The adsorption experiments were performed on the <4 μm fraction, collected by repeated sedimentation-suspension cycles in deionized water, and then exchanged with K^+. The cation exchange capacity (CEC) was determined based on the affinity of Cu(II)-

triethylenetetramine complex for the clays (Meier and Kahr, 1999). The total CEC yielded 94±3 $cmol^{+}\ kg^{-1}$.

The calculated structural formula of the K-smectite corresponds to a montmorillonite (Newman and Brown, 1987):

$$K_{0.95}Mg_{0.02}Ca_{0.01}(Al_{2.79}Fe^{3+}_{0.35}Mg_{0.86})(Si_{7.84}Al_{0.16})O_{20}(OH)_4$$

Only 0.34 K^{+} ions per formula unit are exchangeable which indicates the presence of a small proportion of non-swelling layers, consistent with the estimation derived from the position of reflections 001 and 002 in the oriented mount diffraction pattern of the ethylene-glycol solvated sample (Moore and Reynolds, 1989).

The organic carbon content determined by the wet oxidation method (Mingorance et al., 2007) yielded 2.57 ± 0.27 g C kg^{-1} (0.26 ± 0.03%), which is consistent with the value 0.35 ± 0.05% obtained for bulk FEBEX bentonite (Fernandez et al., 2004). Although the presence of organic carbon could affect to the adsorption results, the clay was used as adsorbent without any pretreatment. Previous works suggest that the process of removal of organic carbon may affect the mineral surface more than the presence of organic carbon (Brown and Brindley, 1980).

6.2.2. Batch adsorption experiments

Adsorption edges of glycine were carried out at room temperature using the batch equilibrium method. Potassium chloride was added to the solutions as background electrolyte. Individual suspensions were prepared for every point of the adsorption series: 0.058 g of montmorillonite were added to 20 mL of 10 mmol L^{-1} KCl in a polyethylene bottle. The suspensions were stirred for 3-4 minutes and left to equilibrate for 24 h. A volume of glycine stock solution was added to reach a total concentration of 1.5 mmol L^{-1}. A control sample without clay was prepared to quantify the potential loss of glycine likely due to degradation. The pH was adjusted in each sample with an appropriate amount of 1 mol L^{-1} HCl or KOH solution to cover a pH range from 2 to 12. After 5 h the pH was measured in each bottle and an aliquot of 10 mL was withdrawn and filtered through a 0.22 μm Durapore membrane to analyze the glycine remaining in the solution.

For adsorption isotherm experiments the same experimental setup was used, but the quantity of montmorillonite was increased to 0.1 g in 10 mL of solution. A volume of glycine stock solution was added to each batch to reach a total glycine concentration of 0.001, 0.003, 0.01, 0.03, 0.1 and 0.3 mol L^{-1}. A control sample without clay was prepared for every glycine concentration. The pH was adjusted with little amounts of 1 mol L^{-1} HCl to correct the pH shift due to adsorption and cation exchange reactions and obtain a final pH of 3 in each clay/glycine solution suspension. This value of pH was chosen since adsorption edge results showed a high adsorption at acidic pHs. After 5 h, the samples were filtered through a 0.22 µm Durapore membrane and the supernatant was analyzed for glycine, K^+, Mg^{2+}, Ca^{2+} and pH. The solids were kept for subsequent analysis.

Glycine was analyzed colorimetrically with a UV-visible spectrometer, using the ninhydrin method (Sun et al., 2006). The detection limit is 0.1 ppm and the associated error 4%. Potassium, magnesium and calcium were analyzed in every withdrawal by ion chromatography (IC) using a Metrohm 883 Basic IC Plus Ion Chromatograph with a Metrosep C3-250 column. The eluent was prepared with 3.5 mmol L^{-1} HNO_3. The detection limit and associated error were 1 ppb and 3%, respectively.

There was no indication of decreasing of glycine concentration over time in the control solution, indicating that no bacterial degradation took place in the clay suspension during the experiment.

6.2.3. X-Ray diffraction analysis

The solids obtained after the adsorption isotherm experiment were filtered through a Durapore membrane, rinsed with ethanol/water 1:1 to remove the remaining bulk solution, and then let dry at room temperature. The solids were ground with an agate mortar and pestle and re-suspended in 1 mL of deionised water. Every suspension was placed on a glass slide and air-dried at room temperature. The resulting oriented mounts were analyzed using a PANalytical X'Pert Pro diffractometer equipped with a X'Celerator detector, CuKa radiation, operated at 45 kV and 40 mA, Ni filter and ¼° divergence slit.

6.2.4. Infrared spectroscopy

A different set of adsorption experiments was carried out for the IR analysis. The reactions of glycine with montmorillonite were conducted in acid-washed 30 mL glass vials with polytetrafluoroethylene (PTFE) caps. Ten mL of 10 mmol L^{-1} KCl (background electrolyte) were added to each vial with 0.625 g of smectite and the pH was adjusted to 4, 6 or 8. The suspensions were stirred for 3-4 minutes and let equilibrate for 24 h. After equilibration, 2.5 mL of 125 mmol L^{-1} glycine stock solution was added to each vial to reach a total concentration of 25 mmol L^{-1} and a total solid/solution ratio of 50 g clay L^{-1}. The glycine concentration was chosen as the minimum to have a good response of the IR spectrometer. Every suspension had a replicate at the same pH without glycine to use it as a reference in the spectral analysis. All the suspensions were stirred and let equilibrate for 5 h at room temperature. To separate the supernatant and the wet paste with the montmorillonite-glycine complex, the suspensions were filtered through a 0.22 μm Durapore membrane. A fraction of the solid was rinsed with a 10 mmol L^{-1} KCl solution. The clay paste with the montmorillonite-glycine complex (with and without rinsing) was removed from the filter with a spatula and placed in a horizontal flat ATR (HATR) cell. ATR-FTIR spectra were collected with a PerkinElmer Spectrum One FTIR spectrometer equipped with a lithium tantalate ($LiTaO_3$) detector and a HATR sampling accessory. The HATR cell contains a ZnSe crystal with an angle of incidence of 45°. The spectra were obtained by collecting 100 scans with a wavenumber resolution of 4 cm^{-1} in the 4000-400 cm^{-1} range and a scan speed of 0.2 cm/s. Grams/32 (Thermo Fisher Scientific Inc., 2011) program was used to plot and analyze the spectra.

All ATR-FTIR spectra obtained for wet pastes were dominated by the strong infrared absorbance of water. A subtraction procedure was necessary to isolate the spectrum of adsorbed glycine, being the most critical step to correctly remove the band originating from the bulk water. For each sample, the contribution of water was removed by subtracting the ATR-FTIR spectrum of a 0.01 mol L^{-1} KCl solution measured at the same pH. Then, the spectrum of the pure montmorillonite, normalized against the Si-O stretching vibration band at 1027 cm^{-1}, was subtracted to further enhance the signal of the adsorbed glycine over the bulk mineral.

Spectra of glycine in aqueous solutions were measured by placing 1 mL of 25 mmol L^{-1} glycine solution in a ZnSe HATR trough cell with a volume of 2 mL. The solution spectra were collected at pH 4, 6 and 8. The sample spectra were recorded in absorbance mode in the 4000-400 cm^{-1} range with a wavenumber resolution of 4.0 cm^{-1}. A total of 100 scans were collected for each spectrum at a scan speed of 0.2 cm/s.

6.3. Results

6.3.1. Quantitative analysis for glycine adsorption by montmorillonite

Indications on the mechanism of adsorption and the affinity between a particular ligand and a surface can be obtained by studying the dependence of the amount of ligand sorbed as a function of pH. Figure 6.2 illustrates that adsorption of glycine onto montmorillonite was strongly pH dependent, although the amount of glycine adsorbed is low.

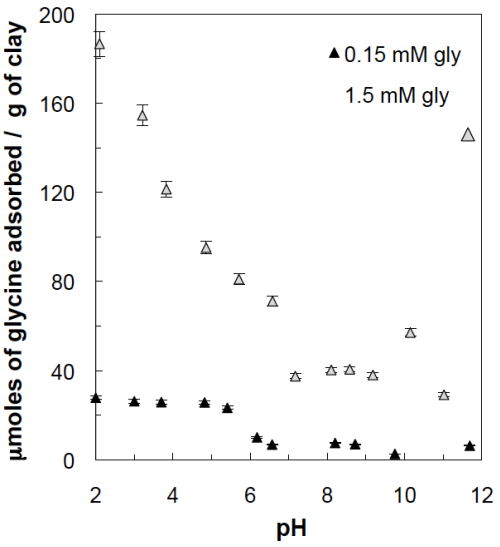

Figure 6.2. Adsorption edge of glycine onto montmorillonite. Data from the 0.15 mmol L^{-1} adsorption edge were taken from Ramos et al. (2011).

The adsorption edge follows a different trend depending on the glycine concentration. For the 0.15 mmol L^{-1} adsorption edge (data from Ramos et al., 2011) the amount of glycine adsorbed is constant from pH 2 to 5.5 with a maximum of 26 µmol g^{-1} in this range. From pH 5.5 the amount of glycine decreases progressively until pH 7, where

the glycine does not absorb onto the montmorillonite surface. For the 1.5 mmol L^{-1} adsorption edge, no adsorption plateau was observed under acidic conditions. The amount of glycine adsorbed increases progressively from pH 6.5 to 2 (maximum of 186 µmol g^{-1}). From pH 6.5 to 11 the adsorbed glycine is approximately constant (35-40 µmol g^{-1}). The concentration of glycine adsorbed is in agreement with the values reported by Hedges and Hare (1987) in their study of adsorption of amino acids onto montmorillonite.

Figure 6.3a shows the amount of glycine adsorbed on montmorillonite as a function of concentration in equilibrium solution along with the concentration of K^+ released to solution. The initial pH of every suspension drifted to higher values after the equilibration (Table 6.1).

Table 6.1. pH values of the suspensions of montmorillonite in glycine solutions before and after 5 h equilibration for the various concentrations of glycine. The pH was adjusted by adding little amounts of 1 mol L^{-1} HCl (for detailed procedure, see section 2.2.).

Glycine (mol L^{-1})	Suspension pH before equilibration	Suspension pH after equilibration
0	2.60	2.66
0.001	2.58	3.11
0.003	2.72	3.20
0.01	2.77	3.18
0.03	2.71	3.05
0.1	2.76	3.06
0.3	2.74	3.01

The isotherm is similar in shape and values to others reported for lysine (Parbhakar et al., 2007), glutamic and aspartic amino acids (Siffert and Naidja, 1992). The shape of the isotherm suggests that the adsorption maximum is not reached at the maximum concentration of glycine studied. The adsorption isotherm is L-type (Giles et al., 1974), suggesting a progressive saturation of the solid. Adsorption data were fitted to the logarithmic form of the Freundlich equation (Fig. 6.3b):

$$\log A = \log K_f + n \log C \qquad (6.1)$$

where A is the concentration of adsorbed glycine (mmol g^{-1}), C is the concentration of glycine in the equilibrium solution (mol L^{-1}) and K_f and n are experimental parameters.

Glycine shows a Freundlich-like sorption behavior throughout all the concentration range studied at pH 3.

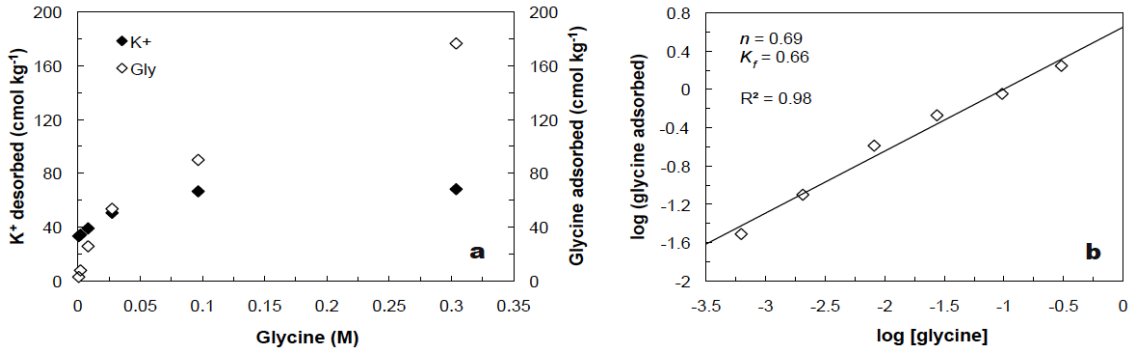

Figure 6.3. a) Potassium desorbed and glycine adsorbed vs. equilibrium concentration of glycine at pH 3. b) Logarithmic plot of the isotherm adsorption data showing the Freundlich sorption behavior.

In Figure 6.3a it is also shown the concentration of potassium released to the solution, which is displaced from the interlayer (41%) even when glycine is not present. Fast release of cations from the interlayer sites of phyllosilicates has been observed by Bibi et al. (2011) at acidic pHs and they suggested that it was due to the exchange reactions with H_3O^+ from the solution. The presence of interlayer hydronium ion may produce an apparent deficit of interlayer cations in some phyllosilicates (Nieto, 2002; Nieto et al., 2010). In order to test the K^+-H_3O^+ exchange, an additional experiment was carried out. Ten mL of a solution at pH 3 (1 mmol L^{-1} HCl) were added to 0.1 g of clay. After 5 h of equilibration, the pH drifted from pH 3.10 to 5.07 and the concentration of K^+ in the supernatant reached 39.5 ppm, equivalent to 10 cmol kg^{-1} of exchanged potassium. The pH drift together with the release of K^+ to the supernatant provide a direct evidence of the K^+- H_3O^+ exchange reaction.

The concentration of released K^+ slightly increases with the concentration of glycine, and it remains constant with a value of 68 cmol kg^{-1} for a concentration of glycine above 0.1 mol L^{-1}. For a concentration of glycine in solution higher that 0.03 mol L^{-1}, the amount of adsorbed glycine exceeds the exchanged K^+. In order to keep the structural charge balanced, only a fraction of the intercalated glycine should contribute to the interlayer charge.

6.3.2. ATR-FTIR analysis of glycine sorption by montmorillonite

The comparison and analysis of the ATR-FTIR spectra of glycine in solution and on montmorillonite surface gives useful information about the nature of the amino acid-clay interaction.

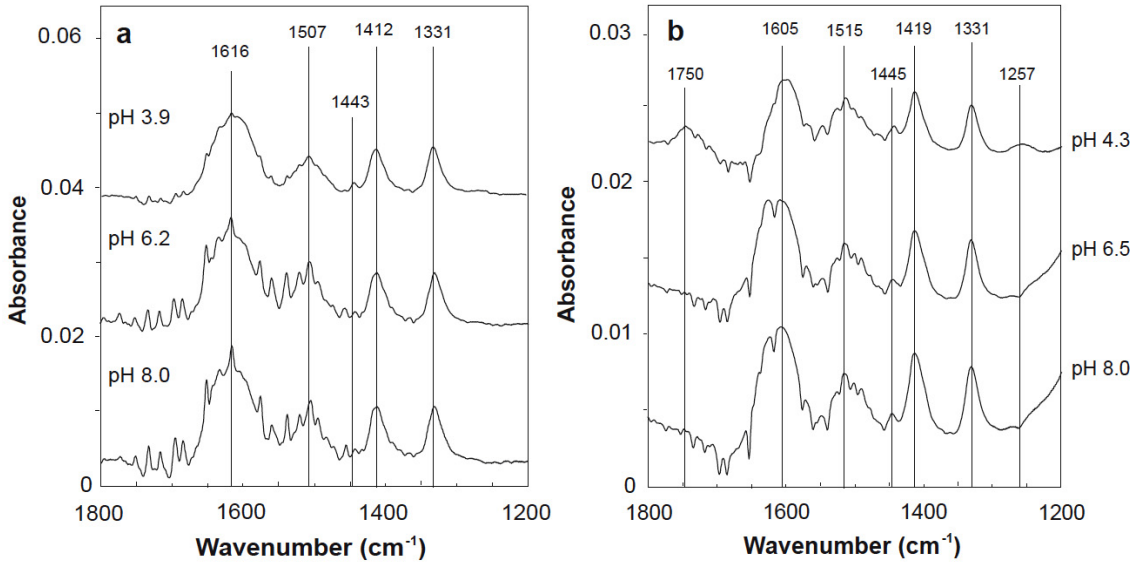

Figure 6.4. a) ATR-FTIR spectra of 25 mmol L^{-1} glycine solutions at pH 3.9, 6.2 and 8. b) ATR-FTIR spectra of paste glycine/montmorillonite complexes at pH 4.3, 6.5 and 8.

Figure 6.4a shows the ATR-FTIR spectra of glycine in aqueous solutions at pH 4, 6 and 8. The studied region is between 1800 and 1200 cm^{-1}. This frequency region covers most of the main vibrational signature of glycine and excludes infrared peaks due to montmorillonite vibrations (Farmer, 1974). At the studied pH values, the most abundant specie is the zwitterionic form of glycine. The characteristic bands of glycine in aqueous solutions fall within the expected ranges. The bands were assigned according to Meng et al. (2004) (Table 6.2).

In Figure 6.4b the ATR-FTIR spectra of glycine adsorbed onto montmorillonite at pH 4, 6 and 8 are shown. The spectra of adsorbed glycine is similar to that found for glycine in aqueous solution, indicating that a part of glycine is in zwitterionic form. Nevertheless, two features appear when the spectra of glycine adsorbed on montmorillonite are compared with the spectra of zwitterion glycine molecules in solution. At the lowest pH studied (pH 4.3), a new band appears at 1750 cm^{-1} due to the carbonyl-stretching mode of the unionized carboxyl group (Meng et al., 2004). Moreover, the band due to δCOH of the carboxylic group can be found at 1257 cm^{-1},

which implies that the glycinium cation is present in this sample. These results are evidences of the presence of glycine in the interlayer space as both glycinium and zwitterion, whose relative abundance should depend on the pH conditions within the smectite interlayer space. The spectra were roughly similar to that of aqueous glycine, which suggests a dominant outer-sphere adsorption mode. Nevertheless the small shift of the bands provides evidences of the interaction between glycine and clay surface. The band $\delta_s NH_3$ shifts from 1507 to 1515 cm^{-1} at all the pHs studied, suggesting an interaction of the amino group with the inner clay surface. Furthermore, the carboxylate-montmorillonite interaction at the edge surface can be derived by the shift in the position of the asymmetric stretch to a lower wavenumber (from 1616 cm^{-1} to 1605 cm^{-1}) and the symmetric stretch to a slightly higher wavenumber (from 1412 cm^{-1} to 1419 cm^{-1}) at all the pHs studied.

Table 6.2. Assignments of main aqueous and adsorbed glycine IR bands in the 1800-1200 cm^{-1} region

Assignment*	Aqueous gly	Adsorbed gly
	Wavenumber (cm^{-1})	Wavenumber (cm^{-1})
$\upsilon C=O$		1750
$\upsilon_{as} COO$	1616	1605
$\delta_{as} NH_3$	1615	1615
$\delta_s NH_3$	1507	1515
$\delta_s CH_2$	1443	1445
$\upsilon_s COO$	1412	1419
$\rho_w CH_2$	1331	1331
δCOH		1257

* υ, stretching mode; $\delta_{as/s}$, asymmetric/symmetric deformation mode; ρ_w, wagging mode.

6.3.3. X-Ray analysis

Figure 6.5 shows the XRD patterns for the montmorillonite after the reaction with glycine solutions with different concentrations at pH 3. The 001 peak has different intensity, position and shape depending on the glycine concentration. The 001 peak is progressively narrower and shifted to lower d-spacing from 14.5 to 12 Å when the concentration of glycine increases. The samples with higher amounts of glycine showed

a narrower basal reflection, thus indicating a more ordered structure than the K smectite.

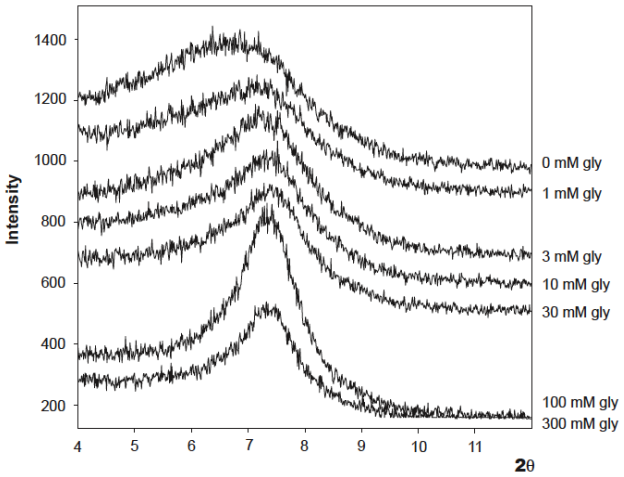

Figure 6.5. XRD patterns of glycine adsorbed on montmorillonite at different glycine concentrations at pH 3.

The shape of low angle peaks in hydrated smectites is the result of several factors, as layer arrangements, hydration of interlayer cations, size of scattering domain, etc. The spacing of the sample without glycine may correspond to a mixture of interlayered cations, mainly K^+ and hydronium (see next section) and, in minor amount, Ca^{2+} and Mg^{2+} (they represent approximately 6% of interlayer charge) that produce a wide range of hydration states, probably within individual layers; this will result in small diffraction domains. As more and more glycine penetrates the interlayer, the interlayer space acquires a more homogeneous arrangement of glycine, water and cations, resulting in more parallel layers, more similar individual d-spacings and larger coherent scattering domains.

6.4. Discussion

Ligand adsorption is the result of the interaction between ligand and smectite at the mineral/solution interface. Glycine adsorption by montmorillonite is influenced by glycine concentration in solution and pH (Fig. 6.2) since the ligand protonation state (Fig. 6.1) and the smectite surface charge (Rozalén et al., 2009a) are both pH-dependent. The shape of the 0.15 mmol L^{-1} adsorption edge is different from that

obtained with 1.5 mmol L^{-1} of glycine, suggesting that the mechanism that controls the adsorption is different in every case.

At low glycine concentrations, the shape of the adsorption edge shows that there is only one mechanism of adsorption in the pH range studied. The shape of this adsorption edge is consistent with the development of positive charge by protonation of aluminol sites below pH ~7 (Rozalén et al., 2009a). Thus, between pH 3 and 7 the zwitterion form of glycine is in contact with the positively charged edges, and electrostatic interaction can occurs. The interaction occurs through the $–COO^-$ group of the zwitterion form of glycine and the $>AlOH_2^+$ groups. From pH 3 to 2, the relative abundance of the zwitterion form diminishes from 77% to 23%, but the adsorption remains constant below pH 5.5. Probably the increase in the relative abundance of $>AlOH_2^+$ groups in more acidic conditions may compensate the decrease of the proportion of the zwitterion form, in such a way that the measured adsorbed concentration remains constant. The quantity of glycine adsorbed, 26 μmol g^{-1}, suggests that adsorption at low concentrations of glycine is likely limited to the smectite edges. The trend of the shifts observed in the ATR-FTIR spectra for the $\upsilon_{as}COO$ and υ_sCOO bands of the adsorbed glycine also provide an evidence for the formation of outer-sphere complexes at the smectite edge surface (Hwang et al., 2007).

At a glycine concentration of 1.5 mmol L^{-1} the shape of the adsorption edge is different from that found at low concentrations. The adsorption of glycine decreases progressively from pH 2 to 6.5 and reaches a plateau from pH 6.5 to 11 (average 35-40 μmol g^{-1}). The quantity of glycine adsorbed exceeds the sites available at the smectite edges, which correspond to an aluminol edge surface concentration of 38 mmoles g^{-1}, equivalent to 3.55 sites nm^{-2} (Rozalen et al., 2009a, Table 6.3). For example, at pH 2 the adsorbed glycine (212 mmoles g^{-1}) is almost 5 times the edge site density. The results shown in Figure 6.2 suggest that glycine is first adsorbed in the smectite edges and after the saturation of the edges, glycine occupies the interlayer sites, through ion exchange with interlayered cations, K^+ in our case.

For glycine concentrations higher than 0.03 mol L^{-1}, the concentration of adsorbed glycine is higher than the amount of K^+ displaced (Fig. 6.3a). This supports that cation exchange is not the only adsorption mechanism to account for glycine adsorption.

Glycine is taken up as glycinium by ion exchange with the interlayered cations. Then the equilibrium glycinium-zwitterion (Gly^+/Gly-zw) within the interlayer space permits the uptake of additional Gly^+. In such a way the equilibrium of glycine species contributes to keep the structural charge balanced. This hypothesis is supported by the ATR-FTIR spectra of adsorbed glycine, as bands characteristics of glycinium and zwitterion are observed at pH 4 (Fig. 6.4b).

Other studies confirm that the adsorption of amino acids onto montmorillonite is a result of the electrostatic interactions between the clay surface and the amino acid (Hedges and Hare 1987; Kitadai et al., 2009) or through hydrogen bonding with the zwitterionic form (Cloos et al., 1966). However, Friebele et al. (1980) found that the very large increase in adsorption with decreasing pH indicates that the adsorption mechanism is due to cationic exchange, because glycine is in cationic form under acidic conditions. They also found that at higher pH values the proportion of amino acids weakly adsorbed (ion-dipole interaction, hydrogen bonding or van der Waals forces) increases with respect to the amino acids strongly adsorbed.

It is generally accepted that amino acids adopt a configuration in the smectite interlayer by which —NH_3^+ groups are near the basal surface of the clay due to coulombic attraction to the residual negative charge of the oxygen atoms, and where —NH_3^+ groups and oxygen atoms can form hydrogen bonds (Parbhakar et al., 2007; Kollár et al., 2003). ATR-FTIR data provides evidence of this type of interaction. The shift in the symmetric deformation band of —NH_3^+ from 1507 to 1515 cm^{-1} (Fig. 6.4b) indicates a direct bond between the —NH_3^+ group and the basal oxygen atoms in the interlayer (Serratosa et al., 1970; Kitadai et al., 2009). Benetoli et al. (2007) also found that the amino group was involved in the adsorption of several amino acids on clays based on FT-IR results. Thus for glutamine, they detected a change in —NH_2 to —NH_3^+ by the interaction of an electron pair of the —NH_2 group with the surface of the clay. Other studies of glycine adsorption on silica support that the adsorption mechanism depends on hydrogen bonds between the amino acid and the silica surface groups (Meng et al., 2004; Stievano et al., 2007).

Bujdak and Rode (1996) studied the polymerization of several amino acids using smectites of varied composition and found that only 1.5% of the adsorbed glycine was polymerized in experiments with Wyoming SWy-1 smectite. In our experiments

glycine oligomerization is unlike to occur to any significant extent. Amide bands corresponding to peptide bonds were not observed in the IR spectra in our glycine–smectite complexes (Fig. 6.4b).

Our results suggest that a fraction of the intercalated glycine do not contribute to interlayer charge. There exist two interlayer sites per smectite unit cell. In our sample, only one is occupied by exchangeable cations to balance structural charge (1.01 per unit cell). Additional space is available to accommodate other interlayered species. Glycine molecule (4.3×3.2×1.8 Å, Accelrys Software Inc., 2009) can be located within the interlayer space (~6.1 Å in diameter, Bailey, 1984). We can try to estimate an average composition of the interlayer space to get to know how glycine is intercalated. The structure neutrality requires layer charge (σ) to be balanced by interlayered species as K^+, hydronium ions (H_3O^+) and glycinium (Gly^+), according to the following charge balance equation:

$$\sigma = \{K^+\} + \{H_3O^+\} + \{Gly^+\} \quad (6.2)$$

where {} denotes concentration in the interlayer.

The concentrations of Mg^{2+} and Ca^{2+} (14.5 and 15.3 ppm, respectively) in the supernatant of the point with higher concentration of glycine in the adsorption isotherm are consistent with the complete desorption of the exchangeable Mg^{2+} and Ca^{2+}. This represents a contribution of 0.03 divalent cations or 0.06 interlayer charges per formula unit. The analysis of the solution 0.3 mol L^{-1} in glycine at pH 3 gives 68 cmol kg^{-1} of K^+ desorbed (equivalent to 0.52 atoms per formula unit). The glycine adsorbed is 176 cmol kg^{-1} (1.35 molecules per formula unit, distributed in the edges (0.03) and the interlayer (1.32) adsorption sites).

Three hypotheses has been explored:

I. The equilibrium of glycine species corresponds to the pH of the solution (pH 3). The layer charge is completed with protons (Eq. 2).

II. The two interlayer sites per formula unit are occupied. Proton concentration is fitted to satisfy this condition:

$$\{K^+\} + \{H_3O^+\} + \{Gly_{total}\} = 2 \quad (6.3)$$

The equilibrium of glycine species is shifted to balance the charge. The interlayer pH is deduced from glycine speciation (Fig. 6.1).

III. No interlayer protons. The equilibrium of glycine species is shifted to balance the layer charge. The interlayer pH is deduced from glycine speciation.

The constraints and results are gathered in table 6.3. The third hypothesis is the less plausible, as without considering exchangeable hydronium, the interlayer pH (~2.6) is lower that the solution pH. In addition this may be inconsistent with the behavior of the sample at low glycine concentration in solution, being K^+ exchanged for hydronium.

Table 6.3. Distribution of ionic and molecular species in the smectite interlayer space in equilibrium with a solution at pH 3 with 0.3 mol L^{-1} of glycine. (See text for details; I, II, II are the three hypotheses explored). If no units are specified, numbers are in atoms per formula unit.

Smectite characteristics			
- $K_{0.95}Mg_{0.02}Ca_{0.01}(Al_{2.79}Fe^{3+}_{0.35}Mg_{0.86})(Si_{7.84}Al_{0.16})O_{20}(OH)_4$			
- Formula weight: 766 g			
- CEC: 94 $cmol^+ kg^{-1}$			
- Exchangeable cations: 0.67			
- Non-exchangeable K^+: 0.34			
- Total layer charge: 1.01			
- Aluminol sites (>AlOH): 3.55 sites nm^{-2} = 0.03			
- Interlayer sites per formula unit: 2			
Equilibrium solution (pH 3.01, 0.3 mol L^{-1} Gly)			
- Gly_{total} adsorbed: 176 cmol kg^{-1} = 1.35			
o Edges: 0.03			
o Interlayer: 1.32			
- Desorbed cations (as monovalent): 0.58			
o K^+: 68 $cmol^+ kg^{-1}$ = 0.52			
o Mg^{2+}: 0.02, equivalent 0.04			
o Ca^{2+}: 0.01, equivalent 0.02			
Interlayer composition (in atoms per formula unit)	I	II	III
K^+	0.47	0.47	0.47
$Gly_{ads, total}$	1.32	1.32	1.32
- Fraction (%) of glycine as Gly^+	23	28	44
- Gly^+	0.30	0.37	0.58
- Gly-zw	1.02	0.95	0.74
H_3O^+	0.25	0.21	-
Interlayer sites occupied per formula unit	2.04	2.00	1.79
pH interlayer	3.0	2.89	2.60

Hypotheses I and II produce quite similar results, both consistent with ATR-FTIR results. In hypothesis I, there is a slight excess of interlayered species, that can be

allocated in the interlayer. Hypothesis II represents a scenario where the pH in the interlayer space (2.85) is slightly lower that in the solution, in agreement with the presence of exchangeable hydronium and the acidic character of the smectite interlayer. Despite the differences, both results are similar within the uncertainty of the analyses. They show that glycine can be allocated within interlayer space in a concentration exceeding the CEC, due to the presence of neutral or zwitterionic glycine.

5. CONCLUSIONS

The combination of ATR-FTIR spectroscopy, X-ray diffraction analysis and macroscopic adsorption data verified that glycine is adsorbed by cation exchange into montmorillonite, although cation exchange is not the only mechanism implicated in the adsorption of glycine. This amino acid can be allocated in the interlayer space as both glycinium and zwitterion. The adsorption edge trend indicates the existence of electrostatic interactions between the carboxylic acid species and the edge surface sites. Once the smectite edge sites are saturated, glycine is adsorbed by intercalation.

The measured adsorption was sufficiently great to potentially affect the distribution and reactions of free amino acids in natural environments. These results have also implications for methodologies that are applied in amino acid analyses of geochemical samples.

7. Modeling the adsorption of oxalate onto montmorillonite

7. MODELING THE ADSORPTION OF OXALATE ONTO MONTMORILLONITE

Abstract.- Previous results from macroscopic adsorption data of oxalate on montmorillonite in 0.01 M of KNO_3 media at 25°C within the pH range from 2.5 to 9 have been used to develop a surface complexation model.

The experimental adsorption edge data were fitted using the Triple Layer Model (TLM) with the aid of the FITEQL 4.0 computer program. Surface complexation of oxalate is described by two reactions:

$>AlOH + Ox^{2-} + 2H^{+} = >AlOxH + H_2O$ logK = 14.39

$>AlOH + Ox^{2-} + H^{+} = >AlOx^{-} + H_2O$ logK = 10.39

The monodentate complex >AlOxH dominated adsorption below pH 4, and the bidentate complex $>AlOx^{-}$ was predominant at higher pH values. Both the proposed inner-sphere oxalate species are qualitatively consistent with previously published diffuse reflectance FTIR spectroscopic results for oxalate on montmorillonite edge surface (Ramos et al., 2013).

7.1. Introduction

The interaction of organic acids with mineral surfaces in electrolyte solutions is of great interest to a wide range of geochemical topics and processes. One of the properties of low molecular weight organic anions is to promote the mineral dissolution. Their capacity to catalyze the dissolution reaction arises from their ability to strongly bind to mineral surfaces in an inner-sphere manner (e.g. Zutic and Stumm, 1984; Furrer and Stumm, 1986; Stumm and Furrer, 1987; Chin and Mills, 1991). The polarization of the surface metal-organic anion bonds gives rise to the release of the metal cations from the surface through a rate-determining detachment step. Although extensive work has been done to identify the type and structure of surface complexes of relatively simple organic acids at mineral/water interfaces (Nordin et al., 1997; Nordin et al., 1998; Dobson and McQuillan, 1999; Axe and Persson, 2001), a molecular-level understanding of these interactions is not complete. Two major types of surface complexes have been suggested: inner-sphere (direct bond between carboxylate oxygen and surface cations) and outer-sphere complexes (carboxylate

oxygen held at the surface through a combination of hydrogen bonding and electrostatic interactions).

In a previous study, Diffuse Reflectance Fourier-Transform Infrared spectroscopy (DR-FTIR) was used to identify the types of oxalate surface complexes on the montmorillonite surface (Ramos et al., 2013). However, due to the limited amount of oxalate sorbed it was difficult to make a statement about the type of complexes formed. The quantitative adsorption was also studied at different oxalate concentrations. In order to better understand the oxalate-montmorillonite interaction, the experimental results obtained are integrated with a surface complexation model, which establishes the stoichiometry of the adsorption reactions and provides a thermodynamic characterization of the equilibria involved.

The phyllosilicate mineral montmorillonite is the focus of the present study because its prevalence in soils and sediments. Montmorillonite dissolution mechanism and reactivity have been widely investigated in previous work (Furrer et al., 1993; Zysset and Schindler, 1996; Baeyens and Bradbury, 1997; Bauer and Berger, 1998; Cama et al., 2000; Huertas et al., 2001; Amram and Ganor, 2005; Metz et al., 2005a,b; Rozalén et al., 2008; Rozalén et al., 2009a,b; Ramos et al., 2011).

In the present work the adsorption of oxalate at the edge surface of montmorillonite has been successfully modeled base on results from previous investigations (Ramos et al., 2013). The results of this study allow making quantitative predictions that can facilitate evaluation of the potential role of mineral surface chemistry in several geochemical processes involving the interactions of organic molecules and mineral surfaces.

7.2. Materials and methods

7.2.1. Materials

The montmorillonite sample used in the present study was the same than the one used by Ramos et al. (2011). The specific surface area measured by BET (Brunauer et al., 1938) was 111 $m^2 g^{-1}$ with an associated uncertainty of 10%. The edge surface area was estimated to be 6.5 $m^2 g^{-1}$ (Rozalen et al., 2008). For a complete montmorillonite characterization the reader is referred to Ramos et al. (2011).

7.2.2. Adsorption experiments

In this study, we used adsorption data previously reported in Ramos et al. (2013). For the sake of clarity, we repeat the experimental information that is relevant to this data.

Quantitative adsorption of oxalate on montmorillonite was studied at 25°C using the batch equilibrium method. Batch samples with a solid concentration of 10 g L^{-1} and a total concentration of oxalate of 0.1 mmol L^{-1} were prepared in 30 mL Corex centrifuge tubes with polytetrafluoroethylene (PTFE) caps. In order to cover a wide range of pH's (from 3 to 9 units), precise volumes of HCl or KOH were added to each sample using 10 mmol L^{-1} KCl as background electrolyte. Preliminary kinetic experiments indicated that the adsorption of oxalate reached a steady state within the first 5 h after addition of oxalate to a montmorillonite suspension. After the filtration of every supernatant, oxalate was analyzed using a Dionex ion chromatograph equipped with an AS50 autosampler, a GP50 gradient pump, an AS50 thermal compartment, EG40 eluent generator and ES50 electrochemical detector. By calculating the difference between the known total concentration and the remaining concentration in the supernatant after equilibration, the quantity of oxalate adsorbed on the surface of montmorillonite was determined in each sample.

The adsorption modes of oxalate on montmorillonite have been examined in a previous work (Ramos et al., 2013) using Diffuse Reflectance Fourier Transform Infrared (DR-FTIR) spectroscopy.

7.2.3. Modeling the adsorption data

The macroscopic adsorption edge data shown in Fig. 7.1 can be tentatively linked with the DR-FTIR data results using a suitable surface complexation model.

Montmorillonite edge surface contains functional groups with oxygen atoms, which are coordinated by different numbers of protons and silicon and aluminum. These groups can accept and release protons and also take part in complexation reactions with metal ions and ligands. Because the low ability of Si to form complexes in solution (Pokrovsky and Schott, 1998), complexation reactions of silanol groups of

the surface have not been considered in our conceptual model. The reactive edge surface can be described as a homogeneous surface with only one type of reactive hydroxyl group (>AlOH), which is responsible for all surface complexation reactions. This relatively simple model of surface groups is often satisfactory for modeling of adsorption data (Nordin et al., 1998).

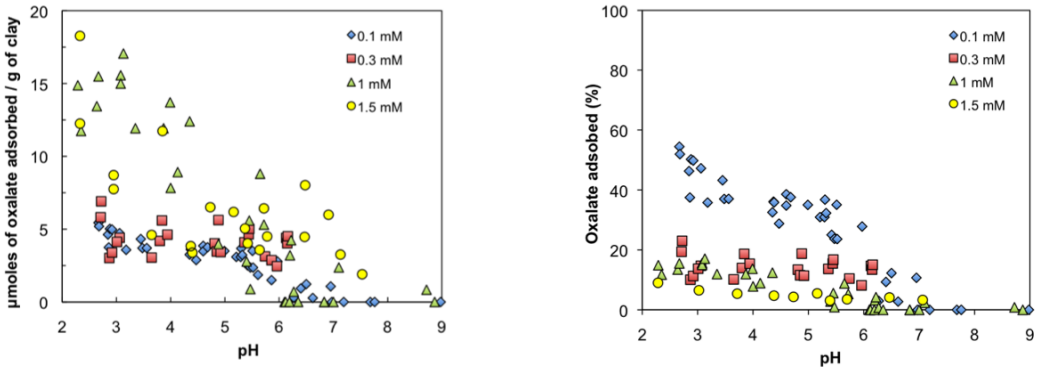

Figure 7.1. Experimental data of adsorption of oxalate on montmorillonite as a function of pH at varying ligand concentrations: (a) ads. in mmol g^{-1} and (b) ads. in % (data from Ramos et al., 2013).

Both inner- and outer-sphere complexation at the montmorillonite surface may be considered according to the experimental DR-FTIR results previously reported in Ramos et al. (2013). The DR-FTIR results also indicated that oxalate adsorbs in a mononuclear manner and therefore, binuclear complexes have not been considered in our conceptual model. The Triple Layer Model (TLM) can distinguish inner- and outer-sphere complexes: sorbates forming inner-sphere complexes are typically placed on the o-plane, whereas those forming outer-sphere complexes are placed on the β-plane (Fig. 7.2). The inner layer (between the surface plane and the β-plane) and the outer layer (between the β-plane and the bulk solution) have their own constant capacitance values, C_1 and C_2, respectively.

In our study, the surface site density and protolysis constants for aluminol edge sites optimized by Rozalen et al. (2009a) were adopted. Protonation and deprotonation reactions are assumed to occur on the inner plane, and are described by the reactions:

$$>AlOH_2^+ = >AlOH + H^+$$

$$>AlOH = >AlO^- + H^+$$

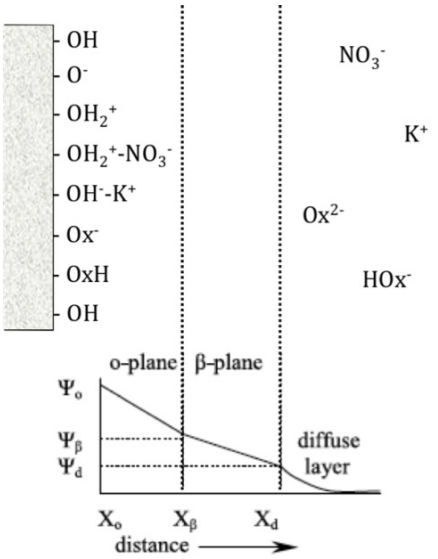

Figure 7.2. Schematic representation of the electrical properties and location of the complexes formed (modified from Hayes et al., 1991).

The free concentration of the background electrolyte ions (K^+, NO_3^-) 0.01 mol L^{-1} is assumed to remain constant in the experiments. The equilibrium constants for the oxalate acid/base reactions and the montmorillonite surface protonation/deprotonation, as well as the density of surface aluminol groups and the outer and inner capacitance for the electrostatic double layer were considered as known parameters and used without modifications (Table 7.1).

The protonation reaction constants of oxalate were collected from Filius et al. (1997). Preliminary tests with the chemical speciation program MEDUSA (Puigdomenech, 2004) showed that the formation of Al-oxalate aqueous complexes is negligible under our experimental conditions (oxalate concentration = 0.1 mmol L^{-1}) and thus they were not considered in the model. The equilibrium constants for the outer-sphere complexes $>AlOH_2^+$-NO_3^- and $>AlO^-$-K^+ published previously for γ-Al_2O_3 (Reich et al., 2011) and illite (Kulik et al., 2000), respectively, were used to complete the set of constants required to implement the TLM. Unfortunately, the assumption that electrolyte ions are bounded in the outer layer plane led to poor fit of the data. Therefore, the formation reactions of $>AlOH_2^+$-NO_3^- and $>AlO^-$-K^+ were modeled by placing the electrolyte ions in the inner plane. The effect of this change is not expected to be substantial according to the low background electrolyte concentration (0.01 mol L^{-1}) used in the macroscopic adsorption experiments (Johnson et al., 2004b).

Table 7.1. Parameters of the surface complexation model

	log K	Reference
Protonation of oxalate		
$Ox^{2-} + H^+ = HOx^-$	4.27	(1)
$Ox^{2-} + 2H^+ = H_2Ox$	5.52	(1)
Surface reactions (*I*=0.01 mol L^{-1})		
$>AlOH_2^+ = >AlOH + H^+$	6.44	(2)
$>AlOH = >AlO^- + H^+$	-9.94	(2)
$>AlOH + H^+ + NO_3^- = >AlOH_2^+\text{-}NO_3^-$	8.30	(3)
$>AlOH - H^+ + K^+ = >AlO^-\text{-}K^+$	-9.20	(4)
$>AlOH + Ox^{2-} + H^+ = >Al\text{-}Ox^- + H_2O$	10.39	(5)
$>AlOH + Ox^{2-} + 2H^+ = >AlOxH + H_2O$	14.39	(5)
Other parameters		
Site density for >AlOH (sites nm^{-2})	3.55	(2)
S_{edges} (m^2 g^{-1})	6.5	(2)
Inner capacitance (F m^{-2})	1.0	(6)
Outer capacitance (F m^{-2})	0.2	(6)

[1] Filius et al. (1997), [2] Rozalen et al. (2009a), [3] Reich et al. (2011), [4] Kulik et al. (2000), [5] This study, [6] Hayes et al. (1991)

The experimental data were evaluated using the program FITEQL 4.0 (Herbelin and Westall, 1999). Since oxalate was present in the solution as H_2Ox, HOx^- and Ox^{2-}; and Ox^{2-} is used as main component in the definition of the equilibrium model for the surface complexation, it is convenient to represent the measured aqueous oxalate concentration by a parameter that is independent of the aqueous speciation. Therefore, the entering of data into FITEQL was done as described in Westall and Herbelin (1992) using a dummy component, Ox(ads), which represents the total concentration of adsorbed oxalate. Ox(ads) was calculated for each data point as the difference between the total concentration of oxalate added and the analyzed total concentration in solution (see section 2.2.).

The evaluation of the experimental data in the system H^+ - >AlOH - oxalate consisted of a systematic test of combinations of inner- or outer-sphere complexes with different compositions and an optimization of the corresponding equilibrium constants. The combination of complexes giving the lowest average WSOS/DF (V(Y)) was considered the best fitting model. Moreover, special attention was focused on

making sure that the final model was in good semiquantitative agreement with previously reported FTIR spectroscopic measurements (Ramos et al., 2013).

7.3. Results and discussion

The TLM fit for oxalate sorption to montmorillonite is satisfactory (V(Y)=21.7), although montmorillonite is not a strong oxalate sorbent. The best fit is achieved when oxalate sorption is represented by the reactions:

$>AlOH + Ox^{2-} + 2H^{+} = >AlOxH + H_2O$

$>AlOH + Ox^{2-} + H^{+} = >AlOx^{-} + H_2O$

These reactions support the hypothesis that oxalate sorption to montmorillonite is dominated by specific sorption to amphoteric aluminol edge sites in the whole pH range studied (3-9). The DR-FTIR data obtained in the previous work (Ramos et al., 2013) agree with the proposed model in acidic conditions, since the spectra suggested that the formation of the complex $>Al\text{-}Ox^{-}$ was favored at low pH. However, modelization results indicate that this complex exist in the whole pH range studied, with a maximum concentration at pH 5. This complex involves one surface Al atom to form a mononuclear, bidentate, 5-member ring, which has been also observed for adsorption of oxalate on Al_2O_3 (corundum) (Johnson et al., 2004b) and γ-AlO(OH) (boehmite) (Axe and Persson, 2001; Yoon et al, 2004). The infrared spectra also suggested the formation of the monodentate outer-sphere complex $>AlOH\cdots Ox^{2-}$ in the whole pH range studied. However, the introduction of outer-sphere complexes in the model led to poor convergence characteristics. On the other hand, the addition of the monodentate inner-sphere complex >AlOxH in the model led to a good fitting at pH < 5.5.

Speciation diagram for 0.1 mmol L^{-1} oxalate adsorbed onto montmorillonite, calculated from the model parameters given in Table 7.1, is shown in Figure 7.3. The monodentate inner-sphere complex >AlOxH dominates from pH 2.5 up to pH 4. The bidentate inner-sphere complex $>AlOx^{-}$ is significant above pH 4.

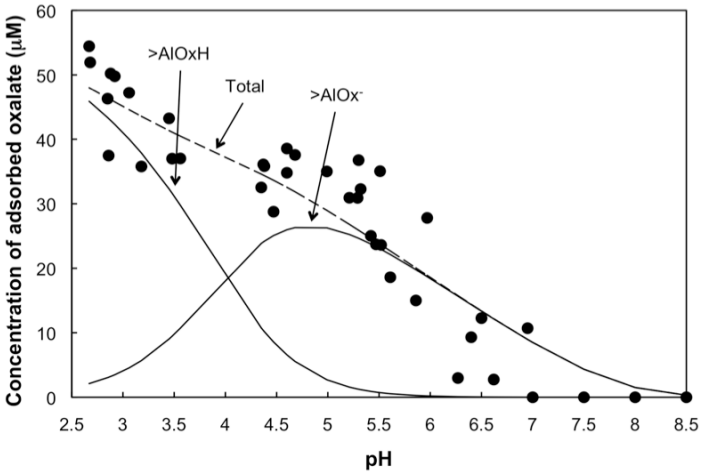

Figure 7.3. Speciation diagram of oxalate adsorption at 25°C from 0.1 mmol L^{-1} solution onto montmorillonite, calculated from the surface complexation model. Model parameters are detailed in Table 7.1. Filled circles: experimental adsorption edge data previously reported in Ramos et al. (2013); Black solid lines: model results for the individual contribution of each oxalate surface complex; Dashed black line: overall model fit to experimental data for oxalate sorption.

In general, there is a good fit to all data. Nevertheless, at pH > 6 the model fit probably overestimates the extent of oxalate adsorption. This phenomenon can be due to competitive solution complexation of oxalate by dissolved Al^{3+} (Ramos et al., 2013).

The model fit for adsorption edges with higher concentrations of oxalate (0.3, 1 and 1.5 mmol L^{-1}) is also satisfactory and the general trend for the model fit is in good agreement with the experimental observations, taking into account the data dispersion.

The adsorption reaction constant for the complex $>AlOx^-$ (logK=10.39) is very similar to that reported for Al_2O_3 by Zutic and Stumm (1984) (logK=11.00) and for α-Al_2O_3 by Johnson et al. (2004b) (logK=10.22).

7.4. Conclusions

The macroscopic behavior the adsorption of oxalate on montmorillonite was successfully modeled using the TLM. Two geometries were identified for the surface complexes: the first one, the monodentate complex >AlOxH dominated adsorption below pH 4, and the bidentate complex $>AlOx^-$ was predominant at higher pH values. Both the proposed inner-sphere oxalate species were qualitatively consistent with DR-FTIR spectroscopic results.

8. Conclusions

8. CONCLUSIONS

The results of this Thesis contribute to a deeper understanding of the dissolution mechanisms of inhaled clay particles in the presence of organic ligands. The effect of lactate, citrate and glycine on the K-montmorillonite dissolution rate was investigated at 37°C at pH 4 and 7.5. The effect of oxalate was also investigated at 25°C from pH 3-8. To elucidate the dissolution mechanism, the adsorption of lactate, citrate, glycine and oxalate onto the montmorillonite surface in the pH range between 2 and 10 was also studied. The partial conclusions of this dissertation have been introduced at the end of each chapter and are gathered below:

Chapter 3: Effect of lactate, glycine and citrate on the kinetics of montmorillonite dissolution

- In ligand-free solutions, the rates show the typical dependence on pH observed for Al-silicates and complex oxides: the rates decrease with increasing pH in acidic conditions, reaching a minimum at near neutral pH and increase with increasing pH at more basic conditions. The dissolution is stoichiometric at steady-state conditions for pH $\leq$ 4.5. Under near neutral pH conditions, the dissolution is incongruent due to a back-precipitation and/or sorption of Al.

- The addition of lactate and glycine does not produce any relevant change in the dissolution rate both at pH 4 and 7.5, and the Si-derived dissolution rates values are very similar to those found in absence of organic ligands.

- Citrate enhances montmorillonite dissolution rate, approximately 3 times (half order of magnitude) at pH 4 and 10 times at pH 7.5 for 15 mmol L^{-1} citrate. Montmorillonite dissolution in citrate solution is stoichiometric at pH 4, but incongruent at pH 7.5.

- The lactate, citrate and glycine adsorbed onto smectite in acidic conditions (pH < 8), although the adsorption pattern and mechanism were different each other. The affinity for the edge surface of montmorillonite follows the tendency: citrate < glycine < lactate.

- The shape of the adsorption edges suggests that surface complexes form by electrostatic interaction between positively charged montmorillonite surface and deprotonated ligands.

- From the reduction of particle diameter with time in this study it can be concluded that the efficiency of lung fluids to induce the chemical degradation of inhaled clayey particles (smectites, illites, micas) is very low. In addition, the release of elements such as Si or Al may have additional consequences for human health. Strong complexants as citrate and oxalate contribute to the transport of released elements such as Al.

- The application of geochemical methods may help health science in the understanding of the hazard of toxic minerals as well as those considered as inert such as clay minerals.

Chapter 4: Effect of oxalate on the kinetics of montmorillonite dissolution

- Oxalate enhances the montmorillonite dissolution reaction from pH 4 to 8, reaching a maximum of 0.5 logarithmic units with respect to ligand-free conditions at pH 7.

- Oxalate adsorbs onto montmorillonite from pH 2 to 8. The adsorption edge trend suggests that the interaction between oxalate and montmorillonite surface occurs at the aluminol sites locates at the particle edges.

- DRIFT results suggest that oxalate adsorbs onto the edge surface in an outer-sphere mode in all the pH range studied. At low pH, the inner-sphere complexation is favored.

Chapter 5: Adsorption of lactate and citrate on montmorillonite

- ATR-FTIR spectroscopic data suggest that lactate is weakly adsorbed at the positively charged edge surface sites.

- The DLM was used to model lactate adsorption with the specie >AlLac.

- ATR-FTIR results indicate that citrate is adsorbed in an inner-sphere manner at acidic pHs.

- Macroscopic data for citrate adsorption on montmorillonite were successfully fitted using the TLM model and the single monodentate, inner-sphere complex >AlCit^{2-}.

Chapter 6: Adsorption of glycine on montmorillonite

- At low concentration there exist electrostatic interactions between the carboxylic acid species and the edge surface sites. Once the smectite edge sites are saturated, glycine is adsorbed by intercalation.

- The combination of ATR-FTIR spectroscopy, X-ray diffraction analysis and macroscopic adsorption data verified that glycine is adsorbed by cation exchange into montmorillonite, although adsorption at the particle edges occurs at low glycine concentrations.

Chapter 7: Modeling the adsorption of oxalate onto montmorillonite

- The experimental adsorption edge data for oxalate were also fitted using the TLM model. Surface complexation of oxalate is described by the formation of two complexes: >AlOxH and >AlOx$^-$. The monodentate complex >AlOxH dominated adsorption below pH 4, and the bidentate complex >AlOx$^-$ was predominant at higher pH values.

A tentative reaction mechanism can be derived from the partial conclusions obtained in this Dissertation. Dissolution mechanism results from proton- and ligand-promoted dissolution reactions. On the other hand, the ligand-promoted dissolution may occur through the formation of surface complexes or a reduction in the ion activity product by complexation of the released cations.

The dissolution experiments reveal a slight catalytic effect of lactate at pH 4. Although lactate is adsorbed on the edge surface at pH<9, the integration of the adsorption experiments indicates that adsorption takes place by unspecific electrostatic interactions. Johnson et al. (2004a) found that the formation of outer-sphere complexes among LMW organic anions and >AlOH$_2^+$ groups at the corundum edge surface of reduced significantly the dissolution rate at acidic pHs. They proposed a mechanism involving steric protection of dissolution-active surface sites and, in consequence, inhibition of the reaction. Since lactate does not form inner-sphere complexes, the catalytic effect observed at pH 4 could be thus explained by the partial complexation of the Al^{3+} released to solution. The strong contribution of the protons

to the global dissolution mechanism at acidic pHs makes negligible the ligand-promoted dissolution induced by lactate.

Glycine does not catalyze the dissolution reactions in all the studied conditions. Thus, the dissolution can be described in the same way that in pure electrolyte solutions.

For citrate and oxalate the ligand-promoted reaction is relevant. The speciation tests indicate citrate and oxalate are able to complex Al in solution within the pH range of the dissolution experiments. Thus, it can be inferred that the formation of soluble chelates contributes to the overall dissolution mechanism by decreasing the activity of Al^{3+} in solution. To confirm this statement, for lactate, citrate and oxalate, the dissolution rates obtained at pH 4 and 7.5 were plotted versus the logarithm of the ligand concentration (Figure 8.1), showing a linear dependence of both variables. The experimental data were fitted to a straight line, whose slope may express a reaction order respect to ligand concentration. These slopes were plotted versus the Al stability constant of the aqueous 1:1 complex ($logK_{Al}$) (Figure 8.2). The stability constant of the monodentate complex is used as a proxy to compare the relative capacity of each ligand to form a stable complex with Al and thus reduce the activity of Al^{3+}: stronger the complex, lower the Al^{3+} activity.

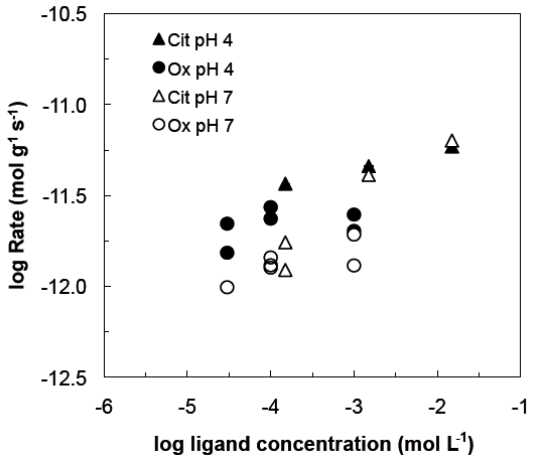

Figure 8.1. Experimental dissolution rates derived from Si concentrations versus log ligand concentration at pH 4 and 7.5.

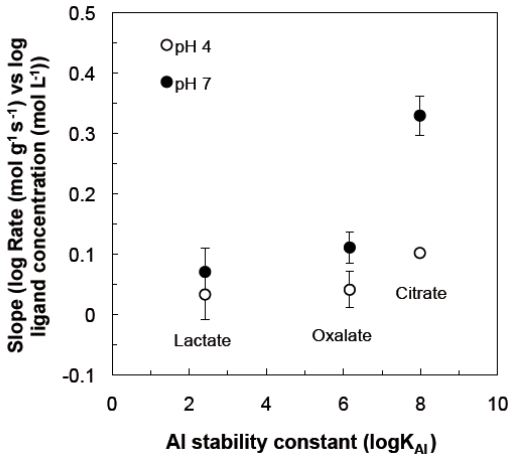

Figure 8.2. Relationship between the slope of the plot log Rate versus log ligand concentration at pH 4 and 7.5, and log K_{Al} values of lactate, oxalate and citrate (Fox et al., 1990).

The graph in Figure 8.2 shows an evidence of the contribution of the formation of soluble Al complexes to the global dissolution mechanism. According to our results (adsorption edges, FTIR spectra and surface modeling), ligands with a strong capacity to form stable aqueous complexes also tend to form inner-sphere surface complexes. At both pHs, the dissolution rates increase with the stability of the aqueous Al complex ($logK_{Al}$), although the effect is stronger at pH 7.5 than at pH 4. This is a consequence of the competition of protons and ligands for the adsorption sites at the edges. From pH 4 to 7 the H^+ concentration decreases approximately 3 orders of magnitude, whereas the total ligand concentration remains constant. Consequently at pH 4 and 7 dissolution reaction is dominated respectively by a proton- and a ligand-promoted mechanism.

LMW organic species bound as inner-sphere surface complexes produce the enhancement of mineral dissolution rates due to their ability to polarize and weaken surface metal-oxygen bonds (Furrer and Stumm, 1986; Drever and Stillings, 1997) and to catalyze the detachment of structural cations, as Al. In the bulk solution, the detached Al^{3+} ions are complexed by the LMW organic ligands, avoiding the back-precipitation and/or sorption of Al, and reducing the activity of free Al^{3+}. The dissolution process under the studied conditions depends on two effects, surface complexation and chelation, which act simultaneously. However, in our experiments it is difficult to split both effects. Only in the case of lactate, that forms outer-sphere surface complexes, the enhancement of the dissolution reaction is produced by aqueous Al complexes. For citrate and oxalate both effects are simultaneous and there is no way to assess the contribution of surface and aqueous complexation. To isolate the effect of the formation of aqueous complexes, it would be necessary the use of large, rigid ligands, capable to form stable aqueous complexes, but not surface complexes due to steric impediments.

The conclusions of this Dissertation have some implications to understand the degradation mechanism of the phyllosilicates in lung conditions. Montmorillonite has been used as a case of study to get a deeper understanding of the dissolution mechanism in synthetic lung fluid. It has been reported in literature (e.g. Rozalén et al., 2008) that the mechanism and rate of the dissolution reaction is similar for 2:1 phyllosilicates (smectites, illites, micas) and also for chlorites. Thus our results can be

extended to other mineral with similar composition and structure. Although the experiments were performed in simplified fluids, where proteins, surfactants and phosphates were suppressed, the conclusions may be considered valid for human health. Even though phyllosilicates are not considered carcinogenic substances as asbestos or quartz, once phyllosilicate particles reach the alveolar cavities the capacity of the body to clear or degrade them is very limited and lung diseases can be developed. The common use of these materials in building and industrial activities all over the world implies frequent potential occupational exposure, which can be easily prevented by the use of adequate masks. Non-occupation exposition may be negligible for the majority of the population, but it may be relevant for communities exposed to dust storms. Continuous inhalation may conduce to incapacity of the lung to particle clearance. Even if this cannot be considered a cause of mortality, it may represent a notable reduction of respiratory capacity and quality of live.

Geochemistry and mineralogy methods are useful to assess the mechanism of solution/mineral interaction, but they cannot suggest medical treatments. Joint research among biochemists, geochemists, toxicologist, physicians, etc. is necessary to obtain a general comprehension of the problem and to get solutions that prevent or minimize the risk derived from inhaled materials. Medical diagnosis and treatment of environmentally induced diseases also require further research and development.

9. REFERENCES

9. REFERENCES

Accelrys Software, Inc. (2009) Materials Studio, version 5.0. San Diego, CA.

Amram K. and Ganor J. (2005) The combined effect of pH and temperature on smectite dissolution rate under acidic conditions. *Geochim. Cosmochim. Acta* **69**, 2535-2546.

Awatani T., Dobson K.D., McQuillan A.J, Ohtani B. and Uosaki K. (1998) In situ infrared spectroscopic studies of adsorption of lactic acid and related compounds on the TiO2 and CdS semiconductor photocatalyst surfaces from aqueous solutions. *Chem. Lett.* **8**, 849-850.

Axe K. and Persson P. (2001) Time-dependent surface speciation of oxalate at the water-boehmite (γ-AlOOH) interface: implications for dissolution. *Geochim. Cosmochim. Acta* **65**, 4481-4492.

Baeyens B. and Bradbury M.H. (1997) A mechanistic description of Ni and Zn sorption on Na-montmorillonite 1. Titration and sorption measurements. *J. Contam. Hydrol.* **27**, 199-222.

Bailey S.W. (1984) Crystal chemistry of the true micas. In *Micas* (eds. S.W. Bailey) Mineralogical Society of America, Reviews in Mineralogy 13, pp 13-60.

Barrenechea M.J., Martínez C., Ferreiroa M.J., Paramá A., Tardón A. and Rego G. (2002) Características del cáncer de pulmón en pacientes con exposición laboral a la sílice. Estudio comparativo entre individuos expuestos y no expuestos. *Arch. Bronconeumol.* **38**, 561-567.

Bauer A. and G. Berger (1998) Kaolinite and smectite dissolution rate in high molar KOH solutions at 35° and 80°C. *Appl. Geochem.* **13**, 905-916.

Becaria A., Campbell A. and Bondy S.C. (2002) Aluminium as a toxicant. *Toxicol. Ind. Health* **18**, 309-320.

Benetoli L.O.B., de Souza C.M.D, da Silva K.L., de Souza I.G. Jr, de Santana H., Paesano A. Jr, da Costa A.C.S., Zaia C.T.B.V. and Zaia D.A.M. (2007) Amino acid interaction with and adsorption on clays: FT-IR and Mossbauer spectroscopy and X-ray diffractometry investigations. *Orig. Life Evol. Biosph.* **37**, 479–493.

Bhatti J.S., Comerford N.B. and Johnston C.T. (1998) Influence of soil organic matter removal and pH on oxalate sorption onto a spodic horizon. *Soil Sci. Soc Am. J.* **62**, 152-158.

Biber M.V. and Stumm W. (1994) An in-situ ATR-FTIR study: The surface coordination of salicylic acid on aluminum and iron (III) oxides. *Environ. Sci. Technol.* **28**, 763-768.

Bibi I., Singh B. and Silvester E. (2011) Dissolution of illite in saline-acidic solutions at 25°C. *Geochim. Cosmochim. Acta* **75**, 3237-3249.

Brown G. and Brindley G. W. (1980) X-ray diffraction procedures for clay and mineral identification. In *Crystal Structures of Clay Minerals and X-ray Identification, Vol. 5* (eds. G.W. Brindley and G. Brown) MSA, London, pp. 305–410.

Brunauer S., Emmett P.H. and Teller E. (1938) Adsorption of gases in multimolecular layers. *J. Am. Chem. Soc.* **60**, 309-319.

Bujdak J. and Rode B.M. (1996) The effect of smectite composition on the catalysis of peptide bond formation. *J. Mol. Evol.* **43**, 326-333.

Buol S.W., Hole F.D. and MdCracken R.J. (1980) Soil genesis and classification. 2nd ed. Iowa State Univ. Press.

Cabaniss S.E. and McVey I.F. (1995) Aqueous infrared carboxylate absorbances: aliphatic monocarboxylates. *Spectroc. Acta Pt. A-Molec. Biomolec. Spectr.* **51**, 2385-2395.

Cama J., Ganor J., Ayora C. and Lasaga A.C. (2000) Smectite dissolution at 80°C and pH 8.8. *Geochim. Cosmochim. Acta* **64**, 2701-2717.

Cama J. and Ganor J. (2006) The effects of organic acids on the dissolution of silicate minerals: A case study of oxalate catalysis of kaolinite dissolution. *Geochim. Cosmochim. Acta* **70**, 2191-2209.

Cambier P. and Sposito G. (1991) Interactions of citric acid and synthetic hydroxy-aluminum montmorillonite. *Clays Clay Miner.* **39**, 158-166.

Carbone M., Emri S., Dogan A.U., Steele I., Tuncer M., Pass H.I. and Baris Y.I. (2007) A mesothelioma epidemia in Cappadocia: scientific developments and unexpected social outcomes. *Nature Reviews* **7**, 147-154.

Carroll-Webb S.A. and Walther J.V. (1988) A surface complex reaction model for the pH-dependence of corundum and kaolinite dissolution rates. *Geochim. Cosmochim. Acta* **52,** 2609-2623.

Charlet L., Schindler P.W., Spadini L., Furrer G. and Zysset M. (1993) Cation adsorption on oxides and clays: The aluminum case. *Aquat. Sci.* **55**, 291-303.

Chin P.F. and Mills G.L. (1991) Kinetics and mechanisms of kaolinite dissolution: effects of organic ligands. *Chem. Geol.* **90**, 307-317.

Churg A. (1993) Asbestos lung burden and disease patterns in man. In *Health Effects on Mineral Dusts* (eds. G.D. Guthrie Jr. and B.T. Mossman). Reviews in Mineralogy 28, Mineralogical Society of America, pp. 410-426.

Cloos P., Calicis B., Fripiat J.J. and Makay K. (1967) Proceedings of the International Clay Conference 1966, vol. 1, Israel Program for Scientific Translations, Jerusalem, pp. 233–245.

Cornell R.M. and Schindler P.W. (1980) Infrared study of the adsorption of hydroxycarboxylic acids on α-FeOOH and amorphous Fe (III) hydroxide. *Colloid & Polymer Sci.* **258**, 1171-1175.

Cuadros J., Aldega L., Vetterlein J., Drickamer K. and Dubbin W. (2009) Reactions of lysine with montmorillonite at 80°C: Implications for optical activity, H^+ transfer and lysine-montmorillonite binding. *J. Colloid Interface Sci.* **333**, 78-84.

Dashman T. and Stotzky T. (1982) Adsorption and binding of amino acids on homoionic montmorillonite and kaolinite. *Soil Biol. Biochem.* **14**, 447-456.

Dashman T. and Stotzky G. (1985) Physical properties of homoionic montmorillonite and kaolinite complexed with amino acids and peptides. *Soil Biol. Biochem.* **17,** 189-195.

Dobson K.D. and McQuillan A.J. (1999) In situ infrared spectroscopic analysis of the adsorption of aliphatic carboxylic acids to TiO_2, ZrO_2, Al_2O_3, and Ta_2O_5 from aqueous solutions. *Spectrochim. Acta Part A* **55,** 1395–1405.

Drever J.I. and Stillings L.L. (1997) The role of organic acids in mineral weathering. *Colloids Surfaces A: Physicochem. Eng. Aspects* **120**, 167-181.

Drever J.I. and Vance G.F. (1994) Role of Soil Organic Acids in Mineral Weathering Processes. In *Organic Acids in Geological Processes* (eds. E.D. Pittman and M.D. Lewan). Springer-Verlag, New York.

Evanko C.R. and Dzombak D.A. (1998) Influence of structural features on sorption of NOM-analogue organic acids to goethite. *Environ. Sci. Technol.* **32**, 2846-2855.

Farmer V.C. (1974) *The Infrared Spectra of Minerals.* Monograph 4. Mineralogical Society, London, 539 pp.

Fein J.B. and Brady P.V. (1995) Mineral surface controls on the diagenetic transport of oxalate and aluminum. *Chem. Geol.* **121**, 11-18.

Fernandez A.M., Baeyens B., Bradbury M. and Rivas P. (2004) Analysis of the pore water chemical composition of a Spanish compacted bentonite used in an engineered barrier. *Phys. Chem. Earth* **29**, 105–118.

Filius J.D., Hiemstra T. and Van Riemsdijk W.H. (1997) Adsorption of small weak organic acids on goethite: Modeling of mechanisms. *J. Colloid Interface Sci.* **195**, 368-380.

Finkelman R.B., Skinner C.W., Plumlee G.S. and Bunnell J.E. (2001) Medical geology. *Geotimes* **46**, 20–23.

Fox T.R., Comerford N.B. and McFee W.W. (1990) Phosphorus and Aluminum Release from a Spodic Horizon Mediated by Organic Acids. *Soil Sci. Soc. Am. J.* **54**, 1763-1767.

Friebele E., Shimoyama A. and Ponnamperuma C. (1980) Adsorption of protein and non-protein amino acids on a clay mineral: A possible role of selection in chemical evolution. *J. Mol Evol.* **16**, 269-278.

Fubini B. and Fenoglio I. (2007) Toxic potential of mineral dusts. *Elements* **3**, 407-414.

Furrer G. and Stumm W. (1986) The coordination chemistry of weathering: I. Dissolution kinetics of Al_2O_3 and BeO. *Geochim. Cosmochim. Acta* **50**, 1847-1860.

Furrer G., Zysset M. and Schindler P.W. (1993) Weathering kinetics of montmorillonite in batch and mixed-flow reactors. In *Geochemistry of Pore/Fluid Interactions* (eds. D.A.C. Manning, P.L. Hall and C.R. Hughes). Chapman & Hall, London, pp. 243–262.

Gadd G.M. (1999) Fungal production of citric and oxalic acid: Importance in metal speciation, physiology and biogeochemical processes. *Adv. Microb. Physiol.* **41**, 47-92.

Gaines R.V., Skinner H.C.W., Foord E.E., Mason B. and Rosenzweig (1997) Dana's New Mineralogy, eighth edition. John Wiley & Sons, Inc. New York. pp. 1819.

Ganor J. and Lasaga A.C. (1994) The effects of oxalate acid on kaolinite dissolution rate. *Mineral Magazine* **58A**, 315.

Giles C.H., Smith D. and Huitson A. (1974) A general treatment and classification of the solute adsorption isotherm. I. Theoretical. *J. Colloid Interface Sci.* **47**, 755-765.

Golubev S.V., Bauer A. and Pokrovsky O.S. (2006) Effect of pH and organic ligands on the kinetics of smectite dissolution at 25°C. *Geochim. Cosmochim. Acta* **70**, 4436-4451.

Golubev S.V. and Pokrovsky O.S. (2006) Experimental study of the effect of organic ligands on diopside dissolution kinetics. *Chem. Geol.* **235**, 377-389.

Grasshoff K., Ehrhardt M. and Kremling K., ed. (1983) Methods of Seawater Analysis, 2nd ed. Verlag Chemie.

Gunter M.E. and Wood S.A. (2000) Can chrysotile alter to tremolite in the human lung? AGU Spring Meeting 2000, M51A.

Gustafsson J.P. (2010) Visual MINTEQ 3.0 For Windows XP/7.

Guthrie G.D.Jr. (1992) Biological effects of inhaled materials. *Am. Miner.* **77**, 1125-1128.

Ha J.Y., Yoon T.H., Wang Y.G., Musgrave C.B. and Brown G.E. (2008) Adsorption of organic matter at mineral/water interfaces: 7. ATR-FTIR and quantum chemical study of lactate interactions with hematite nanoparticles. *Langmuir* **24**, 6683-6692.

Hay M.B. and Myneni S.C.B. (2007) Structural environments of carboxyl groups in natural organic molecules from terrestrial systems. Part 1: Infrared spectroscopy. *Geochim. Cosmochim. Acta* **71**, 3518-3532.

Hayes K.F., Redden G., Ela W. and Leckie J.O. (1991) Surface complexation models: An evaluation of model parameter estimation using FITEQL and oxide mineral titration data. *J. Colloid Interface Sci.* **142**, 448-469.

Hedges J.I. and Hare P.E. (1987) Amino acid adsorption by clay minerals in distilled water. *Geochim. Cosmochim. Acta* **51**, 255-259.

Herbelin A.L. and Westall J.C. (1999) FITEQL 4.0: a Computer Program for Determination of Chemical Equilibrium Constants from Experimental Data. Report 99-01. Department of Chemistry, Oregon State University, Corvallis.

Hoose C., Lohmann U., Erdin R. and Tegen I. (2008) The global influence of dust mineralogical composition on heterogeneous ice nucleation in mixed-phase clouds. *Environ. Res. Lett.* **3**, 14 pp.

Howard A.G., Coxhead A.J., Potter I.A. and Watt A.P. (1986) Determination of dissolved aluminium by the micelle-enhanced fluorescence of its lumogallion complex. *Analyst* **111**, 1379-1381.

Huertas F., Fuentes-Cantillana J.L., Jullien F., Rivas P., Linares J., Farina P., Ghoreychi M., Jockwer N., Kickmaier W., Martinez M.A., Samper J., Alonso E. and Elorza F.J. (2000) Full-scale engineered barriers experiment for a deep geological repository for high-level radioactive waste in crystalline host rock (FEBEX project). European Commission, EUR 19147EN, Brussels.

Huertas F.J., Caballero E., Jiménez de Cisneros C., Huertas F. and Linares J. (2001) Kinetics of montmorillonite dissolution in granitic solutions. *Appl. Geochem.* **16**, 397-407.

Huertas F.J., Chou L. and Wollast R (1999) Mechanism of kaolinite dissolution at room temperature and pressure. II. Kinetic study. *Geochim. Cosmochim. Acta* **63**, 3261-3275.

Huertas F.J., Lei C. and Wollast R. (1998) Mechanism of kaolinite dissolution at room temperature and pressure: Part 1. Surface speciation. *Geochim. Cosmochim. Acta* **62**, 417-431.

Hume L.A. and Rimstidt J.D. (1992) The biodurability of chrysotile asbestos. *Am. Miner.* **77**, 1125-1128.

Hwang Y.S., Liu J., Lenhart J.J. and Hadad C.M. (2007) Surface complexes of phthalic acid at the hematite/water interface. *J. Colloid Interface Sci.* **307**, 124-134.

IARC (1997) IARC Monographs on the evaluation of carcinogenic risks to humans 42, pp. 1-42.

Ikhsan J., Wells J.D., Johnson B.B. and Angove M.J. (2005) Surface complexation modeling of the sorption of Zn(II) by montmorillonite. *Colloid Surf. A-Physicochem. Eng. Asp.* **252**, 33-41.

Jaber M., Bertin F. and Thomas-David G. (1977) Application de la spectrométrie infrarouge, Raman et résonance magnétique nucléaire à l'étude des complexes en solution aqueuse. Al^{3+}–$H_2C_2O_4$. *Can. J. Chem.* **55**, 3689-3699.

Jardine P.M. and Zelazny L.W. (1996) Surface reactions of aqueous aluminum species. In *The Environmental Chemistry of Aluminum* (eds. G. Sposito). Lewis Publishers, pp. 221-270.

Johnson S.B., Yoon T.H., Kocar B.D. Brown G.E. (2004a) Adsorption of organic matter at mineral/water interfaces. 2. Outer-sphere adsorption of maleate and implications for dissolution processes. *Langmuir* **20**, 4996-5006.

Johnson S.B., Yoon T.H., Slowey A.J. and Brown Jr G.E. (2004b) Adsorption of organic matter at mineral/water interfaces: 3. Implications of surface dissolution for adsorption of oxalate. *Langmuir* **20**, 11480-11492.

Johnston C.T. and Sposito G. (1987) Disorder and early sorrow: progress in the chemical speciation of soil surfaces. In *Future Developments in Soil Science Research* (eds. L.L. Boersma). Soil Science Society of America, Madison, Wisconsin, USA, pp. 89-100.

Jonsson C.M., Jonsson C.L., Estrada C., Sverjensky D.A., Cleaves Ii H.J. and Hazen R.M. (2010) Adsorption of L-aspartate to rutile (α-TiO2): Experimental and theoretical surface complexation studies. *Geochim Cosmochim. Acta* **74**, 2356-2367.

Jurinski J.B. and Rimstidt J.D. (2001) Biodurability of talc. *Am. Miner.* **86**, 392-399.

Kang S. and Xing B.S. (2007) Adsorption of dicarboxylic acids by clay minerals as examined by in situ ATR-FTIR and ex situ DRIFT. *Langmuir* **23**, 7024-7031.

Kitadai N., Yokoyama T. and Nakashima S. (2009a) ATR-IR spectroscopic study of L-lysine adsorption on amorphous silica *J. Colloid Interface Sci.* **329**, 31-37.

Kitadai N., Yokoyama T. and Nakashima S. (2009b) In situ ATR-IR investigation of L-lysine adsorption on montmorillonite. *J. Colloid Interface Sci.* **338**, 395-401.

Kollár I. Pálinkó I, Kónya Z. and Kiricsi I. (2003) Intercalating amino acid guests into montmorillonite host. *J. Mol. Struct.* **651-653**, 335-340.

Kubicki J.D., Itoh M.J., Schroeter L.M. and Apitz S.E. (1997) Bonding mechanisms of salicylic acid adsorbed onto illite clay: An ATR−FTIR and molecular orbital study. *Environ. Sci. Technol.* **31**, 1151–1156.

Kubicki J.D., Schroeter L.M., Itoh M.J., Nguyen B.N. and Apitz S.E. (1999) Attenuated total reflectance Fourier-transform infrared spectroscopy of carboxylic acids adsorbed onto mineral surfaces. *Geochim Cosmochim. Acta* **63**, 2709-2725.

Kulik D.A., Aja S.U., Sinitsyn V.A. and Wood S.A. (2000) Acid-base surface chemistry and sorption of some lanthanides on K^+-saturated Marblehead illite: II. A multisite-surface complexation modeling. *Geochim. Cosmochim. Acta* **64**, 195-213.

Kummert R. and Stumm W. (1980) The surface complexation of organic acid and hydrous γ-Al_2O_3. *J. Colloid Interface Sci.* **75**, 373-385.

Lackovic K., Johnson B.B., Angove M.J. and Wells J.D. (2003) Modeling the adsorption of citric acid onto Muloorina illite and related clay minerals. *J. Colloid Interface Sci.* **267**, 49-59.

Lahav N. (2002) Organo-Clay Complexes and Interactions (eds. S. Yariv and H. Cross). Marcel Dekker, New York, pp. 615–638.

Lehnert (1993) Defense mechanisms against inhaled particles and associated particle cell-interactions. In *Health Effects on Mineral Dusts* (eds. G.D. Guthrie Jr. and B.T. Mossman). Reviews in Mineralogy 28, pp. 427-469. Mineralogical Society of America.

Li J., Xu R., Tiwari D. and Ji G. (2006) Effect of low-molecular-weight organic acids on the distribution of mobilized Al between soil solution and solid phase. *Appl. Geochem.* **21**, 1750–1759.

Marklund E., Sjoberg S. and Ohman L.O. (1986) Equilibrium and structural studies of silicon (IV) and aluminum (III) in aqueous-solution .14. Speciation and equilibria in the aluminum (III)-lactic acid-OH system. *Acta Chem. Scand.* **A40**, 367-373.

Martell A.E., Motekaitis R.J. and Smith R.M. (1990) Aluminium complexes of hydroxyaliphatic and hydroxyaromatic ligands in aqueous systems -some problems and solutions. *Polyhedron* **9**, 171-187.

Martell A.E. and Smith R.M. (1974) Critical Stability Constants, Vol 1, Plenum Press, New York.

Meier L.P. and Kahr G. (1999) Determination of the cation exchange capacity (CEC) of clay minerals using the complexes of copper(II) ion with triethylenetetramine and tetraethylenepentamine. *Clay Clay Min.* **47**, 386-388.

Meng M., Stievano L. and Lambert J.F. (2004) Adsorption and thermal condensation mechanisms of amino acids on oxide supports. 1. Glycine on silica. *Langmuir* **20**, 914-923.

Metz V., Amram K. and Ganor J. (2005a) Stoichiometry of smectite dissolution. *Geochim. Cosmochim. Acta* **69**, 1755-1772.

Metz V., Raanan H., Pieper H., Bosbach D. and Ganor J. (2005b) Towards the establishment of a reliable proxy for the reactive surface area of smectite. *Geochim. Cosmochim. Acta* **69**, 2581-2591.

Meunier A. (2003) Argiles. GB Science Publisher. Paris. pp. 434.

Mingorance M.D., Barahona E. and Fernandez-Galvez J. (2007) Guidelines for improving organic carbon recovery by the wet oxidation method. *Chemosphere* **68**, 409-413.

Moore D.M. and Reynolds R.C. (1989) X-Ray Diffraction and the Identification and Analysis of Clay Minerals. Oxford University Press. New York. pp. 340.

Mortland M.M. (1970) Clay organic complexes and interactions. *Adv. Agron.* **22**, 75–117.

Nagy K.L., Cygan R.T., Hanchar J.M. and Sturchio N.C. (1999) Gibbsite growth kinetics on gibbsite, kaolinite, and muscovite substrates: atomic force microscopy evidence for epitaxy and an assessment of reactive surface area. *Geochim. Cosmochim Acta* **63**, 2337-2351.

Nakamoto K. (1997) Infrared and Raman Spectra of Inorganic and Coordination Compounds. John Wiley & Sons.

Newman A.C.D. and Brown G. (1987) The chemical constitution of clays. In *Chemistry of Clays and Clay Minerals* (ed. A.C.D. Newman). Mineralogical Society. Monograph N° 6, John Wiley & sons, New York. pp. 1-128.

Nieto F. (2002) Characterization of coexisting NH_4- and K-micas in very low grade metapelites. *Am. Miner.* **87**, 205-216.

Nieto F., Mellini M. and Abad I. (2010) The role of H_3O^+ in the crystal structure of illite. *Clay Clay Min.* **58**, 238-246.

NIST Standard Reference Database 46 Version 6.0, NIST Critically Selected Stability Constants of Metal Complexes. (eds. A.E. Martell and R.M. Smith, 2001) NIST Standard Reference Data, Gaithersberg, MD, 20899, USA.

Nordin J., Persson P., Laiti E. and Sjöberg S. (1997) Adsorption of o-phthalate at the water−boehmite (γ-AlOOH) interface: Evidence for two coordination modes. *Langmuir* **13**, 4085-4093.

Nordin J., Persson P., Nordin A. and Sjöberg S. (1998) Inner-sphere and outer-sphere complexation of a polycarboxylic acid at the water−boehmite (γ-AlOOH) interface: A combined potentiometric and IR spectroscopic study. *Langmuir* **14**, 3655–3662.

Noren K., Loring J.S. and Persson P. (2008) Adsorption of alpha amino acids at the water/goethite interface. *J. Colloid Interface Sci.* **319**, 416-428.

Noren K. and Persson P. (2007) Adsorption of monocarboxylates at the water/goethite interface: The importance of hydrogen bonding. *Geochim. Cosmochim. Acta* **71**, 5717-5730.

Nyberg K., Johansson U., Johansson A. and Camner P. (1992) Phagolysosomal pH in alveolar macrophages. *Environ. Health Perspect.* **97**, 149-152.

Oberdorster G. (2000) Toxicology of ultrafine particles: in vivo studies. *Philos. Trans. Roy. Soc. London Ser. A – Math. Phys. Eng. Sci.* **358**, 2719-2739.

Oberdorster G., Ferin J., Gelein R., Soderholm S.C. and Finkelstein J. (1992). Role of the alveolar macrophage in lung injury: studies with ultrafine particles. *Environ. Health Perspect.* **97**, 193-199.

Oberdorster G., Oberdorster E., Oberdorster J. (2005) Nanotoxicology: An emerging discipline evolving from studies of ultrafine particles. *Environ. Health Perspect.* **113**, 823-839.

Oelkers E.H. and Schott J. (1998) Does organic acid adsorption affect alkali-feldspar dissolution rates? *Chem. Geol.* **151**, 235-245.

Oliver M.A. (1997) Soil and human health: a review. *Eur. J. Soil Sci.* **48**, 573–592.

Olsen A.A. and Rimstidt J.D. (2008) Oxalate-promoted forsterite dissolution at low pH. *Geochim. Cosmochim. Acta* **72**, 1758-1766.

Oze C. and Solt K. (2010) Biodurability of chrysotile and tremolite asbestos in simulated lung and gastric fluids. *Am. Miner.* **95**, 825–831.

Parbhakar A., Cuadros J., Sephton M.A. Dubbin W., Coles B.J. and Weiss D. (2007) Adsorption of L-lysine on montmorillonite. *Colloid Surf. A-Physicochem. Eng. Asp.* **307**, 142-149.

Plumlee G.S. and Ziegler T.L. (2003) The medical geochemistry of dusts, soils, and other earth materials. In *Environmental Geochemistry*. (eds.H.D. Holland and K.K. Turekian) Treatise on Geochemistry Vol. 9, Elsevier. pp. 263-310.

Pokrovsky O.S., Golubev S.V. and Jordan G. (2009) Effect of organic and inorganic ligands on calcite and magnesite dissolution rates at 60°C and 30 atm pCO_2. *Chem. Geol.* **265**, 33–43.

Pokrovski G.S. and Schott J. (1998) Experimental study of the complexation of silicon and germanium with aqueous organic species: Implications for germanium and silicon transport and Ge/Si ratio in natural waters. *Geochim. Cosmochim. Acta* **62**, 3413-3428.

Pokrovsky O.S., Schott J. and Castillo A. (2005) Kinetics of brucite dissolution at 25°C in the presence of organic and inorganic ligands and divalent metals. *Geochim. Cosmochim. Acta* **69**, 905-918.

Polubesova T. and Borisover M. (2009). Two components of chloride anion exclusion volume in montmorillonitic soils. *Colloids and Surf. A. Physicochem. Eng. Aspects.* **347**, 175-179.

Puigdomenech I. (2004) HYDRA and MEDUSA chemical equilibrium software. Software and documentation. <http://web.telia.com/~u15651596/>.

Ramos M.E., Cappelli C., Rozalén M., Fiore S. and Huertas F.J. (2011) Effect of lactate, glycine and citrate on the kinetics of montmorillonite dissolution. *Am. Miner.* **96**, 768-780.

Ramos M.E., Rozalen M., Johnston C.T. and Huertas F.J. (2013) Effect of oxalate on the kinetics of montmorillonite dissolution. (To be submitted).

Reich T.J. and Koretsky C.M. (2011) Adsorption of Cr(VI) on γ-alumina in the presence and absence of CO_2: Comparison of three surface complexation models. *Geochim. Cosmochim. Acta* **75**, 7006-7017.

Rengel Z. (2004) Aluminium cycling in the soil-plant-animal-human continuum. *Biometals* **17**, 669-689.

Robie R.A. and Hemingway B.S. (1995) Thermodynamic properties of minerals and related substances at 298.15 K and 1 Bar (10^5 Pascals) pressure and at higher temperatures. *U.S. Geological Survey* 2131, 1-461.

Rozalén M.L., Huertas F.J., Brady P.V., Cama J., Garcia-Palma S. and Linares J. (2008) Experimental study of the effect of pH on the kinetics of montmorillonite dissolution at 25°C. *Geochim. Cosmochim. Acta*. **72**, 4224-4253.

Rozalén M., Brady P.V. and Huertas F.J. (2009a) Surface chemistry of K-montmorillonite: ionic strength, temperature dependence and dissolution kinetics. *J. Colloid Interface Sci.* **333**, 474-484.

Rozalén M., Huertas F.J. and Brady P.V. (2009b) Experimental study of the effect of pH and temperature on the kinetics of montmorillonite dissolution. *Geochim. Cosmochim. Acta* **73,** 3752-3766.

Ryan P.R., Delhaize E. and Jones D.L. (2001) Function and mechanism of organic anion exudation from plant roots. *Annu. Rev. Plant Physiol. Plant Mol. Biol.* **52**, 527-560.

Scholze H. and Conradt R. (1987) An in vitro study of the chemical durability of siliceous fibres. *Ann. Occupational Higiene* **31** (4B), 683-692.

Selinus O. and Frank A. (2000) Medical geology. Environmental Medicine (ed. L. Moller). Joint Industrial Safety Council/Sweden, pp. 164–183.

Serratosa J.M., Johns W.D. and Shimoyama A. (1970) IR study of alkylammonium vermiculite complexes: *Clays Clay Min.* **18**, 107-113.

Siffert B. and Naidja A. (1992) Stereoselectivity of montmorillonite in the adsorption and deamination of some amino acids. *Clay Min.* **27**, 109-118.

Sigg L. and Stumm W. (1981) The interactions of anions and weak acids with the hydrous goethite surface. *Colloids Surf.* **2**, 101-117.

Singer J.M., Adlersberg L., Hoenig E.M., Ende E. and Tchorsch Y. (1969) Radiolabeled latex particles in the investigation of phagocytosis in vivo: clearance curves and histological observations. *J. Reticuloendothel. Soc.* **6**, 561–589.

Skinner H.C.W. and Berger A.R. (2003) Geology and Health: Closing the Gap. Oxford University Press, Oxford.

Socrates G. (1994) *Infrared characteristic group frequencies.* Wiley, Chichester, 2nd end.

Specht C.H. and Frimmel F.H. (2001) An in situ ATR-FTIR study on the adsorption of dicarboxylic acids onto kaolinite in aqueous suspensions. *Phys. Chem. Chem. Phys.* **3**, 5444-5449.

Stievano L., Piao L.Y., Lopes I., Meng M., Costa D. and Lambert J.F. (2007) Glycine and lysine adsorption and reactivity on the surface of amorphous silica. *Eur. J. Mineral.* **19**, 321-331.

Stillings L.L., Drever J.I. and Poulson S.R. (1998) Oxalate adsorption at a plagioclase (An(47)) surface and models for ligand-promoted dissolution. *Environ. Sci. Technol.* **32**, 2856-2864.

Strathmann T.J. and Myneni S.C.B. (2004) Speciation of aqueous Ni(II)-carboxylate and Ni(II)-fulvic acid solutions: Combined ATR-FTIR and XAFS analysis. *Geochim. Cosmochim. Acta* **68**, 3441-3458.

Stumm W. and Furrer G. (1987) The dissolution of oxides and aluminum silicates; examples of surface-coordination-controlled kinetics. In *Aquatic Surface Chemistry*. (ed. Stumm W.). Wiley-Interscience: New York, pp. 197.

Stumm W., Kummert R. and Sigg L. (1980) A ligand exchange model for the adsorption of inorganic and organic ligands at hydrous oxide interfaces. *Croat. Chem. Acta* **53**, 291-312.

Sun S.W., Lin Y.C., Weng Y.M., and Chen, M.J. (2006) Efficiency improvements on ninhydrin method for amino acid quantification. *J. Food Comp. Anal.* **19**, 112-117.

Theng B.K. (1974) The Chemistry of Clay-Organic Reactions. Adan Hilger, London.

Thermo Fisher Scientific Inc. (2011) GRAMS/32 software v.9.1. Waltham, MA (USA).

van Oss C.J., Naim J.O., Costanzo P.M., Giese R.F., Wu W. and Sorling A.F. (1999) Impact of different asbestos species and other mineral particles on pulmonary pathogenesis. *Clays Clay Miner.* **47**, 697-707.

Venturini M. and Berthon G. (1989) Aluminum speciation studies in biological fluids. Part 2. Quantitative investigation of aluminum-citrate complexes and appraisal of their potential significance in vivo. *J. Inorg. Biochem.* **37**, 69-90.

Verburg K. and Baveye P. (1994) Hysteresis in binary exchange of cations on 2:1 clay minerals: A critical review. *Clays Clay Miner.* **42**, 207-220.

Vieillard Ph. (2000) A new method for the prediction of Gibbs free energies of formation of hydrated clay minerals based on the electronegativity scale. *Clays Clay Minerals* **48,** 459–473.

Wang X.X., Li Q.M., Hu H.F., Zhang T.L. and Zhou Y.Y. (2005) Dissolution of kaolinite induced by citric, oxalic, and malic acids. *J. Colloid Interface Sci.* **290**, 481-488.

Ward D.B. and Brady P.V. (1998) Effect of Al and organic acids on the surface chemistry of kaolinite. *Clays Clay Miner*. **46**, 453-465.

Weiss A. (1969) Organic derivatives of clay minerals, zeolites, and related minerals. In *Organic Geochemistry* (eds. G. Eglinton and M.T.J. Murphy). Springer-Verlag, Berlin.

Welch S.A. and Ullman W.J. (1993) The effect of organic acids on plagioclase dissolution rates and stoichiometry. *Geochim. Cosmochim. Acta* **57**, 2725-2736.

Werner A.J., Hochella M.F., Guthrie G.C., Hardy J.A., Aust A.E. and Rimstidt J.D. (1995) Asbestiform riebeckite (crocidolite) dissolution in the presence of Fe chelators; implications for mineral-induced disease. *Am. Miner.* **80**, 1093-1103.

Westall J.C. and Herbelin A. (1992) Addendum to FITEQL 2.0 Manual. Oregon State Univ.

White K.N., Ejim A.I., Walton R.C., Brown A.P., Judgaohsingh R., Powell J.J. and Mccrohan C.R. (2008) Avoidance of aluminium toxicity in freshwater snails involves intracellular silicon-aluminium biointeraction. *Environ. Sci. Technol.* **42**, 2189-2194.

WHO (2000) Cristalline silica, quartz. Concise Inernational Chemical Assessment Document 24, 1-50.

WHO (2005) Bentonite, kaolin and selected minerals. Environmental Health Criteria 231, pp. 1-174.

Wieland E. and Stumm W. (1992) Dissolution kinetics of kaolinite in acidic aqueous solutions at 25 °C. *Geochim. Cosmochim. Acta* **56**, 3339-3355.

Wolery T.J. (1992) EQ3NR, a computer program for geochemical aqueous speciation-solubility calculations: theoretical manual, user's guide, and related documentation (Version 7). UCRL-MA-110662 PT III. Laurence Livermore National Laboratory.

Yadava H.L., Singh S., Prasad P., Singh R.K.P., Yadava P.C. and Yadava K.L. (1984) Stability constants of glycinate complexes of nickel (II), lead (II), chromium (III), aluminium (III) and thorium (IV) by paper electrophoresis. *Bull. Soc. Chim. Fr.* **1**, 314-316.

Yoon T.H., Johnson S.B., Musgrave C.B. and Brown Jr G.E. (2004) Adsorption of organic matter at mineral/water interfaces: I. ATR-FTIR spectroscopic and quantum chemical study of oxalate adsorbed at boehmite/water and corundum/water interfaces. *Geochim. Cosmochim. Acta* **68**, 4505-4518.

Zutic V. and Stumm W. (1984) Effect of organic acids and fluoride on the dissolution kinetics of hydrous alumina. *Geochim. Cosmochim. Acta* **48**, 1493-1503.

Zysset M. and Schindler P.W. (1996) The proton promoted dissolution kinetics of Kmontmorillonite. *Geochim. Cosmochim. Acta* **60**, 921-931.

10. Appendix I. Chemical analysis

10. APPENDIX I. CHEMICAL ANALYSIS

10.1. Silicon analysis

Si concentration in the output solutions was determined by colorimetry by using the molybdate blue method (Grasshoff et al., 1983). This method is based on the capacity of ammonium molybdate to form a yellow complex with silica in acidic media. The complex is reduced to form a silicamolybdate blue complex. This reaction is favored with a soft heat of the solutions.

Equipment:

- Perkin Elmer Lambda 25 UV/Vis spectrometer set at 825 nm
- Spectrophotometric cuvettes (quartz or disposable pastic)
- Pipettes
- Polyethylene vials (20 mL) with caps

Reagents:

- Ammonium molybdate solution: Dissolve 7.5 g of ammonium molybdate ($(NH_4)_6Mo_7O_{24}\cdot 4H_2O$) in 75 mL of Milli Q water. Introduce in an ice bath and add little by little 25 mL of 1:1 H_2SO_4.
- Tartaric acid solution: Prepare a 10% (weight) aqueous solution. It is necessary to take in account the biological activity and the appearance of sediments. To prevent fungi development, add a crystal of thymol or sodium azide (final concentration 2 ppm).
- Reductant solution: Dissolve 0.07 g of Na_2SO_3 in 1 mL of Milli Q water. Add 0.015 g of 1-amino-2-naphthol-4-sulfonic acid and shake until it is complete dissolved. Dissolve separately 0.9 g of $Na_2S_2O_3$ in 9 mL of Milli Q water. Mix both solutions. Prepare a fresh reductant solution for every analysis.
- Acidified Milli Q water (pH ~3) (AW): Add 1 mL of 1 N HCl (aproximately 10% HCl concentrated in Milli Q water) to 1 L of Milli Q water. This solution is used for dilutions and as background, both in standard and problem solutions.

Prodecure:

Standard solutions: Prepare a 50 ppm Si solution from a stock standard solution of 1000 ppm. Store in cold to avoid evaporation. Prepare standard solutions from the 50

ppm solution with Si concentration of 0.05, 0.10, 0.15, 0.20, 0.25, 0.30, 0.40 and 0.50 ppm. Acidify all the solutions to pH 3 with 1 N HCl.

- Add 5 mL of standard or sample solution to acid cleaned vials.
- Heat the vials at 40°C for 15 minutes before the addition of the reactants.
- Add 0.1 mL of ammonium molybdate solution and keep the vials at 40°C for 15 minutes.
- Add 0.2 mL of tartaric acid solution.
- Add 0.05 mL of reductant solution, shake and heat again for 30 minutes.
- Let cold down the samples at room temperature.
- Read the absorption in a UV/Vis spectrometer at 825 nm.

The detection limit is 5 ppb and the associate error is 5%.

10.2. Aluminium analysis

Al concentration was determined by fluorimetry, using lumogallion as complexing agent (Howard et al., 1986). The fluorescence involves the excitation of a fluorescent complex with a monochromatic light, and it is relaxed with the emission of a photon with a higher wavelength than the excitation one. To favor the formation of the fluorescent complex, samples were buffered at pH 4.86 and heated for two hours at 80°C.

Equipment:

- FluoDia T70 High Temperature Fluorescence Microplate Reader
- 96-well microplate
- Pipettes
- Polyethylene vials (20 mL) with caps

Reagents:

- Acetic/acetate buffer solution (pH 5.0 ± 0.1): Weight 6.875 g of sodium acetate (Merk Suprapur) and dilute with Milli Q water in a 250 mL volumetric flask. Add 2 mL of acetic acid (Merk Suprapur), shake and bring to volume.
- Lumogallion solution: Prepare a 0.1% (volume) solution in Milli Q water. Dilute 20 times to prepare a 0.005% solution for the 0-100 ppb calibration curve. For

the 0-10 ppb calibration curve prepare a 0.0025% solution by diluting 40 times the initial solution.

- 1 N HCl solution.
- Acidified Milli Q water (pH ~3) (AW): Add 1 mL of 1 N HCl (aproximately 10% HCl concentrated in Milli Q water) to 1 L of Milli Q water. This solution is used for dilutions and as background, both in standard and problem solutions.

Prodecure:

Standard solutions: Prepare a 50 ppm Al solution from a stock standard solution of 1000 ppm. Prepare 2 calibration curves of 0-10 or 0-100 ppb depending on the estimated Al concentration in the samples.

- Add 2 mL of standard or sample solution to acid cleaned vials. Use acidified Milli Q water to dilute the samples.
- Buffer the samples and standards at pH 5 by adding 0.2 mL of acetic/acetate solution and shake.
- Add 0.1 mL of lumogallion solution (0.005 or 0.0025% for 0-10 or 0-100 ppb calibration curve respectively) and shake.
- Heat the samples at 80°C during 2 hours to favor the complex formation. Let cold down in a refrigerator during 1 hour.
- Add 250 µL of each sample of standard in a 96-well microplate.
- Read the microplate in a fluorometer (microplate reader) using λ_{em}= 486 nm and λ_{ex}= 550 nm.

The detection limit is 0.2 ppb and the associate error 5%.

10.3. Potassium analysis

The concentration of K^+ was determined by ion chromatography. Ion chromatography is a form of liquid chromatography that uses ion-exchange resin columns and polar eluents to separate ions or polar molecules based on their interaction with the resin.

Equipment:

- Metrohm 883 Basic IC Plus Ion Chromatograph
- Metrosep C3-250 column (working pressure of approximately 12 MPa)

- Pipettes
- Polypropylene sample tubes (11 mL)

Reagents:

- Milli Q water
- Eluent: 3.5 mmol L^{-1} HNO_3

Prodecure:

Prepare a 0-1 ppm calibration curve.

- Dilute the samples with Milli Q water.
- Inject the samples using a flow of 1 mL/min by setting an analysis time of 30 min.
- Read the area at the retention time of 7.5 min.

The detection limit and associated error were 1 ppb and 3%, respectively.

10.4. Lactate and citrate analysis.

The concentration of lactate and citrate was determined by ion chromatography. Ion chromatography is a form of liquid chromatography that uses ion-exchange resins to separate atomic or molecular ions based on their interaction with the resin.

Equipment:

- Metrohm 761 Ion Chromatograph
- Metrosep Organic Acids ion exclusion column (working pressure of approximately 6 MPa)
- Pipettes
- Polypropylene sample tubes (11 mL)

Reagents:

- Milli Q water
- Eluent: 0.5 mmol L^{-1} H_2SO_4 / 15% acetone

Prodecure:

Prepare a 0-10 mmol L^{-1} calibration curve.

- Dilute the samples with Milli Q water.
- Inject the samples using a flow of 1 mL/min by setting an analysis time of 20

min.

- Read the area at the retention time of 13 min for lactate and 8 min for citrate

The detection limits are 0.9 ppm for lactate and 9 ppm for citrate. The associated error was 6%.

10.5. Oxalate analysis

The concentration of oxalate was determined by ion chromatography with chemical suppression. Ion chromatography is a form of liquid chromatography that uses ion-exchange resins to separate atomic or molecular ions based on their interaction with the resin.

Equipment:

- Metrohm 761 Ion Chromatograph
- Metrosep A Supp 4-250 column (working pressure of approximately 6 MPa)
- Pipettes
- Polypropylene sample tubes (11 mL)

Reagents:

- Milli Q water
- Eluent: 1.7 mmol L^{-1} $NaHCO_3$ and 1.8 mmol L^{-1} $NaCO_3$
- Suppressor: 50 mol L^{-1} H_2SO_4

Prodecure:

Prepare a 0-10 mmol L^{-1} calibration curve.

- Dilute the samples with Milli Q water.
- Inject the samples using a flow of 1 mL/min by setting an analysis time of 20 min..
- Read the area at the retention time of 13 min.

The detection limit and associated error were 0.9 ppm and 5%, respectively.

10.6. Glycine analysis

Glycine was analyzed colorimetrically with a UV-visible spectrometer, using the ninhydrin method (Sun et al. 2006). This method is based on the reaction of the amino

group with ninhydrin to form the ninhydrin colored chromophore called 'Ruhemann's purple'.

Equipment:

- Perkin Elmer Lambda 25 UV/Vis spectrometer at 570 nm
- Spectrophotometric cuvettes (quartz or disposable pastic)
- Pipettes
- Polyethylene vials (20 mL) with caps.

Reagents:

- 1 mmol L^{-1} acetic/acetate buffer solution (pH 5.0 ± 0.1): Weight 5.166 g of sodium acetate (Merk Suprapur) and dilute with Milli Q water in a 100 mL volumetric flask. Add 2 mL of acetic acid (Merk Suprapur), shake and bring to volume.
- 2% ninhydrin solution: Dissolve 2 g of ninhydrin and 0.30 g of hydridantin in 75 mL of dimethyl sulfoxide (DMSO). Sonicate during 10 minutes. Add 25 mL of acetic/acetate buffer solution and store in cold. Due to the instability of the solution, prepare a fresh solution for every new analysis.
- Stabilizing solution: 50% ethanol in Milli Q water.

Prodecure:

Prepare a 0-1 mmol L^{-1} calibration curve.

- Add 1 mL of standard or sample solution to acid cleaned vials.
- Add 0.5 mL 2% ninhydrin solution.
- Heat at 80°C during 10 minutes.
- Let cold down in a refrigerator during 30 minutes.
- Add 2 mL of stabilizing solution and shake.
- Read the absorption in a UV/Vis spectrometer at 570 nm

The detection limit is 0.1 ppm (1.3 mmol/L) and the associated error 3%.

11. Appendix II. EQ3 and FITEQL files

11. APPENDIX II. EQ3 AND FITEQL FILES

11.1. Changes introduced in the EQ3 data0.cmp database

```
+------------------------------------------------------------------------
bdot parameters
+------------------------------------------------------------------------
```

* species name	azer0	neutral ion type
Al(Cit)-	4	0
AlCit(OH)--	4	0
Al(Ox)2-	4	0
Al(Ox)3---	4	0
Citrate-	4	0
Citrate--	4	0
Citrate---	4	0
Oxalate	4	0
Lactate	4	0
Al(Lac)3(aq)	3	0
Al(Cit)(aq)	3	0
Citric_acid(aq)	3	0
Lactic_acid(aq)	3	0
Oxalic_acid(aq)	3	0
AlH(Cit)+	4	0
Al(Ox)+	4	0
Al(Lac)2+	4	0
Al(Lac)++	4.5	0

```
+------------------------------------------------------------------------
auxiliary basis species
+------------------------------------------------------------------------
Citric_acid(aq)             C6H8O7
     sp.type =  aux
*    EQ3/6   =  com, alt, sup
     revised =  05-feb-2010
*    mol.wt. = 192.124 g/mol
*    DHazero =   3.0
     charge  =   0.0
****
     3 element(s):
      6.0000 C              8.0000 H              7.0000 O
****
     4 species in aqueous dissociation reaction:
    -1.0000  Citric_acid(aq)            -2.0000  H2O
     1.5000  O2(g)                       3.0000  Acetic_acid(aq)
*
**** logK grid [0-25-60-100C @1.0132bar; 150-200-250-300C @Psat-H2O]:
       500.0000 -124.6666  500.0000  500.0000
       500.0000  500.0000  500.0000  500.0000
*
*    gflag = 1 [reported delG0f used]
*    extrapolation algorithm: supcrt92 [92joh/oel]
*    ref-state data  [source: 90sho/hel ]
*         delG0f =     32.000 kcal/mol     [reported]
*         delH0f =     12.230 kcal/mol     [reported]
*         S0PrTr =     35.500 cal/(mol*K)  [reported]
+------------------------------------------------------------------------
Citrate-                    C6H7O7
     sp.type =  aux
*    EQ3/6   =  com, alt, sup
     revised =  04-feb-2010
*    mol.wt. = 191.124 g/mol
*    DHazero =   4.0
     charge  =  -1.0
```

```
****
     3 element(s):
      6.0000 C              7.0000 H              7.0000 O
****
     3 species in aqueous dissociation reaction:
    -1.0000  Citrate-                    -1.0000  H+
     1.0000  Citric_acid(aq)
*
**** logK grid [0-25-60-100C @1.0132bar; 150-200-250-300C @Psat-H2O]:
       500.0000    3.1000  500.0000  500.0000
       500.0000  500.0000  500.0000  500.0000
*
*    gflag = 1 [reported delG0f used]
*    extrapolation algorithm: supcrt92 [92joh/oel]
*    ref-state data  [source: 95sho     ]
*         delG0f =   -292.912 kcal/mol     [reported]
*         delH0f =   -363.530 kcal/mol     [reported]
*         S0PrTr =     67.920 cal/(mol*K)  [reported]
+--------------------------------------------------------------------
Citrate--                 C6H7O7
     sp.type =  aux
*    EQ3/6   =  com, alt, sup
     revised =  04-feb-2010
*    mol.wt. = 190.124 g/mol
*    DHazero =   4.0
     charge  =  -2.0
****
     3 element(s):
      6.0000 C              6.0000 H              7.0000 O
****
     3 species in aqueous dissociation reaction:
    -1.0000  Citrate--                   -2.0000  H+
     1.0000  Citric_acid(aq)
*
**** logK grid [0-25-60-100C @1.0132bar; 150-200-250-300C @Psat-H2O]:
       500.0000    7.9000  500.0000  500.0000
       500.0000  500.0000  500.0000  500.0000
*
*    gflag = 1 [reported delG0f used]
*    extrapolation algorithm: supcrt92 [92joh/oel]
*    ref-state data  [source: 95sho     ]
*         delG0f =   -286.417 kcal/mol     [reported]
*         delH0f =   -362.947 kcal/mol     [reported]
*         S0PrTr =     48.090 cal/(mol*K)  [reported]
+--------------------------------------------------------------------
Citrate---                C6H7O7
     sp.type =  aux
*    EQ3/6   =  com, alt, sup
     revised =  04-feb-2010
*    mol.wt. = 189.124 g/mol
*    DHazero =   4.0
     charge  =  -3.0
****
     3 element(s):
      6.0000 C              5.0000 H              7.0000 O
****
     3 species in aqueous dissociation reaction:
    -1.0000  Citrate---                  -3.0000  H+
     1.0000  Citric_acid(aq)
*
**** logK grid [0-25-60-100C @1.0132bar; 150-200-250-300C @Psat-H2O]:
       500.0000   14.3000  500.0000  500.0000
       500.0000  500.0000  500.0000  500.0000
*
*    gflag = 1 [reported delG0f used]
*    extrapolation algorithm: supcrt92 [92joh/oel]
*    ref-state data  [source: 95sho     ]
*         delG0f =   -277.690 kcal/mol     [reported]
```

```
*         delH0f =   -363.750 kcal/mol     [reported]
*         S0PrTr =     16.130 cal/(mol*K)  [reported]
+--------------------------------------------------------------------
Lactic_acid(aq)          C3H6O3
     sp.type =  aux
*    EQ3/6   =  com, alt, sup
     revised =  07-mar-1996
*    mol.wt. =  90.079 g/mol
*    DHazero =   3.0
     charge  =   0.0
****
     3 element(s):
      3.0000 C              6.0000 H              3.0000 O
****
     2 species in aqueous dissociation reaction:
    -1.0000  Lactic_acid(aq)              1.5000  Acetic_acid(aq)
*
**** logK grid [0-25-60-100C @1.0132bar; 150-200-250-300C @Psat-H2O]:
        11.1804   10.5113    9.7286    9.0087
         8.2988    7.7390    7.2850    6.9058
*
*    gflag = 1 [reported delG0f used]
*    extrapolation algorithm: supcrt92 [92joh/oel]
*    ref-state data  [source: 95sho     ]
*         delG0f =   -127.800 kcal/mol     [reported]
*         delH0f =   -164.000 kcal/mol     [reported]
*         S0PrTr =     49.800 cal/(mol*K)  [reported]
+--------------------------------------------------------------------
Oxalic_acid(aq)          C2H2O4
     sp.type =  aux
*    EQ3/6   =  com, alt, sup
     revised =  07-mar-1996
*    mol.wt. =  90.035 g/mol
*    DHazero =   3.0
     charge  =   0.0
****
     3 element(s):
      2.0000 C              2.0000 H              4.0000 O
****
     4 species in aqueous dissociation reaction:
    -1.0000  Oxalic_acid(aq)             -1.0000  H2O
     1.0000  Acetic_acid(aq)              1.5000  O2(g)
*
**** logK grid [0-25-60-100C @1.0132bar; 150-200-250-300C @Psat-H2O]:
      -105.5636  -95.7070  -84.3648  -73.9846
       -63.7444  -55.6502  -49.0940  -43.6868
*
*    gflag = 1 [reported delG0f used]
*    extrapolation algorithm: supcrt92 [92joh/oel]
*    ref-state data  [source: 95sho     ]
*         delG0f =   -168.640 kcal/mol     [reported]
*         delH0f =   -194.580 kcal/mol     [reported]
*         S0PrTr =     44.000 cal/(mol*K)  [reported]
+--------------------------------------------------------------------
aqueous species
+--------------------------------------------------------------------
Al(Cit)(aq)                    AlC6H5O7(aq)
     sp.type =  aux
*    EQ3/6   =  com, alt, sup
     revised =  05-feb-2010
*    mol.wt. =
*    DHazero =   3.0
     charge  =   0.0
****
     4 element(s):
      6.0000 C              1.0000 Al             5.0000 H
      7.0000 O
```

```
****
     4 species in aqueous dissociation reaction:
    -1.0000  Al(Cit)(aq)                  -3.0000  H+
     1.0000  Al+++                         1.0000  Citric_acid(aq)
*
**** logK grid [0-25-60-100C @1.0132bar; 150-200-250-300C @Psat-H2O]:
       500.0000    6.3200  500.0000  500.0000
       500.0000  500.0000  500.0000  500.0000
*
*    Source data: Martell et al. (1990) Polyhedrom 9 pp 171-187
*    Comment: Reaction written in terms of `citric acid´for
*    consistency with this auxiliary basis species in this database.
*    See spreadsheet `Organic_Acids_Al_Marisa.xls´for conversion
*    calculations
*
+------------------------------------------------------------------------
AlH(Cit)+                       Al(C6H6O7)+
     sp.type =  aux
*    EQ3/6   =  com, alt, sup
     revised =  05-feb-2010
*    mol.wt. =
*    DHazero =   4.0
     charge  =   1.0
****
     4 element(s):
      6.0000 C              1.0000 Al             6.0000 H
      7.0000 O
****
     4 species in aqueous dissociation reaction:
    -1.0000  AlH(Cit)+                    -2.0000  H+
     1.0000  Al+++                         1.0000  Citric_acid(aq)
*
**** logK grid [0-25-60-100C @1.0132bar; 150-200-250-300C @Psat-H2O]:
       500.0000    3.3800  500.0000  500.0000
       500.0000  500.0000  500.0000  500.0000
*
*    Source data: Martell et al. (1990) Polyhedrom 9 pp 171-187
*    Comment: Reaction written in terms of `citric acid´for
*    consistency with this auxiliary basis species in this database.
*    See spreadsheet `Organic_Acids_Al_Marisa.xls´for conversion
*    calculations
*
+------------------------------------------------------------------------
Al(Cit)-                        Al(C6H4O7)-
     sp.type =  aux
*    EQ3/6   =  com, alt, sup
     revised =  05-feb-2010
*    mol.wt. =
*    DHazero =   4.0
     charge  =  -1.0
****
     4 element(s):
      6.0000 C              1.0000 Al             4.0000 H
      7.0000 O
****
     4 species in aqueous dissociation reaction:
    -1.0000  Al(Cit)-                     -4.0000  H+
     1.0000  Al+++                         1.0000  Citric_acid(aq)
*
**** logK grid [0-25-60-100C @1.0132bar; 150-200-250-300C @Psat-H2O]:
       500.0000    9.6300  500.0000  500.0000
       500.0000  500.0000  500.0000  500.0000
*
```

```
*   Source data: Martell et al. (1990) Polyhedrom 9 pp 171-187
*   Comment: Reaction written in terms of `citric acid´for
*   consistency with this auxiliary basis species in this database.
*   See spreadsheet `Organic_Acids_Al_Marisa.xls´for conversion
*   calculations
*
+--------------------------------------------------------------------------
AlCit(OH)--                        Al(C6H5O8)--
     sp.type =  aux
*    EQ3/6   =  com, alt, sup
     revised =  05-feb-2010
*    mol.wt. =
*    DHazero =   4.0
     charge  =  -2.0
****
     4 element(s):
      6.0000 C              1.0000 Al             5.0000 H
      8.0000 O
****
     5 species in aqueous dissociation reaction:
    -1.0000  AlCit(OH)--                 -5.0000  H+
     1.0000  Al+++                        1.0000  Citric_acid(aq)
     1.0000  H2O
*
**** logK grid [0-25-60-100C @1.0132bar; 150-200-250-300C @Psat-H2O]:
       500.0000   15.8600  500.0000  500.0000
       500.0000  500.0000  500.0000  500.0000
*
*   Source data: Martell et al. (1990) Polyhedrom 9 pp 171-187
*   Comment: Reaction written in terms of `citric acid´for
*   consistency with this auxiliary basis species in this database.
*   See spreadsheet `Organic_Acids_Al_Marisa.xls´for conversion
*   calculations
*
+--------------------------------------------------------------------------
Al(Ox)+                            Al(C2O4)+
     sp.type =  aux
*    EQ3/6   =  com, alt, sup
     revised =  10-oct-2010
*    mol.wt. =  115.91 g/mol
*    DHazero =   4.0
     charge  =   1.0
****
     3 element(s):
      2.0000 C              1.0000 Al             4.0000 O
****
     4 species in aqueous dissociation reaction:
    -1.0000  Al(Ox)+                     -2.0000  H+
     1.0000  Al+++                        1.0000  Oxalic_acid(aq)
*
**** logK grid [0-25-60-100C @1.0132bar; 150-200-250-300C @Psat-H2O]:
       500.0000   -1.7800  500.0000  500.0000
       500.0000  500.0000  500.0000  500.0000
*
*   Source data: Jaber et al. (1977) Can J Chem 55 pp 3689-3699
*   Comment: Reaction written in terms of `oxalic acid´for
*   consistency with this auxiliary basis species in this database.
*   See spreadsheet `Organic_Acids_Al_Marisa.xls´for conversion
*   calculations
*
+--------------------------------------------------------------------------
Al(Ox)2-                           Al(C2O4)2-
     sp.type =  aux
*    EQ3/6   =  com, alt, sup
     revised =  10-oct-2010
*    mol.wt. =  203.04 g/mol
*    DHazero =   4.0
     charge  =  -1.0
```

```
****      -
     3 element(s):
      4.0000 C              1.0000 Al             8.0000 O
****
     4 species in aqueous dissociation reaction:
    -1.0000  Al(Ox)2-                    -4.0000  H+
     1.0000  Al+++                        2.0000  Oxalic_acid(aq)
*
**** logK grid [0-25-60-100C @1.0132bar; 150-200-250-300C @Psat-H2O]:
       500.0000   -2.2600  500.0000  500.0000
       500.0000  500.0000  500.0000  500.0000
*
*    Source data: Jaber et al. (1977) Can J Chem 55 pp 3689-3699
*    Comment: Reaction written in terms of `oxalic acid´for
*    consistency with this auxiliary basis species in this database.
*    See spreadsheet `Organic_Acids_Al_Marisa.xls´for conversion
*    calculations
*
+---------------------------------------------------------------------
Al(Ox)3---                        Al(C2O4)3---
     sp.type =  aux
*    EQ3/6   =  com, alt, sup
     revised =  10-oct-2010
*    mol.wt. =  291.07 g/mol
*    DHazero =   4.0
     charge  =  -3.0
****
     3 element(s):
      6.0000 C              1.0000 Al            12.0000 O
****
     4 species in aqueous dissociation reaction:
    -1.0000  Al(Ox)3---                  -6.0000  H+
     1.0000  Al+++                        3.0000  Oxalic_acid(aq)
*
**** logK grid [0-25-60-100C @1.0132bar; 150-200-250-300C @Psat-H2O]:
       500.0000   -0.6400  500.0000  500.0000
       500.0000  500.0000  500.0000  500.0000
*
*    Source data: Jaber et al. (1977) Can J Chem 55 pp 3689-3699
*    Comment: Reaction written in terms of `oxalic acid´for
*    consistency with this auxiliary basis species in this database.
*    See spreadsheet `Organic_Acids_Al_Marisa.xls´for conversion
*    calculations
*
+---------------------------------------------------------------------
Al(Lac)++                  Al(C3H5O3)++
     sp.type =  aqueous
     revised =  09-25-2008
     charge  =   2.0
****
     4 element(s):
      3.0000 C              1.0000 Al             5.0000 H
      3.0000 O
****
     4 species in aqueous dissociation reaction:
    -1.0000  Al(Lac)++                   -1.0000  H+
     1.0000  Al+++                        1.0000  Lactic_acid(aq)
*
****logK grid [0-25-60-100C@1.0132bar; 150-200-250-300C @Psat-H2O]:
       500.0000    1.5000  500.0000  500.0000
       500.0000  500.0000  500.0000  500.0000
*
*    Source data: Solubility constants in Sposito (1996), The
*    Environmental Chemistry of Aluminium Table 8
*    Comment: Reaction written in terms of `lactic acid´for
*    consistency with this auxiliary basis species in this database.
*    See spreadsheet `Organic_Acids_Al_Marisa.xls´for conversion
*    calculations
*
+---------------------------------------------------------------------
```

```
Al(Lac)2+                Al(C3H5O3)2+
     sp.type =  aqueous
     revised =  09-25-2008
     charge  =   1.0
****
     4 element(s):
      6.0000 C              1.0000 Al            10.0000 H
      6.0000 O
****
     4 species in aqueous dissociation reaction:
    -1.0000  Al(Lac)2+                  -2.0000  H+
     1.0000  Al+++                       2.0000  Lactic_acid(aq)
*
****logK grid [0-25-60-100C@1.0132bar; 150-200-250-300C @Psat-H2O]:

       500.0000    3.3000  500.0000  500.0000
       500.0000  500.0000  500.0000  500.0000
*
*   Source data: Solubility constants in Sposito (1996), The
*   Environmental Chemistry of Aluminium Table 8
*   Comment: Reaction written in terms of `lactic acid´for
*   consistency with this auxiliary basis species in this database.
*   See spreadsheet `Organic_Acids_Al_Marisa.xls´for conversion
*   calculations
*
+---------------------------------------------------------------------
Al(Lac)3(aq)             Al(C3H5O3)3(aq)
     sp.type =  aqueous
     revised =  09-25-2008
     charge  =   0.0
****
     4 element(s):
      9.0000 C              1.0000 Al            15.0000 H
      9.0000 O
****
     4 species in aqueous dissociation reaction:
    -1.0000  Al(Lac)3(aq)               -3.0000  H+
     1.0000  Al+++                       3.0000  Lactic_acid(aq)
*
****logK grid [0-25-60-100C@1.0132bar; 150-200-250-300C @Psat-H2O]:

       500.0000    5.7900  500.0000  500.0000
       500.0000  500.0000  500.0000  500.0000
*
*   Source data: Solubility constants in Sposito (1996), The
*   Environmental Chemistry of Aluminium Table 8
*   Comment: Reaction written in terms of `lactic acid´for
*   consistency with this auxiliary basis species in this database.
*   See spreadsheet `Organic_Acids_Al_Marisa.xls´for conversion
*   calculations
*
+---------------------------------------------------------------------
```

11.2. Example of EQ3 input file for the experiment Sm-SEmL15-7

```
|-------------------------------------------------------------------------|
|EQ3NR input file name= Sm_SEmL15_7.3i                                    |
|Description= disolucion sm pH7 en sistema abierto tipo celda de flujo    |
|celdas con lactico de Elena                                              |
|Version level= 7.2                                                       |
|Revised 08/04/95    Revisor= T. J. Wolery                                |
|This is part of the EQ3NR Test Case Library (EQ3/6-V7-EQ3NR-TST-R04)      |
|                                                                         |
|Temperatura trabajo: 25 +/- 2ºC                                          |
|SoluciÚn en equilibrio con el CO2 atmosfÈrico.                           |
|SoluciÚn en equilibrio con el O2 atmosfÈrico.                            |
|                                                                         |
|                                                                         |
|                           References                                    |
|                                                                         |
|Nordstrom, D. K., et al., 1979, A comparison of computerized chemical    |
|  models for equilibrium calculations in aqueous systems, in Jenne,      |
|  E. A., editor, Chemical Modeling in Aqueous Systems, ACS Symposium     |
|  Series, v. 93, American Chemical Society, Washington, DC, p. 857-892|
|                                                                         |
|-------------------------------------------------------------------------|
|Temperature (C)         | 25.00        |Density(gm/cm3)|  1.02336      |
|-------------------------------------------------------------------------|
|Total Dissolved Salts   |              | mg/kg | mg/l  |*not used      |
|-------------------------------------------------------------------------------|
|Electrical Balancing on |                        | code selects|*not performed|
|-------------------------------------------------------------------------------|
| SPECIES                | BASIS SWITCH/CONSTRAINT| CONC/ETC  | UNITS OR TYPE  |
|-------------------------------------------------------------------------------|
|redox                   |                        |-0.7000    |logfo2          |
|K+                      |                        | 0.1134    |Molality        |
|Cl-                     |                        | 0.1125    |Molality        |
|SO4--                   |                        | 0.0056    |Molality        |
|SiO2(aq)                |                        | 0.1158    |mg/kg           |
|H+                      |                        | 7.7900    |pH              |
|HCO3-                   |CO2(g)                  |-3.5000    |Log fugacity    |
|Al+++                   |                        | 0.0059    |mg/kg           |
|Mg++                    |                        | 0.0164    |mg/kg           |
|Fe++                    |Fe(OH)3                 | 0.0000    |mineral         |
|Lactic_acid(aq)         |                        | 0.0150    |mg/kg           |
|-------------------------------------------------------------------------------|
|Input Solid Solutions                                                          |
|-------------------------------------------------------------------------------|
| none                   |                        |           |                |
|-------------------------------------------------------------------------------|
|SUPPRESSED SPECIES   (suppress,replace,augmentk,augmentg)    value     |
|-------------------------------------------------------------------------|
| Oxalic_acid(aq)        |aqueous         |suppress  |0.0000          |
| Oxalate                |aqueous         |suppress  |0.0000          |
| H-Oxalate              |aqueous         |suppress  |0.0000          |
| Formic_acid(aq)        |aqueous         |suppress  |0.0000          |
| Formate                |aqueous         |suppress  |0.0000          |
| Malonic_acid(aq)       |aqueous         |suppress  |0.0000          |
| Malonate               |aqueous         |suppress  |0.0000          |
| H-Malonate             |aqueous         |suppress  |0.0000          |
```

```
| Glycolic_acid(aq)      |aqueous         |suppress  |0.0000          |
| Glycolate              |aqueous         |suppress  |0.0000          |
| Succinic_acid(aq)      |aqueous         |suppress  |0.0000          |
| Succinate              |aqueous         |suppress  |0.0000          |
| H-Succinate            |aqueous         |suppress  |0.0000          |
| o-Phthalic_acid(aq)    |aqueous         |suppress  |0.0000          |
| o-Phthalate            |aqueous         |suppress  |0.0000          |
| H(o-Phthalate)-        |aqueous         |suppress  |0.0000          |
| Aspartic_acid(aq)      |aqueous         |suppress  |0.0000          |
| Glutaric_acid(aq)      |aqueous         |suppress  |0.0000          |
| Glutarate              |aqueous         |suppress  |0.0000          |
| H-Glutarate            |aqueous         |suppress  |0.0000          |
|-------------------------------------------------------------------------|
|OPTIONS                                                                  |
|-------------------------------------------------------------------------|
| - SOLID SOLUTIONS -                                                     |
|   * ignore solid solutions                                              |
|     process hypothetical solid solutions                                |
|     process input and hypothetical solid solutions                      |
| - LOADING OF SPECIES INTO MEMORY -                                      |
|   * does nothing                                                        |
|     lists species loaded into memory                                    |
| - ECHO DATABASE INFORMATION -                                           |
|   * does nothing                                                        |
|     lists all reactions                                                 |
|     lists reactions and log K values                                    |
|     lists reactions, log K values and polynomial coef.                  |
| - LIST OF AQUEOUS SPECIES (ordering) -                                  |
|   * in order of decreasing concentration                                |
|     in same order as input file                                         |
| - LIST OF AQUEOUS SPECIES (concentration limit) -                       |
|     all species                                                         |
|   * only species > 10**-20 molal                                        |
|     only species > 10**-12 molal                                        |
|     not printed                                                         |
| - LIST OF AQUEOUS SPECIES (by element) -                                |
|   * print major species                                                 |
|     print all species                                                   |
|     don't print                                                         |
| - MINERAL SATURATION STATES -                                           |
|     print if affinity > -10 kcals                                       |
|   * print all                                                           |
|     don't print                                                         |
| - pH SCALE CONVENTION -                                                 |
|   * modified NBS                                                        |
|     internal                                                            |
|     rational                                                            |
| - ACTIVITY COEFFICIENT OPTIONS -                                        |
|   * use B-dot equation                                                  |
|     Davies' equation                                                    |
|     Pitzer's equations                                                  |
| - AUTO BASIS SWITCHING -                                                |
|   * off                                                                 |
|     on                                                                  |
```

```
| - PITZER DATABASE INFORMATION -                                          |
|   * print only warnings                                                  |
|     print species in model and number of Pitzer coefficients            |
|     print species in model and names of Pitzer coefficients             |
| - PICKUP FILE -                                                          |
|   * write pickup file                                                    |
|     don't write pickup file                                              |
| - LIST MEAN IONIC PROPERTIES -                                           |
|   * don't print                                                          |
|     print                                                                |
| - LIST AQUEOUS SPECIES, ION SIZES, AND HYDRATION NUMBERS -               |
|   * print                                                                |
|     don't print                                                          |
| - CONVERGENCE CRITERIA -                                                 |
|   * test both residual functions and correction terms                    |
|     test only residual functions                                         |
|--------------------------------------------------------------------------|
|DEBUGGING SWITCHES (0 = off, 1,2 = on                                     |
|--------------------------------------------------------------------------|
|0  generic debugging information                                         |2
|0  print details of pre-Newton-Raphson iteration                         |2
|0  print details of Newton-Raphson iteration                             |
|0  print details of stoichiometric factors                               |2
|0  print details of stoichiometric factors calculation                   |
|0  write reactions on RLIST                                              |
|0  list stoichiometric concentrations of master species                  |
|0  request iteration variables to be killed                              |
|--------------------------------------------------------------------------|
|DEVELOPMENT OPTIONS  (used for code development)                          |
|--------------------------------------------------------------------------|
| none                                                                     |
|--------------------------------------------------------------------------|
|TOLERANCES                  (desired values)        (defaults)            |
|--------------------------------------------------------------------------|
|      residual functions  |                      |1.0e-10  tolbt         |
|        correction terms  |                      |1.0e-10  toldl         |
|        saturation state  |                      |0.5      tolsat        |
|number of N-R iterations  |                      |30       itermx        |
|--------------------------------------------------------------------------|
```

11.3. FITEQL input file for the modeling of the adsorption of 0.15 mmol L^{-1} lactate on montmorillonite.

```
': PROGRAM: FITEQL Version 4.0
': FILENAME: C:\FITEQL4\FITDATA\INPUTL~1\FIT-TEMP.DAT
': PATH: C:\FITEQL4\FITDATA\INPUTL~1\
': DESCRIPTION:
     1
     1
     1
     0
     0
    20
     4     1     1     9     1     1
   160 PSI(0)        -1.000  0.000E+00
   170 I              0.000  1.015E-02
     1 Lac-           0.000  1.500E-04
     3 AlOH           0.000  6.750E-05
     4 Lac(ads)       0.000  0.000E+00
     2 H+             0.000  0.000E+00

     1 H+             0.000    2    1
     2 OH-          -14.000  170   -2   2   -1
     3 Lac-           0.000  170   -2   1    1
     4 HLac           3.860    1    1   2    1
     6 AlOH           0.000    3    1
     7 AlOH2+         6.440  160    1   3    1   2    1
     8 AlO-          -9.440  160   -1   3    1   2   -1
     9 AlOHLac-     -20.000  160   -1   1    1   3    1   4    1
    10 AlOH2Lac       1.500    1    1   3    1   4    1   2    1

     1 H+           170    0.500
     2 OH-          170    0.500
     3 Lac-         170    0.500
     4 HLac
     6 AlOH
     7 AlOH2+
     8 AlO-
     9 AlOHLac-
    10 AlOH2Lac

     2   6.500000   1.160000
  0.010150   1.000000

     1     0     0
    10
     0    '* NDIS

     1    14
     T          logX
     4          2
'*   Lac(ads)    H+
   1  6.610E-05  -2.310000
   2  5.340E-05  -3.930000
   3  6.670E-05  -5.050000
   4  5.810E-05  -5.820000
   5  8.760E-05  -6.040000
   6  6.720E-05  -6.630000
   7  5.390E-05  -6.810000
   8  4.360E-05  -6.910000
   9  3.410E-05  -7.010000
```

```
  10  1.730E-05  -7.890000
  11  2.250E-08  -8.320000
  12  1.140E-06  -9.500000
  13  1.010E-05  -9.760000
  14  2.020E-06 -10.600000

     0     0     0     '* NST, NSX, KUWSOS

'* Graph Information
'*  Type  ID    RangeI  RangeF  Format    Axis  Name        Format   Series Type
    3       1     1      14          '*  X     H+
    3       4     1      14    1     '*  Y 1   Lac(ads)    Symbols  Component Total
    5       9     1      14    1     '*  Y 2   AlOHLac-    Symbols  Species Conc.
    5      10     1      14    1     '*  Y 3   AlOH2Lac    Symbols  Species Conc.
    4       4     1      14    2     '*  Y 4   Lac(ads)    Line     Component Sum
    1       0     1      14    1     '*  Y 5   None        Symbols  None
    1       0     1      14    1     '*  Y 6   None        Symbols  None
    1       0                       '*  D     None                 None

'*  Max         Min         Step            Type
3   12.000E+00  20.000E-01  20.000E-01  '*  -log
1   10.000E-05  00.000E+00  20.000E-06  '*  linear
lactato                                                '* Graph Title
pH                                                     '* X - Axis Title
Ox(ads) (M)                                            '* Y - Axis Title
```

11.4. FITEQL input file for the modeling of the adsorption of 0.15 mmol L^{-1} citrate on montmorillonite.

```
': PROGRAM: FITEQL Version 4.0
': FILENAME: C:\FITEQL4\FITDATA\INPUTC~1\FIT-TEMP.DAT
': PATH: C:\FITEQL4\FITDATA\INPUTC~1\
': DESCRIPTION:
     1
     1
     1
     0
     0
    20
     9     1     1    22     1     1
     1 Cit3-          0.000  1.500E-04
     5 SiOH           0.000  1.980E-04
     3 AlOH           0.000  2.220E-04
   170 I              0.000  1.015E-02
   160 PSI(0)        -1.000  0.000E+00
   161 PSI(b)        -0.500  0.000E+00
   162 PSI(d)        -0.200  0.000E+00
     7 NO3-           0.000  1.000E-02
     6 K+             0.000  1.000E-02
     4 Cit(ads)       0.000  0.000E+00
     2 H+             0.000  0.000E+00

     1 H+             0.000    2    1
     2 OH-          -14.000  170   -2   2   -1
     3 Cit3-          0.000    1    1 170  -18
     4 HCit2-         6.400    1    1 170  -12   2    1
     5 H2Cit-        11.200    1    1 170   -8   2    2
     4 H3Cit         14.300    1    1 170   -6   2    3
     6 AlOH           0.000    3    1
     7 AlOH2+         6.440    3    1 160    1   2    1
     8 AlO-          -9.440    3    1 160   -1   2   -1
    18 SiOH           0.000    5    1
    14 SiO-          -8.800    5    1 160   -1   2   -1
    22 K+             0.000    6    1
    21 NO3-           0.000    7    1
    20 AlOH2+NO3-     8.290    3    1 160    1 161   -1   7    1   2    1
    19 AlO-K+        -9.000    3    1 160   -1 161    1   6    1   2   -1
     9 AlOCit2-      10.500    1    1   3    1 160    1 161   -3   4    1   2    1
    13 AlOCitH-    -20.000    1    1   3    1 160    1 161   -3   4    1   2    2
    12 AlOCit      -20.000    1    1   3    1 160    1 161   -3   4    1   2    3
    11 AlOHCit3-   -20.000    1    1   3    1 162   -3   4    1
    16 AlOH2Cit2-  -20.000    1    1   3    1 160    1 162   -3   4    1   2    1
    17 AlOH22Cit-  -20.000    1    1   3    1 160    1 162   -3   4    1   2    2
    15 AlOH22CitH  -20.000    1    1   3    1 160    1 162   -3   4    1   2    3

     1 H+           170    0.500
     2 OH-          170    0.500
     3 Cit3-        170    4.500
     4 HCit2-       170    2
     5 H2Cit-       170    0.500
     4 H3Cit        170    0
     6 AlOH
     7 AlOH2+
     8 AlO-
    18 SiOH
    14 SiO-
    22 K+
    21 NO3-
```

```
    20 AlOH2+NO3-
    19 AlO-K+
     9 AlOCit2-
    13 AlOCitH-
    12 AlOCit
    11 AlOHCit3-
    16 AlOH2Cit2-
    17 AlOH22Cit-    3    2
    15 AlOH22CitH    3    2

     4   6.500000   5.800000   7.000000   3.000000
  0.010150   1.000000

     1     0     0
     9
     0    '* NDIS

     1    14
     T          logX
     4          2
'*   Cit(ads)    H+
   1  4.400E-06  -2.400000
   2  4.400E-06  -2.500000
   3  4.610E-06  -2.630000
   4  5.460E-06  -2.950000
   5  8.850E-06  -3.840000
   6  1.360E-05  -4.170000
   7  1.800E-05  -4.570000
   8  2.210E-05  -5.040000
   9  2.500E-05  -5.550000
  10  2.710E-05  -5.720000
  11  2.620E-05  -6.310000
  12  2.280E-05  -6.870000
  13  1.680E-05  -7.060000
  14  1.160E-05  -9.120000

     0     0     0     '* NST, NSX, KUWSOS

'* Graph Information
'*  Type  ID    RangeI  RangeF  Format    Axis  Name        Format   Series Type
    3       1     1      14          '*  X     H+
    3       4     1      14    1     '*  Y 1   Cit(ads)    Symbols  Component Total
    5       9     1      14    3     '*  Y 2   AlOCit2-    Both     Species Conc.
    5      15     1      14    3     '*  Y 3   AlOH22CitH  Both     Species Conc.
    4       4     1      14    2     '*  Y 4   Cit(ads)    Line     Component Sum
    5      11     1      14    3     '*  Y 5   AlOHCit3-   Both     Species Conc.
    5      12     1      14    3     '*  Y 6   AlOCit      Both     Species Conc.
    1       0                        '*  D     None                 None

'*  Max         Min         Step           Type
3   95.000E-01  20.000E-01  20.000E-01  '*  -log
1   40.000E-06  00.000E+00  10.000E-06  '*  linear
citrato                                              '* Graph Title
pH                                                   '* X - Axis Title
Cit(ads)(M)                                          '* Y - Axis Title
```

11.5. FITEQL input file for the modeling of the adsorption of 0.15 mmol L^{-1} oxalate on montmorillonite.

```
': PROGRAM: FITEQL Version 4.0
': FILENAME: C:\FITEQL4\FITDATA\INPUTO~1\FIT-TEMP.DAT
': PATH: C:\FITEQL4\FITDATA\INPUTO~1\
': DESCRIPTION:
     1
     1
     1
     0
     0
    20
     9     1     1    19     1     1
     1 Ox2-          0.000  1.000E-04
     3 AlOH          0.000  3.830E-04
   170 I             0.000  1.010E-02
   162 PSI(d)       -0.200  0.000E+00
   161 PSI(b)       -0.500  0.000E+00
   160 PSI(0)       -1.000  0.000E+00
     5 SiOH          0.000  3.410E-04
     7 NO3-          0.000  1.000E-02
     6 K+            0.000  1.000E-02
     4 Ox(ads)       0.000  0.000E+00
     2 H+            0.000  0.000E+00

     1 H+            0.000    2    1
     2 OH-         -14.000  170   -2   2   -1
     3 Ox2-          0.000    1    1
     4 HOx-          4.270    1    1 170    4   2    1
     5 H2Ox          5.520    1    1 170    6   2    2
     6 AlOH          0.000    3    1
     7 AlOH2+        6.440    3    1 160    1   2    1
     8 AlO-         -9.440    3    1 160   -1   2   -1
     9 Al(OH)Ox-2  -20.000    1    1   3    1 162   -2   4    1
    10 AlOx-         1.500    1    1   3    1 161   -2 160    1   4    1   2    1
    13 (AlOH2)2Ox  -20.000    1    1   3    1 162   -2 160    1   4    1
    12 AlOxH         1.500    1    1   3    1 161   -2 160    1   4    1   2    2
    11 Al2Ox       -20.000    1    1   3    1 161   -2 160    1   4    1   2    2
    14 SiOH          0.000    5    1
    15 SiO-         -8.800  160   -1   5    1   2   -1
    16 NO3-          0.000    7    1
    20 K+            0.000    6    1
    17 AlOH2+NO3-    8.290    3    1 161   -1 160    1   7    1   2    1
    18 AlO-K+       -9.000    3    1 161    1 160   -1   6    1   2   -1

     1 H+          170    0.500
     2 OH-         170    0.500
     3 Ox2-        170    2
     4 HOx-        170    0.500
     5 H2Ox        170    0
     6 AlOH
     7 AlOH2+
     8 AlO-
     9 Al(OH)Ox-2
    10 AlOx-
    13 (AlOH2)2Ox    3    2
    12 AlOxH
    11 Al2Ox         3    2
    14 SiOH
```

```
    15 SiO-
    16 NO3-
    20 K+
    17 AlOH2+NO3-
    18 AlO-K+

     4   6.500000  10.000000   1.000000   0.200000
  0.010100   1.000000

     2     0     0
    10
    12
     0    '* NDIS

     1    40
     T          logX
     4          2
'*   Ox(ads)     H+
   1  5.444E-05  -2.670000
   2  5.194E-05  -2.680000
   3  3.747E-05  -2.860000
   4  4.629E-05  -2.850000
   5  5.022E-05  -2.880000
   6  4.979E-05  -2.920000
   7  4.722E-05  -3.060000
   8  4.323E-05  -3.450000
   9  3.699E-05  -3.480000
  10  3.578E-05  -3.180000
  11  3.702E-05  -3.560000
  12  3.253E-05  -4.350000
  13  3.610E-05  -4.370000
  14  3.583E-05  -4.380000
  15  2.877E-05  -4.470000
  16  3.856E-05  -4.600000
  17  3.480E-05  -4.600000
  18  3.757E-05  -4.680000
  19  3.501E-05  -4.990000
  20  3.093E-05  -5.210000
  21  3.091E-05  -5.290000
  22  3.676E-05  -5.300000
  23  3.228E-05  -5.320000
  24  2.503E-05  -5.420000
  25  2.371E-05  -5.470000
  26  3.505E-05  -5.510000
  27  2.362E-05  -5.520000
  28  1.860E-05  -5.610000
  29  1.500E-05  -5.860000
  30  2.781E-05  -5.970000
  31  2.984E-06  -6.270000
  32  9.304E-06  -6.400000
  33  1.226E-05  -6.500000
  34  2.753E-06  -6.620000
  35  1.070E-05  -6.950000
  36  0.000E+00  -7.000000
  37  0.000E+00  -7.500000
  38  0.000E+00  -8.000000
  39  0.000E+00  -8.500000
```

```
  40  0.000E+00  -9.000000

     0     0     0     '* NST, NSX, KUWSOS

'* Graph Information
'*  Type  ID    RangeI  RangeF  Format    Axis  Name        Format   Series Type
    3       1     1      40          '*  X     H+
    3       4     1      40    1     '*  Y 1   Ox(ads)     Symbols  Component Total
    5       9     1      40    3     '*  Y 2   Al(OH)Ox-2  Both     Species Conc.
    5      10     1      40    3     '*  Y 3   AlOx-       Both     Species Conc.
    4       4     1      40    2     '*  Y 4   Ox(ads)     Line     Component Sum
    5      13     1      40    3     '*  Y 5   (AlOH2)2Ox  Both     Species Conc.
    5      12     1      40    3     '*  Y 6   AlOxH       Both     Species Conc.
    1       0                        '*  D     None                 None

'*  Max         Min         Step            Type
3   90.000E-01  20.000E-01  10.000E-01  '*  -log
1   60.000E-06  00.000E+00  10.000E-06  '*  linear
Oxalate adsorption onto Montmorillonite                          '* Graph Title
pH                                                               '* X - Axis Title
Ox(ads) (M)                                                      '* Y - Axis Title
```

12. Appendix III. Experimental conditions, pH and Si, Al and ligand concentration in the output solutions of the montmorillonite dissolution experiments

12. APPENDIX III. EXPERIMENTAL CONDITIONS, pH AND Si, Al AND LIGAND CONCENTRATION IN THE OUTPUT SOLUTIONS OF THE MONTMORILLONITE DISSOLUTION EXPERIMENTS.

Sm-SEm-3		**Temperature 37ºC**		**Initial pH 3.21**	
Mass 0.1005 g		**Solution 112 mM KCl + 0.556 mM K_2SO_4 + 1 mM HCl**			
Run	Time (h)	pH	Flow (mL min^{-1})	Si (µM)	Al (µM)
Sm-SEm-3-1	20.7	3.09	0.0268	65.06	1.52
Sm-SEm-3-2	43.5	3.09	0.0246	58.41	0.92
Sm-SEm-3-3	65.0	3.10	0.0244	49.52	0.50
Sm-SEm-3-4	90.5	3.09	0.0243	38.73	0.36
Sm-SEm-3-5	158.3	3.08	0.0243	29.38	0.26
Sm-SEm-3-6	182.6	3.08	0.0242	23.84	0.22
Sm-SEm-3-7	206.4	3.08	0.0241	20.22	0.22
Sm-SEm-3-8	230.7	3.08	0.0240	19.45	0.20
Sm-SEm-3-9	258.1	3.18	0.0240	18.00	0.18
Sm-SEm-3-10	283.5	3.10	0.0240	16.86	0.17
Sm-SEm-3-11	326.5	3.09	0.0240	15.97	0.16
Sm-SEm-3-12	352.7	3.07	0.0240	15.07	0.15
Sm-SEm-3-13	375.5	3.08	0.0241	14.43	0.15
Sm-SEm-3-14	398.7	3.08	0.0241	13.94	0.14
Sm-SEm-3-15	422.7	3.10	0.0241	13.64	0.14
Sm-SEm-3-16	448.7	3.09	0.0240	13.39	0.14
Sm-SEm-3-17	494.3	3.07	0.0240	12.96	0.14
Sm-SEm-3-18	519.2	3.07	0.0239	12.57	0.13
Sm-SEm-3-19	543.5	3.06	0.0241	12.67	0.13
Sm-SEm-3-20	566.0	3.04	0.0239	12.15	0.13
Sm-SEm-3-21	590.2	3.13	0.0238	12.12	0.13
Sm-SEm-3-22	617.6	3.11	0.0238	11.76	0.12
Sm-SEm-3-23	662.0	3.06	0.0240	11.10	0.13
Sm-SEm-3-24	686.4	3.06	0.0237	10.90	0.12
Sm-SEm-3-25	710.5	3.05	0.0238	10.86	0.12
Sm-SEm-3-26	738.0	3.05	0.0237	10.49	0.11
Sm-SEm-3-27	762.9	3.05	0.0237	10.09	0.11
Sm-SEm-3-28	830.4	3.04	0.0237	10.01	0.11
Sm-SEm-3-29	858.9	3.05	0.0237	9.43	0.11
Sm-SEm-3-30	901.9	3.05	0.0237	9.24	0.11
Sm-SEm-3-31	930.8	3.04	0.0237	8.99	0.10
Sm-SEm-3-32	998.4	3.08	0.0238	9.15	0.10
Sm-SEm-3-33	1022.2	3.03	0.0236	8.77	0.10
Sm-SEm-3-34	1046.8	3.07	0.0237	8.90	0.11
Sm-SEm-3-35	1072.0	3.06	0.0235	8.82	0.10
Sm-SEm-3-36	1098.7	3.14	0.0236	8.79	0.10
Sm-SEm-3-37	1123.7	3.06	0.0237	8.33	0.10
Sm-SEm-3-38	1166.4	3.07	0.0238	8.32	0.10
Sm-SEm-3-39	1190.5	3.05	0.0237	8.18	0.10
Sm-SEm-3-40	1214.4	3.07	0.0238	8.19	0.10
Sm-SEm-3-41	1238.5	3.06	0.0237	8.07	0.10
Sm-SEm-3-42	1267.2	3.05	0.0237	8.04	0.10
Sm-SEm-3-43	1334.1	3.05	0.0236	7.96	0.09
Sm-SEm-3-44	1357.9	3.05	0.0235	7.78	0.09
Sm-SEm-3-45	1382.1	3.05	0.0235	7.40	0.09

Sm-SEm-4		**Temperature 37ºC**		**Initial pH 4.24**	
Mass 0.1013 g		**Solution 112 mM KCl + 0.556 mM K_2SO_4 + 0.1 mM HCl**			
Run	Time (h)	pH	Flow (mL min^{-1})	Si (µM)	Al (µM)
Sm-SEm-4-1	20.7	3.44	0.0235	60.34	45.71
Sm-SEm-4-2	43.5	3.67	0.0235	53.10	25.28
Sm-SEm-4-3	65.0	3.93	0.0228	40.33	5.77
Sm-SEm-4-4	90.5	4.05	0.0227	27.78	2.75
Sm-SEm-4-5	158.3	4.11	0.0227	17.40	1.89
Sm-SEm-4-6	182.6	4.12	0.0225	14.10	2.08
Sm-SEm-4-7	206.4	4.11	0.0225	10.95	2.03
Sm-SEm-4-8	230.7	4.11	0.0224	11.35	1.91
Sm-SEm-4-9	258.1	4.11	0.0225	9.53	1.80
Sm-SEm-4-10	283.5	4.14	0.0223	8.62	1.86
Sm-SEm-4-11	326.5	4.10	0.0223	8.10	1.75
Sm-SEm-4-12	352.7	4.13	0.0222	7.49	1.75
Sm-SEm-4-13	375.5	4.11	0.0222	7.18	1.78
Sm-SEm-4-14	398.7	4.11	0.0223	6.96	1.74
Sm-SEm-4-15	422.7	4.10	0.0222	6.82	1.73
Sm-SEm-4-16	448.7	4.11	0.0222	6.50	1.67
Sm-SEm-4-17	494.3	4.10	0.0223	6.25	1.66
Sm-SEm-4-18	519.2	4.11	0.0221	6.07	1.67
Sm-SEm-4-19	543.5	4.09	0.0221	6.14	1.68
Sm-SEm-4-20	566.0	4.09	0.0223	13.07	1.66
Sm-SEm-4-21	590.2	4.10	0.0221	5.85	1.65
Sm-SEm-4-22	617.6	4.18	0.0220	5.48	1.64
Sm-SEm-4-23	662.0	4.12	0.0221	5.17	1.61
Sm-SEm-4-24	686.4	4.11	0.0220	5.52	1.71
Sm-SEm-4-25	710.5	4.14	0.0220	5.22	1.60
Sm-SEm-4-26	738.0	4.09	0.0220	4.86	1.59
Sm-SEm-4-27	762.9	4.10	0.0220	4.67	1.56
Sm-SEm-4-28	830.4	4.08	0.0220	4.86	1.69
Sm-SEm-4-29	858.9	4.11	0.0219	4.43	1.50
Sm-SEm-4-30	901.9	4.12	0.0220	4.40	1.50
Sm-SEm-4-31	930.8	4.09	0.0218	4.43	1.49
Sm-SEm-4-32	998.4	4.09	0.0220	4.34	1.32
Sm-SEm-4-33	1022.2	4.10	0.0220	4.01	1.39
Sm-SEm-4-34	1046.8	4.10	0.0220	3.97	1.39
Sm-SEm-4-35	1072.0	4.12	0.0219	3.88	1.35
Sm-SEm-4-36	1098.7	4.09	0.0218	4.03	1.61
Sm-SEm-4-37	1123.7	4.02	0.0219	3.49	1.38
Sm-SEm-4-38	1166.4	4.10	0.0219	3.43	1.28
Sm-SEm-4-39	1190.5	4.11	0.0219	3.95	1.22
Sm-SEm-4-40	1214.4	4.09	0.0221	3.56	1.41
Sm-SEm-4-41	1238.5	4.09	0.0220	3.43	1.22
Sm-SEm-4-42	1267.2	4.14	0.0220	3.58	1.29
Sm-SEm-4-43	1334.1	4.09	0.0219	3.39	1.29
Sm-SEm-4-44	1357.9	4.12	0.0219	3.24	1.36
Sm-SEm-4-45	1382.1	4.10	0.0219	3.17	1.28

Sm-SEm-5		**Temperature 37ºC**		**Initial pH 5.52**	
Mass 0.1008 g		**Solution 112 mM KCl + 0.556 mM K_2SO_4**			
Run	Time (h)	pH	Flow (mL min^{-1})	Si (µM)	Al (µM)
Sm-SEm-5-1	20.7	3.59	0.0238	54.49	35.40
Sm-SEm-5-2	43.5	3.88	0.0233	46.97	18.09
Sm-SEm-5-3	65.0	4.30	0.0232	34.47	2.78
Sm-SEm-5-4	90.5	4.63	0.0229	24.89	1.76
Sm-SEm-5-5	158.3	4.86	0.0229	16.41	0.58
Sm-SEm-5-6	182.6	5.06	0.0228	11.61	0.70
Sm-SEm-5-7	206.4	5.10	0.0228	9.48	0.08
Sm-SEm-5-8	230.7	5.14	0.0227	8.60	0.11
Sm-SEm-5-9	258.1	5.15	0.0227	7.58	0.01
Sm-SEm-5-10	283.5	5.13	0.0228	6.55	0.02
Sm-SEm-5-11	326.5	5.15	0.0227	6.03	< d.l.
Sm-SEm-5-12	352.7	5.15	0.0227	5.22	0.01
Sm-SEm-5-13	375.5	5.07	0.0228	4.85	0.01
Sm-SEm-5-14	398.7	5.28	0.0227	4.64	0.04
Sm-SEm-5-15	422.7	5.16	0.0227	4.19	0.00
Sm-SEm-5-16	448.7	5.11	0.0228	3.70	0.01
Sm-SEm-5-17	494.3	5.11	0.0227	3.56	0.03
Sm-SEm-5-18	519.2	5.18	0.0226	3.13	0.00
Sm-SEm-5-19	543.5	5.08	0.0228	2.98	0.02
Sm-SEm-5-20	566.0	5.18	0.0226	2.91	0.02
Sm-SEm-5-21	590.2	5.18	0.0225	2.66	0.04
Sm-SEm-5-22	617.6	5.13	0.0226	2.50	0.03
Sm-SEm-5-23	662.0	4.92	0.0227	2.96	0.26
Sm-SEm-5-24	686.4	5.23	0.0225	2.44	0.04
Sm-SEm-5-25	710.5	5.17	0.0225	2.16	0.05
Sm-SEm-5-26	738.0	5.17	0.0225	2.08	0.04
Sm-SEm-5-27	762.9	5.16	0.0226	2.15	0.09
Sm-SEm-5-28	830.4	4.64	0.0226	2.52	0.43
Sm-SEm-5-29	858.9	5.15	0.0225	1.76	0.07
Sm-SEm-5-30	901.9	5.07	0.0225	1.63	0.03
Sm-SEm-5-31	930.8	5.21	0.0226	1.53	0.04
Sm-SEm-5-32	998.4	5.13	0.0226	1.62	0.07
Sm-SEm-5-33	1022.2	5.22	0.0225	1.77	0.13
Sm-SEm-5-34	1046.8	5.30	0.0225	1.83	0.23
Sm-SEm-5-35	1072.0	5.19	0.0225	1.36	0.04
Sm-SEm-5-36	1098.7	5.22	0.0225	1.40	0.08
Sm-SEm-5-37	1123.7	5.25	0.0226	1.40	0.04
Sm-SEm-5-38	1166.4	5.16	0.0226	1.40	0.06
Sm-SEm-5-39	1190.5	5.11	0.0226	1.34	0.07
Sm-SEm-5-40	1214.4	5.36	0.0226	1.48	0.20
Sm-SEm-5-41	1238.5	5.37	0.0226	1.51	0.21
Sm-SEm-5-42	1267.2	5.21	0.0224	1.26	0.08
Sm-SEm-5-43	1334.1	5.22	0.0225	1.30	0.04
Sm-SEm-5-44	1357.9	5.22	0.0224	1.25	0.09
Sm-SEm-5-45	1382.1	5.21	0.0224	1.56	0.15

*d.l.: detection limit

Sm-SEm-6		**Temperature 37ºC**		**Initial pH 6.17**	
Mass 0.0999 g		**Solution 112 mM KCl + 0.556 mM K_2SO_4 + 0.018 mM $KHCO_3$**			
Run	Time (h)	pH	Flow (mL min^{-1})	Si (µM)	Al (µM)
Sm-SEm-6-1	20.7	3.17	0.0187	56.29	31.09
Sm-SEm-6-2	43.5	4.13	0.0234	40.95	9.88
Sm-SEm-6-3	65.0	4.53	0.0232	30.50	1.52
Sm-SEm-6-4	90.5	4.97	0.0232	22.78	0.85
Sm-SEm-6-5	158.3	5.28	0.0230	15.30	0.29
Sm-SEm-6-6	182.6	5.75	0.0229	11.25	0.19
Sm-SEm-6-7	206.4	5.80	0.0229	8.98	0.08
Sm-SEm-6-8	230.7	5.93	0.0229	7.95	0.06
Sm-SEm-6-9	258.1	5.98	0.0228	7.08	< d.l.
Sm-SEm-6-10	283.5	5.88	0.0229	6.35	< d.l.
Sm-SEm-6-11	326.5	5.74	0.0228	5.94	0.25
Sm-SEm-6-12	352.7	5.92	0.0225	5.38	0.09
Sm-SEm-6-13	375.5	6.00	0.0229	4.49	0.01
Sm-SEm-6-14	398.7	5.98	0.0229	4.78	0.01
Sm-SEm-6-15	422.7	5.96	0.0229	4.51	0.07
Sm-SEm-6-16	448.7	5.95	0.0228	3.55	0.01
Sm-SEm-6-17	494.3	5.96	0.0228	3.24	0.04
Sm-SEm-6-18	519.2	6.00	0.0227	2.97	0.00
Sm-SEm-6-19	543.5	5.99	0.0229	2.82	< d.l.
Sm-SEm-6-20	566.0	5.94	0.0228	2.60	< d.l.
Sm-SEm-6-21	590.2	5.85	0.0226	2.70	0.09
Sm-SEm-6-22	617.6	5.91	0.0227	2.29	0.00
Sm-SEm-6-23	662.0	5.91	0.0228	2.30	0.06
Sm-SEm-6-24	686.4	5.96	0.0227	2.10	0.02
Sm-SEm-6-25	710.5	6.01	0.0226	2.20	0.07
Sm-SEm-6-26	738.0	5.92	0.0226	1.99	0.05
Sm-SEm-6-27	762.9	6.08	0.0226	2.02	0.01
Sm-SEm-6-28	830.4	6.14	0.0226	1.67	0.00
Sm-SEm-6-29	858.9	5.96	0.0226	1.76	0.10
Sm-SEm-6-30	901.9	5.96	0.0227	-	< d.l.
Sm-SEm-6-31	930.8	5.90	0.0226	1.68	0.03
Sm-SEm-6-32	998.4	5.77	0.0228	2.51	0.06
Sm-SEm-6-33	1022.2	6.15	0.0227	1.40	0.03
Sm-SEm-6-34	1046.8	6.01	0.0226	1.50	0.04
Sm-SEm-6-35	1072.0	5.89	0.0225	1.38	0.00
Sm-SEm-6-36	1098.7	5.89	0.0225	1.38	0.11
Sm-SEm-6-37	1123.7	5.93	0.0226	1.41	0.02
Sm-SEm-6-38	1166.4	4.34	0.0227	1.31	0.03
Sm-SEm-6-39	1190.5	5.99	0.0228	1.37	0.03
Sm-SEm-6-40	1214.4	6.18	0.0226	1.47	0.23
Sm-SEm-6-41	1238.5	6.02	0.0227	1.52	0.15
Sm-SEm-6-42	1267.2	5.94	0.0225	1.24	0.06
Sm-SEm-6-43	1334.1	6.08	0.0226	1.26	0.03
Sm-SEm-6-44	1357.9	5.92	0.0225	1.32	0.03
Sm-SEm-6-45	1382.1	5.86	0.0223	1.43	0.09

*d.l.: detection limit

Sm-SEm-7		**Temperature 37ºC**		**Initial pH 6.91**	
Mass 0.0990 g		**Solution 112 mM KCl + 0.556 mM K_2SO_4 + 0.300 mM $KHCO_3$**			
Run	Time (h)	pH	Flow (mL min^{-1})	Si (µM)	Al (µM)
Sm-SEm-7-1	21.2	3.94	0.0232	46.80	21.73
Sm-SEm-7-2	44.2	5.80	0.0235	33.40	3.03
Sm-SEm-7-3	72.8	6.79	0.0238	23.64	0.80
Sm-SEm-7-4	116.0	7.10	0.0234	20.21	0.09
Sm-SEm-7-5	140.2	7.25	0.0234	13.91	0.08
Sm-SEm-7-6	165.2	6.96	0.0233	11.35	0.17
Sm-SEm-7-7	191.1	7.08	0.0232	9.39	0.14
Sm-SEm-7-8	215.7	7.08	0.0232	7.91	0.13
Sm-SEm-7-9	242.0	7.08	0.0232	7.04	0.10
Sm-SEm-7-10	284.0	7.14	0.0232	6.14	0.06
Sm-SEm-7-11	308.2	6.90	0.0231	5.15	0.14
Sm-SEm-7-12	332.0	7.24	0.0231	4.87	0.13
Sm-SEm-7-13	356.0	7.17	0.0233	4.38	0.22
Sm-SEm-7-14	382.7	7.11	0.0231	3.99	0.14
Sm-SEm-7-15	406.8	7.18	0.0231	3.62	0.18
Sm-SEm-7-16	452.0	7.24	0.0231	3.34	0.09
Sm-SEm-7-17	476.0	7.13	0.0231	2.98	0.13
Sm-SEm-7-18	500.0	7.32	0.0233	2.88	0.10
Sm-SEm-7-19	524.2	7.20	0.0232	2.92	0.19
Sm-SEm-7-20	548.5	6.98	0.0232	2.70	0.15
Sm-SEm-7-21	578.2	7.13	0.0231	2.39	0.11
Sm-SEm-7-22	620.2	7.30	0.0232	2.16	0.06
Sm-SEm-7-23	651.2	7.02	0.0231	2.08	0.11
Sm-SEm-7-24	673.2	7.01	0.0232	1.95	0.13
Sm-SEm-7-25	696.8	6.98	0.0231	1.88	0.13
Sm-SEm-7-26	720.0	6.93	0.0230	1.86	0.19
Sm-SEm-7-27	745.1	6.95	0.0229	1.84	0.14
Sm-SEm-7-28	788.4	7.20	0.0236	1.83	0.10
Sm-SEm-7-29	812.2	6.97	0.0230	1.73	0.06
Sm-SEm-7-30	836.2	6.98	0.0230	1.76	0.12
Sm-SEm-7-31	863.4	7.11	0.0229	1.60	0.11
Sm-SEm-7-32	887.3	7.16	0.0230	1.75	0.14
Sm-SEm-7-33	912.0	6.79	0.0231	1.69	0.09
Sm-SEm-7-34	956.1	7.25	0.0229	1.65	0.13
Sm-SEm-7-35	980.2	6.96	0.0230	1.72	0.13
Sm-SEm-7-36	1004.1	7.23	0.0230	1.60	0.15
Sm-SEm-7-37	1028.3	6.93	0.0230	1.83	0.13
Sm-SEm-7-38	1055.0	6.98	0.0230	1.67	0.12
Sm-SEm-7-39	1080.5	6.99	0.0231	1.49	0.10
Sm-SEm-7-40	1124.0	7.23	0.0229	1.49	0.07
Sm-SEm-7-41	1148.2	7.03	0.0229	1.63	0.20
Sm-SEm-7-42	1172.0	7.14	0.0229	1.00	0.16
Sm-SEm-7-43	1197.0	6.99	0.0229	1.71	0.12
Sm-SEm-7-44	1221.1	6.98	0.0230	1.68	0.13
Sm-SEm-7-45	1248.7	7.00	0.0229	1.48	0.19
Sm-SEm-7-46	1293.0	7.15	0.0228	1.63	0.08
Sm-SEm-7-47	1316.2	7.02	0.0228	1.66	0.15
Sm-SEm-7-48	1340.4	7.00	0.0229	1.49	0.12
Sm-SEm-7-49	1364.8	7.07	0.0231	1.49	0.11

Run	Time (h)	pH	Flow (mL min^{-1})	Si (µM)	Al (µM)
Sm-SEm-7-50	1391.3	7.07	0.0230	1.43	0.12
Sm-SEm-7-51	1417.0	7.03	0.0230	1.54	0.11
Sm-SEm-7-52	1460.3	7.21	0.0229	1.56	0.10
Sm-SEm-7-53	1484.4	7.24	0.0227	1.51	0.12
Sm-SEm-7-54	1508.7	6.63	0.0228	1.60	0.20
Sm-SEm-7-55	1533.0	7.00	0.0228	1.53	0.12
Sm-SEm-7-56	1559.3	6.92	0.0228	1.90	0.23
Sm-SEm-7-57	1584.4	7.01	0.0219	1.61	0.15
Sm-SEm-7-58	1629.0	7.15	0.0227	1.65	0.10
Sm-SEm-7-59	1653.6	7.03	0.0224	1.43	0.17
Sm-SEm-7-60	1681.0	6.98	0.0225	1.56	0.14

Sm-SEm-8	**Temperature 37ºC**		**Initial pH 7.92**		
Mass 0.0993 g	**Solution 112 mM KCl + 0.556 mM K_2SO_4 + 0.500 mM $KHCO_3$**				
Run	Time (h)	pH	Flow (mL min^{-1})	Si (µM)	Al (µM)
Sm-SEm-8-1	69.3	7.24	0.0234	32.65	2.65
Sm-SEm-8-2	93.0	7.46	0.0235	24.68	0.47
Sm-SEm-8-3	116.9	7.38	0.0233	17.43	0.44
Sm-SEm-8-4	142.0	7.49	0.0213	13.67	0.33
Sm-SEm-8-5	165.0	7.61	0.0230	12.63	0.34
Sm-SEm-8-6	193.6	7.51	0.0231	9.68	0.34
Sm-SEm-8-7	236.8	7.65	0.0231	7.91	0.30
Sm-SEm-8-8	261.0	7.65	0.0231	6.27	0.34
Sm-SEm-8-9	286.0	7.37	0.0231	6.49	0.38
Sm-SEm-8-10	311.9	7.50	0.0230	5.29	0.37
Sm-SEm-8-11	336.5	7.33	0.0231	4.91	0.39
Sm-SEm-8-12	362.8	7.43	0.0231	4.35	0.36
Sm-SEm-8-13	404.8	7.47	0.0230	3.82	0.29
Sm-SEm-8-14	429.0	7.51	0.0230	3.41	0.40
Sm-SEm-8-15	452.8	7.46	0.0229	3.20	0.40
Sm-SEm-8-16	476.8	7.29	0.0231	3.04	0.37
Sm-SEm-8-17	503.5	7.46	0.0229	2.78	0.34
Sm-SEm-8-18	527.6	7.31	0.0230	2.62	0.37
Sm-SEm-8-19	572.8	7.50	0.0230	2.81	0.24
Sm-SEm-8-20	596.8	7.66	0.0230	2.49	0.41
Sm-SEm-8-21	620.8	7.61	0.0231	3.34	0.34
Sm-SEm-8-22	645.0	7.41	0.0230	2.44	0.30
Sm-SEm-8-23	669.3	7.43	0.0230	2.27	0.32
Sm-SEm-8-24	699.0	7.47	0.0230	2.34	0.30
Sm-SEm-8-25	741.0	7.52	0.0230	2.52	0.16
Sm-SEm-8-26	772.0	7.47	0.0230	2.25	0.32
Sm-SEm-8-27	794.0	7.53	0.0230	2.35	0.37
Sm-SEm-8-28	817.5	7.55	0.0230	2.09	0.33
Sm-SEm-8-29	840.7	7.34	0.0229	1.99	0.22
Sm-SEm-8-30	865.9	7.09	0.0230	2.13	0.29
Sm-SEm-8-31	909.2	7.52	0.0235	1.91	0.27
Sm-SEm-8-32	933.0	7.61	0.0229	1.92	0.29
Sm-SEm-8-33	957.0	7.28	0.0230	1.92	0.30
Sm-SEm-8-34	984.2	7.44	0.0229	1.99	0.29

Run	Time (h)	pH	Flow (mL min^{-1})	Si (µM)	Al (µM)
Sm-SEm-8-35	1008.1	7.49	0.0229	2.04	0.34
Sm-SEm-8-36	1032.8	7.40	0.0230	1.98	0.30
Sm-SEm-8-37	1076.9	7.58	0.0229	2.56	0.24
Sm-SEm-8-38	1101.0	7.46	0.0229	1.87	0.28
Sm-SEm-8-39	1124.9	7.39	0.0229	1.80	0.39
Sm-SEm-8-40	1149.0	7.61	0.0227	1.85	0.25
Sm-SEm-8-41	1175.8	7.47	0.0229	1.79	0.25
Sm-SEm-8-42	1201.3	7.50	0.0230	1.79	0.24
Sm-SEm-8-43	1244.8	7.58	0.0229	1.81	0.14
Sm-SEm-8-44	1269.0	7.52	0.0229	1.75	0.22
Sm-SEm-8-45	1292.8	7.39	0.0229	1.87	0.28
Sm-SEm-8-46	1317.7	7.44	0.0229	1.77	0.28
Sm-SEm-8-47	1341.9	7.37	0.0229	1.69	0.24
Sm-SEm-8-48	1369.5	7.40	0.0229	1.67	0.23
Sm-SEm-8-49	1413.8	7.63	0.0228	1.70	0.31
Sm-SEm-8-50	1437.0	7.43	0.0228	1.73	0.23
Sm-SEm-8-51	1461.2	7.62	0.0229	1.64	0.21
Sm-SEm-8-52	1485.6	7.40	0.0229	1.61	0.22
Sm-SEm-8-53	1512.1	7.69	0.0230	1.57	0.22
Sm-SEm-8-54	1537.8	7.61	0.0229	1.63	0.25
Sm-SEm-8-55	1581.1	7.64	0.0228	1.48	0.19
Sm-SEm-8-56	1605.2	7.55	0.0227	1.58	0.23
Sm-SEm-8-57	1629.5	7.62	0.0228	1.62	0.25
Sm-SEm-8-58	1653.8	7.49	0.0227	1.76	0.24
Sm-SEm-8-59	1680.1	7.37	0.0227	2.29	0.54
Sm-SEm-8-60	1705.2	7.56	0.0219	1.70	0.31
Sm-SEm-8-61	1749.8	7.67	0.0227	1.63	0.22
Sm-SEm-8-62	1774.4	7.34	0.0227	1.76	0.26
Sm-SEm-8-63	1801.8	7.54	0.0229	1.64	0.25

Sm-SEmL0.15-4	**Temperature 37ºC**	**Initial pH 3.90**
Mass 0.0991 g	**Solution 112 mM KCl + 0.556 mM K_2SO_4 + 0.1 mM HCl + 0.15 mM Lactate**	

Run	Time (h)	pH	Flow (mL min^{-1})	Si (µM)	Al (µM)	Lactate output (mM)	Lactate input (mM)
Sm-SEmL0.15-4-1	21.2	3.34	0.0201	52.12	50.22	0.159	-
Sm-SEmL0.15-4-2	45.4	3.65	0.0209	64.56	26.29	0.147	-
Sm-SEmL0.15-4-3	75.2	3.89	0.0203	42.27	7.03	0.141	-
Sm-SEmL0.15-4-4	117.2	3.91	0.0201	26.51	4.29	0.141	-
Sm-SEmL0.15-4-5	148.2	3.96	0.0201	16.21	3.04	0.151	-
Sm-SEmL0.15-4-6	170.2	3.91	0.0201	18.45	2.95	0.141	-
Sm-SEmL0.15-4-7	193.7	3.93	0.0200	14.67	2.96	0.148	-
Sm-SEmL0.15-4-8	216.9	3.94	0.0199	13.75	2.93	0.141	-
Sm-SEmL0.15-4-9	242.1	3.90	0.0200	12.67	2.98	0.147	-
Sm-SEmL0.15-4-10	285.4	3.88	0.0204	11.50	2.92	0.149	-
Sm-SEmL0.15-4-11	309.1	3.93	0.0199	10.54	2.84	0.150	0.197
Sm-SEmL0.15-4-12	333.1	3.95	0.0199	10.14	2.76	0.139	-
Sm-SEmL0.15-4-13	360.3	3.96	0.0198	9.63	2.75	0.141	-
Sm-SEmL0.15-4-14	384.3	3.94	0.0198	9.31	2.70	0.153	-

Run	Time (h)	pH	Flow (mL min^{-1})	Si (µM)	Al (µM)	Lactate output (mM)	Lactate input (mM)
Sm-SEmL0.15-4-15	409.0	3.97	0.0198	8.91	2.73	0.145	-
Sm-SEmL0.15-4-16	453.1	3.90	0.0198	8.61	3.19	0.155	-
Sm-SEmL0.15-4-17	477.1	3.94	0.0198	8.36	2.77	0.150	0.146
Sm-SEmL0.15-4-18	501.0	3.94	0.0199	8.43	2.66	0.156	-
Sm-SEmL0.15-4-19	525.2	3.95	0.0198	7.97	2.66	0.152	-
Sm-SEmL0.15-4-20	551.9	3.95	0.0198	7.99	2.69	0.151	-
Sm-SEmL0.15-4-21	577.5	3.97	0.0198	7.52	2.50	0.146	-
Sm-SEmL0.15-4-22	621.0	3.94	0.0198	7.33	2.53	0.148	-
Sm-SEmL0.15-4-23	645.1	3.93	0.0197	7.04	2.38	0.143	-
Sm-SEmL0.15-4-24	669.0	3.93	0.0198	7.28	2.52	0.156	-
Sm-SEmL0.15-4-25	693.9	3.95	0.0198	6.59	2.36	0.152	0.150
Sm-SEmL0.15-4-26	718.1	3.94	0.0198	6.63	2.20	0.156	-
Sm-SEmL0.15-4-27	745.7	3.91	0.0197	6.73	2.31	0.152	-
Sm-SEmL0.15-4-28	790.0	3.90	0.0198	6.35	2.43	0.149	-
Sm-SEmL0.15-4-29	813.2	3.93	0.0197	6.19	2.42	0.134	-
Sm-SEmL0.15-4-30	837.4	3.94	0.0197	6.21	2.42	0.149	-
Sm-SEmL0.15-4-31	861.8	3.94	0.0198	6.26	2.15	0.142	0.145
Sm-SEmL0.15-4-32	888.3	3.89	0.0198	6.14	2.33	0.157	-
Sm-SEmL0.15-4-33	913.9	3.92	0.0199	6.07	2.26	0.151	-
Sm-SEmL0.15-4-34	957.3	3.92	0.0197	6.00	2.23	0.151	-
Sm-SEmL0.15-4-35	981.4	3.94	0.0197	5.98	2.25	0.154	-
Sm-SEmL0.15-4-36	1005.7	3.95	0.0199	5.78	2.25	0.147	0.158
Sm-SEmL0.15-4-37	1029.9	3.93	0.0198	6.13	2.16	0.152	-
Sm-SEmL0.15-4-38	1056.3	3.93	0.0178	5.51	2.01	0.145	-
Sm-SEmL0.15-4-39	1081.3	3.94	0.0190	5.44	1.84	0.154	-
Sm-SEmL0.15-4-40	1125.9	3.90	0.0198	5.45	1.75	0.210	-
Sm-SEmL0.15-4-41	1150.5	3.93	0.0196	5.04	1.86	0.165	-
Sm-SEmL0.15-4-42	1178.1	3.95	0.0198	4.92	1.91	0.148	0.150

Sm-SEmL0.15-4b	**Temperature 37ºC**	**Initial pH 3.95**
Mass 0.0998 g	**Solution 112 mM KCl + 0.556 mM K_2SO_4 + 0.06 mM HCl + 0.15 mM Lactate**	

Run	Time (h)	pH	Flow (mL min^{-1})	Si (µM)	Al (µM)	Lactate output (mM)
Sm-SEmL0.15b-4-1	20.0	3.15	0.0238	54.12	45.77	0.212
Sm-SEmL0.15b-4-2	44.4	3.59	0.0228	39.36	22.40	0.171
Sm-SEmL0.15b-4-3	68.0	3.84	0.0228	25.57	6.95	0.162
Sm-SEmL0.15b-4-4	93.4	3.92	0.0226	28.07	2.92	0.156
Sm-SEmL0.15b-4-5	139.7	3.93	0.0224	28.76	2.87	0.157
Sm-SEmL0.15b-4-6	163.6	3.94	0.0222	22.97	2.29	0.153
Sm-SEmL0.15b-4-7	187.7	3.96	0.0222	17.26	2.32	0.152
Sm-SEmL0.15b-4-8	216.0	3.95	0.0220	15.51	2.30	0.161
Sm-SEmL0.15b-4-9	237.4	3.95	0.0221	12.45	2.32	0.155
Sm-SEmL0.15b-4-10	261.2	3.98	0.0221	11.92	2.32	0.155
Sm-SEmL0.15b-4-11	307.7	3.95	0.0219	10.97	2.27	0.148
Sm-SEmL0.15b-4-12	331.8	3.98	0.0219	9.95	6.44	0.148
Sm-SEmL0.15b-4-13	355.6	3.97	0.0219	9.50	2.29	0.227

Run	Time (h)	pH	Flow (mL min^{-1})	Si (μM)	Al (μM)	Lactate output (mM)
Sm-SEmL0.15b-4-14	379.7	3.96	0.0219	9.22	2.34	0.169
Sm-SEmL0.15b-4-15	406.3	3.96	0.0218	10.03	2.26	0.170
Sm-SEmL0.15b-4-16	429.9	3.98	0.0220	8.17	2.18	0.167
Sm-SEmL0.15b-4-17	475.8	3.94	0.0217	7.97	2.36	0.159
Sm-SEmL0.15b-4-18	500.0	3.95	0.0217	8.21	2.15	0.158
Sm-SEmL0.15b-4-19	523.9	3.95	0.0218	7.17	2.04	0.160
Sm-SEmL0.15b-4-20	547.9	3.95	0.0218	8.52	2.44	0.143
Sm-SEmL0.15b-4-21	571.7	3.96	0.0218	7.68	2.26	0.162
Sm-SEmL0.15b-4-22	597.1	3.96	0.0218	7.09	2.32	0.157
Sm-SEmL0.15b-4-23	643.6	3.94	0.0218	6.94	2.40	0.163
Sm-SEmL0.15b-4-24	667.6	3.95	0.0218	6.52	2.10	-
Sm-SEmL0.15b-4-25	691.7	3.94	0.0218	6.45	2.09	0.302
Sm-SEmL0.15b-4-26	715.6	3.95	0.0217	6.60	2.28	0.166
Sm-SEmL0.15b-4-27	739.6	3.96	0.0218	6.32	1.98	0.233
Sm-SEmL0.15b-4-28	768.0	3.97	0.0218	6.25	2.14	0.184
Sm-SEmL0.15b-4-29	811.8	3.95	0.0217	6.41	2.01	0.175
Sm-SEmL0.15b-4-30	836.6	3.95	0.0216	6.56	1.92	0.177
Sm-SEmL0.15b-4-31	860.7	3.97	0.0216	6.21	1.89	0.171
Sm-SEmL0.15b-4-32	883.8	3.97	0.0217	5.88	1.81	0.171
Sm-SEmL0.15b-4-33	907.8	3.94	0.0217	5.41	1.83	0.167
Sm-SEmL0.15b-4-34	936.3	3.98	0.0217	5.33	1.81	0.176
Sm-SEmL0.15b-4-35	979.5	3.97	0.0209	5.41	1.97	0.174
Sm-SEmL0.15b-4-36	1003.5	3.96	0.0217	5.59	1.95	0.171
Sm-SEmL0.15b-4-37	1027.6	3.94	0.0215	5.01	1.80	0.238
Sm-SEmL0.15b-4-38	1051.6	3.93	0.0218	5.50	1.70	0.196
Sm-SEmL0.15b-4-39	1075.5	3.95	0.0214	5.15	1.84	0.190
Sm-SEmL0.15b-4-40	1104.4	3.96	0.0217	5.25	1.89	0.179
Sm-SEmL0.15b-4-41	1147.4	3.94	0.0218	4.70	1.88	0.185
Sm-SEmL0.15b-4-42	1171.5	3.94	0.0217	4.87	1.81	0.191
Sm-SEmL0.15b-4-43	1195.6	3.93	0.0217	4.38	1.73	0.192
Sm-SEmL0.15b-4-44	1219.4	3.93	0.0216	4.15	1.60	0.182
Sm-SEmL0.15b-4-45	1243.7	3.94	0.0215	4.27	1.56	0.189
Sm-SEmL0.15b-4-46	1268.5	3.95	0.0217	4.51	1.62	0.194
Sm-SEmL0.15b-4-47	1314.8	3.93	0.0217	4.38	1.57	0.181
Sm-SEmL0.15b-4-48	1340.3	3.95	0.0212	3.86	1.46	0.192
Sm-SEmL0.15b-4-49	1366.9	3.96	0.0217	4.11	1.58	0.189
Sm-SEmL0.15b-4-50	1392.4	3.95	0.0218	4.08	1.81	0.190
Sm-SEmL0.15b-4-51	1415.6	3.94	0.0215	4.03	1.89	0.190
Sm-SEmL0.15b-4-52	1439.4	3.99	0.0217	4.68	1.68	0.256
Sm-SEmL0.15b-4-53	1485.0	3.93	0.0211	4.38	3.29	0.190
Sm-SEmL0.15b-4-54	1507.3	3.96	0.0225	4.16	1.72	0.192
Sm-SEmL0.15b-4-55	1531.5	3.92	0.0218	4.13	1.64	0.186
Sm-SEmL0.15b-4-56	1555.1	3.92	0.0219	3.77	1.60	0.191
Sm-SEmL0.15b-4-57	1578.8	3.92	0.0217	3.88	1.58	0.200
Sm-SEmL0.15b-4-58	1614.2	3.95	0.0218	3.89	1.49	0.185
Sm-SEmL0.15b-4-59	1651.3	3.94	0.0217	3.87	1.50	0.197
Sm-SEmL0.15b-4-60	1675.5	3.93	0.0217	3.72	1.51	0.183

Sm-SEmL1.5-4	**Temperature 37ºC**	**Initial pH 4.51**
Mass 0.0994 g	**Solution 112 mM KCl + 0.556 mM K_2SO_4 + 0.899 mM $KHCO_3$+ 1.5 mM Lactate**	

Run	Time (h)	pH	Flow (mL min^{-1})	Si (µM)	Al (µM)	Lactate output (mM)	Lactate input (mM)
Sm-SEmL1.5-4-1	20.9	4.70	0.0173	39.39	6.90	1.51	-
Sm-SEmL1.5-4-2	45.2	4.60	0.0204	34.91	4.24	1.51	-
Sm-SEmL1.5-4-3	74.9	4.56	0.0198	30.13	2.82	1.51	-
Sm-SEmL1.5-4-4	116.9	4.56	0.0197	20.79	2.54	1.52	-
Sm-SEmL1.5-4-5	147.9	4.52	0.0195	15.46	2.31	1.51	-
Sm-SEmL1.5-4-6	169.9	4.51	0.0195	12.18	2.25	1.50	-
Sm-SEmL1.5-4-7	193.5	4.53	0.0195	10.65	2.08	1.48	-
Sm-SEmL1.5-4-8	216.7	4.53	0.0194	9.46	1.91	1.44	-
Sm-SEmL1.5-4-9	241.8	4.52	0.0195	8.54	1.70	1.44	-
Sm-SEmL1.5-4-10	285.1	4.52	0.0199	7.54	1.56	1.42	-
Sm-SEmL1.5-4-11	308.9	4.56	0.0193	6.92	1.49	1.42	1.48
Sm-SEmL1.5-4-12	332.9	4.55	0.0194	6.53	1.46	1.43	-
Sm-SEmL1.5-4-13	360.1	4.56	0.0193	6.11	1.45	1.43	-
Sm-SEmL1.5-4-14	384.0	4.56	0.0194	5.76	1.40	1.42	-
Sm-SEmL1.5-4-15	408.8	4.58	0.0194	3.74	1.38	1.39	-
Sm-SEmL1.5-4-16	452.8	4.61	0.0194	5.01	1.41	1.36	-
Sm-SEmL1.5-4-17	476.9	4.65	0.0192	4.60	1.17	1.31	1.50
Sm-SEmL1.5-4-18	500.8	4.68	0.0193	4.66	1.09	1.30	-
Sm-SEmL1.5-4-19	525.0	4.70	0.0193	4.53	1.03	1.24	-
Sm-SEmL1.5-4-20	551.7	4.70	0.0193	4.31	1.01	1.23	-
Sm-SEmL1.5-4-21	577.2	4.71	0.0193	4.22	0.98	1.23	-
Sm-SEmL1.5-4-22	620.7	4.64	0.0193	3.95	1.00	1.24	-
Sm-SEmL1.5-4-23	644.9	4.65	0.0193	3.59	0.99	1.25	-
Sm-SEmL1.5-4-24	668.7	4.64	0.0193	3.75	0.97	1.25	-
Sm-SEmL1.5-4-25	693.7	4.63	0.0193	3.36	1.04	1.27	1.55
Sm-SEmL1.5-4-26	717.8	4.59	0.0193	3.68	1.00	1.26	-
Sm-SEmL1.5-4-27	745.4	4.58	0.0193	3.19	0.97	1.29	-
Sm-SEmL1.5-4-28	789.7	4.56	0.0193	3.27	0.96	1.27	-
Sm-SEmL1.5-4-29	812.9	4.55	0.0192	3.10	1.00	1.28	-
Sm-SEmL1.5-4-30	837.1	4.55	0.0193	2.98	1.00	1.26	-
Sm-SEmL1.5-4-31	861.5	4.55	0.0194	3.15	1.00	1.26	1.56
Sm-SEmL1.5-4-32	888.0	4.52	0.0192	3.07	1.00	1.26	-
Sm-SEmL1.5-4-33	913.7	4.54	0.0192	2.97	1.03	1.28	-
Sm-SEmL1.5-4-34	957.0	4.53	0.0192	2.82	1.02	1.29	-
Sm-SEmL1.5-4-35	981.1	4.52	0.0192	2.83	1.09	1.29	-
Sm-SEmL1.5-4-36	1005.4	4.51	0.0192	2.84	1.12	1.28	1.53
Sm-SEmL1.5-4-37	1029.7	4.51	0.0192	2.76	1.04	1.25	-
Sm-SEmL1.5-4-38	1056.0	4.50	0.0192	3.23	1.18	1.27	-
Sm-SEmL1.5-4-39	1081.1	4.50	0.0185	2.71	1.16	1.28	-
Sm-SEmL1.5-4-40	1125.7	4.50	0.0193	2.98	1.05	1.27	-
Sm-SEmL1.5-4-41	1150.3	4.53	0.0192	2.99	1.12	1.29	-
Sm-SEmL1.5-4-42	1177.9	4.52	0.0193	2.93	1.09	1.27	1.57

Sm-SEmL1.5-4b	**Temperature 37ºC**	**Initial pH 3.96**
Mass 0.0999 g	**Solution 112 mM KCl + 0.556 mM K_2SO_4 + 0.7 mM $KHCO_3$ + 1.5 mM Lactate**	

Run	Time (h)	pH	Flow (mL min^{-1})	Si (µM)	Al (µM)	Lactate output (mM)
Sm-SEmL1.5-4-1	19.7	3.39	0.0248	50.20	42.04	1.42
Sm-SEmL1.5-4-2	44.2	3.76	0.0225	39.56	19.45	1.45
Sm-SEmL1.5-4-3	67.8	3.91	0.0224	22.54	7.30	1.46
Sm-SEmL1.5-4-4	93.2	3.98	0.0229	23.87	3.09	1.45
Sm-SEmL1.5-4-5	139.4	3.94	0.0222	31.43	2.98	1.42
Sm-SEmL1.5-4-6	163.4	3.96	0.0219	24.62	2.51	1.49
Sm-SEmL1.5-4-7	187.4	3.96	0.0220	15.96	2.43	1.47
Sm-SEmL1.5-4-8	215.8	3.97	0.0218	14.01	2.37	1.49
Sm-SEmL1.5-4-9	237.1	3.96	0.0218	11.78	2.23	1.51
Sm-SEmL1.5-4-10	260.9	3.97	0.0217	11.08	2.26	1.48
Sm-SEmL1.5-4-11	307.4	3.95	0.0216	9.72	2.13	1.48
Sm-SEmL1.5-4-12	331.5	3.97	0.0217	8.97	2.15	1.48
Sm-SEmL1.5-4-13	355.4	3.96	0.0217	9.08	2.18	1.50
Sm-SEmL1.5-4-14	379.5	3.96	0.0216	8.17	2.11	1.54
Sm-SEmL1.5-4-15	406.0	3.95	0.0214	7.75	2.05	1.57
Sm-SEmL1.5-4-16	429.7	3.95	0.0217	7.79	2.00	1.57
Sm-SEmL1.5-4-17	475.6	3.95	0.0215	7.06	1.88	1.56
Sm-SEmL1.5-4-18	499.7	3.95	0.0213	6.99	1.92	1.55
Sm-SEmL1.5-4-19	523.6	3.96	0.0215	6.55	1.80	1.54
Sm-SEmL1.5-4-20	547.7	3.95	0.0215	6.42	0.22	1.60
Sm-SEmL1.5-4-21	571.5	3.95	0.0215	6.40	1.74	1.57
Sm-SEmL1.5-4-22	596.9	3.96	0.0216	6.56	1.88	1.57
Sm-SEmL1.5-4-23	643.4	3.95	0.0216	5.68	1.74	1.56
Sm-SEmL1.5-4-24	667.4	3.95	0.0214	5.45	1.67	-
Sm-SEmL1.5-4-25	691.4	3.94	0.0215	5.45	1.70	1.56
Sm-SEmL1.5-4-26	715.3	3.95	0.0215	6.64	2.01	1.63
Sm-SEmL1.5-4-27	739.4	3.96	0.0216	5.81	1.78	1.58
Sm-SEmL1.5-4-28	767.7	3.96	0.0215	5.29	1.62	1.60
Sm-SEmL1.5-4-29	811.5	3.96	0.0215	5.05	1.49	1.61
Sm-SEmL1.5-4-30	836.3	3.96	0.0213	5.09	1.52	1.60
Sm-SEmL1.5-4-31	860.4	3.96	0.0214	4.93	1.61	1.62
Sm-SEmL1.5-4-32	883.5	3.96	0.0215	5.18	1.94	1.61
Sm-SEmL1.5-4-33	907.5	3.95	0.0214	4.97	1.86	1.61
Sm-SEmL1.5-4-34	936.1	3.96	0.0215	5.07	1.66	1.60
Sm-SEmL1.5-4-35	979.3	3.97	0.0215	4.75	0.89	1.64
Sm-SEmL1.5-4-36	1003.2	3.95	0.0214	4.75	1.75	1.64
Sm-SEmL1.5-4-37	1027.3	3.95	0.0218	4.60	1.62	1.74
Sm-SEmL1.5-4-38	1051.4	3.94	0.0212	4.55	1.57	1.73
Sm-SEmL1.5-4-39	1075.2	3.95	0.0218	4.62	1.79	1.72
Sm-SEmL1.5-4-40	1104.1	3.95	0.0214	4.74	1.76	1.73
Sm-SEmL1.5-4-41	1147.2	3.95	0.0215	4.24	1.83	1.74
Sm-SEmL1.5-4-42	1171.3	3.94	0.0214	3.98	1.74	1.74
Sm-SEmL1.5-4-43	1195.3	3.93	0.0214	3.99	1.68	1.74
Sm-SEmL1.5-4-44	1219.2	3.94	0.0213	3.73	1.53	1.73
Sm-SEmL1.5-4-45	1243.5	3.94	0.0211	3.97	1.75	1.77
Sm-SEmL1.5-4-46	1268.2	3.94	0.0213	3.86	1.71	1.75
Sm-SEmL1.5-4-47	1314.6	3.93	0.0213	4.08	1.86	1.74

Run	Time (h)	pH	Flow (mL min^{-1})	Si (µM)	Al (µM)	Lactate output (mM)
Sm-SEmL1.5-4-48	1340.0	3.94	0.0216	4.01	1.57	1.77
Sm-SEmL1.5-4-49	1366.6	3.95	0.0213	3.93	1.56	1.75
Sm-SEmL1.5-4-50	1392.2	3.94	0.0214	4.00	1.76	1.87
Sm-SEmL1.5-4-51	1415.3	3.95	0.0211	3.83	1.78	1.75
Sm-SEmL1.5-4-52	1439.2	3.97	0.0213	3.80	1.66	1.78
Sm-SEmL1.5-4-53	1484.8	3.96	0.0208	3.71	1.61	1.78
Sm-SEmL1.5-4-54	1507.1	3.93	0.0222	3.65	3.22	1.76
Sm-SEmL1.5-4-55	1531.2	3.92	0.0214	3.87	1.45	1.76
Sm-SEmL1.5-4-56	1554.8	3.92	0.0215	3.68	1.52	1.77
Sm-SEmL1.5-4-57	1578.5	3.93	0.0214	3.45	1.46	1.76
Sm-SEmL1.5-4-58	1614.0	3.94	0.0214	3.57	1.32	1.78
Sm-SEmL1.5-4-59	1651.1	3.93	0.0214	3.64	1.45	1.82
Sm-SEmL1.5-4-60	1675.3	3.93	0.0213	3.38	1.55	1.84

Sm-SEmL15-4	**Temperature 37ºC**	**Initial pH 4.39**
Mass 0.0998 g	**Solution 112 mM KCl + 0.556 mM K_2SO_4 + 9 mM $KHCO_3$ + 15 mM Lactate**	

Run	Time (h)	pH	Flow (mL min^{-1})	Si (µM)	Al (µM)	Lactate output (mM)	Lactate input (mM)
Sm-SEmL15-4-1	20.7	4.43	0.0189	59.19	33.10	14.5	-
Sm-SEmL15-4-2	45.0	4.41	0.0201	48.44	20.26	14.7	-
Sm-SEmL15-4-3	74.7	4.39	0.0196	43.27	9.51	14.6	-
Sm-SEmL15-4-4	116.7	4.38	0.0196	27.20	6.72	14.7	-
Sm-SEmL15-4-5	147.7	4.38	0.0193	20.04	4.75	14.7	-
Sm-SEmL15-4-6	169.8	4.34	0.0193	17.60	4.34	14.7	-
Sm-SEmL15-4-7	193.3	4.36	0.0193	15.69	3.80	14.7	-
Sm-SEmL15-4-8	216.5	4.34	0.0193	13.76	3.54	14.6	-
Sm-SEmL15-4-9	241.7	4.32	0.0194	12.78	3.29	14.6	-
Sm-SEmL15-4-10	285.0	4.31	0.0198	11.20	3.16	14.7	-
Sm-SEmL15-4-11	308.7	4.34	0.0193	10.17	2.93	14.5	14.4
Sm-SEmL15-4-12	332.7	4.37	0.0193	9.51	2.71	14.6	-
Sm-SEmL15-4-13	359.9	4.35	0.0193	9.07	2.63	14.7	-
Sm-SEmL15-4-14	383.8	4.34	0.0193	8.47	2.57	14.8	-
Sm-SEmL15-4-15	408.6	4.35	0.0193	8.21	2.38	14.7	-
Sm-SEmL15-4-16	452.7	4.34	0.0193	7.86	2.39	14.7	-
Sm-SEmL15-4-17	476.7	4.33	0.0193	7.27	2.21	14.8	14.6
Sm-SEmL15-4-18	500.6	4.33	0.0193	6.87	2.14	15.0	-
Sm-SEmL15-4-19	524.8	4.33	0.0194	6.80	2.12	14.9	-
Sm-SEmL15-4-20	551.5	4.33	0.0193	7.17	2.09	14.9	-
Sm-SEmL15-4-21	577.0	4.34	0.0192	7.24	2.08	14.9	-
Sm-SEmL15-4-22	620.5	4.33	0.0193	7.31	2.05	14.9	-
Sm-SEmL15-4-23	644.7	4.32	0.0193	6.24	1.99	14.9	-
Sm-SEmL15-4-24	668.6	4.32	0.0193	6.84	1.99	15.0	-
Sm-SEmL15-4-25	693.5	4.33	0.0193	6.13	1.96	15.1	15.0
Sm-SEmL15-4-26	717.7	4.31	0.0193	5.84	1.86	15.2	-
Sm-SEmL15-4-27	745.3	4.30	0.0193	6.74	1.82	15.2	-
Sm-SEmL15-4-28	789.5	4.29	0.0193	5.88	2.07	15.3	-

Run	Time (h)	pH	Flow (mL min^{-1})	Si (µM)	Al (µM)	Lactate output (mM)	Lactate input (mM)
Sm-SEmL15-4-29	812.7	4.30	0.0193	5.47	1.80	16.8	-
Sm-SEmL15-4-30	837.0	4.32	0.0193	5.71	1.93	-	-
Sm-SEmL15-4-31	861.3	4.31	0.0194	5.43	1.84	15.2	15.1
Sm-SEmL15-4-32	887.8	4.28	0.0194	5.39	1.78	15.3	-
Sm-SEmL15-4-33	913.5	4.31	0.0194	5.37	1.83	15.4	-
Sm-SEmL15-4-34	956.9	4.30	0.0193	5.97	1.79	15.4	-
Sm-SEmL15-4-35	981.0	4.29	0.0193	5.84	1.76	15.4	-
Sm-SEmL15-4-36	1005.3	4.30	0.0194	6.17	1.79	15.2	15.0
Sm-SEmL15-4-37	1029.5	4.31	0.0193	5.12	1.70	15.4	-
Sm-SEmL15-4-38	1055.9	4.29	0.0193	5.14	1.74	15.6	-
Sm-SEmL15-4-39	1080.9	4.30	0.0186	4.96	1.77	15.3	-
Sm-SEmL15-4-40	1125.5	4.29	0.0193	4.83	1.78	15.2	-
Sm-SEmL15-4-41	1150.1	4.30	0.0193	4.85	1.70	15.3	-
Sm-SEmL15-4-42	1177.7	4.30	0.0194	5.38	1.87	15.3	15.2

Sm-SEm15-4b	**Temperature 37ºC**	**Initial pH 3.92**
Mass 0.1000 g	**Solution 112 mM KCl + 0.556 mM K_2SO_4 + 0.8 mM $KHCO_3$ + 15 mM Lactate**	

Run	Time (h)	pH	Flow (mL min^{-1})	Si (µM)	Al (µM)	Lactate output (mM)
Sm-SEmL15-4b-1	19.5	3.74	0.0221	56.53	56.87	14.3
Sm-SEmL15-4b-2	43.9	3.87	0.0232	45.96	20.32	14.6
Sm-SEmL15-4b-3	67.5	3.90	0.0230	26.51	7.35	14.5
Sm-SEmL15-4b-4	92.9	3.93	0.0233	35.45	4.84	14.5
Sm-SEmL15-4b-5	139.2	3.91	0.0228	34.50	5.08	14.8
Sm-SEmL15-4b-6	163.1	3.90	0.0228	26.26	4.44	14.6
Sm-SEmL15-4b-7	187.2	3.91	0.0230	20.27	3.76	14.4
Sm-SEmL15-4b-8	215.5	3.90	0.0224	17.67	3.96	14.9
Sm-SEmL15-4b-9	236.9	3.91	0.0230	15.44	3.63	14.6
Sm-SEmL15-4b-10	260.7	3.92	0.0223	14.48	3.48	14.8
Sm-SEmL15-4b-11	307.2	3.90	0.0222	12.98	3.45	14.9
Sm-SEmL15-4b-12	331.3	3.91	0.0221	12.40	3.34	14.9
Sm-SEmL15-4b-13	355.1	3.90	0.0221	11.41	3.03	15.3
Sm-SEmL15-4b-14	379.2	3.91	0.0221	11.16	2.86	15.4
Sm-SEmL15-4b-15	405.8	3.90	0.0220	10.08	2.91	15.4
Sm-SEmL15-4b-16	429.4	3.90	0.0221	10.50	2.83	15.5
Sm-SEmL15-4b-17	475.3	3.89	0.0220	9.78	3.00	15.3
Sm-SEmL15-4b-18	499.5	3.89	0.0220	9.36	2.78	15.3
Sm-SEmL15-4b-19	523.4	3.90	0.0221	9.29	2.49	15.3
Sm-SEmL15-4b-20	547.4	3.91	0.0220	9.03	2.65	15.6
Sm-SEmL15-4b-21	571.2	3.89	0.0220	8.58	2.79	15.5
Sm-SEmL15-4b-22	596.6	3.90	0.0220	8.34	2.52	15.4
Sm-SEmL15-4b-23	643.1	3.89	0.0220	8.52	3.67	15.5
Sm-SEmL15-4b-24	667.1	3.89	0.0219	7.90	2.45	15.6
Sm-SEmL15-4b-25	691.2	3.89	0.0220	8.33	2.65	15.7
Sm-SEmL15-4b-26	715.1	3.89	0.0220	8.21	2.58	15.7
Sm-SEmL15-4b-27	739.1	3.90	0.0220	7.45	2.44	15.7
Sm-SEmL15-4b-28	767.5	3.90	0.0220	7.74	2.45	16.0

Run	Time (h)	pH	Flow (mL min^{-1})	Si (µM)	Al (µM)	Lactate output (mM)
Sm-SEmL15-4b-29	811.3	3.90	0.0217	7.41	2.51	15.9
Sm-SEmL15-4b-30	836.1	3.90	0.0218	7.99	2.57	16.0
Sm-SEmL15-4b-31	860.2	3.89	0.0219	6.68	2.49	16.0
Sm-SEmL15-4b-32	883.3	3.89	0.0218	6.58	2.45	16.0
Sm-SEmL15-4b-33	907.3	3.91	0.0219	6.68	2.46	16.1
Sm-SEmL15-4b-34	935.8	3.89	0.0220	6.81	2.78	16.4
Sm-SEmL15-4b-35	979.0	3.88	0.0218	6.68	0.00	16.6

Sm-SEmL0.15-7	**Temperature 37ºC**	**Initial pH 6.98**
Mass 0.0996 g	**Solution 112 mM KCl + 0.556 mM K_2SO_4 + 0.599 mM $KHCO_3$+ 0.15 mM Lactate**	

Run	Time (h)	pH	Flow (mL min^{-1})	Si (µM)	Al (µM)	Lactate output (mM)	Lactate input (mM)
Sm-SEmL0.15-7-1	23.6	7.16	0.0240	30.05	0.83	0.205	0.152
Sm-SEmL0.15-7-2	48.1	7.34	0.0239	25.18	0.98	0.185	-
Sm-SEmL0.15-7-3	76.6	7.40	0.0233	33.10	0.39	0.097	-
Sm-SEmL0.15-7-4	139.5	7.70	0.0230	16.92	0.11	0.015	0.148
Sm-SEmL0.15-7-5	163.5	7.59	0.0229	11.40	0.22	0.036	-
Sm-SEmL0.15-7-6	187.5	7.56	0.0228	9.58	0.12	0.026	-
Sm-SEmL0.15-7-7	211.7	7.69	0.0175	8.04	0.29	0.044	0.147
Sm-SEmL0.15-7-8	243.3	7.39	0.0228	7.59	0.16	0.027	-
Sm-SEmL0.15-7-9	307.3	7.63	0.0227	4.84	0.07	0.021	0.139
Sm-SEmL0.15-7-10	331.3	7.46	0.0226	4.28	0.28	0.034	-
Sm-SEmL0.15-7-11	355.4	7.25	0.0226	4.80	0.17	0.014	-
Sm-SEmL0.15-7-12	379.7	7.20	0.0226	4.51	0.10	0.033	-
Sm-SEmL0.15-7-13	406.3	7.23	0.0225	4.36	0.11	0.015	-
Sm-SEmL0.15-7-14	433.1	7.24	0.0225	4.08	0.10	0.018	-
Sm-SEmL0.15-7-15	475.5	7.18	0.0225	3.45	0.06	0.015	0.124
Sm-SEmL0.15-7-16	499.5	7.01	0.0225	3.18	0.07	0.024	-
Sm-SEmL0.15-7-17	523.5	7.18	0.0225	2.28	0.07	0.023	-
Sm-SEmL0.15-7-18	547.3	7.11	0.0226	2.54	0.08	0.024	-
Sm-SEmL0.15-7-19	575.7	7.00	0.0226	2.39	0.10	0.026	-
Sm-SEmL0.15-7-20	598.3	7.02	0.0224	2.60	0.17	0.023	-
Sm-SEmL0.15-7-21	643.4	7.16	0.0225	2.38	0.08	0.026	0.126
Sm-SEmL0.15-7-22	667.4	7.33	0.0224	2.05	0.11	0.036	-
Sm-SEmL0.15-7-23	691.4	7.20	0.0225	1.56	0.08	0.026	-
Sm-SEmL0.15-7-24	715.6	7.00	0.0225	1.51	0.07	0.030	-
Sm-SEmL0.15-7-25	742.9	7.20	0.0224	1.48	0.11	0.037	-
Sm-SEmL0.15-7-26	768.2	7.22	0.0225	1.71	0.10	0.032	-
Sm-SEmL0.15-7-27	811.6	7.20	0.0140	1.46	0.04	0.031	0.110
Sm-SEmL0.15-7-28	835.4	7.17	0.0224	2.54	0.06	0.031	-
Sm-SEmL0.15-7-29	859.4	7.23	0.0225	1.91	0.11	0.019	-
Sm-SEmL0.15-7-30	883.3	7.13	0.0225	1.41	0.09	0.032	-
Sm-SEmL0.15-7-31	909.9	7.34	0.0226	1.16	0.11	0.032	-
Sm-SEmL0.15-7-32	934.7	7.06	0.0225	1.14	0.09	0.065	-
Sm-SEmL0.15-7-33	979.4	7.22	0.0226	1.15	0.05	0.034	0.118
Sm-SEmL0.15-7-34	1003.6	7.01	0.0225	1.08	0.10	0.024	-

Run	Time (h)	pH	Flow (mL min^{-1})	Si (µM)	Al (µM)	Lactate output (mM)	Lactate input (mM)
Sm-SEmL0.15-7-35	1029.9	7.33	0.0225	1.34	0.16	0.031	-
Sm-SEmL0.15-7-36	1054.3	6.91	0.0225	1.12	0.16	0.027	-
Sm-SEmL0.15-7-37	1078.9	7.23	0.0225	1.08	0.14	0.034	-
Sm-SEmL0.15-7-38	1104.6	7.19	0.0225	1.11	0.16	0.027	-
Sm-SEmL0.15-7-39	1147.6	7.16	0.0210	1.20	0.10	0.030	0.129
Sm-SEmL0.15-7-40	1174.4	6.98	0.0225	1.01	0.13	0.022	-
Sm-SEmL0.15-7-41	1198.3	7.15	0.0223	0.98	0.10	0.034	-
Sm-SEmL0.15-7-42	1222.4	7.14	0.0222	1.00	0.13	0.028	-
Sm-SEmL0.15-7-43	1247.3	6.85	0.0222	2.12	0.49	0.040	-
Sm-SEmL0.15-7-44	1270.6	7.05	0.0223	0.92	0.11	0.030	-
Sm-SEmL0.15-7-45	1315.6	7.11	0.0222	0.94	0.07	0.024	-
Sm-SEmL0.15-7-46	1339.4	7.09	0.0220	0.92	0.07	0.031	-
Sm-SEmL0.15-7-47	1363.3	7.11	0.0221	0.86	0.10	0.030	-
Sm-SEmL0.15-7-48	1387.4	7.13	0.0222	0.85	0.16	0.032	-
Sm-SEmL0.15-7-49	1415.3	6.97	0.0222	0.86	0.08	0.040	-
Sm-SEmL0.15-7-50	1440.1	7.19	0.0222	0.92	0.14	0.011	-
Sm-SEmL0.15-7-51	1483.8	7.10	0.0221	1.82	0.03	0.024	-
Sm-SEmL0.15-7-52	1507.9	7.10	0.0221	1.04	0.15	0.038	-
Sm-SEmL0.15-7-53	1534.6	7.12	0.0219	0.83	0.10	0.043	-
Sm-SEmL0.15-7-54	1560.5	7.14	0.0221	0.87	0.09	0.032	-
Sm-SEmL0.15-7-55	1584.3	7.19	0.0221	0.96	0.09	0.024	-
Sm-SEmL0.15-7-56	1608.6	7.12	0.0220	1.30	0.16	0.029	-
Sm-SEmL0.15-7-57	1651.4	7.06	0.0058	1.51	0.17	0.032	-
Sm-SEmL0.15-7-58	1679.4	7.10	0.0218	1.64	0.11	0.033	-

Sm-SEmL0.15-7b	**Temperature 37ºC**	**Initial pH 7.05**
Mass 0.1001 g	**Solution 112 mM KCl + 0.556 mM K_2SO_4 + 0.599 mM $KHCO_3$+ 0.15 mM Lactate**	

Run	Time (h)	pH	Flow (mL min^{-1})	Si (µM)	Al (µM)
Sm-SEmL0.15-7b-1	64.3	7.07	0.0231	28.11	2.21
Sm-SEmL0.15-7b-2	88.6	7.54	0.0243	11.54	0.15
Sm-SEmL0.15-7b-3	112.6	7.54	0.0237	15.18	1.09
Sm-SEmL0.15-7b-4	139.8	7.47	0.0234	18.07	0.27
Sm-SEmL0.15-7b-5	164.9	7.36	0.0233	13.88	0.21
Sm-SEmL0.15-7b-6	188.9	7.42	0.0232	11.00	0.24
Sm-SEmL0.15-7b-7	232.7	7.61	0.0232	8.68	0.17
Sm-SEmL0.15-7b-8	257.1	7.31	0.0232	9.07	1.25
Sm-SEmL0.15-7b-9	280.6	7.66	0.0232	6.09	0.15
Sm-SEmL0.15-7b-10	304.4	7.55	0.0230	5.58	0.16
Sm-SEmL0.15-7b-11	332.3	7.61	0.0232	5.03	0.16
Sm-SEmL0.15-7b-12	399.9	7.50	0.0232	4.61	0.15
Sm-SEmL0.15-7b-13	424.1	7.40	0.0231	3.63	0.16
Sm-SEmL0.15-7b-14	447.8	7.33	0.0232	3.37	0.12
Sm-SEmL0.15-7b-15	471.9	7.20	0.0231	3.07	0.18
Sm-SEmL0.15-7b-16	498.7	7.50	0.0231	2.88	0.10
Sm-SEmL0.15-7b-17	567.9	7.54	0.0231	2.69	0.02
Sm-SEmL0.15-7b-18	591.9	7.44	0.0231	2.35	0.12
Sm-SEmL0.15-7b-19	616.0	7.41	0.0231	2.24	0.10

Run	Time (h)	pH	Flow (mL min^{-1})	Si (µM)	Al (µM)
Sm-SEmL0.15-7b-20	640.0	7.39	0.0232	2.12	0.07
Sm-SEmL0.15-7b-21	667.8	7.43	0.0231	2.13	0.07
Sm-SEmL0.15-7b-22	736.4	7.33	0.0231	2.18	0.08
Sm-SEmL0.15-7b-23	760.4	7.28	0.0232	1.90	0.15
Sm-SEmL0.15-7b-24	784.6	7.34	0.0232	1.87	0.12
Sm-SEmL0.15-7b-25	808.5	7.43	0.0232	1.90	0.15
Sm-SEmL0.15-7b-26	833.0	7.26	0.0232	1.79	0.18
Sm-SEmL0.15-7b-27	858.5	7.40	0.0232	1.73	0.12
Sm-SEmL0.15-7b-28	903.9	7.50	0.0231	1.66	0.10
Sm-SEmL0.15-7b-29	928.5	7.29	0.0231	1.64	0.12
Sm-SEmL0.15-7b-30	954.4	7.36	0.0231	1.65	0.16
Sm-SEmL0.15-7b-31	978.8	7.41	0.0232	1.66	0.12
Sm-SEmL0.15-7b-32	1003.5	7.41	0.0232	1.76	0.12
Sm-SEmL0.15-7b-33	1028.3	7.30	0.0231	1.59	0.16
Sm-SEmL0.15-7b-34	1072.1	7.44	0.0231	1.61	0.07
Sm-SEmL0.15-7b-35	1095.8	7.41	0.0231	1.70	0.12
Sm-SEmL0.15-7b-36	1122.0	7.34	0.0232	1.59	0.14
Sm-SEmL0.15-7b-37	1146.5	7.38	0.0232	1.59	0.12
Sm-SEmL0.15-7b-38	1172.7	7.26	0.0232	1.61	0.08
Sm-SEmL0.15-7b-39	1195.8	7.31	0.0232	1.50	0.18
Sm-SEmL0.15-7b-40	1239.8	7.41	0.0226	3.69	0.05
Sm-SEmL0.15-7b-41	1263.9	7.51	0.0230	1.45	0.13
Sm-SEmL0.15-7b-42	1288.6	7.46	0.0231	1.87	0.10
Sm-SEmL0.15-7b-43	1313.0	7.40	0.0231	2.16	0.07
Sm-SEmL0.15-7b-44	1337.5	7.45	0.0232	1.65	1.69
Sm-SEmL0.15-7b-45	1362.8	7.42	0.0231	1.29	0.07
Sm-SEmL0.15-7b-46	1407.9	7.39	0.0231	1.45	0.01
Sm-SEmL0.15-7b-47	1432.6	7.54	0.0231	1.48	0.07
Sm-SEmL0.15-7b-48	1457.0	7.47	0.0231	1.39	0.07
Sm-SEmL0.15-7b-49	1484.0	7.48	0.0230	1.96	0.09
Sm-SEmL0.15-7b-50	1506.1	7.41	0.0230	1.29	0.07
Sm-SEmL0.15-7b-51	1576.5	7.51	0.0218	1.59	0.05
Sm-SEmL0.15-7b-52	1601.1	7.51	0.0230	1.48	0.09
Sm-SEmL0.15-7b-53	1624.9	7.57	0.0231	1.52	0.09
Sm-SEmL0.15-7b-54	1648.4	7.36	0.0232	1.51	0.14
Sm-SEmL0.15-7b-55	1676.3	7.44	0.0194	1.54	0.22
Sm-SEmL0.15-7b-56	1743.7	7.60	0.0231	1.56	0.09
Sm-SEmL0.15-7b-57	1767.9	7.43	0.0232	1.29	0.17
Sm-SEmL0.15-7b-58	1792.2	7.45	0.0232	1.45	0.11
Sm-SEmL0.15-7b-59	1816.5	7.56	0.0232	1.36	0.15
Sm-SEmL0.15-7b-60	1844.7	7.46	0.0232	1.28	0.16
Sm-SEmL0.15-7b-61	1912.7	7.48	0.0232	1.32	0.06

Sm-SEmL1.5-7	**Temperature 37ºC**	**Initial pH 7.22**
Mass 0.0997 g	**Solution 112 mM KCl + 0.556 mM K_2SO_4 + 4.99 mM $KHCO_3$+ 1.5 mM Lactate**	

Run	Time (h)	pH	Flow (mL min^{-1})	Si (µM)	Al (µM)	Lactate output (mM)	Lactate input (mM)
Sm-SEmL1.5-7-1	23.5	7.84	0.0245	27.95	0.71	1.87	1.42
Sm-SEmL1.5-7-2	48.0	8.27	0.0245	31.36	0.14	1.82	-
Sm-SEmL1.5-7-3	76.5	8.17	0.0242	26.15	0.28	1.85	-
Sm-SEmL1.5-7-4	139.4	8.51	0.0239	14.14	0.34	1.66	1.42
Sm-SEmL1.5-7-5	163.4	8.21	0.0239	9.59	0.74	1.69	-
Sm-SEmL1.5-7-6	187.5	8.29	0.0238	7.63	0.47	1.72	-
Sm-SEmL1.5-7-7	211.6	8.38	0.0238	6.09	0.50	1.74	1.46
Sm-SEmL1.5-7-8	243.2	8.06	0.0237	6.18	0.32	1.70	-
Sm-SEmL1.5-7-9	307.2	8.07	0.0236	4.60	0.27	1.69	1.46
Sm-SEmL1.5-7-10	331.2	7.94	0.0236	4.12	0.31	1.73	-
Sm-SEmL1.5-7-11	355.3	7.55	0.0236	4.79	0.37	1.71	-
Sm-SEmL1.5-7-12	379.6	7.25	0.0236	3.76	0.15	1.68	-
Sm-SEmL1.5-7-13	406.2	7.38	0.0235	3.55	0.46	1.62	-
Sm-SEmL1.5-7-14	433.0	7.35	0.0236	3.05	0.12	1.61	-
Sm-SEmL1.5-7-15	475.4	7.48	0.0234	2.39	0.08	1.60	1.48
Sm-SEmL1.5-7-16	499.4	7.27	0.0235	2.60	0.14	1.69	-
Sm-SEmL1.5-7-17	523.4	7.36	0.0235	1.97	0.13	1.65	-
Sm-SEmL1.5-7-18	547.2	7.38	0.0236	2.24	0.13	1.65	-
Sm-SEmL1.5-7-19	575.6	7.21	0.0236	1.68	0.14	1.62	-
Sm-SEmL1.5-7-20	598.2	7.37	0.0235	1.57	0.14	1.65	-
Sm-SEmL1.5-7-21	643.3	7.44	0.0235	1.89	0.10	1.61	1.51
Sm-SEmL1.5-7-22	667.3	7.50	0.0234	1.65	0.17	1.66	-
Sm-SEmL1.5-7-23	691.3	7.26	0.0235	1.26	0.13	1.65	-
Sm-SEmL1.5-7-24	715.5	7.37	0.0235	1.72	0.11	1.69	-
Sm-SEmL1.5-7-25	742.8	7.28	0.0235	1.16	0.12	1.63	-
Sm-SEmL1.5-7-26	768.1	7.36	0.0235	1.13	0.11	1.65	-
Sm-SEmL1.5-7-27	811.5	7.48	0.0146	1.71	0.08	1.64	1.53
Sm-SEmL1.5-7-28	835.3	7.25	0.0235	1.93	0.12	1.62	-
Sm-SEmL1.5-7-29	859.3	7.26	0.0235	1.20	0.13	1.66	-
Sm-SEmL1.5-7-30	883.2	7.36	0.0235	0.97	0.13	1.65	-
Sm-SEmL1.5-7-31	909.8	7.41	0.0236	2.79	0.43	1.64	-
Sm-SEmL1.5-7-32	934.6	7.34	0.0235	1.31	0.18	1.65	-
Sm-SEmL1.5-7-33	979.3	7.35	0.0235	0.95	0.07	1.63	1.53
Sm-SEmL1.5-7-34	1003.5	7.38	0.0236	1.13	0.13	1.64	-
Sm-SEmL1.5-7-35	1029.8	7.30	0.0236	0.90	0.14	1.64	-
Sm-SEmL1.5-7-36	1054.2	7.06	0.0236	0.97	0.26	1.64	-
Sm-SEmL1.5-7-37	1078.8	7.36	0.0236	0.90	0.21	1.66	-
Sm-SEmL1.5-7-38	1104.5	7.36	0.0236	1.34	0.22	1.66	-
Sm-SEmL1.5-7-39	1147.5	7.47	0.0234	1.20	0.12	1.66	1.82
Sm-SEmL1.5-7-40	1174.3	7.21	0.0235	0.78	0.17	1.65	-
Sm-SEmL1.5-7-41	1198.2	7.18	0.0235	0.78	0.13	1.67	-
Sm-SEmL1.5-7-42	1222.3	7.33	0.0233	1.11	0.27	1.68	-
Sm-SEmL1.5-7-43	1247.2	7.21	0.0233	1.78	0.43	1.67	-
Sm-SEmL1.5-7-44	1270.5	7.31	0.0233	0.70	0.13	1.66	-
Sm-SEmL1.5-7-45	1315.5	7.46	0.0233	0.68	0.08	1.65	-
Sm-SEmL1.5-7-46	1339.3	7.25	0.0233	0.68	0.17	1.66	-
Sm-SEmL1.5-7-47	1363.2	7.31	0.0233	0.99	0.14	1.67	-

Run	Time (h)	pH	Flow (mL min^{-1})	Si (µM)	Al (µM)	Lactate output (mM)	Lactate input (mM)
Sm-SEmL1.5-7-48	1387.3	7.22	0.0234	0.77	0.13	1.66	-
Sm-SEmL1.5-7-49	1415.2	7.11	0.0233	0.64	0.15	1.65	-
Sm-SEmL1.5-7-50	1440.0	7.27	0.0235	0.97	0.14	1.65	-
Sm-SEmL1.5-7-51	1483.7	7.28	0.0234	1.16	0.07	1.64	-
Sm-SEmL1.5-7-52	1507.8	7.31	0.0233	1.03	0.21	1.66	-
Sm-SEmL1.5-7-53	1534.5	7.25	0.0233	0.63	0.13	1.67	-
Sm-SEmL1.5-7-54	1560.4	7.31	0.0233	0.73	0.15	1.67	-
Sm-SEmL1.5-7-55	1584.2	7.25	0.0233	0.87	0.15	1.64	-
Sm-SEmL1.5-7-56	1608.5	6.95	0.0233	1.06	0.20	1.67	-
Sm-SEmL1.5-7-57	1651.3	7.28	0.0063	1.55	0.20	1.73	-
Sm-SEmL1.5-7-58	1679.3	7.30	0.0231	1.11	0.11	1.64	1.60

Sm-SEmL1.5-7b	**Temperature 37ºC**	**Initial pH 7.12**
Mass 0.0997 g	**Solution 112 mM KCl + 0.556 mM K_2SO_4 + 4.99 mM $KHCO_3$+ 1.5 mM Lactate**	

Run	Time (h)	pH	Flow (mL min^{-1})	Si (µM)	Al (µM)
Sm-SEmL1.5-7b-1	67.7	8.47	0.0229	21.70	0.17
Sm-SEmL1.5-7b-2	92.1	8.49	0.0231	11.01	0.17
Sm-SEmL1.5-7b-3	116.0	8.48	0.0228	16.24	0.17
Sm-SEmL1.5-7b-4	143.3	8.39	0.0226	17.23	0.23
Sm-SEmL1.5-7b-5	168.4	8.39	0.0225	14.57	0.36
Sm-SEmL1.5-7b-6	192.3	8.35	0.0224	12.26	0.39
Sm-SEmL1.5-7b-7	236.1	8.58	0.0223	13.82	0.40
Sm-SEmL1.5-7b-8	260.5	8.37	0.0224	8.35	0.54
Sm-SEmL1.5-7b-9	284.0	8.40	0.0223	6.95	0.50
Sm-SEmL1.5-7b-10	307.9	8.35	0.0222	6.52	0.56
Sm-SEmL1.5-7b-11	335.7	8.36	0.0223	5.91	0.54
Sm-SEmL1.5-7b-12	403.3	8.30	0.0221	5.16	0.46
Sm-SEmL1.5-7b-13	427.5	8.10	0.0221	4.41	0.42
Sm-SEmL1.5-7b-14	451.2	8.03	0.0221	4.29	0.33
Sm-SEmL1.5-7b-15	475.3	7.93	0.0221	3.77	0.35
Sm-SEmL1.5-7b-16	502.2	8.09	0.0222	3.23	0.38
Sm-SEmL1.5-7b-17	571.3	7.78	0.0222	3.64	0.24
Sm-SEmL1.5-7b-18	595.4	7.46	0.0221	3.25	0.19
Sm-SEmL1.5-7b-19	619.4	7.47	0.0222	3.12	0.23
Sm-SEmL1.5-7b-20	643.4	7.30	0.0222	2.99	0.23
Sm-SEmL1.5-7b-21	671.3	7.56	0.0221	2.65	0.13
Sm-SEmL1.5-7b-22	739.8	7.44	0.0221	2.52	0.14
Sm-SEmL1.5-7b-23	763.8	7.29	0.0221	2.56	0.68
Sm-SEmL1.5-7b-24	788.0	7.48	0.0221	2.44	0.18
Sm-SEmL1.5-7b-25	811.9	7.42	0.0221	2.29	0.17
Sm-SEmL1.5-7b-26	836.4	7.44	0.0221	2.33	0.18
Sm-SEmL1.5-7b-27	861.9	7.56	0.0221	2.16	0.11
Sm-SEmL1.5-7b-28	907.3	7.62	0.0221	2.36	0.13
Sm-SEmL1.5-7b-29	931.9	7.50	0.0221	2.04	0.18
Sm-SEmL1.5-7b-30	957.9	7.49	0.0220	2.02	0.35
Sm-SEmL1.5-7b-31	982.2	7.42	0.0221	2.07	0.19
Sm-SEmL1.5-7b-32	1007.0	7.48	0.0220	1.98	0.17

Run	Time (h)	pH	Flow (mL min^{-1})	Si (µM)	Al (µM)
Sm-SEmL1.5-7b-33	1031.7	7.39	0.0220	1.90	0.18
Sm-SEmL1.5-7b-34	1075.5	7.46	0.0220	2.14	0.03
Sm-SEmL1.5-7b-35	1099.3	7.55	0.0220	1.95	0.14
Sm-SEmL1.5-7b-36	1125.4	7.39	0.0220	1.80	0.15
Sm-SEmL1.5-7b-37	1149.9	7.53	0.0220	1.92	0.08
Sm-SEmL1.5-7b-38	1176.1	7.41	0.0220	2.29	0.08
Sm-SEmL1.5-7b-39	1199.3	7.35	0.0220	1.80	0.29
Sm-SEmL1.5-7b-40	1243.2	7.46	0.0215	1.79	0.05
Sm-SEmL1.5-7b-41	1267.3	7.45	0.0219	1.75	0.20
Sm-SEmL1.5-7b-42	1292.0	7.45	0.0220	1.65	0.35
Sm-SEmL1.5-7b-43	1316.4	7.43	0.0220	1.69	0.11
Sm-SEmL1.5-7b-44	1340.9	7.50	0.0220	1.69	0.12
Sm-SEmL1.5-7b-45	1366.2	7.53	0.0220	1.76	0.14
Sm-SEmL1.5-7b-46	1411.4	7.41	0.0220	1.67	0.08
Sm-SEmL1.5-7b-47	1436.0	7.53	0.0220	1.60	0.23
Sm-SEmL1.5-7b-48	1460.5	7.45	0.0220	1.61	0.19
Sm-SEmL1.5-7b-49	1487.4	7.44	0.0219	1.71	0.09
Sm-SEmL1.5-7b-50	1509.5	7.42	0.0219	1.69	0.08
Sm-SEmL1.5-7b-51	1580.0	7.40	0.0219	2.01	0.04
Sm-SEmL1.5-7b-52	1604.5	7.36	0.0219	1.80	0.18
Sm-SEmL1.5-7b-53	1628.3	7.43	0.0221	1.67	0.16
Sm-SEmL1.5-7b-54	1651.8	7.44	0.0221	1.78	0.23
Sm-SEmL1.5-7b-55	1679.8	7.47	0.0220	1.74	0.16
Sm-SEmL1.5-7b-56	1747.2	7.58	0.0219	1.69	0.16
Sm-SEmL1.5-7b-57	1771.4	7.49	0.0218	1.60	0.12
Sm-SEmL1.5-7b-58	1795.6	7.51	0.0219	1.64	0.16
Sm-SEmL1.5-7b-59	1820.0	7.54	0.0219	1.79	0.08
Sm-SEmL1.5-7b-60	1848.1	7.49	0.0220	1.70	0.10
Sm-SEmL1.5-7b-61	1916.1	7.50	0.0220	1.85	0.04

Sm-SEmL15-7	**Temperature 37ºC**	**Initial pH 7.20**
Mass 0.1000 g	**Solution 112 mM KCl + 0.556 mM K_2SO_4 + 49.9 mM $KHCO_3$+ 15 mM Lactate**	

Run	Time (h)	pH	Flow (mL min^{-1})	Si (µM)	Al (µM)	Lactate output (mM)	Lactate input (mM)
Sm-SEmL15-7-1	23.3	8.44	0.0235	29.34	< d.l.	18.4	14.4
Sm-SEmL15-7-2	47.9	8.59	0.0243	31.78	0.08	18.2	-
Sm-SEmL15-7-3	76.4	8.87	0.0239	26.31	0.45	18.6	-
Sm-SEmL15-7-4	139.2	9.09	0.0236	14.23	1.07	18.8	14.7
Sm-SEmL15-7-5	163.2	8.90	0.0235	11.73	1.31	19.3	-
Sm-SEmL15-7-6	187.3	8.90	0.0235	7.82	0.69	19.3	-
Sm-SEmL15-7-7	211.4	8.90	0.0234	6.56	0.63	19.3	14.9
Sm-SEmL15-7-8	243.1	8.78	0.0234	5.77	0.52	19.3	-
Sm-SEmL15-7-9	307.0	8.79	0.0233	4.14	0.40	19.2	15.5
Sm-SEmL15-7-10	331.1	8.71	0.0232	5.21	< d.l.	19.2	-
Sm-SEmL15-7-11	355.2	8.44	0.0232	4.81	< d.l.	19.1	-
Sm-SEmL15-7-12	379.5	7.78	0.0231	3.69	0.33	19.2	-
Sm-SEmL15-7-13	406.0	7.91	0.0231	2.66	0.60	18.5	-
Sm-SEmL15-7-14	432.8	6.90	0.0232	7.20	3.76	17.6	-

Run	Time (h)	pH	Flow (mL min^{-1})	Si (µM)	Al (µM)	Lactate output (mM)	Lactate input (mM)
Sm-SEmL15-7-15	475.2	4.16	0.0229	18.55	3.73	18.2	15.2
Sm-SEmL15-7-16	499.3	4.07	0.0230	15.81	3.66	18.6	-
Sm-SEmL15-7-17	523.2	4.05	0.0230	14.03	3.53	18.7	-
Sm-SEmL15-7-18	547.0	4.20	0.0232	17.01	3.32	18.6	-
Sm-SEmL15-7-19	575.4	7.79	0.0230	20.01	0.04	16.8	-
Sm-SEmL15-7-20	598.1	7.98	0.0229	13.42	0.00	17.2	-
Sm-SEmL15-7-21	643.1	8.36	0.0227	9.97	0.01	16.8	13.7
Sm-SEmL15-7-22	667.2	8.33	0.0227	6.41	0.00	18.0	-
Sm-SEmL15-7-23	691.2	8.29	0.0229	5.38	< d.l.	16.9	-
Sm-SEmL15-7-24	715.3	8.01	0.0229	5.02	0.04	17.0	-
Sm-SEmL15-7-25	742.6	7.81	0.0228	4.55	0.22	16.9	-
Sm-SEmL15-7-26	768.0	7.94	0.0229	3.98	0.10	17.2	-
Sm-SEmL15-7-27	811.3	8.18	0.0141	3.81	< d.l.	17.2	14.0
Sm-SEmL15-7-28	835.2	7.87	0.0228	4.62	0.04	17.2	-
Sm-SEmL15-7-29	859.1	7.98	0.0229	3.30	0.06	17.3	-
Sm-SEmL15-7-30	883.1	7.96	0.0229	2.85	0.21	17.4	-
Sm-SEmL15-7-31	909.7	8.07	0.0229	2.72	0.58	17.1	-
Sm-SEmL15-7-32	934.4	7.85	0.0229	2.68	0.12	17.3	-
Sm-SEmL15-7-33	979.1	8.02	0.0229	3.20	0.08	18.8	14.6
Sm-SEmL15-7-34	1003.3	8.07	0.0228	2.40	0.10	18.7	-
Sm-SEmL15-7-35	1029.6	8.03	0.0229	2.38	0.15	18.4	-
Sm-SEmL15-7-36	1054.1	7.69	0.0229	2.77	0.16	18.8	-
Sm-SEmL15-7-37	1078.6	8.08	0.0228	2.32	0.17	18.7	-
Sm-SEmL15-7-38	1104.4	7.92	0.0229	2.61	0.18	18.6	-
Sm-SEmL15-7-39	1147.3	8.02	0.0227	2.23	0.09	18.2	17.5
Sm-SEmL15-7-40	1174.1	7.81	0.0227	2.02	0.11	20.0	-
Sm-SEmL15-7-41	1198.1	7.91	0.0227	2.33	0.17	18.9	-
Sm-SEmL15-7-42	1222.2	7.82	0.0226	4.15	1.04	19.3	-
Sm-SEmL15-7-43	1247.0	7.67	0.0225	2.61	0.25	-	-
Sm-SEmL15-7-44	1270.4	7.89	0.0226	2.31	0.13	19.0	-
Sm-SEmL15-7-45	1315.3	7.93	0.0226	2.07	0.09	18.4	-
Sm-SEmL15-7-46	1339.1	7.82	0.0225	1.90	0.18	19.0	-
Sm-SEmL15-7-47	1363.1	7.60	0.0226	1.99	0.21	18.9	-
Sm-SEmL15-7-48	1387.1	7.72	0.0226	1.83	0.18	18.9	-
Sm-SEmL15-7-49	1415.0	7.62	0.0227	3.06	0.21	18.5	-
Sm-SEmL15-7-50	1439.8	7.82	0.0227	1.91	0.18	18.8	-
Sm-SEmL15-7-51	1483.5	7.83	0.0224	1.84	0.20	18.5	-
Sm-SEmL15-7-52	1507.6	7.86	0.0226	1.84	0.32	18.9	-
Sm-SEmL15-7-53	1534.3	7.77	0.0224	2.10	0.18	19.2	-
Sm-SEmL15-7-54	1560.2	7.82	0.0226	2.05	0.19	19.0	-
Sm-SEmL15-7-55	1584.1	7.61	0.0226	1.86	0.25	19.1	-
Sm-SEmL15-7-56	1608.3	7.44	0.0226	1.73	0.24	19.2	-
Sm-SEmL15-7-57	1651.1	7.69	0.0060	2.23	0.08	20.7	-
Sm-SEmL15-7-58	1679.1	7.67	0.0223	3.29	0.21	18.8	18.2

*d.l.: detection limit

Sm-SEmL15-7b **Mass 0.1006 g**	**Temperature 37ºC** **Solution 112 mM KCl + 0.556 mM K_2SO_4 + 0.25 mM HCl + 32.5 mM $KHCO_3$ + 15 mM Lactate**		**Initial pH 7.07**		
Run	Time (h)	pH	Flow (mL min^{-1})	Si (µM)	Al (µM)
Sm-SEmL15-7b-1	67.5	8.89	0.0233	28.65	20.15
Sm-SEmL15-7b-2	91.8	8.80	0.0232	11.32	3.49
Sm-SEmL15-7b-3	115.8	8.83	0.0230	19.21	1.08
Sm-SEmL15-7b-4	143.0	8.78	0.0227	23.77	0.84
Sm-SEmL15-7b-5	168.1	8.80	0.0225	18.24	0.75
Sm-SEmL15-7b-6	192.1	8.84	0.0223	11.85	0.72
Sm-SEmL15-7b-7	235.8	9.03	0.0223	10.61	0.76
Sm-SEmL15-7b-8	260.3	8.83	0.0223	8.83	0.80
Sm-SEmL15-7b-9	283.8	8.84	0.0222	7.66	0.75
Sm-SEmL15-7b-10	307.6	8.82	0.0222	7.05	0.90
Sm-SEmL15-7b-11	335.4	8.77	0.0222	6.64	0.90
Sm-SEmL15-7b-12	403.0	8.92	0.0221	5.69	0.87
Sm-SEmL15-7b-13	427.2	8.72	0.0221	5.40	0.90
Sm-SEmL15-7b-14	451.0	8.70	0.0222	5.54	0.92
Sm-SEmL15-7b-15	475.0	8.67	0.0221	4.82	0.96
Sm-SEmL15-7b-16	501.9	8.68	0.0223	3.64	0.89
Sm-SEmL15-7b-17	571.1	8.74	0.0221	3.93	0.84
Sm-SEmL15-7b-18	595.1	8.47	0.0222	3.79	0.82
Sm-SEmL15-7b-19	619.2	8.40	0.0221	3.61	0.80
Sm-SEmL15-7b-20	643.1	8.44	0.0221	3.46	0.80
Sm-SEmL15-7b-21	671.0	8.34	0.0219	3.24	0.78
Sm-SEmL15-7b-22	739.6	8.21	0.0215	2.72	0.77
Sm-SEmL15-7b-23	763.5	8.00	0.0221	2.68	0.91
Sm-SEmL15-7b-24	787.7	8.08	0.0221	2.62	0.83
Sm-SEmL15-7b-25	811.6	8.15	0.0220	2.80	0.79
Sm-SEmL15-7b-26	836.1	7.96	0.0220	2.46	0.78
Sm-SEmL15-7b-27	861.6	8.00	0.0220	2.50	0.81
Sm-SEmL15-7b-28	907.1	8.11	0.0221	2.42	0.79
Sm-SEmL15-7b-29	931.6	8.03	0.0220	2.28	0.75
Sm-SEmL15-7b-30	957.6	7.85	0.0220	2.24	0.79
Sm-SEmL15-7b-31	981.9	8.04	0.0221	2.22	0.86
Sm-SEmL15-7b-32	1006.7	8.16	0.0220	2.14	0.77
Sm-SEmL15-7b-33	1031.4	7.98	0.0220	2.12	0.70
Sm-SEmL15-7b-34	1075.2	7.76	0.0220	2.17	0.69
Sm-SEmL15-7b-35	1099.0	7.68	0.0220	2.05	0.76
Sm-SEmL15-7b-36	1125.1	7.47	0.0220	2.25	0.69
Sm-SEmL15-7b-37	1149.6	7.58	0.0221	2.08	0.69
Sm-SEmL15-7b-38	1175.9	7.56	0.0220	2.42	0.66
Sm-SEmL15-7b-39	1199.0	7.49	0.0220	1.92	0.71
Sm-SEmL15-7b-40	1242.9	7.57	0.0213	1.94	0.64
Sm-SEmL15-7b-41	1267.0	7.60	0.0219	2.00	0.69
Sm-SEmL15-7b-42	1291.8	7.68	0.0220	1.91	0.66
Sm-SEmL15-7b-43	1316.2	7.56	0.0219	1.93	0.79
Sm-SEmL15-7b-44	1340.6	7.62	0.0220	1.91	0.77
Sm-SEmL15-7b-45	1366.0	7.54	0.0220	1.88	0.65
Sm-SEmL15-7b-46	1411.1	7.46	0.0220	1.93	0.69
Sm-SEmL15-7b-47	1435.8	7.62	0.0220	1.88	0.67
Sm-SEmL15-7b-48	1460.2	7.49	0.0220	1.96	0.67

Run	Time (h)	pH	Flow (mL min^{-1})	Si (µM)	Al (µM)
Sm-SEmL15-7b-49	1487.2	7.31	0.0220	2.33	0.66
Sm-SEmL15-7b-50	1509.2	7.40	0.0201	1.80	0.69
Sm-SEmL15-7b-51	1579.7	7.49	0.0218	1.81	0.69
Sm-SEmL15-7b-52	1604.3	7.44	0.0219	1.77	0.69
Sm-SEmL15-7b-53	1628.0	7.44	0.0221	2.24	0.64
Sm-SEmL15-7b-54	1651.6	7.42	0.0221	1.74	0.62
Sm-SEmL15-7b-55	1679.5	7.30	0.0220	1.77	0.67
Sm-SEmL15-7b-56	1746.9	7.59	0.0221	1.78	0.64
Sm-SEmL15-7b-57	1771.1	7.49	0.0221	1.73	0.72
Sm-SEmL15-7b-58	1795.4	7.43	0.0220	1.68	0.73
Sm-SEmL15-7b-59	1819.7	7.42	0.0220	1.73	0.68
Sm-SEmL15-7b-60	1847.9	7.50	0.0221	1.71	0.64
Sm-SEmL15-7b-61	1915.9	7.40	0.0221	1.74	0.58

Sm-SEC0.15-4	**Temperature 37ºC**	**Initial pH 4.00**
Mass 0.0999 g	**Solution 112 mM KCl + 0.556 mM K_2SO_4 + 0.45 mM HCl + 0.15 mM Citrate**	

Run	Time (h)	pH	Flow (mL min^{-1})	Si (µM)	Al (µM)	Citrate output (mM)
Sm-SEC0.15-4-1	17.0	3.02	0.0248	57.13	44.99	0.127
Sm-SEC0.15-4-2	64.2	3.57	0.0239	51.87	25.96	-
Sm-SEC0.15-4-3	87.3	3.91	0.0237	24.70	6.25	0.125
Sm-SEC0.15-4-4	111.2	3.96	0.0236	21.55	5.57	-
Sm-SEC0.15-4-5	135.4	3.97	0.0237	25.11	6.00	-
Sm-SEC0.15-4-6	159.0	3.96	0.0234	39.45	8.64	0.133
Sm-SEC0.15-4-7	187.8	4.03	0.0234	31.35	7.90	-
Sm-SEC0.15-4-8	231.2	3.98	0.0233	27.17	6.83	-
Sm-SEC0.15-4-9	255.2	3.98	0.0232	22.02	6.20	0.134
Sm-SEC0.15-4-10	279.6	3.98	0.0233	22.07	5.78	-
Sm-SEC0.15-4-11	303.5	3.98	0.0237	17.89	5.45	-
Sm-SEC0.15-4-12	327.2	3.97	0.0232	17.06	5.12	0.142
Sm-SEC0.15-4-13	362.6	3.99	0.0233	15.21	4.85	-
Sm-SEC0.15-4-14	399.7	3.98	0.0232	13.95	4.71	-
Sm-SEC0.15-4-15	423.9	4.01	0.0232	14.62	4.47	0.142
Sm-SEC0.15-4-16	448.2	3.98	0.0232	12.81	4.34	-
Sm-SEC0.15-4-17	471.9	3.99	0.0231	12.97	4.03	0.133
Sm-SEC0.15-4-18	495.8	3.99	0.0231	12.68	3.93	0.132
Sm-SEC0.15-4-19	523.0	3.98	0.0230	12.58	3.82	0.142
Sm-SEC0.15-4-20	567.8	4.01	0.0231	11.60	3.71	-
Sm-SEC0.15-4-21	591.7	3.98	0.0231	11.37	3.91	0.134
Sm-SEC0.15-4-22	615.6	3.98	0.0230	12.17	3.28	-
Sm-SEC0.15-4-23	639.7	3.97	0.0231	11.32	3.16	-
Sm-SEC0.15-4-24	663.9	3.97	0.0230	10.54	3.11	0.138
Sm-SEC0.15-4-25	691.1	3.98	0.0231	10.72	3.01	-
Sm-SEC0.15-4-26	714.9	3.98	0.0231	8.58	3.00	-
Sm-SEC0.15-4-27	736.2	3.98	0.0231	10.98	3.02	0.141
Sm-SEC0.15-4-28	760.4	3.99	0.0231	8.87	3.02	-
Sm-SEC0.15-4-29	784.0	3.98	0.0230	10.06	2.99	0.149

Run	Time (h)	pH	Flow (mL min^{-1})	Si (µM)	Al (µM)	Citrate output (mM)
Sm-SEC0.15-4-30	808.1	3.99	0.0230	9.05	2.98	-
Sm-SEC0.15-4-31	832.0	3.98	0.0229	9.44	2.97	0.144
Sm-SEC0.15-4-32	857.8	3.98	0.0229	9.13	2.77	-
Sm-SEC0.15-4-33	904.1	3.99	0.0229	8.22	2.81	0.144
Sm-SEC0.15-4-34	928.2	3.98	0.0219	7.68	2.85	-
Sm-SEC0.15-4-35	952.4	3.99	0.0229	7.54	2.68	0.140
Sm-SEC0.15-4-36	975.8	3.98	0.0230	7.53	2.84	-
Sm-SEC0.15-4-37	1000.4	4.01	0.0229	7.49	3.03	0.143
Sm-SEC0.15-4-38	1025.8	3.99	0.0229	7.40	3.11	0.132
Sm-SEC0.15-4-39	1072.0	3.99	0.0225	7.41	2.89	0.147
Sm-SEC0.15-4-40	1095.3	3.99	0.0228	7.35	2.78	0.145
Sm-SEC0.15-4-41	1119.2	3.98	0.0230	7.38	2.76	0.140
Sm-SEC0.15-4-42	1143.6	3.99	0.0229	7.05	2.79	0.155
Sm-SEC0.15-4-43	1168.7	3.99	0.0230	7.41	2.53	0.145

Sm-SEC1.5-4	**Temperature 37ºC**	**Initial pH 4.14**
Mass 0.0999 g	**Solution 112 mM KCl + 0.556 mM K_2SO_4 + 2.70 mM HCl + 1.5 mM Citrate**	

Run	Time (h)	pH	Flow (mL min^{-1})	Si (µM)	Al (µM)	Citrate output (mM)
Sm-SEC1.5-4-1	16.8	3.68	0.0256	76.92	46.53	1.52
Sm-SEC1.5-4-2	64.0	4.07	0.0252	46.02	19.09	1.55
Sm-SEC1.5-4-3	87.1	4.13	0.0250	27.08	6.81	1.53
Sm-SEC1.5-4-4	111.0	4.12	0.0249	22.43	5.88	1.52
Sm-SEC1.5-4-5	135.2	4.13	0.0248	31.37	7.51	1.55
Sm-SEC1.5-4-6	158.9	4.13	0.0248	42.27	9.98	1.52
Sm-SEC1.5-4-7	187.7	4.18	0.0248	35.07	8.47	1.54
Sm-SEC1.5-4-8	231.0	4.12	0.0247	28.67	7.54	1.53
Sm-SEC1.5-4-9	255.0	4.12	0.0247	25.02	7.08	1.54
Sm-SEC1.5-4-10	279.4	4.12	0.0248	21.69	6.41	1.52
Sm-SEC1.5-4-11	303.3	4.12	0.0248	21.53	6.15	1.51
Sm-SEC1.5-4-12	327.0	4.12	0.0246	18.30	5.75	1.56
Sm-SEC1.5-4-13	362.4	4.13	0.0247	21.10	5.20	1.55
Sm-SEC1.5-4-14	399.5	4.12	0.0247	17.67	5.66	1.56
Sm-SEC1.5-4-15	423.8	4.13	0.0246	12.35	4.41	1.51
Sm-SEC1.5-4-16	448.0	4.13	0.0246	14.94	4.50	1.51
Sm-SEC1.5-4-17	471.7	4.13	0.0246	12.46	4.30	-
Sm-SEC1.5-4-18	495.6	4.13	0.0245	12.11	4.02	1.50
Sm-SEC1.5-4-19	522.8	4.13	0.0245	12.25	3.95	-
Sm-SEC1.5-4-20	567.6	4.14	0.0247	12.01	3.89	1.50
Sm-SEC1.5-4-21	591.5	4.14	0.0246	14.28	3.64	-
Sm-SEC1.5-4-22	615.4	4.13	0.0246	12.09	4.21	1.54
Sm-SEC1.5-4-23	639.5	4.13	0.0246	11.06	3.84	-
Sm-SEC1.5-4-24	663.8	4.13	0.0245	10.90	3.54	1.53
Sm-SEC1.5-4-25	690.9	4.13	0.0245	11.88	3.91	-
Sm-SEC1.5-4-26	714.7	4.13	0.0245	10.42	3.46	-
Sm-SEC1.5-4-27	736.0	4.13	0.0247	9.81	3.41	1.52
Sm-SEC1.5-4-28	760.2	4.13	0.0246	11.13	3.47	-

Run	Time (h)	pH	Flow (mL min^{-1})	Si (µM)	Al (µM)	Citrate output (mM)
Sm-SEC1.5-4-29	783.9	4.13	0.0245	9.53	4.23	1.51
Sm-SEC1.5-4-30	807.9	4.13	0.0247	9.34	3.55	-
Sm-SEC1.5-4-31	831.8	4.13	0.0245	9.51	3.36	1.55
Sm-SEC1.5-4-32	857.6	4.13	0.0245	9.53	3.29	-
Sm-SEC1.5-4-33	903.9	4.13	0.0246	9.05	3.29	1.51
Sm-SEC1.5-4-34	928.0	4.13	0.0246	8.65	3.23	-
Sm-SEC1.5-4-35	952.2	4.14	0.0246	8.86	3.03	1.55
Sm-SEC1.5-4-36	975.6	4.14	0.0245	8.98	0.00	-
Sm-SEC1.5-4-37	1000.2	4.14	0.0244	8.74	2.84	1.51
Sm-SEC1.5-4-38	1025.6	4.14	0.0245	8.54	3.00	-
Sm-SEC1.5-4-39	1071.8	4.12	0.0226	8.75	3.05	1.56
Sm-SEC1.5-4-40	1095.1	4.13	0.0244	8.58	2.87	-
Sm-SEC1.5-4-41	1119.1	4.13	0.0246	8.61	2.85	-
Sm-SEC1.5-4-42	1143.4	4.13	0.0244	7.89	2.67	1.57
Sm-SEC1.5-4-43	1168.6	4.13	0.0246	8.07	2.87	-

Sm-SEC15-4	**Temperature 37ºC**	**Initial pH 4.04**
Mass 0.1006 g	**Solution 112 mM KCl + 0.556 mM K_2SO_4 + 23.3 mM HCl + 15 mM Citrate**	

Run	Time (h)	pH	Flow (mL min^{-1})	Si (µM)	Al (µM)	Citrate output (mM)
Sm-SEC15-4-1	16.6	3.98	0.0237	75.28	78.88	
Sm-SEC15-4-2	63.9	4.01	0.0236	56.90	26.47	15.9
Sm-SEC15-4-3	87.0	4.03	0.0234	33.89	10.35	16.0
Sm-SEC15-4-4	110.9	4.02	0.0233	27.36	8.61	15.7
Sm-SEC15-4-5	135.1	4.02	0.0231	37.42	13.35	15.6
Sm-SEC15-4-6	158.7	4.02	0.0230	53.48	15.70	15.6
Sm-SEC15-4-7	187.5	4.08	0.0229	46.20	12.52	16.9
Sm-SEC15-4-8	230.9	4.02	0.0228	38.07	10.71	16.1
Sm-SEC15-4-9	254.9	4.02	0.0228	31.32	9.67	15.7
Sm-SEC15-4-10	279.2	4.02	0.0229	29.29	14.36	15.6
Sm-SEC15-4-11	303.1	4.01	0.0228	26.94	9.49	16.0
Sm-SEC15-4-12	326.9	4.02	0.0228	25.01	8.83	15.6
Sm-SEC15-4-13	362.3	4.03	0.0229	22.90	8.71	15.6
Sm-SEC15-4-14	399.4	4.02	0.0228	21.14	8.37	15.7
Sm-SEC15-4-15	423.6	4.03	0.0227	20.91	6.50	15.6
Sm-SEC15-4-16	447.8	4.03	0.0228	18.24	9.58	-
Sm-SEC15-4-17	471.5	4.03	0.0227	19.08	6.56	-
Sm-SEC15-4-18	495.5	4.02	0.0227	18.16	7.06	15.6
Sm-SEC15-4-19	522.7	4.03	0.0227	17.09	7.27	-
Sm-SEC15-4-20	567.5	4.03	0.0227	17.09	7.38	15.7
Sm-SEC15-4-21	591.3	4.03	0.0227	15.87	5.74	-
Sm-SEC15-4-22	615.2	4.03	0.0226	15.03	5.41	-
Sm-SEC15-4-23	639.4	4.03	0.0228	15.11	5.91	-
Sm-SEC15-4-24	663.6	4.02	0.0226	15.57	8.07	15.7
Sm-SEC15-4-25	690.7	4.02	0.0227	15.03	6.75	-
Sm-SEC15-4-26	714.6	4.03	0.0227	15.34	5.85	-
Sm-SEC15-4-27	735.9	4.03	0.0227	13.88	6.53	15.7

Run	Time (h)	pH	Flow (mL min^{-1})	Si (µM)	Al (µM)	Citrate output (mM)
Sm-SEC15-4-28	760.0	4.03	0.0227	14.04	5.54	-
Sm-SEC15-4-29	783.7	4.03	0.0227	13.73	4.96	15.8
Sm-SEC15-4-30	807.8	4.03	0.0226	13.84	5.53	-
Sm-SEC15-4-31	831.7	4.03	0.0225	15.39	5.66	16.0
Sm-SEC15-4-32	857.4	4.03	0.0225	13.36	5.89	-
Sm-SEC15-4-33	903.8	4.04	0.0226	12.45	5.49	17.8
Sm-SEC15-4-34	927.8	4.03	0.0225	12.72	5.99	-
Sm-SEC15-4-35	952.0	4.04	0.0225	11.92	4.93	16.0
Sm-SEC15-4-36	975.5	4.03	0.0225	13.63	4.83	-
Sm-SEC15-4-37	1000.1	4.05	0.0224	12.13	5.61	15.7
Sm-SEC15-4-38	1025.4	4.05	0.0225	12.45	4.80	-
Sm-SEC15-4-39	1071.7	4.03	0.0215	13.25	5.06	16.3
Sm-SEC15-4-40	1094.9	4.03	0.0224	12.08	4.73	-
Sm-SEC15-4-41	1118.9	4.03	0.0224	11.97	4.15	-
Sm-SEC15-4-42	1143.3	4.03	0.0225	12.02	5.08	15.8
Sm-SEC15-4-43	1168.4	4.03	0.0225	12.29	4.64	-

Sm-SEC0.15-5a	**Temperature 37ºC**	**Initial pH 5.56**
Mass 0.1000 g	**Solution 112 mM KCl + 0.556 mM K_2SO_4 + 0.1 mM HCl + 0.15 mM Citrate**	

Run	Time (h)	pH	Flow (mL min^{-1})	Si (µM)	Al (µM)	Citrate output (mM)
Sm-SEC0.15-5a-1	17.8	3.76	0.0229	45.31	48.97	0.133
Sm-SEC0.15-5a-2	41.7	4.61	0.0220	49.88	28.97	-
Sm-SEC0.15-5a-3	63.0	5.09	0.0219	36.58	11.06	-
Sm-SEC0.15-5a-4	87.1	5.26	0.0218	29.87	6.24	-
Sm-SEC0.15-5a-5	110.8	5.37	0.0219	26.01	5.14	0.151
Sm-SEC0.15-5a-6	134.8	5.38	0.0218	28.95	5.66	-
Sm-SEC0.15-5a-7	158.7	5.53	0.0216	23.67	5.28	-
Sm-SEC0.15-5a-8	184.5	5.78	0.0216	18.80	3.92	-
Sm-SEC0.15-5a-9	230.9	5.88	0.0216	13.92	3.36	-
Sm-SEC0.15-5a-10	254.9	6.09	0.0215	10.62	2.13	0.122
Sm-SEC0.15-5a-11	279.1	6.16	0.0216	8.83	1.87	-
Sm-SEC0.15-5a-12	302.5	6.15	0.0216	7.73	1.57	-
Sm-SEC0.15-5a-13	327.2	6.19	0.0215	7.14	1.53	-
Sm-SEC0.15-5a-14	352.5	6.28	0.0216	5.89	1.33	-
Sm-SEC0.15-5a-15	398.7	6.36	0.0216	5.67	1.19	0.119
Sm-SEC0.15-5a-16	422.0	6.56	0.0216	4.99	1.23	-
Sm-SEC0.15-5a-17	446.0	6.55	0.0217	4.99	1.05	-
Sm-SEC0.15-5a-18	470.3	6.64	0.0216	4.64	0.91	-
Sm-SEC0.15-5a-19	495.5	6.52	0.0216	4.30	0.96	-
Sm-SEC0.15-5a-20	518.7	6.58	0.0216	4.20	0.89	-
Sm-SEC0.15-5a-21	567.2	6.74	0.0217	4.05	0.86	-
Sm-SEC0.15-5a-22	590.6	6.73	0.0218	4.01	1.12	-
Sm-SEC0.15-5a-23	614.5	6.77	0.0218	3.68	0.68	-
Sm-SEC0.15-5a-24	638.8	6.73	0.0220	3.67	0.74	-
Sm-SEC0.15-5a-25	662.8	6.75	0.0218	3.57	0.57	-
Sm-SEC0.15-5a-26	689.3	6.75	0.0218	3.50	0.54	-

Run	Time (h)	pH	Flow (mL min^{-1})	Si (µM)	Al (µM)	Citrate output (mM)
Sm-SEC0.15-5a-27	734.7	6.83	0.0217	3.36	0.69	-
Sm-SEC0.15-5a-28	759.0	6.88	0.0217	3.25	0.54	-
Sm-SEC0.15-5a-29	782.8	6.94	0.0218	3.00	0.49	-
Sm-SEC0.15-5a-30	806.3	6.77	0.0218	3.13	0.52	-
Sm-SEC0.15-5a-31	830.7	6.94	0.0217	3.05	0.46	-
Sm-SEC0.15-5a-32	858.5	6.93	0.0218	2.75	0.52	-
Sm-SEC0.15-5a-33	902.6	6.76	0.0218	2.97	0.49	-
Sm-SEC0.15-5a-34	927.3	6.89	0.0218	2.81	0.63	-
Sm-SEC0.15-5a-35	950.7	6.88	0.0218	2.69	0.64	-
Sm-SEC0.15-5a-36	975.0	6.78	0.0217	2.67	0.56	-
Sm-SEC0.15-5a-37	999.0	6.78	0.0219	2.67	0.62	-
Sm-SEC0.15-5a-38	1026.6	6.83	0.0217	2.62	0.52	-
Sm-SEC0.15-5a-39	1070.7	6.78	0.0217	2.83	0.64	-
Sm-SEC0.15-5a-40	1094.7	6.57	0.0217	2.56	0.43	-
Sm-SEC0.15-5a-41	1118.6	6.64	0.0217	2.56	0.45	-
Sm-SEC0.15-5a-42	1142.9	6.73	0.0224	2.51	0.45	-
Sm-SEC0.15-5a-43	1166.9	6.61	0.0218	2.45	0.51	-

Sm-SEC0.15-5b	**Temperature 37ºC**	**Initial pH 5.36**
Mass 0.1018 g	**Solution 112 mM KCl + 0.556 mM K_2SO_4 + 0.06 mM HCl + 0.15 mM Citrate**	

Run	Time (h)	pH	Flow (mL min^{-1})	Si (µM)	Al (µM)	Citrate output (mM)
Sm-SEC0.15-5b-1	20.3	5.29	0.0217	37.28	14.37	0.151
Sm-SEC0.15-5b-2	43.9	5.30	0.0211	48.90	17.30	-
Sm-SEC0.15-5b-3	68.3	5.33	0.0209	31.11	11.36	-
Sm-SEC0.15-5b-4	96.0	5.31	0.0209	37.80	9.47	-
Sm-SEC0.15-5b-5	140.2	5.30	0.0206	33.72	10.71	0.145
Sm-SEC0.15-5b-6	164.9	5.34	0.0206	26.60	8.67	-
Sm-SEC0.15-5b-7	188.3	5.37	0.0204	22.62	7.30	-
Sm-SEC0.15-5b-8	212.6	5.43	0.0203	22.46	6.79	-
Sm-SEC0.15-5b-9	236.5	5.54	0.0204	16.76	4.41	-
Sm-SEC0.15-5b-10	264.2	5.57	0.0205	14.56	3.86	0.150
Sm-SEC0.15-5b-11	308.3	5.58	0.0204	11.73	3.47	-
Sm-SEC0.15-5b-12	332.3	5.60	0.0203	9.74	3.03	-
Sm-SEC0.15-5b-13	356.2	5.63	0.0203	13.25	2.85	-
Sm-SEC0.15-5b-14	380.5	5.64	0.0204	8.30	2.57	-
Sm-SEC0.15-5b-15	404.9	5.62	0.0204	7.33	2.34	-
Sm-SEC0.15-5b-16	431.4	5.62	0.0205	7.72	2.34	-
Sm-SEC0.15-5b-17	476.5	5.63	0.0204	6.60	2.17	-
Sm-SEC0.15-5b-18	501.6	5.65	0.0204	6.29	2.31	-
Sm-SEC0.15-5b-19	523.9	5.61	0.0205	5.94	2.29	-
Sm-SEC0.15-5b-20	548.2	5.61	0.0204	6.02	1.99	0.153
Sm-SEC0.15-5b-21	572.1	5.65	0.0204	5.84	1.98	-
Sm-SEC0.15-5b-22	600.9	5.64	0.0204	5.49	1.91	-
Sm-SEC0.15-5b-23	644.3	5.63	0.0204	5.75	1.81	-
Sm-SEC0.15-5b-24	668.2	5.63	0.0203	5.23	1.71	-
Sm-SEC0.15-5b-25	692.0	5.62	0.0204	5.09	1.88	0.148

Run	Time (h)	pH	Flow (mL min^{-1})	Si (µM)	Al (µM)	Citrate output (mM)
Sm-SEC0.15-5b-26	716.4	5.64	0.0204	5.00	1.81	-
Sm-SEC0.15-5b-27	742.4	5.65	0.0203	4.80	1.69	-
Sm-SEC0.15-5b-28	768.3	5.65	0.0203	4.62	1.55	-
Sm-SEC0.15-5b-29	812.2	5.67	0.0203	4.55	1.60	-
Sm-SEC0.15-5b-30	836.3	5.68	0.0203	4.50	1.81	0.149
Sm-SEC0.15-5b-31	860.4	5.62	0.0203	4.51	1.55	-
Sm-SEC0.15-5b-32	884.3	5.61	0.0205	4.48	1.60	-
Sm-SEC0.15-5b-33	908.4	5.61	0.0204	4.52	1.65	-
Sm-SEC0.15-5b-34	934.2	5.68	0.0205	4.26	1.47	-
Sm-SEC0.15-5b-35	984.5	5.64	0.0205	4.43	1.51	-
Sm-SEC0.15-5b-36	1004.1	5.62	0.0204	4.08	1.50	-
Sm-SEC0.15-5b-37	1028.3	5.66	0.0204	4.16	1.47	-
Sm-SEC0.15-5b-38	1052.9	5.66	0.0203	4.41	2.30	-
Sm-SEC0.15-5b-39	1079.3	5.65	0.0204	3.89	1.37	-
Sm-SEC0.15-5b-40	1104.9	5.65	0.0204	3.94	1.62	-
Sm-SEC0.15-5b-41	1149.2	5.66	0.0203	4.15	1.71	-
Sm-SEC0.15-5b-42	1172.8	5.67	0.0204	3.84	1.34	-
Sm-SEC0.15-5b-43	1196.8	5.65	0.0204	3.84	1.34	-

Sm-SEC1.5-5	**Temperature 37ºC**	**Initial pH 5.57**
Mass 0.1005 g	**Solution 112 mM KCl + 0.556 mM K_2SO_4 + 1.05 mM HCl + 1.5 mM Citrate**	

Run	Time (h)	pH	Flow (mL min^{-1})	Si (µM)	Al (µM)	Citrate output (mM)
Sm-SEC1.5-5-1	20.3	5.29	0.0218	48.23	27.17	1.57
Sm-SEC1.5-5-2	43.9	5.30	0.0210	48.23	20.89	-
Sm-SEC1.5-5-3	68.3	5.33	0.0210	33.38	12.81	-
Sm-SEC1.5-5-4	96.0	5.31	0.0209	27.57	8.29	-
Sm-SEC1.5-5-5	140.2	5.30	0.0207	36.91	10.01	1.57
Sm-SEC1.5-5-6	164.9	5.34	0.0210	27.28	7.87	-
Sm-SEC1.5-5-7	188.3	5.37	0.0204	21.83	6.61	-
Sm-SEC1.5-5-8	212.6	5.43	0.0204	18.77	5.59	-
Sm-SEC1.5-5-9	236.5	5.54	0.0204	23.91	5.08	-
Sm-SEC1.5-5-10	264.2	5.57	0.0205	13.89	4.24	1.54
Sm-SEC1.5-5-11	308.3	5.58	0.0209	11.81	3.81	-
Sm-SEC1.5-5-12	332.3	5.60	0.0204	10.41	3.57	-
Sm-SEC1.5-5-13	356.2	5.63	0.0203	9.84	3.35	-
Sm-SEC1.5-5-14	380.5	5.64	0.0203	9.93	2.87	-
Sm-SEC1.5-5-15	404.9	5.62	0.0199	8.94	2.62	1.59
Sm-SEC1.5-5-16	431.4	5.62	0.0208	9.67	2.88	-
Sm-SEC1.5-5-17	476.5	5.63	0.0203	8.84	2.74	-
Sm-SEC1.5-5-18	501.6	5.65	0.0204	9.10	2.75	-
Sm-SEC1.5-5-19	523.9	5.61	0.0200	9.25	2.84	-
Sm-SEC1.5-5-20	548.2	5.61	0.0204	7.67	2.69	1.55
Sm-SEC1.5-5-21	572.1	5.65	0.0204	7.49	2.25	-
Sm-SEC1.5-5-22	600.9	5.64	0.0204	8.42	2.66	-
Sm-SEC1.5-5-23	644.3	5.63	0.0194	7.62	2.49	-
Sm-SEC1.5-5-24	668.2	5.63	0.0203	7.20	2.27	-

Run	Time (h)	pH	Flow (mL min^{-1})	Si (µM)	Al (µM)	Citrate output (mM)
Sm-SEC1.5-5-25	692.0	5.62	0.0202	6.81	2.35	1.54
Sm-SEC1.5-5-26	716.4	5.64	0.0205	6.94	2.01	-
Sm-SEC1.5-5-27	742.4	5.65	0.0203	6.30	2.12	-
Sm-SEC1.5-5-28	768.3	5.65	0.0202	6.81	1.82	-
Sm-SEC1.5-5-29	812.2	5.67	0.0204	7.02	2.19	-
Sm-SEC1.5-5-30	836.3	5.68	0.0203	6.45	1.62	1.57
Sm-SEC1.5-5-31	860.4	5.62	0.0203	6.19	2.05	-
Sm-SEC1.5-5-32	884.3	5.61	0.0204	6.04	1.86	-
Sm-SEC1.5-5-33	908.4	5.61	0.0206	6.17	1.91	-
Sm-SEC1.5-5-34	934.2	5.68	0.0203	5.41	2.08	-
Sm-SEC1.5-5-35	984.5	5.64	0.0201	5.80	1.78	1.54
Sm-SEC1.5-5-36	1004.1	5.62	0.0205	5.86	1.77	-
Sm-SEC1.5-5-37	1028.3	5.66	0.0205	5.67	1.67	-
Sm-SEC1.5-5-38	1052.9	5.59	0.0218	6.01	2.07	-
Sm-SEC1.5-5-39	1079.3	5.58	0.0218	5.78	2.24	-
Sm-SEC1.5-5-40	1104.9	5.59	0.0218	5.86	1.81	1.53
Sm-SEC1.5-5-41	1149.2	5.60	0.0219	5.76	2.21	-
Sm-SEC1.5-5-42	1172.8	5.69	0.0218	5.48	1.91	-
Sm-SEC1.5-5-43	1196.8	5.60	0.0219	5.40	1.61	1.56

Sm-SEC15-5	**Temperature 37ºC**	**Initial pH 5.47**
Mass 0.1003 g	**Solution 112 mM KCl + 0.556 mM K_2SO_4 + 9.57 mM HCl + 15 mM Citrate**	

Run	Time (h)	pH	Flow (mL min^{-1})	Si (µM)	Al (µM)	Citrate output (mM)
Sm-SEC15-5-1	17.8	5.38	0.0236	68.44	46.89	15.6
Sm-SEC15-5-2	41.7	5.45	0.0220	89.60	34.96	-
Sm-SEC15-5-3	63.0	5.48	0.0216	59.78	17.01	15.6
Sm-SEC15-5-4	87.1	5.47	0.0215	39.87	12.36	-
Sm-SEC15-5-5	110.8	5.47	0.0217	31.01	9.35	15.9
Sm-SEC15-5-6	134.8	5.47	0.0212	37.89	11.55	-
Sm-SEC15-5-7	158.7	5.47	0.0211	36.43	11.02	15.9
Sm-SEC15-5-8	184.5	5.47	0.0209	30.77	7.36	-
Sm-SEC15-5-9	230.9	5.47	0.0210	22.44	6.93	15.7
Sm-SEC15-5-10	254.9	5.47	0.0210	21.69	6.35	-
Sm-SEC15-5-11	279.1	5.48	0.0210	17.43	5.83	15.7
Sm-SEC15-5-12	302.5	5.48	0.0210	17.02	6.14	-
Sm-SEC15-5-13	327.2	5.48	0.0209	16.23	5.24	15.9
Sm-SEC15-5-14	352.5	5.48	0.0209	22.23	5.14	-
Sm-SEC15-5-15	398.7	5.47	0.0209	15.56	4.73	15.7
Sm-SEC15-5-16	422.0	5.48	0.0210	13.26	3.99	-
Sm-SEC15-5-17	446.0	5.48	0.0210	13.52	4.01	15.5
Sm-SEC15-5-18	470.3	5.49	0.0209	16.49	3.68	-
Sm-SEC15-5-19	495.5	5.49	0.0210	14.41	3.51	-
Sm-SEC15-5-20	518.7	5.49	0.0209	16.49	3.48	-
Sm-SEC15-5-21	567.2	5.48	0.0209	15.14	3.75	15.7
Sm-SEC15-5-22	590.6	5.49	0.0210	11.02	3.38	-
Sm-SEC15-5-23	614.5	5.49	0.0209	13.26	4.93	-

Run	Time (h)	pH	Flow (mL min^{-1})	Si (µM)	Al (µM)	Citrate output (mM)
Sm-SEC15-5-24	638.8	5.49	0.0210	13.89	3.57	15.4
Sm-SEC15-5-25	662.8	5.49	0.0210	18.37	3.60	-
Sm-SEC15-5-26	689.3	5.48	0.0210	9.04	4.45	-
Sm-SEC15-5-27	734.7	5.48	0.0209	10.60	4.07	15.5
Sm-SEC15-5-28	759.0	5.49	0.0209	10.86	4.21	-
Sm-SEC15-5-29	782.8	5.50	0.0209	11.65	2.78	-
Sm-SEC15-5-30	806.3	5.49	0.0209	9.25	3.44	15.4
Sm-SEC15-5-31	830.7	5.49	0.0209	9.14	2.62	-
Sm-SEC15-5-32	858.5	5.49	0.0209	8.57	3.61	-
Sm-SEC15-5-33	902.6	5.49	0.0209	7.63	3.18	15.5
Sm-SEC15-5-34	927.3	5.50	0.0210	8.62	3.71	-
Sm-SEC15-5-35	950.7	5.49	0.0209	8.31	4.23	-
Sm-SEC15-5-36	975.0	5.50	0.0209	8.00	4.35	-
Sm-SEC15-5-37	999.0	5.49	0.0210	7.63	3.56	15.5
Sm-SEC15-5-38	1026.6	5.50	0.0209	8.26	3.84	-
Sm-SEC15-5-39	1070.7	5.50	0.0207	9.25	3.41	-
Sm-SEC15-5-40	1094.7	5.51	0.0208	7.16	2.40	15.2
Sm-SEC15-5-41	1118.6	5.50	0.0208	7.84	2.80	-
Sm-SEC15-5-42	1142.9	5.48	0.0208	6.96	2.42	-
Sm-SEC15-5-43	1166.9	5.50	0.0209	7.42	2.37	13.3

Sm-SEC0.15-7	**Temperature 37ºC**	**Initial pH 7.16**
Mass 0.0999 g	**Solution 112 mM KCl + 0.556 mM K_2SO_4 + 0.20 mM $KHCO_3$ + 0.15 mM Citrate**	

Run	Time (h)	pH	Flow (mL min^{-1})	Si (µM)	Al (µM)	Citrate output (mM)
Sm-SEC0.15-7-1	22.0	3.73	0.0257	56.72	62.46	-
Sm-SEC0.15-7-2	57.4	6.42	0.0239	61.67	13.34	-
Sm-SEC0.15-7-3	94.5	7.26	0.0235	29.24	1.54	-
Sm-SEC0.15-7-4	118.7	7.34	0.0238	19.54	0.73	-
Sm-SEC0.15-7-5	142.9	7.19	0.0230	18.51	0.89	-
Sm-SEC0.15-7-6	166.7	7.39	0.0231	14.52	1.10	0.128
Sm-SEC0.15-7-7	190.6	7.29	0.0231	10.54	0.86	-
Sm-SEC0.15-7-8	217.8	7.39	0.0230	8.58	0.80	-
Sm-SEC0.15-7-9	262.6	7.26	0.0231	7.64	0.70	-
Sm-SEC0.15-7-10	286.4	7.25	0.0230	6.03	0.80	0.134
Sm-SEC0.15-7-11	310.3	7.28	0.0231	6.78	0.73	0.156
Sm-SEC0.15-7-12	334.5	7.33	0.0230	5.60	0.56	0.135
Sm-SEC0.15-7-13	358.7	7.26	0.0230	5.51	0.47	-
Sm-SEC0.15-7-14	385.8	7.28	0.0231	5.45	0.57	-
Sm-SEC0.15-7-15	409.7	7.37	0.0231	5.06	0.58	-
Sm-SEC0.15-7-16	431.0	7.29	0.0231	5.00	0.88	0.156
Sm-SEC0.15-7-17	455.2	7.30	0.0231	5.19	0.55	-
Sm-SEC0.15-7-18	478.8	7.38	0.0231	4.91	0.50	-
Sm-SEC0.15-7-19	502.9	7.34	0.0230	4.32	0.47	-
Sm-SEC0.15-7-20	526.8	7.29	0.0231	4.76	0.47	0.159
Sm-SEC0.15-7-21	552.5	7.38	0.0229	4.37	0.50	-
Sm-SEC0.15-7-22	598.9	7.37	0.0230	4.12	0.44	-
Sm-SEC0.15-7-23	622.9	7.37	0.0231	4.42	0.46	-

Run	Time (h)	pH	Flow (mL min^{-1})	Si (µM)	Al (µM)	Citrate output (mM)
Sm-SEC0.15-7-24	647.1	7.39	0.0230	4.46	0.51	0.162
Sm-SEC0.15-7-25	670.6	7.38	0.0230	4.17	0.64	-
Sm-SEC0.15-7-26	695.2	7.30	0.0229	3.94	0.49	-
Sm-SEC0.15-7-27	720.5	7.13	0.0230	4.51	0.49	0.132
Sm-SEC0.15-7-28	766.8	7.35	0.0228	4.16	0.46	0.146
Sm-SEC0.15-7-29	790.1	7.38	0.0229	4.19	0.46	0.140
Sm-SEC0.15-7-30	814.0	7.39	0.0230	4.33	0.46	0.165
Sm-SEC0.15-7-31	838.4	7.41	0.0229	4.32	0.76	-
Sm-SEC0.15-7-32	863.5	7.32	0.0229	3.74	0.47	-
Sm-SEC0.15-7-33	886.7	7.27	0.0228	4.07	0.55	-
Sm-SEC0.15-7-34	935.2	7.42	0.0228	4.03	0.49	-
Sm-SEC0.15-7-35	958.7	7.40	0.0228	3.95	0.00	-
Sm-SEC0.15-7-36	982.6	7.40	0.0228	3.46	0.40	-
Sm-SEC0.15-7-37	1006.8	7.20	0.0231	3.50	0.49	-
Sm-SEC0.15-7-38	1030.9	7.40	0.0231	3.69	0.54	-
Sm-SEC0.15-7-39	1057.3	7.33	0.0231	3.48	0.51	-
Sm-SEC0.15-7-40	1102.7	7.42	0.0230	3.72	0.39	-
Sm-SEC0.15-7-41	1127.0	7.21	0.0230	3.48	0.57	-
Sm-SEC0.15-7-42	1150.8	7.42	0.0230	3.50	0.35	-
Sm-SEC0.15-7-43	1174.5	7.34	0.0230	4.89	0.36	-

Sm-SEC1.5-7	**Temperature 37ºC**	**Initial pH 6.98**
Mass 0.1001 g	**Solution 112 mM KCl + 0.556 mM K_2SO_4 + 0.05 mM HCl + 1.5 mM Citrate**	

Run	Time (h)	pH	Flow (mL min^{-1})	Si (µM)	Al (µM)	Citrate output (mM)
Sm-SEC1.5-7-1	16.2	5.09	0.0203	60.52	31.02	1.48
Sm-SEC1.5-7-2	63.5	6.24	0.0205	70.04	20.20	1.51
Sm-SEC1.5-7-3	86.6	7.08	0.0203	31.90	6.49	1.52
Sm-SEC1.5-7-4	110.4	7.11	0.0204	22.43	7.40	1.47
Sm-SEC1.5-7-5	134.7	7.15	0.0206	25.34	5.06	1.50
Sm-SEC1.5-7-6	158.3	7.26	0.0205	25.45	6.08	1.44
Sm-SEC1.5-7-7	187.1	7.14	0.0204	20.66	5.32	1.47
Sm-SEC1.5-7-8	230.5	6.99	0.0204	17.01	4.65	1.50
Sm-SEC1.5-7-9	254.4	7.07	0.0204	14.04	4.31	1.51
Sm-SEC1.5-7-10	278.8	7.18	0.0205	14.41	3.90	1.48
Sm-SEC1.5-7-11	302.7	7.10	0.0204	13.17	3.72	1.47
Sm-SEC1.5-7-12	326.4	7.12	0.0203	11.29	3.41	1.52
Sm-SEC1.5-7-13	361.9	6.99	0.0205	10.68	2.99	1.48
Sm-SEC1.5-7-14	399.0	7.05	0.0204	11.40	2.81	1.50
Sm-SEC1.5-7-15	423.2	7.08	0.0204	9.89	2.41	1.47
Sm-SEC1.5-7-16	447.4	7.08	0.0204	11.90	3.38	1.47
Sm-SEC1.5-7-17	471.1	7.07	0.0203	10.71	2.17	-
Sm-SEC1.5-7-18	495.1	7.01	0.0203	11.06	2.65	1.47
Sm-SEC1.5-7-19	522.2	7.07	0.0202	10.45	2.07	-
Sm-SEC1.5-7-20	567.1	7.09	0.0202	10.55	1.91	1.47
Sm-SEC1.5-7-21	590.9	7.13	0.0202	10.95	2.55	-
Sm-SEC1.5-7-22	614.8	7.09	0.0202	10.21	1.95	1.47
Sm-SEC1.5-7-23	639.0	7.12	0.0202	10.61	2.04	-
Sm-SEC1.5-7-24	663.2	7.16	0.0201	10.29	2.50	1.49

Run	Time (h)	pH	Flow (mL min^{-1})	Si (µM)	Al (µM)	Citrate output (mM)
Sm-SEC1.5-7-25	690.3	7.18	0.0202	10.74	1.92	-
Sm-SEC1.5-7-26	714.2	7.13	0.0202	10.98	1.89	-
Sm-SEC1.5-7-27	735.5	7.11	0.0202	11.58	2.69	1.46
Sm-SEC1.5-7-28	759.6	7.14	0.0202	11.27	1.74	-
Sm-SEC1.5-7-29	783.3	7.13	0.0202	9.63	1.85	1.46
Sm-SEC1.5-7-30	807.3	7.11	0.0202	9.90	3.57	-
Sm-SEC1.5-7-31	831.2	7.14	0.0202	9.25	1.95	1.46
Sm-SEC1.5-7-32	857.0	7.16	0.0201	9.62	1.75	-
Sm-SEC1.5-7-33	903.4	7.24	0.0201	9.51	1.91	1.46
Sm-SEC1.5-7-34	927.4	7.20	0.0201	9.71	1.70	-
Sm-SEC1.5-7-35	951.6	7.18	0.0201	9.58	1.89	1.46
Sm-SEC1.5-7-36	975.0	7.18	0.0201	9.78	3.05	-
Sm-SEC1.5-7-37	999.7	7.16	0.0200	9.23	1.61	1.46
Sm-SEC1.5-7-38	1025.0	7.08	0.0201	9.65	1.60	-
Sm-SEC1.5-7-39	1071.2	7.19	0.0199	9.65	1.66	1.47
Sm-SEC1.5-7-40	1094.5	7.18	0.0200	9.42	1.60	-
Sm-SEC1.5-7-41	1118.5	7.16	0.0201	9.37	2.96	-
Sm-SEC1.5-7-42	1142.9	7.17	0.0200	8.84	1.59	1.51
Sm-SEC1.5-7-43	1168.0	7.16	0.0201	8.93	1.50	-

Sm-SEC15-7	**Temperature 37ºC**	**Initial pH 6.98**
Mass 0.1007 g	**Solution 112 mM KCl + 0.556 mM K_2SO_4 + 0.70 mM HCl + 15 mM Citrate**	

Run	Time (h)	pH	Flow (mL min^{-1})	Si (µM)	Al (µM)	Citrate output (mM)
Sm-SEC15-7-1	16.0	6.54	0.0251	61.38	31.43	15.8
Sm-SEC15-7-2	63.3	6.85	0.0238	56.23	27.60	15.8
Sm-SEC15-7-3	86.4	6.98	0.0233	27.33	10.24	16.0
Sm-SEC15-7-4	110.3	6.98	0.0234	19.80	7.46	16.2
Sm-SEC15-7-5	134.5	6.98	0.0236	25.39	10.18	16.4
Sm-SEC15-7-6	158.1	6.98	0.0231	31.43	10.92	16.3
Sm-SEC15-7-7	186.9	6.95	0.0231	29.45	7.87	16.2
Sm-SEC15-7-8	230.3	6.98	0.0230	24.84	10.85	15.9
Sm-SEC15-7-9	254.3	6.97	0.0230	21.59	6.02	15.9
Sm-SEC15-7-10	278.6	7.01	0.0231	21.46	5.33	15.9
Sm-SEC15-7-11	302.5	7.01	0.0230	20.80	4.75	15.9
Sm-SEC15-7-12	326.3	7.01	0.0230	17.65	5.00	15.9
Sm-SEC15-7-13	361.7	7.00	0.0231	18.23	3.28	16.2
Sm-SEC15-7-14	398.8	7.00	0.0230	19.89	3.44	16.0
Sm-SEC15-7-15	423.0	7.01	0.0229	17.22	3.94	15.6
Sm-SEC15-7-16	447.2	7.00	0.0229	19.18	2.22	-
Sm-SEC15-7-17	471.0	7.01	0.0233	19.61	2.36	-
Sm-SEC15-7-18	494.9	7.00	0.0229	19.30	2.75	15.8
Sm-SEC15-7-19	522.1	6.99	0.0228	18.63	2.39	-
Sm-SEC15-7-20	566.9	7.01	0.0227	17.92	2.38	16.0
Sm-SEC15-7-21	590.8	6.99	0.0229	18.50	3.30	-
Sm-SEC15-7-22	614.6	7.00	0.0228	18.28	3.06	-
Sm-SEC15-7-23	638.8	7.00	0.0228	18.44	2.97	-
Sm-SEC15-7-24	663.0	7.00	0.0228	17.36	2.49	15.6
Sm-SEC15-7-25	690.1	7.01	0.0228	17.48	3.27	-

Run	Time (h)	pH	Flow (mL min^{-1})	Si (µM)	Al (µM)	Citrate output (mM)
Sm-SEC15-7-26	714.0	7.00	0.0228	17.30	3.11	-
Sm-SEC15-7-27	735.3	7.01	0.0229	18.12	4.00	15.6
Sm-SEC15-7-28	759.5	7.00	0.0229	16.93	2.43	-
Sm-SEC15-7-29	783.1	7.01	0.0227	16.94	2.44	15.7
Sm-SEC15-7-30	807.2	7.00	0.0228	15.82	2.71	-
Sm-SEC15-7-31	831.1	7.00	0.0228	15.70	2.59	15.7
Sm-SEC15-7-32	856.8	7.02	0.0228	15.49	2.55	-
Sm-SEC15-7-33	903.2	7.01	0.0228	18.11	3.42	15.8
Sm-SEC15-7-34	927.2	7.01	0.0228	14.35	3.20	-
Sm-SEC15-7-35	951.4	7.02	0.0228	14.16	3.29	15.7
Sm-SEC15-7-36	974.9	7.02	0.0228	14.47	2.66	-
Sm-SEC15-7-37	999.5	7.02	0.0227	13.16	3.03	15.7
Sm-SEC15-7-38	1024.8	7.01	0.0228	13.14	2.63	-
Sm-SEC15-7-39	1071.1	7.01	0.0208	13.67	2.44	-
Sm-SEC15-7-40	1094.4	7.02	0.0228	12.99	2.07	15.7
Sm-SEC15-7-41	1118.3	7.02	0.0227	12.34	2.71	-
Sm-SEC15-7-42	1142.7	7.04	0.0228	11.53	2.52	15.6
Sm-SEC15-7-43	1167.8	7.02	0.0228	11.44	2.86	-

Sm-SEmG0.15-4	**Temperature 37ºC**	**Initial pH 4.37**
Mass 0.0992 g	**Solution 112 mM KCl + 0.556 mM K_2SO_4 + 0.08 mM HCl + 0.15 mM Glycine**	

Run	Time (h)	pH	Flow (mL min^{-1})	Si (µM)	Al (µM)	Glycine output (mM)	Glycine input (mM)
Sm-SEmG0.15-4-1	23.6	2.98	0.0232	61.08	69.85	-	-
Sm-SEmG0.15-4-2	47.2	3.45	0.0236	35.45	30.40	0.152	-
Sm-SEmG0.15-4-3	71.3	3.97	0.0241	29.53	5.07	-	-
Sm-SEmG0.15-4-4	95.7	4.25	0.0235	39.78	0.76	-	-
Sm-SEmG0.15-4-5	119.4	4.36	0.0235	29.53	0.50	-	-
Sm-SEmG0.15-4-6	162.4	4.38	0.0235	17.83	0.41	-	-
Sm-SEmG0.15-4-7	186.4	4.44	0.0234	14.21	0.53	-	-
Sm-SEmG0.15-4-8	210.6	4.44	0.0235	11.05	0.54	-	-
Sm-SEmG0.15-4-9	237.9	4.46	0.0236	9.29	0.60	-	-
Sm-SEmG0.15-4-10	262.0	4.41	0.0236	11.30	0.77	0.150	-
Sm-SEmG0.15-4-11	330.4	4.39	0.0233	7.53	0.77	-	-
Sm-SEmG0.15-4-12	355.1	4.36	0.0235	6.37	0.84	-	-
Sm-SEmG0.15-4-13	378.9	4.36	0.0234	7.13	0.86	-	-
Sm-SEmG0.15-4-14	403.1	4.39	0.0234	5.12	0.87	-	-
Sm-SEmG0.15-4-15	430.2	4.36	0.0234	4.95	0.89	-	-
Sm-SEmG0.15-4-16	498.9	4.34	0.0234	4.68	0.92	-	-
Sm-SEmG0.15-4-17	523.0	4.35	0.0234	4.21	0.96	-	-
Sm-SEmG0.15-4-18	547.0	4.35	0.0234	3.81	0.95	-	-
Sm-SEmG0.15-4-19	571.1	4.32	0.0235	3.83	1.00	-	-
Sm-SEmG0.15-4-20	595.0	4.37	0.0236	3.21	0.89	0.149	0.145
Sm-SEmG0.15-4-21	619.1	4.40	0.0235	3.47	0.93	-	-
Sm-SEmG0.15-4-22	667.0	4.38	0.0235	3.34	0.85	-	-
Sm-SEmG0.15-4-23	691.1	4.36	0.0235	3.32	0.86	-	-
Sm-SEmG0.15-4-24	715.0	4.36	0.0235	3.06	0.87	-	-

Run	Time (h)	pH	Flow (mL min^{-1})	Si (µM)	Al (µM)	Glycine output (mM)	Glycine input (mM)
Sm-SEmG0.15-4-25	740.9	4.40	0.0235	2.67	0.87	-	-
Sm-SEmG0.15-4-26	763.1	4.36	0.0234	2.85	0.86	-	-
Sm-SEmG0.15-4-27	788.4	4.40	0.0235	3.36	0.84	-	-
Sm-SEmG0.15-4-28	835.1	4.35	0.0236	2.81	0.83	-	-
Sm-SEmG0.15-4-29	859.0	4.36	0.0235	2.97	0.91	-	-
Sm-SEmG0.15-4-30	882.9	4.36	0.0236	2.63	1.11	0.149	-
Sm-SEmG0.15-4-31	907.0	4.37	0.0236	2.64	0.86	-	-
Sm-SEmG0.15-4-32	931.0	4.37	0.0236	2.28	0.90	-	-
Sm-SEmG0.15-4-33	959.4	4.41	0.0235	2.38	0.88	-	-
Sm-SEmG0.15-4-34	1003.1	4.36	0.0234	2.54	1.09	-	-
Sm-SEmG0.15-4-35	1027.0	4.36	0.0235	2.46	0.90	-	-
Sm-SEmG0.15-4-36	1051.3	4.41	0.0235	2.37	1.02	-	-
Sm-SEmG0.15-4-37	1075.8	4.42	0.0235	2.71	0.97	-	-
Sm-SEmG0.15-4-38	1099.3	4.39	0.0235	2.05	0.94	-	-
Sm-SEmG0.15-4-39	1124.8	4.42	0.0234	2.85	0.87	-	-
Sm-SEmG0.15-4-40	1171.0	4.26	0.0235	3.14	2.39	0.145	-
Sm-SEmG0.15-4-41	1195.0	4.40	0.0234	2.06	0.86	-	-
Sm-SEmG0.15-4-42	1219.0	4.43	0.0235	1.99	0.86	-	-
Sm-SEmG0.15-4-43	1247.3	4.43	0.0235	2.28	0.80	-	-
Sm-SEmG0.15-4-44	1268.7	4.43	0.0235	1.97	0.77	-	-
Sm-SEmG0.15-4-45	1292.5	4.46	0.0236	2.33	0.83	-	-
Sm-SEmG0.15-4-46	1339.0	4.41	0.0234	2.46	0.76	-	-
Sm-SEmG0.15-4-47	1363.1	4.42	0.0235	1.87	0.78	-	-
Sm-SEmG0.15-4-48	1387.0	4.43	0.0234	1.95	0.79	-	-
Sm-SEmG0.15-4-49	1411.0	4.43	0.0234	1.91	0.86	-	-
Sm-SEmG0.15-4-50	1437.6	4.45	0.0234	1.87	0.80	-	-
Sm-SEmG0.15-4-51	1461.3	4.45	0.0230	1.95	0.79	0.144	-

Sm-SEmG1.5-4	**Temperature 37ºC**	**Initial pH 4.34**
Mass 0.0995 g	**Solution 112 mM KCl + 0.556 mM K_2SO_4 + 0.10 mM HCl + 1.5 mM Glycine**	

Run	Time (h)	pH	Flow (mL min^{-1})	Si (µM)	Al (µM)	Glycine output (mM)	Glycine input (mM)
Sm-SEmG1.5-4-1	21.1	3.37	0.0248	41.55	40.31	-	-
Sm-SEmG1.5-4-2	44.8	3.88	0.0240	29.51	17.23	1.58	-
Sm-SEmG1.5-4-3	68.9	4.12	0.0240	27.00	3.03	-	-
Sm-SEmG1.5-4-4	93.3	4.26	0.0237	31.06	0.77	-	-
Sm-SEmG1.5-4-5	117.0	4.31	0.0237	22.73	0.79	-	-
Sm-SEmG1.5-4-6	160.0	4.32	0.0237	16.91	0.68	-	-
Sm-SEmG1.5-4-7	184.0	4.36	0.0236	12.15	0.72	-	-
Sm-SEmG1.5-4-8	208.1	4.36	0.0236	10.36	0.81	-	-
Sm-SEmG1.5-4-9	235.5	4.37	0.0237	9.41	0.77	-	-
Sm-SEmG1.5-4-10	259.5	4.37	0.0236	8.57	0.89	1.52	-
Sm-SEmG1.5-4-11	328.0	4.36	0.0234	7.07	0.90	-	-
Sm-SEmG1.5-4-12	352.7	4.31	0.0236	6.11	0.84	-	-
Sm-SEmG1.5-4-13	376.5	4.32	0.0235	6.22	1.00	-	-
Sm-SEmG1.5-4-14	400.6	4.32	0.0235	5.28	0.94	-	-
Sm-SEmG1.5-4-15	427.8	4.33	0.0235	5.47	1.20	-	-

Run	Time (h)	pH	Flow (mL min^{-1})	Si (µM)	Al (µM)	Glycine output (mM)	Glycine input (mM)
Sm-SEmG1.5-4-16	496.4	4.33	0.0233	5.20	0.86	-	-
Sm-SEmG1.5-4-17	520.6	4.32	0.0234	4.84	0.89	-	-
Sm-SEmG1.5-4-18	544.6	4.34	0.0234	4.06	0.91	-	-
Sm-SEmG1.5-4-19	568.7	4.30	0.0235	3.99	0.91	-	-
Sm-SEmG1.5-4-20	592.6	4.34	0.0235	4.33	1.26	1.51	1.48
Sm-SEmG1.5-4-21	616.7	4.34	0.0235	3.66	0.90	-	-
Sm-SEmG1.5-4-22	664.6	4.32	0.0235	3.37	0.93	-	-
Sm-SEmG1.5-4-23	688.7	4.33	0.0235	3.10	0.89	-	-
Sm-SEmG1.5-4-24	712.6	4.33	0.0234	3.06	0.94	-	-
Sm-SEmG1.5-4-25	738.5	4.34	0.0233	3.00	0.72	-	-
Sm-SEmG1.5-4-26	760.6	4.32	0.0234	3.18	0.95	-	-
Sm-SEmG1.5-4-27	785.9	4.34	0.0234	2.90	1.04	-	-
Sm-SEmG1.5-4-28	832.7	4.33	0.0235	3.43	0.98	-	-
Sm-SEmG1.5-4-29	856.6	4.33	0.0234	3.00	1.31	-	-
Sm-SEmG1.5-4-30	880.5	4.34	0.0234	2.66	0.85	1.46	-
Sm-SEmG1.5-4-31	904.6	4.34	0.0235	2.70	0.95	-	-
Sm-SEmG1.5-4-32	928.6	4.33	0.0235	2.55	1.00	-	-
Sm-SEmG1.5-4-33	957.0	4.34	0.0235	2.78	0.99	-	-
Sm-SEmG1.5-4-34	1000.6	4.32	0.0233	2.93	0.94	-	-
Sm-SEmG1.5-4-35	1024.6	4.33	0.0233	2.72	1.00	-	-
Sm-SEmG1.5-4-36	1048.9	4.34	0.0233	2.68	1.00	-	-
Sm-SEmG1.5-4-37	1073.3	4.36	0.0233	2.26	0.93	-	-
Sm-SEmG1.5-4-38	1096.9	4.33	0.0233	2.37	0.99	-	-
Sm-SEmG1.5-4-39	1122.4	4.35	0.0232	2.69	1.09	-	-
Sm-SEmG1.5-4-40	1168.6	4.33	0.0233	2.52	1.04	1.51	-
Sm-SEmG1.5-4-41	1192.5	4.33	0.0233	2.14	0.97	-	-
Sm-SEmG1.5-4-42	1216.6	4.34	0.0233	2.49	1.07	-	-
Sm-SEmG1.5-4-43	1244.9	4.32	0.0233	2.20	0.96	-	-
Sm-SEmG1.5-4-44	1266.3	4.33	0.0233	2.08	0.94	-	-
Sm-SEmG1.5-4-45	1290.1	4.39	0.0234	2.06	0.86	-	-
Sm-SEmG1.5-4-46	1336.6	4.23	0.0234	2.76	2.22	-	-
Sm-SEmG1.5-4-47	1360.7	4.34	0.0229	2.29	0.91	-	-
Sm-SEmG1.5-4-48	1384.5	4.34	0.0232	2.07	0.87	-	-
Sm-SEmG1.5-4-49	1408.6	4.34	0.0232	2.33	0.94	-	-
Sm-SEmG1.5-4-50	1435.2	4.33	0.0232	2.35	0.94	1.49	-
Sm-SEmG1.5-4-51	1458.8	4.34	0.0233	1.97	0.85	-	-
Sm-SEmG1.5-4-52	1504.8	4.34	0.0232	2.32	0.76	-	-
Sm-SEmG1.5-4-53	1528.9	4.34	0.0229	1.98	0.89	-	-
Sm-SEmG1.5-4-54	1552.8	4.40	0.0229	1.96	0.87	-	-
Sm-SEmG1.5-4-55	1576.9	4.33	0.0228	1.95	0.87	-	-
Sm-SEmG1.5-4-56	1600.7	4.35	0.0230	2.31	0.96	-	-
Sm-SEmG1.5-4-57	1626.0	4.36	0.0229	2.07	0.88	-	-
Sm-SEmG1.5-4-58	1672.5	4.34	0.0229	1.99	0.82	-	-
Sm-SEmG1.5-4-59	1696.6	4.37	0.0229	1.93	0.82	-	-
Sm-SEmG1.5-4-60	1720.6	4.37	0.0229	1.93	0.79	-	-
Sm-SEmG1.5-4-61	1748.0	4.39	0.0230	1.91	0.78	-	-

Sm-SEmG15-4	**Temperature 37ºC**	**Initial pH 4.30**
Mass 0.1003 g	**Solution 112 mM KCl + 0.556 mM K_2SO_4 + 0.50 mM HCl + 15 mM Glycine**	

Run	Time (h)	pH	Flow (mL min^{-1})	Si (µM)	Al (µM)	Glycine output (mM)	Glycine input (mM)
Sm-SEmG15-4-1	22.4	4.05	0.0210	46.55	53.53	14.3	-
Sm-SEmG15-4-2	49.2	4.17	0.0232	34.27	9.71	-	-
Sm-SEmG15-4-3	91.7	4.27	0.0225	26.05	2.48	-	-
Sm-SEmG15-4-4	115.7	4.30	0.0221	17.00	1.51	-	-
Sm-SEmG15-4-5	139.7	4.29	0.0221	16.12	1.41	-	-
Sm-SEmG15-4-6	163.5	4.29	0.0220	13.80	1.42	-	-
Sm-SEmG15-4-7	191.9	4.31	0.0220	9.39	1.32	-	-
Sm-SEmG15-4-8	214.5	4.26	0.0220	8.57	1.95	-	-
Sm-SEmG15-4-9	259.6	4.26	0.0219	7.10	1.70	-	14.8
Sm-SEmG15-4-10	283.6	4.30	0.0218	6.69	1.68	14.7	-
Sm-SEmG15-4-11	307.6	4.29	0.0218	6.19	1.57	-	-
Sm-SEmG15-4-12	331.7	4.29	0.0218	6.10	1.53	-	-
Sm-SEmG15-4-13	359.0	4.30	0.0217	5.73	1.47	-	-
Sm-SEmG15-4-14	384.4	4.30	0.0219	5.21	1.39	-	-
Sm-SEmG15-4-15	427.8	4.29	0.0135	4.92	1.28	-	-
Sm-SEmG15-4-16	451.6	4.28	0.0218	6.95	1.42	-	-
Sm-SEmG15-4-17	475.5	4.34	0.0218	4.71	1.38	-	-
Sm-SEmG15-4-18	499.5	4.30	0.0217	4.12	1.36	-	-
Sm-SEmG15-4-19	526.1	4.33	0.0218	3.80	1.28	-	-
Sm-SEmG15-4-20	550.9	4.31	0.0217	3.71	1.32	14.8	-
Sm-SEmG15-4-21	595.5	4.33	0.0219	3.50	1.14	-	-
Sm-SEmG15-4-22	619.8	4.33	0.0216	3.54	1.12	-	-
Sm-SEmG15-4-23	646.0	4.33	0.0217	3.10	1.07	-	-
Sm-SEmG15-4-24	670.5	4.37	0.0218	3.59	0.97	-	-
Sm-SEmG15-4-25	695.1	4.39	0.0216	3.03	0.98	-	-
Sm-SEmG15-4-26	720.8	4.37	0.0218	3.40	1.02	-	-
Sm-SEmG15-4-27	763.8	4.39	0.0217	2.80	0.81	-	-
Sm-SEmG15-4-28	790.5	4.39	0.0216	2.64	0.82	-	-
Sm-SEmG15-4-29	814.5	4.38	0.0216	2.61	0.84	-	-
Sm-SEmG15-4-30	838.6	4.43	0.0216	4.27	1.38	14.8	-
Sm-SEmG15-4-31	863.4	4.40	0.0216	3.65	1.11	-	-
Sm-SEmG15-4-32	886.8	4.44	0.0218	2.35	0.76	-	-
Sm-SEmG15-4-33	931.8	4.40	0.0213	2.36	0.77	-	-
Sm-SEmG15-4-34	955.5	4.41	0.0221	3.06	0.96	-	-
Sm-SEmG15-4-35	979.5	4.38	0.0216	2.12	1.00	-	-
Sm-SEmG15-4-36	1003.5	4.39	0.0217	2.67	0.99	-	-
Sm-SEmG15-4-37	1031.4	4.40	0.0217	2.58	1.06	-	-
Sm-SEmG15-4-38	1056.3	4.39	0.0217	2.15	0.83	-	-
Sm-SEmG15-4-39	1100.0	4.40	0.0215	2.14	0.77	-	-
Sm-SEmG15-4-40	1124.1	4.40	0.0216	2.44	0.78	14.5	-
Sm-SEmG15-4-41	1150.8	4.43	0.0216	2.28	0.73	-	-
Sm-SEmG15-4-42	1176.7	4.43	0.0216	2.34	0.68	-	-
Sm-SEmG15-4-43	1200.5	4.38	0.0216	2.40	0.77	-	-
Sm-SEmG15-4-44	1224.8	4.39	0.0217	2.33	0.81	-	-
Sm-SEmG15-4-45	1267.5	4.33	0.0058	4.03	3.28	-	-
Sm-SEmG15-4-46	1295.8	4.48	0.0214	3.53	0.61	-	-
Sm-SEmG15-4-47	1320.0	4.43	0.0215	2.51	0.77	-	-

Run	Time (h)	pH	Flow (mL min^{-1})	Si (µM)	Al (µM)	Glycine output (mM)	Glycine input (mM)
Sm-SEmG15-4-48	1344.3	4.40	0.0215	1.81	0.86	-	-
Sm-SEmG15-4-49	1369.0	4.42	0.0216	2.16	0.82	-	-
Sm-SEmG15-4-50	1392.8	4.43	0.0217	1.74	0.78	14.4	-
Sm-SEmG15-4-51	1435.5	4.42	0.0211	2.20	1.21	-	-
Sm-SEmG15-4-52	1459.8	4.40	0.0214	1.77	0.75	-	-
Sm-SEmG15-4-53	1484.1	4.39	0.0215	1.76	0.80	-	-
Sm-SEmG15-4-54	1511.7	4.41	0.0214	1.89	0.76	-	-
Sm-SEmG15-4-55	1537.0	4.45	0.0215	1.88	0.77	-	-
Sm-SEmG15-4-56	1560.8	4.45	0.0215	1.75	0.76	-	-
Sm-SEmG15-4-57	1603.7	4.41	0.0214	1.74	0.66	-	-
Sm-SEmG15-4-58	1627.8	4.45	0.0213	1.67	0.67	-	-
Sm-SEmG15-4-59	1651.9	4.46	0.0213	2.08	0.69	-	-
Sm-SEmG15-4-60	1680.0	4.44	0.0216	1.61	0.65	14.8	-

Sm-SEmG15-4b	**Temperature 37ºC**	**Initial pH 4.34**
Mass 0.1001 g	**Solution 112 mM KCl + 0.556 mM K_2SO_4 + 0.25 mM HCl + 15 mM Glycine**	

Run	Time (h)	pH	Flow (mL min^{-1})	Si (µM)	Al (µM)	Glycine output (mM)	Glycine input (mM)
Sm-SEmG15-4b-1	68.4	3.86	0.0240	28.65	20.15	11.8	11.0
Sm-SEmG15-4b-2	92.7	4.24	0.0241	11.32	3.49	-	-
Sm-SEmG15-4b-3	116.7	4.28	0.0243	19.21	1.08	-	-
Sm-SEmG15-4b-4	143.9	4.30	0.0241	23.77	0.84	-	-
Sm-SEmG15-4b-5	169.0	4.32	0.0239	18.24	0.75	11.3	-
Sm-SEmG15-4b-6	193.0	4.33	0.0239	11.85	0.72	-	10.8
Sm-SEmG15-4b-7	236.8	4.34	0.0237	10.61	0.76	-	-
Sm-SEmG15-4b-8	261.2	4.32	0.0239	8.83	0.80	-	-
Sm-SEmG15-4b-9	284.7	4.36	0.0238	7.66	0.75	-	-
Sm-SEmG15-4b-10	308.5	4.31	0.0237	7.05	0.90	11.4	-
Sm-SEmG15-4b-11	336.4	4.32	0.0238	6.64	0.90	-	-
Sm-SEmG15-4b-12	404.0	4.33	0.0237	5.69	0.87	-	-
Sm-SEmG15-4b-13	428.2	4.31	0.0237	5.40	0.90	-	-
Sm-SEmG15-4b-14	451.9	4.32	0.0236	5.54	0.92	-	-
Sm-SEmG15-4b-15	476.0	4.31	0.0236	4.82	0.96	11.8	-
Sm-SEmG15-4b-16	502.8	4.27	0.0238	3.64	0.89	-	-
Sm-SEmG15-4b-17	572.0	4.30	0.0236	3.93	0.84	-	-
Sm-SEmG15-4b-18	596.0	4.31	0.0236	3.79	0.82	-	10.7
Sm-SEmG15-4b-19	620.1	4.32	0.0238	3.61	0.80	-	-
Sm-SEmG15-4b-20	644.1	4.31	0.0237	3.46	0.80	10.6	-
Sm-SEmG15-4b-21	671.9	4.36	0.0238	3.24	0.78	-	-
Sm-SEmG15-4b-22	740.5	4.31	0.0237	2.72	0.77	-	-
Sm-SEmG15-4b-23	764.5	4.34	0.0236	2.68	0.91	-	-
Sm-SEmG15-4b-24	788.6	4.32	0.0236	2.62	0.83	-	-
Sm-SEmG15-4b-25	812.5	4.33	0.0237	2.80	0.79	12.1	-
Sm-SEmG15-4b-26	837.0	4.32	0.0236	2.46	0.78	-	-
Sm-SEmG15-4b-27	862.5	4.33	0.0237	2.50	0.81	-	-
Sm-SEmG15-4b-28	908.0	4.33	0.0236	2.42	0.79	-	-
Sm-SEmG15-4b-29	932.5	4.33	0.0236	2.28	0.75	-	-

Run	Time (h)	pH	Flow (mL min^{-1})	Si (µM)	Al (µM)	Glycine output (mM)	Glycine input (mM)
Sm-SEmG15-4b-30	958.5	4.35	0.0237	2.24	0.79	11.8	-
Sm-SEmG15-4b-31	982.8	4.31	0.0237	2.22	0.86	-	-
Sm-SEmG15-4b-32	1007.6	4.31	0.0236	2.14	0.77	-	11.1
Sm-SEmG15-4b-33	1032.3	4.36	0.0236	2.12	0.70	-	-
Sm-SEmG15-4b-34	1076.2	4.34	0.0236	2.17	0.69	-	-
Sm-SEmG15-4b-35	1099.9	4.31	0.0229	2.05	0.76	11.0	-
Sm-SEmG15-4b-36	1126.0	4.36	0.0226	2.25	0.69	-	-
Sm-SEmG15-4b-37	1150.5	4.29	0.0236	2.08	0.69	-	-
Sm-SEmG15-4b-38	1176.8	4.32	0.0236	2.42	0.66	-	-
Sm-SEmG15-4b-39	1199.9	4.36	0.0235	1.92	0.71	-	-
Sm-SEmG15-4b-40	1243.8	4.35	0.0230	1.94	0.64	10.8	-
Sm-SEmG15-4b-41	1267.9	4.33	0.0235	2.00	0.69	-	-
Sm-SEmG15-4b-42	1292.7	4.31	0.0229	1.91	0.66	-	-
Sm-SEmG15-4b-43	1317.1	4.32	0.0235	1.93	0.79	-	-
Sm-SEmG15-4b-44	1341.6	4.32	0.0236	1.91	0.77	-	-
Sm-SEmG15-4b-45	1366.9	4.36	0.0236	1.88	0.65	10.7	-
Sm-SEmG15-4b-46	1412.0	4.31	0.0235	1.93	0.69	-	-
Sm-SEmG15-4b-47	1436.7	4.32	0.0236	1.88	0.67	-	-
Sm-SEmG15-4b-48	1461.1	4.33	0.0235	1.96	0.67	-	-
Sm-SEmG15-4b-49	1488.1	4.32	0.0222	2.33	0.66	-	-
Sm-SEmG15-4b-50	1510.2	4.33	0.0234	1.80	0.69	10.6	-
Sm-SEmG15-4b-51	1580.6	4.33	0.0235	1.81	0.69	-	-
Sm-SEmG15-4b-52	1605.2	4.30	0.0236	1.77	0.69	-	-
Sm-SEmG15-4b-53	1629.0	4.34	0.0236	2.24	0.64	-	-
Sm-SEmG15-4b-54	1652.5	4.29	0.0236	1.74	0.62	-	-
Sm-SEmG15-4b-55	1680.4	4.33	0.0235	1.77	0.67	10.8	-
Sm-SEmG15-4b-56	1747.8	4.35	0.0234	1.78	0.64	-	-
Sm-SEmG15-4b-57	1772.0	4.33	0.0235	1.73	0.72	-	-
Sm-SEmG15-4b-58	1796.3	4.32	0.0234	1.68	0.73	-	-
Sm-SEmG15-4b-59	1820.6	4.33	0.0234	1.73	0.68	-	-
Sm-SEmG15-4b-60	1848.8	4.33	0.0235	1.71	0.64	11.5	-
Sm-SEmG15-4b-61	1916.8	4.33	0.0235	1.74	0.58	-	11.8

Sm-SEmG0.15-7	**Temperature 37ºC**	**Initial pH 7.26**
Mass 0.1002 g	**Solution 112 mM KCl + 0.556 mM K_2SO_4 + 0.30 mM $KHCO_3$ + 0.15 mM Glycine**	

Run	Time (h)	pH	Flow (mL min^{-1})	Si (µM)	Al (µM)	Glycine output (mM)	Glycine input (mM)
Sm-SEmG0.15-7-1	21.0	3.04	0.0229	58.59	69.14	-	-
Sm-SEmG0.15-7-2	44.6	3.55	0.0231	41.59	15.82	0.147	-
Sm-SEmG0.15-7-3	68.8	5.86	0.0231	65.01	1.18	-	-
Sm-SEmG0.15-7-4	93.1	6.93	0.0228	57.89	0.10	-	-
Sm-SEmG0.15-7-5	116.8	7.16	0.0227	29.86	0.08	-	-
Sm-SEmG0.15-7-6	159.8	7.34	0.0226	18.81	0.40	-	-
Sm-SEmG0.15-7-7	183.8	7.01	0.0226	10.40	0.06	-	-
Sm-SEmG0.15-7-8	208.0	7.31	0.0226	9.60	0.21	-	-
Sm-SEmG0.15-7-9	235.3	7.28	0.0226	8.59	0.04	-	-
Sm-SEmG0.15-7-10	259.4	7.31	0.0226	5.11	0.07	0.073	-

Run	Time (h)	pH	Flow (mL min^{-1})	Si (µM)	Al (µM)	Glycine output (mM)	Glycine input (mM)
Sm-SEmG0.15-7-11	327.8	7.44	0.0224	6.60	0.11	-	-
Sm-SEmG0.15-7-12	352.5	7.44	0.0226	4.18	0.12	-	-
Sm-SEmG0.15-7-13	376.3	7.35	0.0225	3.96	0.08	-	-
Sm-SEmG0.15-7-14	400.5	7.30	0.0224	3.84	0.09	-	-
Sm-SEmG0.15-7-15	427.6	7.42	0.0225	3.95	0.11	-	-
Sm-SEmG0.15-7-16	496.3	7.39	0.0224	3.19	0.04	-	-
Sm-SEmG0.15-7-17	520.5	7.39	0.0225	2.96	0.10	-	-
Sm-SEmG0.15-7-18	544.4	7.32	0.0225	2.91	0.22	-	-
Sm-SEmG0.15-7-19	568.5	7.33	0.0225	3.00	0.10	-	-
Sm-SEmG0.15-7-20	592.4	7.33	0.0225	2.77	0.09	0.088	0.139
Sm-SEmG0.15-7-21	616.5	7.21	0.0225	2.69	0.14	-	-
Sm-SEmG0.15-7-22	664.4	7.37	0.0225	2.46	0.08	-	-
Sm-SEmG0.15-7-23	688.5	7.33	0.0225	2.76	0.11	-	-
Sm-SEmG0.15-7-24	712.4	7.32	0.0225	2.31	0.11	-	-
Sm-SEmG0.15-7-25	738.3	7.31	0.0224	2.46	0.12	-	-
Sm-SEmG0.15-7-26	760.5	7.38	0.0224	2.32	0.12	-	-
Sm-SEmG0.15-7-27	785.8	7.24	0.0225	2.06	0.11	-	-
Sm-SEmG0.15-7-28	832.5	7.32	0.0225	2.78	0.09	-	-
Sm-SEmG0.15-7-29	856.4	7.41	0.0225	1.82	0.11	-	-
Sm-SEmG0.15-7-30	880.4	7.41	0.0225	2.30	0.12	0.090	-
Sm-SEmG0.15-7-31	904.4	7.37	0.0225	1.81	0.14	-	-
Sm-SEmG0.15-7-32	928.4	7.32	0.0225	2.27	0.39	-	-
Sm-SEmG0.15-7-33	956.9	7.38	0.0224	2.34	0.16	-	-
Sm-SEmG0.15-7-34	1000.5	7.45	0.0224	1.82	0.07	-	-
Sm-SEmG0.15-7-35	1024.4	7.38	0.0224	1.69	0.16	-	-
Sm-SEmG0.15-7-36	1048.7	7.41	0.0224	1.67	0.19	-	-
Sm-SEmG0.15-7-37	1073.2	7.46	0.0224	2.11	0.18	-	-
Sm-SEmG0.15-7-38	1096.8	7.53	0.0223	1.62	0.22	-	-
Sm-SEmG0.15-7-39	1122.2	7.37	0.0224	1.72	0.18	-	-
Sm-SEmG0.15-7-40	1168.4	7.47	0.0224	1.87	0.14	0.089	-
Sm-SEmG0.15-7-41	1192.4	7.40	0.0224	1.59	0.17	-	-
Sm-SEmG0.15-7-42	1216.4	7.43	0.0224	1.55	0.17	-	-
Sm-SEmG0.15-7-43	1244.8	7.46	0.0224	1.51	0.13	-	-
Sm-SEmG0.15-7-44	1266.1	7.56	0.0224	1.65	0.17	-	-
Sm-SEmG0.15-7-45	1289.9	7.23	0.0224	1.54	0.14	-	-
Sm-SEmG0.15-7-46	1336.4	7.32	0.0224	1.66	0.07	-	-
Sm-SEmG0.15-7-47	1360.5	7.40	0.0224	1.51	0.15	-	-
Sm-SEmG0.15-7-48	1384.4	7.38	0.0223	1.53	0.15	-	-
Sm-SEmG0.15-7-49	1408.5	7.33	0.0223	1.86	0.23	-	-
Sm-SEmG0.15-7-50	1435.0	7.35	0.0224	1.53	0.17	-	-
Sm-SEmG0.15-7-51	1458.7	7.34	0.0224	1.47	0.25	0.092	-
Sm-SEmG0.15-7-52	1504.6	7.30	0.0224	1.61	0.08	-	-
Sm-SEmG0.15-7-53	1528.7	7.17	0.0222	1.61	0.19	-	-
Sm-SEmG0.15-7-54	1552.6	7.33	0.0222	1.67	0.31	-	-
Sm-SEmG0.15-7-55	1576.7	7.49	0.0222	1.53	0.23	-	-
Sm-SEmG0.15-7-56	1600.5	7.39	0.0223	1.71	0.50	-	-
Sm-SEmG0.15-7-57	1625.9	7.22	0.0222	1.48	0.21	-	-
Sm-SEmG0.15-7-58	1672.4	7.35	0.0223	1.86	0.16	-	-
Sm-SEmG0.15-7-59	1696.4	6.93	0.0223	1.53	0.22	-	-
Sm-SEmG0.15-7-60	1720.4	7.30	0.0223	1.54	0.21	-	-
Sm-SEmG0.15-7-61	1747.9	7.30	0.0224	1.57	0.30	-	-

Sm-SEmG1.5-7	**Temperature 37ºC**	**Initial pH 7.24**
Mass 0.1001 g	**Solution 112 mM KCl + 0.556 mM K_2SO_4 + 0.20 mM $KHCO_3$ + 1.5 mM Glycine**	

Run	Time (h)	pH	Flow (mL min^{-1})	Si (µM)	Al (µM)	Glycine output (mM)	Glycine input (mM)
Sm-SEmG1.5-7-1	20.8	3.33	0.0243	54.23	46.54	-	-
Sm-SEmG1.5-7-2	44.4	3.87	0.0246	39.82	13.43	1.48	-
Sm-SEmG1.5-7-3	68.6	5.98	0.0245	56.04	0.56	-	-
Sm-SEmG1.5-7-4	92.9	6.64	0.0242	2.09	0.08	-	-
Sm-SEmG1.5-7-5	116.7	7.09	0.0239	28.31	0.08	-	-
Sm-SEmG1.5-7-6	159.6	7.19	0.0240	18.72	0.51	-	-
Sm-SEmG1.5-7-7	183.7	7.32	0.0239	10.96	0.06	-	-
Sm-SEmG1.5-7-8	207.8	7.27	0.0238	9.93	0.07	-	-
Sm-SEmG1.5-7-9	235.2	7.25	0.0239	8.04	0.07	-	-
Sm-SEmG1.5-7-10	259.2	7.41	0.0238	7.09	0.23	1.34	-
Sm-SEmG1.5-7-11	327.6	7.59	0.0236	0.41	0.05	-	-
Sm-SEmG1.5-7-12	352.3	7.40	0.0238	4.85	0.10	-	-
Sm-SEmG1.5-7-13	376.2	7.38	0.0236	4.38	0.07	-	-
Sm-SEmG1.5-7-14	400.3	7.27	0.0236	3.85	0.09	-	-
Sm-SEmG1.5-7-15	427.4	7.39	0.0236	4.38	0.07	-	-
Sm-SEmG1.5-7-16	496.1	7.42	0.0237	3.80	0.09	-	-
Sm-SEmG1.5-7-17	520.3	7.38	0.0236	3.31	0.11	-	-
Sm-SEmG1.5-7-18	544.3	7.30	0.0236	3.42	0.09	-	-
Sm-SEmG1.5-7-19	568.3	7.33	0.0236	3.01	0.07	-	-
Sm-SEmG1.5-7-20	592.3	7.35	0.0236	3.39	0.33	1.40	1.49
Sm-SEmG1.5-7-21	616.4	7.38	0.0236	3.19	0.07	-	-
Sm-SEmG1.5-7-22	664.3	7.21	0.0236	3.51	0.09	-	-
Sm-SEmG1.5-7-23	688.3	7.36	0.0236	2.86	0.11	-	-
Sm-SEmG1.5-7-24	712.2	7.38	0.0236	2.89	0.09	-	-
Sm-SEmG1.5-7-25	738.1	7.29	0.0235	2.73	0.10	-	-
Sm-SEmG1.5-7-26	760.3	7.30	0.0235	2.67	0.08	-	-
Sm-SEmG1.5-7-27	785.6	7.23	0.0235	2.84	0.10	-	-
Sm-SEmG1.5-7-28	832.4	7.22	0.0236	3.06	0.10	-	-
Sm-SEmG1.5-7-29	856.3	7.30	0.0235	2.58	0.12	-	-
Sm-SEmG1.5-7-30	880.2	7.39	0.0236	2.44	0.08	1.40	-
Sm-SEmG1.5-7-31	904.3	7.38	0.0235	2.67	0.10	-	-
Sm-SEmG1.5-7-32	928.3	7.31	0.0235	2.76	0.18	-	-
Sm-SEmG1.5-7-33	956.7	7.26	0.0235	3.49	0.12	-	-
Sm-SEmG1.5-7-34	1000.3	7.27	0.0234	3.74	0.36	-	-
Sm-SEmG1.5-7-35	1024.3	7.32	0.0234	2.43	0.10	-	-
Sm-SEmG1.5-7-36	1048.5	7.31	0.0234	2.35	0.25	-	-
Sm-SEmG1.5-7-37	1073.0	7.40	0.0234	2.33	0.14	-	-
Sm-SEmG1.5-7-38	1096.6	7.28	0.0234	2.33	0.17	-	-
Sm-SEmG1.5-7-39	1122.0	7.34	0.0233	2.39	0.13	-	-
Sm-SEmG1.5-7-40	1168.3	7.32	0.0234	2.76	0.09	1.41	-
Sm-SEmG1.5-7-41	1192.2	7.35	0.0234	2.32	0.11	-	-
Sm-SEmG1.5-7-42	1216.3	7.31	0.0234	2.29	0.12	-	-
Sm-SEmG1.5-7-43	1244.6	7.34	0.0234	2.27	0.11	-	-
Sm-SEmG1.5-7-44	1266.0	7.39	0.0234	2.28	0.08	-	-
Sm-SEmG1.5-7-45	1289.8	7.31	0.0235	2.37	0.08	-	-
Sm-SEmG1.5-7-46	1336.3	7.33	0.0234	2.75	0.06	-	-
Sm-SEmG1.5-7-47	1360.4	7.34	0.0233	2.14	0.10	-	-

Run	Time (h)	pH	Flow (mL min^{-1})	Si (µM)	Al (µM)	Glycine output (mM)	Glycine input (mM)
Sm-SEmG1.5-7-48	1384.2	7.37	0.0233	2.14	0.11	-	-
Sm-SEmG1.5-7-49	1408.3	7.34	0.0126	2.13	0.15	-	-
Sm-SEmG1.5-7-50	1434.8	7.40	0.0169	2.37	0.09	-	-
Sm-SEmG1.5-7-51	1458.5	7.23	0.0236	2.09	0.09	1.38	-
Sm-SEmG1.5-7-52	1504.4	7.22	0.0233	2.85	0.43	-	-
Sm-SEmG1.5-7-53	1528.5	7.32	0.0233	2.56	0.30	-	-
Sm-SEmG1.5-7-54	1552.5	7.29	0.0233	2.48	0.12	-	-
Sm-SEmG1.5-7-55	1576.5	7.32	0.0232	2.48	0.14	-	-
Sm-SEmG1.5-7-56	1600.3	7.44	0.0233	2.53	0.53	-	-
Sm-SEmG1.5-7-57	1625.7	7.23	0.0233	2.12	0.12	-	-
Sm-SEmG1.5-7-58	1672.2	7.39	0.0233	2.44	0.15	-	-
Sm-SEmG1.5-7-59	1696.2	7.15	0.0225	2.06	0.15	-	-
Sm-SEmG1.5-7-60	1720.3	7.38	0.0233	1.98	0.13	-	-
Sm-SEmG1.5-7-61	1747.7	7.36	0.0234	2.30	0.21	-	-

Sm-SEmG15-7	**Temperature 37ºC**	**Initial pH 7.32**
Mass 0.1000 g	**Solution 112 mM KCl + 0.556 mM K_2SO_4 + 0.50 mM $KHCO_3$ + 15 mM Glycine**	

Run	Time (h)	pH	Flow (mL min^{-1})	Si (µM)	Al (µM)	Glycine output (mM)	Glycine input (mM)
Sm-SEmG15-7-1	22.2	4.92	0.0220	35.13	11.35	14.3	-
Sm-SEmG15-7-2	49.0	7.19	0.0230	35.04	0.41	-	-
Sm-SEmG15-7-3	91.4	7.55	0.0223	23.18	0.26	-	-
Sm-SEmG15-7-4	115.5	7.60	0.0221	14.30	0.33	-	-
Sm-SEmG15-7-5	139.4	7.72	0.0219	12.90	0.23	-	-
Sm-SEmG15-7-6	163.2	7.72	0.0220	10.42	0.22	-	-
Sm-SEmG15-7-7	191.6	7.66	0.0219	9.10	0.19	-	-
Sm-SEmG15-7-8	214.2	7.72	0.0218	6.32	0.20	-	-
Sm-SEmG15-7-9	259.3	7.79	0.0217	7.25	0.13	-	14.6
Sm-SEmG15-7-10	283.3	7.78	0.0217	5.07	0.18	14.5	-
Sm-SEmG15-7-11	307.3	7.77	0.0218	4.70	0.13	-	-
Sm-SEmG15-7-12	331.5	7.65	0.0215	3.83	0.11	-	-
Sm-SEmG15-7-13	358.8	7.70	0.0217	3.59	0.10	-	-
Sm-SEmG15-7-14	384.1	7.73	0.0218	2.76	0.08	-	-
Sm-SEmG15-7-15	427.5	7.86	0.0134	2.96	0.03	-	-
Sm-SEmG15-7-16	451.3	7.67	0.0219	3.49	0.05	-	-
Sm-SEmG15-7-17	475.3	7.68	0.0218	2.75	0.04	-	-
Sm-SEmG15-7-18	499.2	7.62	0.0219	2.37	0.03	-	-
Sm-SEmG15-7-19	525.9	7.82	0.0218	2.04	0.04	-	-
Sm-SEmG15-7-20	550.6	7.67	0.0219	3.24	0.14	14.1	-
Sm-SEmG15-7-21	595.3	7.83	0.0219	1.72	0.01	-	-
Sm-SEmG15-7-22	619.5	7.73	0.0219	1.81	0.02	-	-
Sm-SEmG15-7-23	645.8	7.76	0.0218	2.19	0.03	-	-
Sm-SEmG15-7-24	670.2	7.77	0.0219	1.86	0.03	-	-
Sm-SEmG15-7-25	694.8	7.80	0.0218	1.66	0.02	-	-
Sm-SEmG15-7-26	720.5	7.79	0.0219	1.65	0.02	-	-
Sm-SEmG15-7-27	763.5	7.88	0.0219	1.95	0.01	-	-
Sm-SEmG15-7-28	790.3	7.78	0.0218	1.56	0.01	-	-

Run	Time (h)	pH	Flow (mL min^{-1})	Si (µM)	Al (µM)	Glycine output (mM)	Glycine input (mM)
Sm-SEmG15-7-29	814.2	7.83	0.0218	1.89	< d.l.	-	-
Sm-SEmG15-7-30	838.3	7.78	0.0218	1.77	0.01	14.0	-
Sm-SEmG15-7-31	863.2	7.67	0.0216	2.67	0.04	-	-
Sm-SEmG15-7-32	886.5	7.82	0.0219	1.46	< d.l.	-	-
Sm-SEmG15-7-33	931.5	7.86	0.0218	1.86	< d.l.	-	-
Sm-SEmG15-7-34	955.3	7.69	0.0218	1.39	< d.l.	-	-
Sm-SEmG15-7-35	979.2	7.73	0.0218	1.36	< d.l.	-	-
Sm-SEmG15-7-36	1003.3	7.71	0.0218	1.35	< d.l.	-	-
Sm-SEmG15-7-37	1031.2	7.74	0.0218	1.54	< d.l.	-	-
Sm-SEmG15-7-38	1056.0	7.80	0.0218	1.32	< d.l.	-	-
Sm-SEmG15-7-39	1099.7	7.85	0.0216	1.58	< d.l.	-	-
Sm-SEmG15-7-40	1123.8	7.77	0.0216	1.46	< d.l.	14.1	-
Sm-SEmG15-7-41	1150.5	7.79	0.0219	1.40	< d.l.	-	-
Sm-SEmG15-7-42	1176.4	7.78	0.0218	1.98	< d.l.	-	-
Sm-SEmG15-7-43	1200.2	7.78	0.0218	1.54	< d.l.	-	-
Sm-SEmG15-7-44	1224.5	7.80	0.0219	1.39	< d.l.	-	-
Sm-SEmG15-7-45	1267.3	7.71	0.0058	2.13	< d.l.	-	-
Sm-SEmG15-7-46	1295.5	7.80	0.0217	2.51	< d.l.	-	-
Sm-SEmG15-7-47	1319.8	7.84	0.0219	1.99	< d.l.	-	-
Sm-SEmG15-7-48	1344.0	7.82	0.0218	1.52	< d.l.	-	-
Sm-SEmG15-7-49	1368.7	7.78	0.0219	1.54	< d.l.	-	-
Sm-SEmG15-7-50	1392.6	7.97	0.0219	1.44	< d.l.	13.7	-
Sm-SEmG15-7-51	1435.2	7.96	0.0214	1.94	< d.l.	-	-
Sm-SEmG15-7-52	1459.5	7.88	0.0218	1.60	< d.l.	-	-
Sm-SEmG15-7-53	1483.9	7.86	0.0215	1.19	< d.l.	-	-
Sm-SEmG15-7-54	1511.4	7.86	0.0214	1.71	< d.l.	-	-
Sm-SEmG15-7-55	1536.8	7.77	0.0214	1.67	< d.l.	-	-
Sm-SEmG15-7-56	1560.5	7.86	0.0215	1.36	< d.l.	-	-
Sm-SEmG15-7-57	1603.5	7.94	0.0215	1.47	< d.l.	-	-
Sm-SEmG15-7-58	1627.5	7.92	0.0215	1.43	< d.l.	-	-
Sm-SEmG15-7-59	1651.6	7.90	0.0214	2.07	0.01	-	-
Sm-SEmG15-7-60	1679.8	7.90	0.0216	1.35	0.01	14.6	-

*d.l.: detection limit

Sm-SEmG15-7b	**Temperature 37ºC**	**Initial pH 7.29**
Mass 0.0993 g	**Solution 112 mM KCl + 0.556 mM K_2SO_4 + 0.45 mM $KHCO_3$ + 15 mM Glycine**	

Run	Time (h)	pH	Flow (mL min^{-1})	Si (µM)	Al (µM)
Sm-SEmG15-7b-1	68.1	6.65	0.0238	22.30	4.60
Sm-SEmG15-7b-2	92.5	7.36	0.0250	9.88	0.62
Sm-SEmG15-7b-3	116.4	7.47	0.0251	14.57	0.67
Sm-SEmG15-7b-4	143.7	7.47	0.0248	16.67	0.16
Sm-SEmG15-7b-5	168.8	7.47	0.0246	17.19	0.14
Sm-SEmG15-7b-6	192.7	7.60	0.0245	10.14	0.16
Sm-SEmG15-7b-7	236.5	7.72	0.0245	11.90	0.01
Sm-SEmG15-7b-8	260.9	7.58	0.0245	8.35	0.25
Sm-SEmG15-7b-9	284.4	7.53	0.0245	5.24	0.01
Sm-SEmG15-7b-10	308.3	7.60	0.0243	4.70	0.15
Sm-SEmG15-7b-11	336.1	7.56	0.0245	4.31	0.10

Run	Time (h)	pH	Flow (mL min^{-1})	Si (µM)	Al (µM)
Sm-SEmG15-7b-12	403.7	7.57	0.0244	3.69	0.04
Sm-SEmG15-7b-13	427.9	7.48	0.0244	3.00	0.10
Sm-SEmG15-7b-14	451.6	7.57	0.0244	2.86	2.19
Sm-SEmG15-7b-15	475.7	7.46	0.0243	2.75	0.17
Sm-SEmG15-7b-16	502.6	7.44	0.0244	2.60	0.11
Sm-SEmG15-7b-17	571.8	7.65	0.0243	2.23	0.05
Sm-SEmG15-7b-18	595.8	7.50	0.0244	1.93	0.15
Sm-SEmG15-7b-19	619.9	7.40	0.0244	1.81	0.20
Sm-SEmG15-7b-20	643.8	7.46	0.0244	1.97	0.20
Sm-SEmG15-7b-21	671.7	7.48	0.0243	1.66	0.10
Sm-SEmG15-7b-22	740.3	7.46	0.0243	1.71	< d.l.
Sm-SEmG15-7b-23	764.2	7.43	0.0244	1.54	0.23
Sm-SEmG15-7b-24	788.4	7.33	0.0245	1.65	0.09
Sm-SEmG15-7b-25	812.3	7.36	0.0244	1.65	0.10
Sm-SEmG15-7b-26	836.8	7.36	0.0244	1.61	0.39
Sm-SEmG15-7b-27	862.3	7.53	0.0243	1.64	0.20
Sm-SEmG15-7b-28	907.8	7.52	0.0244	1.57	0.09
Sm-SEmG15-7b-29	932.3	7.39	0.0243	1.40	0.17
Sm-SEmG15-7b-30	958.3	7.44	0.0243	1.45	0.14
Sm-SEmG15-7b-31	982.6	7.45	0.0244	1.86	0.15
Sm-SEmG15-7b-32	1007.4	7.44	0.0243	1.43	0.21
Sm-SEmG15-7b-33	1032.1	7.58	0.0242	1.89	0.15
Sm-SEmG15-7b-34	1075.9	7.57	0.0242	1.47	0.97
Sm-SEmG15-7b-35	1099.7	7.44	0.0242	1.41	0.33
Sm-SEmG15-7b-36	1125.8	7.43	0.0243	1.80	0.33
Sm-SEmG15-7b-37	1150.3	7.49	0.0243	1.35	0.05
Sm-SEmG15-7b-38	1176.5	7.37	0.0242	1.40	0.12
Sm-SEmG15-7b-39	1199.7	7.60	0.0243	1.27	0.12
Sm-SEmG15-7b-40	1243.6	7.59	0.0233	1.33	0.10
Sm-SEmG15-7b-41	1267.7	7.49	0.0242	1.52	0.16
Sm-SEmG15-7b-42	1292.4	7.48	0.0242	1.38	0.16
Sm-SEmG15-7b-43	1316.8	7.44	0.0242	1.37	0.14
Sm-SEmG15-7b-44	1341.3	7.42	0.0243	1.53	0.06
Sm-SEmG15-7b-45	1366.6	7.49	0.0243	2.06	0.16
Sm-SEmG15-7b-46	1411.8	7.50	0.0242	1.95	0.03
Sm-SEmG15-7b-47	1436.4	7.48	0.0242	1.35	0.10
Sm-SEmG15-7b-48	1460.9	7.49	0.0242	1.33	0.08
Sm-SEmG15-7b-49	1487.8	7.55	0.0242	1.47	0.11
Sm-SEmG15-7b-50	1509.9	7.62	0.0241	1.20	0.10
Sm-SEmG15-7b-51	1580.4	7.57	0.0241	2.36	0.03
Sm-SEmG15-7b-52	1604.9	7.47	0.0242	1.31	0.09
Sm-SEmG15-7b-53	1628.7	7.46	0.0243	1.32	0.10
Sm-SEmG15-7b-54	1652.3	7.47	0.0243	2.17	0.24

*d.l.: detection limit

Sm-Ox0.03-3		**Temperature 25ºC**				**Initial pH 2.87**	
Mass 0.0914 g		**Solution 2.33 mM HNO_3 + 10 mM KNO_3 + 0.03 mM Oxalate**					
Run	Time (h)	pH	Flow (mL min^{-1})	Si (µM)	Al (µM)	Oxalate output (mM)	Oxalate input (mM)
Sm-Ox0.03-3-1	70.1	2.87	0.0311	78.77	-	0.035	0.042
Sm-Ox0.03-3-2	97.4	2.61	0.0217	39.81	-	-	-
Sm-Ox0.03-3-3	142.1	2.64	0.0216	47.40	-	0.046	0.046
Sm-Ox0.03-3-4	170.1	2.69	0.0210	50.76	-	-	-
Sm-Ox0.03-3-5	238.2	2.63	0.0206	27.76	-	0.048	0.020
Sm-Ox0.03-3-6	262.1	2.65	0.0218	30.07	-	-	-
Sm-Ox0.03-3-7	286.2	2.63	0.0217	28.04	-	0.030	0.029
Sm-Ox0.03-3-8	310.1	2.67	0.0217	26.33	-	-	-
Sm-Ox0.03-3-9	333.8	2.65	0.0216	25.76	-	0.046	0.030
Sm-Ox0.03-3-10	405.9	2.66	0.0216	22.99	-	0.013	-
Sm-Ox0.03-3-11	430.3	2.65	0.0217	23.11	-	0.036	0.024
Sm-Ox0.03-3-12	453.8	2.65	0.0217	22.91	-	0.034	0.033
Sm-Ox0.03-3-13	477.8	2.68	0.0217	23.60	-	-	-
Sm-Ox0.03-3-14	507.0	2.71	0.0215	21.65	-	0.021	0.029
Sm-Ox0.03-3-15	573.9	2.64	0.0217	21.24	-	-	-
Sm-Ox0.03-3-16	621.8	2.63	0.0213	18.88	-	0.013	0.029
Sm-Ox0.03-3-17	646.2	2.67	0.0217	13.86	-	0.021	0.032
Sm-Ox0.03-3-18	672.8	2.67	0.0218	13.42	-	-	-
Sm-Ox0.03-3-19	741.8	2.69	0.0217	13.23	-	0.027	0.031
Sm-Ox0.03-3-20	766.3	2.68	0.0217	11.52	6.55	-	-
Sm-Ox0.03-3-21	790.3	2.67	0.0216	11.52	6.41	0.022	0.027
Sm-Ox0.03-3-22	814.1	2.68	0.0215	11.48	6.44	0.023	0.025
Sm-Ox0.03-3-23	840.4	2.69	0.0216	10.92	6.05	-	-
Sm-Ox0.03-3-24	910.3	2.67	0.0216	11.25	6.19	0.035	0.042

Sm-Ox0.03-3.5		**Temperature 25ºC**				**Initial pH 3.64**	
Mass 0.0902 g		**Solution 0.28 mM HNO_3 + 10 mM KNO_3 + 0.03 mM Oxalate**					
Run	Time (h)	pH	Flow (mL min^{-1})	Si (µM)	Al (µM)	Oxalate output (mM)	Oxalate input (mM)
Sm-Ox0.03.3.5-1	21.3	4.47	0.0248	56.00	-	0.022	0.024
Sm-Ox0.03.3.5-2	48.0	3.92	0.0238	35.64	-	-	-
Sm-Ox0.03.3.5-3	117.0	3.64	0.0238	23.88	-	0.024	0.026
Sm-Ox0.03.3.5-4	141.5	3.63	0.0237	17.98	-	-	-
Sm-Ox0.03.3.5-5	165.4	3.56	0.0239	43.47	-	0.023	0.026
Sm-Ox0.03.3.5-6	189.3	3.59	0.0237	15.02	-	-	-
Sm-Ox0.03.3.5-7	215.6	3.60	0.0240	13.75	-	0.023	0.023
Sm-Ox0.03.3.5-8	285.4	3.59	0.0239	12.12	-	0.025	0.025
Sm-Ox0.03.3.5-9	309.4	3.60	0.0239	12.33	-	0.023	0.023
Sm-Ox0.03.3.5-10	333.6	3.58	0.0241	9.53	-	-	-
Sm-Ox0.03.3.5-11	357.3	3.60	0.0239	9.85	-	0.021	0.022
Sm-Ox0.03.3.5-12	384.6	3.60	0.0239	9.90	-	-	-
Sm-Ox0.03.3.5-13	453.5	3.56	0.0241	-	-	0.022	0.021
Sm-Ox0.03.3.5-14	477.5	3.58	0.0240	9.69	-	-	-
Sm-Ox0.03.3.5-15	501.3	3.58	0.0241	10.54	-	0.021	0.025
Sm-Ox0.03.3.5-16	525.3	3.58	0.0239	8.04	-	0.023	0.024

Run	Time (h)	pH	Flow (mL min^{-1})	Si (µM)	Al (µM)	Oxalate output (mM)	Oxalate input (mM)
Sm-Ox0.03.3.5-17	552.0	3.54	0.0240	4.18	-	0.025	0.024
Sm-Ox0.03.3.5-18	621.4	3.54	0.0240	3.95	-	0.025	0.025
Sm-Ox0.03.3.5-19	645.3	3.60	0.0241	3.62	-	0.020	0.026
Sm-Ox0.03.3.5-20	669.4	3.58	0.0240	2.70	-	-	-
Sm-Ox0.03.3.5-21	693.6	3.57	0.0237	2.71	-	0.022	0.021
Sm-Ox0.03.3.5-22	719.4	3.56	0.0241	2.55	-	-	-
Sm-Ox0.03.3.5-23	789.3	3.58	0.0240	2.56	-	0.022	0.025
Sm-Ox0.03.3.5-24	837.3	3.58	0.0241	2.76	-	-	-
Sm-Ox0.03.3.5-25	887.3	3.56	0.0240	2.62	-	0.023	0.027
Sm-Ox0.03.3.5-26	957.5	3.58	0.0241	2.48	-	-	0.027
Sm-Ox0.03.3.5-27	981.6	3.58	0.0234	2.35	-	0.027	0.023
Sm-Ox0.03.3.5-28	1005.6	3.58	0.0243	2.05	-	-	0.025
Sm-Ox0.03.3.5-29	1029.5	3.58	0.0242	1.78	5.57	0.023	0.026
Sm-Ox0.03.3.5-30	1056.8	3.56	0.0242	1.74	5.19	0.024	0.026
Sm-Ox0.03.3.5-31	1125.3	3.57	0.0241	1.64	4.89	0.021	0.024
Sm-Ox0.03.3.5-32	1149.3	3.58	0.0243	1.86	4.94	0.022	0.026
Sm-Ox0.03.3.5-33	1173.8	3.58	0.0240	1.77	3.23	0.020	0.026

Sm-Ox0.03-4.5a	**Temperature 25ºC**	**Initial pH 4.56**
Mass 0.0909 g	**Solution 0.07 mM HNO_3 + 10 mM KNO_3 + 0.03 mM Oxalate**	

Run	Time (h)	pH	Flow (mL min^{-1})	Si (µM)	Al (µM)	Oxalate output (mM)	Oxalate input (mM)
Sm-Ox0.03-4.5a-1	44.5	5.63	0.0226	-	-	0.028	0.031
Sm-Ox0.03-4.5a-2	72.5	5.29	0.0223	22.52	-	-	-
Sm-Ox0.03-4.5a-3	140.6	6.04	0.0251	17.72	-	0.024	0.033
Sm-Ox0.03-4.5a-4	164.5	5.17	0.0228	17.47	-	-	-
Sm-Ox0.03-4.5a-5	188.6	5.45	0.0249	15.05	-	0.023	0.025
Sm-Ox0.03-4.5a-6	212.5	4.93	0.0222	15.92	-	-	-
Sm-Ox0.03-4.5a-7	236.2	4.92	0.0233	12.74	-	0.027	0.027
Sm-Ox0.03-4.5a-8	308.3	4.72	0.0222	13.25	-	-	-
Sm-Ox0.03-4.5a-9	332.7	4.56	0.0222	11.02	-	0.027	0.029
Sm-Ox0.03-4.5a-10	356.2	4.60	0.0189	6.08	-	-	-
Sm-Ox0.03-4.5a-11	380.3	4.58	0.0225	12.07	-	0.027	0.029
Sm-Ox0.03-4.5a-12	409.4	4.52	0.0221	7.33	-	0.022	0.028
Sm-Ox0.03-4.5a-13	476.3	4.63	0.0224	7.16	-	0.034	-
Sm-Ox0.03-4.5a-14	524.2	4.56	0.0218	7.44	-	-	0.025
Sm-Ox0.03-4.5a-15	548.6	4.40	0.0222	6.28	-	0.022	0.043
Sm-Ox0.03-4.5a-16	575.3	4.40	0.0222	4.26	-	0.025	0.047
Sm-Ox0.03-4.5a-17	644.3	4.38	0.0218	4.46	-	-	-
Sm-Ox0.03-4.5a-18	668.8	4.38	0.0223	4.21	-	0.023	0.025
Sm-Ox0.03-4.5a-19	692.7	4.38	0.0220	3.40	-	0.023	0.029
Sm-Ox0.03-4.5a-20	716.5	4.36	0.0220	4.06	-	-	-
Sm-Ox0.03-4.5a-21	742.8	4.46	0.0222	3.44	-	0.024	0.030
Sm-Ox0.03-4.5a-22	812.7	4.34	0.0221	3.51	-	-	-
Sm-Ox0.03-4.5a-23	836.6	4.34	0.0222	3.78	-	0.025	0.027
Sm-Ox0.03-4.5a-24	860.8	4.36	0.0216	3.72	-	-	-
Sm-Ox0.03-4.5a-25	884.5	4.36	0.0230	4.64	-	0.026	0.027
Sm-Ox0.03-4.5a-26	911.8	4.35	0.0221	4.71	-	-	-

Run	Time (h)	pH	Flow (mL min^{-1})	Si (μM)	Al (μM)	Oxalate output (mM)	Oxalate input (mM)
Sm-Ox0.03-4.5a-27	980.8	4.37	0.0228	4.07	1.52	0.023	0.028
Sm-Ox0.03-4.5a-28	1004.8	4.40	0.0225	4.11	1.39	-	-
Sm-Ox0.03-4.5a-29	1028.5	4.43	0.0221	4.33	1.60	0.025	0.030
Sm-Ox0.03-4.5a-30	1052.6	4.38	0.0221	4.48	1.56	0.026	0.035

Sm-Ox0.03-4.5b	**Temperature 25ºC**	**Initial pH 4.41**
Mass 0.0910 g	**Solution 0.09 mM HNO_3 + 10 mM KNO_3 + 0.03 mM Oxalate**	

Run	Time (h)	pH	Flow (mL min^{-1})	Si (μM)	Al (μM)	Oxalate output (mM)	Oxalate input (mM)
Sm-Ox0.03-4.5b-1	21.4	5.36	0.0218	35.40	-	0.026	0.030
Sm-Ox0.03-4.5b-2	45.3	5.13	0.0232	23.40	-	-	-
Sm-Ox0.03-4.5b-3	71.6	4.80	0.0234	14.85	-	0.028	0.027
Sm-Ox0.03-4.5b-4	141.4	4.41	0.0231	11.63	-	-	0.030
Sm-Ox0.03-4.5b-5	165.4	4.39	0.0231	9.18	-	0.023	-
Sm-Ox0.03-4.5b-6	189.6	4.40	0.0233	8.02	-	-	0.029
Sm-Ox0.03-4.5b-7	213.3	4.42	0.0231	8.31	-	0.026	-
Sm-Ox0.03-4.5b-8	240.6	4.42	0.0231	8.73	-	-	0.031
Sm-Ox0.03-4.5b-9	309.5	4.38	0.0236	7.99	-	0.025	-
Sm-Ox0.03-4.5b-10	333.5	4.38	0.0233	6.73	-	-	0.029
Sm-Ox0.03-4.5b-11	357.3	4.43	0.0242	7.29	-	0.026	-
Sm-Ox0.03-4.5b-12	381.3	4.55	0.0231	7.49	-	-	0.029
Sm-Ox0.03-4.5b-13	408.0	4.45	0.0231	6.84	-	0.027	-
Sm-Ox0.03-4.5b-14	477.4	4.51	0.0230	5.38	-	-	0.031
Sm-Ox0.03-4.5b-15	501.3	4.45	0.0230	3.75	-	0.029	-
Sm-Ox0.03-4.5b-16	525.4	4.44	0.0228	5.10	-	-	0.030
Sm-Ox0.03-4.5b-17	549.6	4.47	0.0227	4.37	-	0.024	-
Sm-Ox0.03-4.5b-18	575.4	4.43	0.0230	4.13	-	-	0.030
Sm-Ox0.03-4.5b-19	645.3	4.47	0.0231	4.43	-	0.027	-
Sm-Ox0.03-4.5b-20	693.3	4.51	0.0229	4.31	-	-	0.029
Sm-Ox0.03-4.5b-21	743.3	4.48	0.0230	4.09	-	0.026	-
Sm-Ox0.03-4.5b-22	813.5	4.50	0.0231	3.44	-	0.025	0.030
Sm-Ox0.03-4.5b-23	837.6	4.52	0.0232	2.82	1.14	-	-
Sm-Ox0.03-4.5b-24	861.6	4.52	0.0231	3.04	1.27	0.024	0.030
Sm-Ox0.03-4.5b-25	885.5	4.49	0.0231	2.72	1.14	-	-
Sm-Ox0.03-4.5b-26	912.8	4.50	0.0232	2.74	1.19	0.025	0.030

Sm-Ox0.03-7	**Temperature 25ºC**	**Initial pH 6.71**
Mass 0.0903 g	**Solution 10 mM KNO_3 + 0.03 mM Oxalate**	

Run	Time (h)	pH	Flow (mL min^{-1})	Si (μM)	Al (μM)	Oxalate output (mM)	Oxalate input (mM)
Sm-Ox0.03-7-1	20.2	6.38	0.0247	45.75	-	0.021	0.023
Sm-Ox0.03-7-2	44.3	6.31	0.0237	23.81	-	0.025	0.024
Sm-Ox0.03-7-3	73.4	6.71	0.0232	11.96	-	0.023	-
Sm-Ox0.03-7-4	140.3	6.69	0.0234	8.62	-	-	0.024
Sm-Ox0.03-7-5	188.2	6.79	0.0230	6.16	-	0.022	-

Run	Time (h)	pH	Flow (mL min^{-1})	Si (µM)	Al (µM)	Oxalate output (mM)	Oxalate input (mM)
Sm-Ox0.03-7-6	212.6	6.78	0.0228	5.41	-	-	0.028
Sm-Ox0.03-7-7	239.3	6.86	0.0230	5.48	-	0.023	-
Sm-Ox0.03-7-8	308.3	6.74	0.0229	3.94	-	-	0.025
Sm-Ox0.03-7-9	332.8	6.90	0.0230	3.95	-	0.022	0.027
Sm-Ox0.03-7-10	356.7	6.82	0.0228	3.31	-	-	-
Sm-Ox0.03-7-11	380.5	6.74	0.0227	3.19	-	0.023	0.026
Sm-Ox0.03-7-12	406.8	6.61	0.0229	3.08	-	0.021	0.027
Sm-Ox0.03-7-13	476.7	6.73	0.0234	3.19	-	-	-
Sm-Ox0.03-7-14	500.6	6.79	0.0228	2.83	-	0.028	0.023
Sm-Ox0.03-7-15	524.8	6.78	0.0229	3.61	-	-	-
Sm-Ox0.03-7-16	548.5	6.75	0.0229	2.54	-	0.020	0.024
Sm-Ox0.03-7-17	575.8	6.78	0.0228	2.59	-	-	-
Sm-Ox0.03-7-18	644.8	6.74	0.0239	2.32	-	0.022	0.022
Sm-Ox0.03-7-19	668.8	6.82	0.0231	2.01	-	-	-
Sm-Ox0.03-7-20	692.5	6.70	0.0230	2.15	-	0.020	0.016
Sm-Ox0.03-7-21	716.6	6.75	0.0228	1.98	-	-	-
Sm-Ox0.03-7-22	743.3	6.63	0.0229	2.44	-	0.022	0.025
Sm-Ox0.03-7-23	812.7	6.75	0.0232	2.14	-	-	-
Sm-Ox0.03-7-24	836.6	6.62	0.0231	1.72	-	0.020	0.026
Sm-Ox0.03-7-25	860.7	6.69	0.0231	1.96	1.11	-	-
Sm-Ox0.03-7-26	884.8	6.72	0.0227	1.88	1.44	0.022	0.023
Sm-Ox0.03-7-27	910.7	6.84	0.0230	1.83	0.82	-	-
Sm-Ox0.03-7-28	980.5	6.84	0.0228	1.74	-	0.021	0.027

Sm-Ox0.1-3.5a	**Temperature 25ºC**	**Initial pH 3.61**
Mass 0.0914 g	**Solution 0.42 mM HNO_3 + 10 mM KNO_3 + 0.1 mM Oxalate**	

Run	Time (h)	pH	Flow (mL min^{-1})	Si (µM)	Al (µM)	Oxalate output (mM)	Oxalate input (mM)
Sm-Ox0.1-3.5a-1	40.8	4.06	0.0169	43.71	-	0.091	0.099
Sm-Ox0.1-3.5a-2	72.3	3.69	0.0221	38.50	-	0.085	0.095
Sm-Ox0.1-3.5a-3	112.8	3.61	0.0227	26.14	-	0.092	0.088
Sm-Ox0.1-3.5a-4	136.6	3.58	0.0228	20.83	-	0.086	0.096
Sm-Ox0.1-3.5a-5	160.6	3.52	0.0219	20.80	-	0.095	0.096
Sm-Ox0.1-3.5a-6	184.9	3.57	0.0235	17.50	-	0.089	0.094
Sm-Ox0.1-3.5a-7	216.3	3.57	0.0220	16.51	-	-	0.099
Sm-Ox0.1-3.5a-8	280.8	3.53	0.0219	15.63	-	0.089	0.090
Sm-Ox0.1-3.5a-9	304.9	3.51	0.0220	12.00	-	0.097	0.097
Sm-Ox0.1-3.5a-10	328.8	3.52	0.0219	12.54	-	0.095	0.096
Sm-Ox0.1-3.5a-11	352.5	3.48	0.0220	12.44	-	0.097	0.095
Sm-Ox0.1-3.5a-12	376.8	3.52	0.0222	12.64	-	0.092	0.098
Sm-Ox0.1-3.5a-13	404.8	3.60	0.0218	14.60	-	0.094	0.093
Sm-Ox0.1-3.5a-14	450.8	3.53	0.0218	11.13	-	0.095	0.098
Sm-Ox0.1-3.5a-15	473.1	3.50	0.0219	10.71	-	0.096	0.099
Sm-Ox0.1-3.5a-16	497.0	3.50	0.0220	11.58	-	-	0.098
Sm-Ox0.1-3.5a-17	520.8	3.51	0.0220	11.03	-	0.093	0.096
Sm-Ox0.1-3.5a-18	553.9	3.53	0.0218	10.98	-	0.094	0.097
Sm-Ox0.1-3.5a-19	618.3	3.56	0.0219	11.88	-	0.097	0.096
Sm-Ox0.1-3.5a-20	641.5	3.51	0.0219	12.20	-	0.092	0.095

Run	Time (h)	pH	Flow (mL min^{-1})	Si (µM)	Al (µM)	Oxalate output (mM)	Oxalate input (mM)
Sm-Ox0.1-3.5a-21	664.6	3.51	0.0219	12.83	-	0.092	0.096
Sm-Ox0.1-3.5a-22	688.8	3.51	0.0219	12.35	-	0.101	0.093
Sm-Ox0.1-3.5a-23	720.3	3.49	0.0218	12.96	-	0.095	0.097
Sm-Ox0.1-3.5a-24	771.0	3.58	0.0216	10.50	-	0.094	0.096
Sm-Ox0.1-3.5a-25	810.3	3.49	0.0217	9.23	-	0.097	0.096
Sm-Ox0.1-3.5a-26	832.8	3.47	0.0221	9.21	-	0.096	0.098
Sm-Ox0.1-3.5a-27	857.0	3.47	0.0217	8.14	-	0.099	0.097
Sm-Ox0.1-3.5a-28	881.9	3.49	0.0202	8.88	-	0.092	0.096
Sm-Ox0.1-3.5a-29	908.5	3.61	0.0222	7.68	-	0.094	0.094
Sm-Ox0.1-3.5a-30	952.9	3.49	0.0216	7.94	-	0.094	0.096
Sm-Ox0.1-3.5a-31	976.8	3.50	0.0220	7.79	-	0.095	0.097
Sm-Ox0.1-3.5a-32	1000.8	3.51	0.0220	7.48	2.06	0.097	0.095
Sm-Ox0.1-3.5a-33	1024.7	3.49	0.0218	7.50	1.96	0.097	0.096
Sm-Ox0.1-3.5a-34	1048.8	3.48	0.0217	7.59	2.01	0.095	0.098
Sm-Ox0.1-3.5a-35	1081.6	3.53	0.0219	7.26	1.91	0.093	0.096
Sm-Ox0.1-3.5a-36	1120.5	3.49	0.0081	7.44	2.19	-	-

Sm-Ox0.1-3.5b	**Temperature 25ºC**	**Initial pH 3.57**
Mass 0.0924 g	**Solution 0.42 mM HNO_3 + 10 mM KNO_3 + 0.1 mM Oxalate**	

Run	Time (h)	pH	Flow (mL min^{-1})	Si (µM)	Al (µM)	Oxalate output (mM)	Oxalate input (mM)
Sm-Ox0.1-3.5b-1	21.5	3.96	0.0215	47.28	-	0.080	-
Sm-Ox0.1-3.5b-2	45.5	3.86	0.0219	53.00	-	0.090	0.099
Sm-Ox0.1-3.5b-3	77.0	3.70	0.0217	38.66	-	0.098	0.095
Sm-Ox0.1-3.5b-4	117.5	3.57	0.0213	30.97	-	0.095	0.088
Sm-Ox0.1-3.5b-5	141.3	3.53	0.0215	24.43	-	0.086	0.096
Sm-Ox0.1-3.5b-6	165.4	3.51	0.0214	17.72	-	0.091	0.096
Sm-Ox0.1-3.5b-7	189.6	3.54	0.0213	19.73	-	0.092	0.094
Sm-Ox0.1-3.5b-8	221.0	3.59	0.0214	18.47	-	-	0.099
Sm-Ox0.1-3.5b-9	285.5	3.54	0.0211	16.52	-	0.090	0.090
Sm-Ox0.1-3.5b-10	309.7	3.51	0.0210	12.95	-	0.099	0.097
Sm-Ox0.1-3.5b-11	333.6	3.53	0.0212	11.80	-	0.095	0.096
Sm-Ox0.1-3.5b-12	357.2	3.53	0.0212	12.06	-	0.092	0.095
Sm-Ox0.1-3.5b-13	381.5	3.52	0.0213	12.52	-	0.090	0.098
Sm-Ox0.1-3.5b-14	409.5	3.60	0.0210	12.51	-	0.090	0.093
Sm-Ox0.1-3.5b-15	455.6	3.49	0.0209	11.14	-	0.100	0.098
Sm-Ox0.1-3.5b-16	477.8	3.50	0.0211	10.37	-	0.097	0.099
Sm-Ox0.1-3.5b-17	501.8	3.52	0.0211	10.63	-	0.093	0.098
Sm-Ox0.1-3.5b-18	525.5	3.52	0.0212	10.38	-	0.096	0.096
Sm-Ox0.1-3.5b-19	558.7	3.52	0.0211	10.33	-	0.100	0.097
Sm-Ox0.1-3.5b-20	623.0	3.54	0.0210	11.13	-	0.096	0.096
Sm-Ox0.1-3.5b-21	646.3	3.52	0.0211	11.51	-	0.092	0.095
Sm-Ox0.1-3.5b-22	669.3	3.51	0.0212	12.32	-	0.096	0.096
Sm-Ox0.1-3.5b-23	693.5	3.52	0.0210	12.10	-	0.095	0.093
Sm-Ox0.1-3.5b-24	725.0	3.51	0.0211	11.81	-	0.087	0.097
Sm-Ox0.1-3.5b-25	775.7	3.58	0.0209	9.69	-	0.096	0.096
Sm-Ox0.1-3.5b-26	815.0	3.49	0.0209	8.70	-	0.091	0.096
Sm-Ox0.1-3.5b-27	837.5	3.49	0.0213	7.22	-	0.095	0.098

Run	Time (h)	pH	Flow (mL min^{-1})	Si (µM)	Al (µM)	Oxalate output (mM)	Oxalate input (mM)
Sm-Ox0.1-3.5b-28	861.8	3.48	0.0209	7.45	-	0.092	-
Sm-Ox0.1-3.5b-29	886.7	3.50	0.0194	8.34	-	0.094	0.096
Sm-Ox0.1-3.5b-30	913.3	3.58	0.0209	7.51	-	0.095	0.094
Sm-Ox0.1-3.5b-31	957.7	3.49	0.0207	7.31	-	0.092	0.096
Sm-Ox0.1-3.5b-32	981.6	3.53	0.0209	7.24	-	0.095	0.097
Sm-Ox0.1-3.5b-33	1005.5	3.51	0.0209	6.94	2.06	0.102	0.095
Sm-Ox0.1-3.5b-34	1029.4	3.50	0.0203	6.86	2.01	0.095	0.096
Sm-Ox0.1-3.5b-35	1053.5	3.50	0.0208	6.98	2.04	0.098	0.094
Sm-Ox0.1-3.5b-36	1086.3	3.55	0.0208	6.81	2.16	0.099	0.095
Sm-Ox0.1-3.5b-37	1125.2	3.49	0.0081	6.88	1.99	0.092	0.096

Sm-Ox0.1-4a	**Temperature 25ºC**	**Initial pH 4.67**
Mass 0.0906 g	**Solution 0.25 mM HNO_3 + 10 mM KNO_3 + 0.1 mM Oxalate**	

Run	Time (h)	pH	Flow (mL min^{-1})	Si (µM)	Al (µM)	Oxalate output (mM)	Oxalate input (mM)
Sm-Ox0.1-4a-1	20.1	4.34	0.0221	45.49	-	0.081	-
Sm-Ox0.1-4a-2	51.5	4.15	0.0215	46.85	-	-	0.095
Sm-Ox0.1-4a-3	116.0	3.86	0.0215	26.87	-	0.094	0.098
Sm-Ox0.1-4a-4	140.2	3.83	0.0213	17.80	-	0.088	0.089
Sm-Ox0.1-4a-5	164.1	3.83	0.0215	16.98	-	0.091	0.095
Sm-Ox0.1-4a-6	187.7	3.82	0.0214	17.19	-	0.091	0.098
Sm-Ox0.1-4a-7	212.0	3.83	0.0217	17.26	-	0.093	0.094
Sm-Ox0.1-4a-8	240.0	3.87	0.0214	15.37	-	0.091	0.099
Sm-Ox0.1-4a-9	286.1	3.84	0.0214	14.02	-	0.093	-
Sm-Ox0.1-4a-10	308.3	3.81	0.0216	12.17	-	0.097	0.093
Sm-Ox0.1-4a-11	332.3	3.83	0.0215	12.23	-	0.094	0.101
Sm-Ox0.1-4a-12	356.0	3.82	0.0215	12.01	-	0.097	0.096
Sm-Ox0.1-4a-13	389.2	3.82	0.0216	11.41	-	0.090	0.101
Sm-Ox0.1-4a-14	453.5	3.85	0.0214	11.67	-	0.099	0.094
Sm-Ox0.1-4a-15	476.8	3.85	0.0215	11.57	-	0.095	0.098
Sm-Ox0.1-4a-16	499.8	3.80	0.0216	11.55	-	0.098	0.095
Sm-Ox0.1-4a-17	524.0	3.82	0.0215	11.23	-	-	0.097
Sm-Ox0.1-4a-18	555.5	3.82	0.0232	11.46	-	0.094	0.093
Sm-Ox0.1-4a-19	606.2	3.87	0.0213	8.84	-	0.092	0.096
Sm-Ox0.1-4a-20	645.5	3.79	0.0214	8.11	-	0.093	0.094
Sm-Ox0.1-4a-21	668.0	3.79	0.0217	8.06	-	0.092	0.093
Sm-Ox0.1-4a-22	692.3	3.77	0.0214	7.32	-	0.095	0.095
Sm-Ox0.1-4a-23	717.2	3.78	0.0199	8.10	-	0.092	0.096
Sm-Ox0.1-4a-24	743.8	3.87	0.0215	7.57	-	0.092	0.098
Sm-Ox0.1-4a-25	788.2	3.78	0.0212	7.12	-	0.091	0.095
Sm-Ox0.1-4a-26	812.1	3.80	0.0216	7.01	-	0.093	0.093
Sm-Ox0.1-4a-27	836.0	3.79	0.0217	6.64	-	0.099	0.093
Sm-Ox0.1-4a-28	859.9	3.79	0.0215	7.00	-	0.094	0.096
Sm-Ox0.1-4a-29	884.0	3.78	0.0214	6.77	-	0.093	0.095
Sm-Ox0.1-4a-30	916.8	3.80	0.0216	6.57	-	0.099	0.093
Sm-Ox0.1-4a-31	955.7	3.81	0.0214	6.52	2.16	0.095	0.092
Sm-Ox0.1-4a-32	980.3	3.81	0.0213	6.35	1.87	0.096	0.098
Sm-Ox0.1-4a-33	1003.9	3.79	0.0217	6.42	1.93	0.094	0.098
Sm-Ox0.1-4a-34	1028.0	3.81	0.0212	6.39	2.42	-	-

Sm-Ox0.1-4b		**Temperature 25ºC**					**Initial pH 4.47**
Mass 0.0914 g		**Solution 0.25 mM HNO_3 + 10 mM KNO_3 + 0.1 mM Oxalate**					
Run	Time (h)	pH	Flow (mL min^{-1})	Si (µM)	Al (µM)	Oxalate output (mM)	Oxalate input (mM)
Sm-Ox0.1-4b-1	22.4	5.61	0.0249	46.79	-	-	0.111
Sm-Ox0.1-4b-2	46.5	5.63	0.0217	23.54	-	0.093	-
Sm-Ox0.1-4b-3	80.5	5.27	0.0220	22.76	-	0.091	-
Sm-Ox0.1-4b-4	142.5	4.67	0.0216	13.82	-	0.096	0.104
Sm-Ox0.1-4b-5	166.7	4.56	0.0219	-	-	0.106	0.108
Sm-Ox0.1-4b-6	190.5	4.57	0.0218	12.01	-	0.103	-
Sm-Ox0.1-4b-7	265.0	4.48	0.0217	9.54	-	0.105	-
Sm-Ox0.1-4b-8	310.5	4.48	0.0214	11.90	-	0.099	0.109
Sm-Ox0.1-4b-9	334.6	4.39	0.0218	10.54	-	0.107	0.108
Sm-Ox0.1-4b-10	359.7	4.47	0.0220	10.33	-	0.108	-
Sm-Ox0.1-4b-11	382.5	4.47	0.0217	9.20	-	0.101	0.104
Sm-Ox0.1-4b-12	410.8	4.50	0.0218	6.77	-	0.108	0.100
Sm-Ox0.1-4b-13	478.3	4.41	0.0217	7.96	-	0.109	0.109
Sm-Ox0.1-4b-14	502.6	4.42	0.0217	5.77	-	0.104	0.101
Sm-Ox0.1-4b-15	526.6	4.43	0.0216	7.44	-	0.110	0.106
Sm-Ox0.1-4b-16	550.8	4.42	0.0219	6.81	-	0.105	0.101
Sm-Ox0.1-4b-17	579.5	4.49	0.0217	6.76	-	0.108	0.105
Sm-Ox0.1-4b-18	646.7	4.41	0.0217	6.06	-	0.106	0.107
Sm-Ox0.1-4b-19	670.4	4.34	0.0218	5.74	-	0.108	0.105
Sm-Ox0.1-4b-20	694.6	4.40	0.0214	6.28	-	0.119	0.111
Sm-Ox0.1-4b-21	718.5	4.40	0.0219	5.61	-	0.102	0.105
Sm-Ox0.1-4b-22	742.7	4.43	0.0218	5.68	-	0.110	0.102
Sm-Ox0.1-4b-23	769.2	4.41	0.0216	5.06	-	0.099	-
Sm-Ox0.1-4b-24	814.6	4.39	0.0215	5.58	-	0.101	0.101
Sm-Ox0.1-4b-25	838.5	4.40	0.0216	5.11	-	0.100	0.109
Sm-Ox0.1-4b-26	862.5	4.34	0.0217	5.32	-	0.101	0.100
Sm-Ox0.1-4b-27	886.7	4.33	0.0217	4.49	1.50	0.105	0.102
Sm-Ox0.1-4b-28	910.8	4.39	0.0216	4.73	1.79	0.103	0.100
Sm-Ox0.1-4b-29	936.5	4.39	0.0218	4.85	1.52	0.099	-
Sm-Ox0.1-4b-30	982.7	4.32	0.0216	4.65	1.41	0.110	0.100
Sm-Ox0.1-4b-31	1006.7	4.30	0.0216	4.78	1.30	0.104	0.102

Sm-Ox0.1-4c		**Temperature 25ºC**					**Initial pH 3.86**
Mass 0.0907 g		**Solution 0.33 mM HNO_3 + 10 mM KNO_3 + 0.1 mM Oxalate**					
Run	Time (h)	pH	Flow (mL min^{-1})	Si (µM)	Al (µM)	Oxalate output (mM)	Oxalate input (mM)
Sm-Ox0.1-4c-1	19.9	5.10	0.0234	26.48	-	0.100	0.109
Sm-Ox0.1-4c-2	43.8	5.30	0.0209	97.98	-	0.101	0.106
Sm-Ox0.1-4c-3	67.7	5.14	0.0206	37.75	-	0.098	0.108
Sm-Ox0.1-4c-4	91.8	4.84	0.0204	19.83	-	0.102	-
Sm-Ox0.1-4c-5	124.7	4.66	0.0206	13.52	-	0.100	-
Sm-Ox0.1-4c-6	163.7	4.56	0.0221	15.37	-	0.105	0.106
Sm-Ox0.1-4c-7	188.1	4.47	0.0205	11.18	-	0.100	0.105
Sm-Ox0.1-4c-8	211.7	4.41	0.0207	11.86	-	0.100	0.111
Sm-Ox0.1-4c-9	235.8	4.42	0.0204	11.77	-	0.102	-

Run	Time (h)	pH	Flow (mL min^{-1})	Si (µM)	Al (µM)	Oxalate output (mM)	Oxalate input (mM)
Sm-Ox0.1-4c-10	269.8	4.45	0.0204	10.80	-	0.100	-
Sm-Ox0.1-4c-11	331.8	4.35	0.0200	11.00	-	0.108	0.104
Sm-Ox0.1-4c-12	356.1	4.42	0.0205	8.87	-	0.099	0.108
Sm-Ox0.1-4c-13	379.8	4.41	0.0204	8.24	-	0.099	-
Sm-Ox0.1-4c-14	454.3	4.42	0.0211	8.52	-	0.114	-
Sm-Ox0.1-4c-15	499.8	4.40	0.0204	7.90	-	0.100	0.109
Sm-Ox0.1-4c-16	523.9	4.40	0.0205	7.78	-	0.104	0.108
Sm-Ox0.1-4c-17	549.1	4.38	0.0206	7.33	-	0.101	-
Sm-Ox0.1-4c-18	571.8	4.55	0.0203	8.23	-	0.106	0.104
Sm-Ox0.1-4c-19	600.2	-	0.0018	-	-	0.100	0.100
Sm-Ox0.1-4c-20	667.7	4.42	0.0203	7.23	-	0.106	0.109
Sm-Ox0.1-4c-21	691.9	4.43	0.0205	6.64	-	0.103	0.101
Sm-Ox0.1-4c-22	715.9	4.40	0.0204	6.77	-	0.106	0.106
Sm-Ox0.1-4c-23	740.2	4.37	0.0205	6.44	-	0.109	0.101
Sm-Ox0.1-4c-24	768.8	4.40	0.0204	6.18	-	0.107	0.105
Sm-Ox0.1-4c-25	836.0	4.35	0.0204	6.15	-	0.107	0.107
Sm-Ox0.1-4c-26	859.7	4.35	0.0204	5.95	1.63	0.105	0.105
Sm-Ox0.1-4c-27	883.9	4.36	0.0201	5.74	1.62	0.104	0.111
Sm-Ox0.1-4c-28	907.8	4.35	0.0204	5.74	1.43	0.106	0.105
Sm-Ox0.1-4c-29	932.0	4.36	0.0204	5.56	1.53	0.106	0.102

Sm-Ox0.1-5	**Temperature 25ºC**	**Initial pH 5.67**
Mass 0.0907 g	**Solution 0.07 mM HNO_3 + 10 mM KNO_3 + 0.1 mM Oxalate**	

Run	Time (h)	pH	Flow (mL min^{-1})	Si (µM)	Al (µM)	Oxalate output (mM)	Oxalate input (mM)
Sm-Ox0.1-5-1	27.3	6.25	0.0227	26.33	-	0.096	0.099
Sm-Ox0.1-5-2	47.0	5.66	0.0224	28.96	-	-	-
Sm-Ox0.1-5-3	71.2	5.67	0.0221	19.24	-	0.096	-
Sm-Ox0.1-5-4	141.8	5.73	0.0220	14.61	-	0.096	0.095
Sm-Ox0.1-5-5	166.4	5.15	0.0219	12.13	-	0.097	0.101
Sm-Ox0.1-5-6	190.5	5.06	0.0218	11.53	-	-	-
Sm-Ox0.1-5-7	214.5	5.09	0.0220	11.57	-	-	-
Sm-Ox0.1-5-8	242.4	5.11	0.0218	9.22	-	0.091	0.094
Sm-Ox0.1-5-9	310.5	-	0.0212	10.56	-	-	-
Sm-Ox0.1-5-10	334.5	4.95	0.0219	9.09	-	0.093	0.095
Sm-Ox0.1-5-11	358.5	4.87	0.0218	8.32	-	0.097	-
Sm-Ox0.1-5-12	382.5	4.91	0.0217	7.77	-	0.098	0.094
Sm-Ox0.1-5-13	410.3	4.85	0.0218	7.23	-	0.098	-
Sm-Ox0.1-5-14	458.3	4.88	0.0214	7.40	-	-	0.095
Sm-Ox0.1-5-15	502.8	4.88	0.0213	6.79	-	-	-
Sm-Ox0.1-5-16	526.4	4.81	0.0218	6.75	-	0.099	0.094
Sm-Ox0.1-5-17	550.3	4.82	0.0218	6.19	-	0.071	-
Sm-Ox0.1-5-18	574.4	4.82	0.0217	5.86	-	0.086	0.096
Sm-Ox0.1-5-19	602.4	-	0.0216	-	-	0.094	0.095
Sm-Ox0.1-5-20	646.3	4.86	0.0213	5.99	-	0.096	-
Sm-Ox0.1-5-21	670.3	4.89	0.0216	5.48	-	0.096	0.094
Sm-Ox0.1-5-22	694.4	4.87	0.0213	5.74	-	-	0.095
Sm-Ox0.1-5-23	718.4	4.92	0.0081	5.67	-	0.094	-

Run	Time (h)	pH	Flow (mL min^{-1})	Si (µM)	Al (µM)	Oxalate output (mM)	Oxalate input (mM)
Sm-Ox0.1-5-24	742.6	4.98	0.0208	7.79	-	-	0.096
Sm-Ox0.1-5-25	770.6	5.01	0.0219	5.40	-	0.090	-
Sm-Ox0.1-5-26	814.9	5.05	0.0218	4.80	-	-	0.092
Sm-Ox0.1-5-27	838.6	4.95	0.0218	4.35	2.62	0.089	-
Sm-Ox0.1-5-28	862.6	4.97	0.0218	4.40	1.20	-	0.093
Sm-Ox0.1-5-29	886.6	5.03	0.0218	4.40	1.12	0.089	-
Sm-Ox0.1-5-30	910.4	4.98	0.0219	4.22	1.16	-	0.091
Sm-Ox0.1-5-31	934.8	5.24	0.0218	4.13	1.15	0.093	-

Sm-Ox0.1-6a	**Temperature 25ºC**				**Initial pH 6.56**		
Mass 0.0913 g	**Solution 10 mM KNO_3 + 0.1 mM Oxalate**						
Run	Time (h)	pH	Flow (mL min^{-1})	Si (µM)	Al (µM)	Oxalate output (mM)	Oxalate input (mM)
Sm-Ox0.1-6a-1	20.8	6.77	0.0229	52.75	-	0.085	0.091
Sm-Ox0.1-6a-2	45.0	6.88	0.0232	-	-	0.093	-
Sm-Ox0.1-6a-3	69.0	6.94	0.0223	22.45	-	0.083	0.097
Sm-Ox0.1-6a-4	93.0	6.69	0.0230	16.84	-	-	0.092
Sm-Ox0.1-6a-5	124.5	6.56	0.0227	12.00	-	0.085	0.098
Sm-Ox0.1-6a-6	165.0	6.52	0.0223	10.79	-	0.090	0.099
Sm-Ox0.1-6a-7	188.8	6.42	0.0228	9.64	-	0.090	0.095
Sm-Ox0.1-6a-8	212.9	6.37	0.0226	7.05	-	0.093	0.097
Sm-Ox0.1-6a-9	237.1	6.34	0.0227	5.51	-	-	0.093
Sm-Ox0.1-6a-10	268.5	6.28	0.0227	7.93	-	-	0.099
Sm-Ox0.1-6a-11	333.0	6.37	0.0224	7.43	-	0.091	0.090
Sm-Ox0.1-6a-12	357.2	6.22	0.0227	6.72	-	0.088	0.099
Sm-Ox0.1-6a-13	381.1	6.21	0.0228	5.68	-	0.093	0.096
Sm-Ox0.1-6a-14	404.7	6.16	0.0228	6.87	-	0.093	0.094
Sm-Ox0.1-6a-15	429.0	5.99	0.0231	5.26	-	0.094	0.096
Sm-Ox0.1-6a-16	457.0	6.04	0.0226	6.42	-	0.093	0.100
Sm-Ox0.1-6a-17	503.1	0.00	0.0226	4.28	-	0.096	0.093
Sm-Ox0.1-6a-18	525.3	6.06	0.0228	3.64	-	0.092	0.097
Sm-Ox0.1-6a-19	549.2	6.12	0.0227	3.97	-	0.097	0.096
Sm-Ox0.1-6a-20	573.0	6.09	0.0228	4.10	-	0.099	0.101
Sm-Ox0.1-6a-21	606.2	6.01	0.0227	3.69	-	-	0.097
Sm-Ox0.1-6a-22	670.5	6.04	0.0226	4.14	-	-	0.099
Sm-Ox0.1-6a-23	693.8	5.94	0.0226	3.87	1.50	0.096	0.094
Sm-Ox0.1-6a-24	716.8	6.01	0.0226	3.83	1.30	-	0.106
Sm-Ox0.1-6a-25	741.0	6.04	0.0226	4.10	1.21	0.105	0.096
Sm-Ox0.1-6a-26	772.5	5.98	0.0225	3.83	1.40	0.091	0.100

Sm-Ox0.1-6b		**Temperature 25ºC**				**Initial pH 6.40**	
Mass 0.0902 g		**Solution 10 mM KNO_3 + 0.1 mM Oxalate**					
Run	Time (h)	pH	Flow (mL min^{-1})	Si (µM)	Al (µM)	Oxalate output (mM)	Oxalate input (mM)
Sm-Ox0.1-6b-1	22.6	6.54	0.0207	27.48	-	0.088	0.093
Sm-Ox0.1-6b-2	54.0	6.40	0.0200	27.73	-	0.093	0.099
Sm-Ox0.1-6b-3	118.5	6.60	0.0197	13.83	-	0.082	0.090
Sm-Ox0.1-6b-4	142.7	6.54	0.0196	13.80	-	0.081	0.099
Sm-Ox0.1-6b-5	166.6	6.48	0.0196	12.64	-	0.086	0.096
Sm-Ox0.1-6b-6	190.2	6.57	0.0195	9.13	-	0.086	0.094
Sm-Ox0.1-6b-7	214.5	6.51	0.0197	8.38	-	0.087	0.096
Sm-Ox0.1-6b-8	242.5	6.53	0.0193	8.33	-	0.086	0.100
Sm-Ox0.1-6b-9	288.6	6.52	0.0193	8.42	-	0.089	0.093
Sm-Ox0.1-6b-10	310.8	6.52	0.0195	8.42	-	-	0.097
Sm-Ox0.1-6b-11	334.7	6.48	0.0194	8.62	-	0.091	0.096
Sm-Ox0.1-6b-12	358.5	6.52	0.0195	7.25	-	0.093	0.101
Sm-Ox0.1-6b-13	391.7	6.40	0.0194	7.18	-	0.096	0.097
Sm-Ox0.1-6b-14	456.0	6.41	0.0192	7.28	-	0.094	0.099
Sm-Ox0.1-6b-15	479.3	6.40	0.0194	7.05	-	0.095	0.094
Sm-Ox0.1-6b-16	502.3	6.41	0.0191	7.07	-	0.097	0.106
Sm-Ox0.1-6b-17	526.5	6.47	0.0192	6.85	-	0.097	0.096
Sm-Ox0.1-6b-18	558.0	6.45	0.0192	7.01	-	0.092	0.100
Sm-Ox0.1-6b-19	608.7	6.17	0.0191	5.31	-	0.095	0.096
Sm-Ox0.1-6b-20	648.0	6.36	0.0191	5.47	-	0.092	0.096
Sm-Ox0.1-6b-21	670.5	6.39	0.0193	5.27	-	0.096	0.099
Sm-Ox0.1-6b-22	694.7	6.34	0.0190	4.66	1.80	0.093	0.097
Sm-Ox0.1-6b-23	719.7	6.33	0.0169	5.21	1.90	0.097	0.095
Sm-Ox0.1-6b-24	746.3	6.32	0.0192	4.81	1.99	0.093	0.097
Sm-Ox0.1-6b-25	790.7	6.34	0.0186	4.75	2.06	0.093	0.094

Sm-Ox0.1-6.5a		**Temperature 25ºC**				**Initial pH 6.45**	
Mass 0.0912 g		**Solution 10 mM KNO_3 + 0.1 mM Oxalate**					
Run	Time (h)	pH	Flow (mL min^{-1})	Si (µM)	Al (µM)	Oxalate output (mM)	Oxalate input (mM)
Sm-Ox0.1-6.5a-1	15.1	6.41	0.0225	64.61	-	0.092	0.101
Sm-Ox0.1-6.5a-2	39.0	6.45	0.0232	29.60	-	0.090	-
Sm-Ox0.1-6.5a-3	62.9	6.45	0.0231	20.91	-	0.093	0.104
Sm-Ox0.1-6.5a-4	87.0	6.27	0.0228	15.03	-	0.093	-
Sm-Ox0.1-6.5a-5	119.8	6.46	0.0229	14.95	-	0.093	0.102
Sm-Ox0.1-6.5a-6	158.7	6.44	0.0226	10.53	-	0.088	-
Sm-Ox0.1-6.5a-7	183.2	6.22	0.0225	11.45	-	0.097	-
Sm-Ox0.1-6.5a-8	206.9	6.40	0.0228	10.89	-	0.100	0.094
Sm-Ox0.1-6.5a-9	231.0	6.33	0.0224	8.04	-	0.100	-
Sm-Ox0.1-6.5a-10	265.0	6.27	0.0225	7.43	-	0.101	-
Sm-Ox0.1-6.5a-11	327.0	6.32	0.0221	5.27	-	0.103	0.102
Sm-Ox0.1-6.5a-12	351.2	6.38	0.0223	5.35	-	0.096	-
Sm-Ox0.1-6.5a-13	375.0	6.30	0.0222	5.43	-	0.099	-
Sm-Ox0.1-6.5a-14	449.5	6.26	0.0225	4.97	-	0.104	0.095
Sm-Ox0.1-6.5a-15	495.0	6.35	0.0220	4.66	-	0.092	0.101

Run	Time (h)	pH	Flow (mL min^{-1})	Si (µM)	Al (µM)	Oxalate output (mM)	Oxalate input (mM)
Sm-Ox0.1-6.5a-16	519.1	6.39	0.0223	6.80	-	0.101	-
Sm-Ox0.1-6.5a-17	544.2	6.44	0.0224	4.90	-	0.097	0.099
Sm-Ox0.1-6.5a-18	567.0	6.44	0.0280	4.51	-	0.093	0.100
Sm-Ox0.1-6.5a-19	595.3	6.36	0.0224	4.43	-	0.098	0.098
Sm-Ox0.1-6.5a-20	662.8	6.31	0.0231	3.62	-	0.099	-
Sm-Ox0.1-6.5a-21	687.1	6.23	0.0221	4.82	-	0.095	0.100
Sm-Ox0.1-6.5a-22	711.0	6.37	0.0221	3.73	-	0.099	0.099
Sm-Ox0.1-6.5a-23	735.3	6.47	0.0209	3.91	-	0.106	0.100
Sm-Ox0.1-6.5a-24	764.0	6.45	0.0221	3.62	-	0.098	0.098
Sm-Ox0.1-6.5a-25	831.2	6.45	0.0235	2.84	1.86	0.096	0.096
Sm-Ox0.1-6.5a-26	854.9	6.32	0.0221	2.56	1.83	0.103	0.096
Sm-Ox0.1-6.5a-27	879.1	6.41	0.0219	2.91	2.14	-	0.098
Sm-Ox0.1-6.5a-28	903.0	6.51	0.0224	2.45	-	0.080	0.097
Sm-Ox0.1-6.5a-29	927.2	6.42	0.0222	2.75	2.21	0.074	0.100

Sm-Ox0.1-6.5b	**Temperature 25ºC**	**Initial pH 6.27**
Mass 0.0900 g	**Solution 10 mM KNO_3 + 0.1 mM Oxalate**	

Run	Time (h)	pH	Flow (mL min^{-1})	Si (µM)	Al (µM)	Oxalate output (mM)	Oxalate input (mM)
Sm-Ox0.1-6.5b-1	20.0	7.28	0.0456	7.16	-	0.124	-
Sm-Ox0.1-6.5b-2	44.2	7.38	0.0233	24.85	-	0.094	0.096
Sm-Ox0.1-6.5b-3	68.2	6.86	0.0222	18.29	-	-	-
Sm-Ox0.1-6.5b-4	92.3	6.27	0.0218	15.05	-	0.091	0.092
Sm-Ox0.1-6.5b-5	120.3	6.31	0.0218	10.73	-	-	-
Sm-Ox0.1-6.5b-6	164.7	5.66	0.0209	10.57	-	0.093	0.093
Sm-Ox0.1-6.5b-7	188.3	6.58	0.0216	7.39	-	0.090	-
Sm-Ox0.1-6.5b-8	212.3	6.71	0.0215	6.69	-	-	0.091
Sm-Ox0.1-6.5b-9	236.3	6.73	0.0216	5.48	-	0.091	-
Sm-Ox0.1-6.5b-10	260.2	6.57	0.0216	4.80	-	0.090	0.096
Sm-Ox0.1-6.5b-11	284.6	6.51	0.0216	4.19	-	-	-
Sm-Ox0.1-6.5b-12	332.4	6.66	0.0215	4.00	-	0.086	0.093
Sm-Ox0.1-6.5b-13	356.5	6.68	0.0216	3.49	-	-	-
Sm-Ox0.1-6.5b-14	380.3	6.83	0.0211	3.62	-	0.088	0.096
Sm-Ox0.1-6.5b-15	404.4	6.53	0.0211	3.08	-	-	-
Sm-Ox0.1-6.5b-16	434.3	6.52	0.0212	2.83	-	0.086	0.096
Sm-Ox0.1-6.5b-17	500.8	6.70	0.0005	2.67	-	0.079	-
Sm-Ox0.1-6.5b-18	524.5	6.77	0.0215	2.85	-	0.091	0.100
Sm-Ox0.1-6.5b-19	548.3	6.68	0.0217	2.46	-	-	-
Sm-Ox0.1-6.5b-20	601.2	6.72	0.0068	3.55	-	0.093	0.098
Sm-Ox0.1-6.5b-21	668.3	6.71	0.0076	3.95	-	-	-
Sm-Ox0.1-6.5b-22	692.3	6.73	0.0193	3.55	-	0.091	0.100
Sm-Ox0.1-6.5b-23	716.3	6.44	0.0219	3.69	-	-	0.097
Sm-Ox0.1-6.5b-24	740.5	6.55	0.0218	4.23	-	0.102	-
Sm-Ox0.1-6.5b-25	768.5	6.56	0.0218	3.40	-	-	0.097
Sm-Ox0.1-6.5b-26	836.5	6.64	0.0240	2.81	-	0.100	0.103
Sm-Ox0.1-6.5b-27	860.5	6.55	0.0217	2.26	-	-	-
Sm-Ox0.1-6.5b-28	884.6	6.69	0.0222	2.22	1.77	0.099	0.096
Sm-Ox0.1-6.5b-29	909.0	6.29	0.0220	1.94	1.85	-	-

Run	Time (h)	pH	Flow (mL min^{-1})	Si (µM)	Al (µM)	Oxalate output (mM)	Oxalate input (mM)
Sm-Ox0.1-6.5b-30	936.67	6.32	0.0220	2.15	1.68	0.099	0.100
Sm-Ox0.1-6.5b-31	1004.50	6.35	0.0219	2.02	1.64	-	-

Sm-Ox0.1-7a	**Temperature 25ºC**	**Initial pH 6.79**
Mass 0.0908 g	**Solution 0.06 mM KOH + 10 mM KNO_3 + 0.1 mM Oxalate**	

Run	Time (h)	pH	Flow (mL min^{-1})	Si (µM)	Al (µM)	Oxalate output (mM)	Oxalate input (mM)
Sm-Ox0.1-7a-1	20.3	6.79	0.0280	24.31	-	0.093	-
Sm-Ox0.1-7a-2	44.3	6.85	0.0222	26.02	-	0.092	-
Sm-Ox0.1-7a-3	78.3	6.68	0.0224	10.19	-	0.094	-
Sm-Ox0.1-7a-4	140.3	7.02	0.0229	8.95	-	0.091	0.101
Sm-Ox0.1-7a-5	164.6	6.75	0.0222	6.51	-	0.097	0.099
Sm-Ox0.1-7a-6	188.3	6.93	0.0222	5.21	-	0.095	0.099
Sm-Ox0.1-7a-7	262.8	6.96	0.0220	5.35	-	0.094	0.099
Sm-Ox0.1-7a-8	308.3	6.91	0.0217	4.53	-	0.101	0.102
Sm-Ox0.1-7a-9	332.4	6.92	0.0218	4.06	-	0.095	0.095
Sm-Ox0.1-7a-10	357.6	6.89	0.0222	2.94	-	-	0.101
Sm-Ox0.1-7a-11	380.3	6.90	0.0218	4.16	-	0.098	0.099
Sm-Ox0.1-7a-12	408.7	6.75	0.0220	3.91	-	0.092	0.099
Sm-Ox0.1-7a-13	476.2	6.82	0.0217	2.99	-	0.098	-
Sm-Ox0.1-7a-14	500.4	6.81	0.0219	2.29	-	0.099	0.100
Sm-Ox0.1-7a-15	524.4	6.81	0.0218	3.62	-	0.098	0.097
Sm-Ox0.1-7a-16	548.7	6.83	0.0220	2.81	-	0.099	0.098
Sm-Ox0.1-7a-17	577.3	6.91	0.0218	3.65	-	0.100	0.099
Sm-Ox0.1-7a-18	644.5	6.97	0.0215	3.10	-	0.096	0.101
Sm-Ox0.1-7a-19	668.3	6.73	0.0218	2.91	-	0.100	0.099
Sm-Ox0.1-7a-20	692.4	6.87	0.0214	3.73	-	0.097	0.100
Sm-Ox0.1-7a-21	716.3	6.72	0.0215	3.18	-	0.114	0.100
Sm-Ox0.1-7a-22	740.5	6.84	0.0219	2.96	1.17	0.096	0.101
Sm-Ox0.1-7a-23	767.0	6.70	0.0216	2.77	1.22	0.097	-
Sm-Ox0.1-7a-24	812.4	6.81	0.0214	2.75	1.15	0.095	0.102
Sm-Ox0.1-7a-25	836.3	6.88	0.0217	2.93	1.25	0.093	0.095

Sm-Ox0.1-7b	**Temperature 25ºC**	**Initial pH 6.85**
Mass 0.0918 g	**Solution 0.06 mM KOH + 10 mM KNO_3 + 0.1 mM Oxalate**	

Run	Time (h)	pH	Flow (mL min^{-1})	Si (µM)	Al (µM)	Oxalate output (mM)	Oxalate input (mM)
Sm-Ox0.1-7b-1	68.0	6.85	0.0189	15.91	-	0.096	0.101
Sm-Ox0.1-7b-2	92.3	6.83	0.0116	12.86	-	0.095	0.099
Sm-Ox0.1-7b-3	116.0	6.68	0.0190	10.51	-	0.096	0.099
Sm-Ox0.1-7b-4	190.5	6.64	0.0191	8.14	-	0.097	0.099
Sm-Ox0.1-7b-5	236.0	6.72	0.0188	5.01	-	0.096	0.102
Sm-Ox0.1-7b-6	260.1	6.76	0.0189	5.93	-	0.100	0.095
Sm-Ox0.1-7b-7	285.2	6.84	0.0191	5.06	-	0.099	0.101
Sm-Ox0.1-7b-8	308.0	6.80	0.0188	5.73	-	0.096	0.099

Run	Time (h)	pH	Flow (mL min^{-1})	Si (µM)	Al (µM)	Oxalate output (mM)	Oxalate input (mM)
Sm-Ox0.1-7b-9	336.3	6.74	0.0191	4.96	-	0.099	0.099
Sm-Ox0.1-7b-10	403.8	6.77	0.0190	5.00	-	0.099	-
Sm-Ox0.1-7b-11	428.1	6.71	0.0189	3.02	-	0.095	0.100
Sm-Ox0.1-7b-12	452.1	6.81	0.0189	4.17	-	0.098	0.097
Sm-Ox0.1-7b-13	476.3	6.74	0.0191	2.74	-	0.099	0.098
Sm-Ox0.1-7b-14	505.0	6.72	0.0190	1.94	-	0.097	0.099
Sm-Ox0.1-7b-15	572.2	6.79	0.0189	2.71	-	0.099	0.101
Sm-Ox0.1-7b-16	595.9	6.73	0.0189	2.47	-	0.100	0.099
Sm-Ox0.1-7b-17	620.1	6.68	0.0187	3.85	-	0.094	0.100
Sm-Ox0.1-7b-18	644.0	6.80	0.0189	4.52	-	0.094	0.100
Sm-Ox0.1-7b-19	668.2	6.81	0.0190	3.70	-	0.082	0.101
Sm-Ox0.1-7b-20	694.7	6.70	0.0187	4.35	-	0.097	-
Sm-Ox0.1-7b-21	740.1	6.82	0.0185	3.62	-	0.099	0.102
Sm-Ox0.1-7b-22	764.0	6.78	0.0187	4.19	-	0.097	0.095
Sm-Ox0.1-7b-23	788.0	6.69	0.0187	2.38	-	0.092	0.099
Sm-Ox0.1-7b-24	812.2	6.70	0.0188	3.64	-	0.093	0.099
Sm-Ox0.1-7b-25	836.3	6.80	0.0188	3.04	1.43	0.093	0.100
Sm-Ox0.1-7b-26	862.0	6.75	0.0195	2.88	1.09	0.087	0.099
Sm-Ox0.1-7b-27	908.2	6.70	0.0190	3.41	-	0.093	0.100
Sm-Ox0.1-7b-28	932.3	6.68	0.0187	2.61	1.04	0.092	0.093
Sm-Ox0.1-7b-29	956.3	6.68	0.0188	3.00	0.97	0.093	0.103

Sm-Ox0.1-8	**Temperature 25ºC**	**Initial pH 7.60**
Mass 0.0910 g	**Solution 0.38 mM KOH + 10 mM KNO_3 + 0.1 mM Oxalate**	

Run	Time (h)	pH	Flow (mL min^{-1})	Si (µM)	Al (µM)	Oxalate output (mM)	Oxalate input (mM)
Sm-Ox0.1-8-1	15.4	7.30	0.0625	29.84	-	0.101	0.103
Sm-Ox0.1-8-2	39.2	7.60	0.0281	14.57	-	0.097	0.100
Sm-Ox0.1-8-3	113.7	7.49	0.0214	14.70	-	0.080	0.100
Sm-Ox0.1-8-4	159.2	7.70	0.0222	4.68	-	0.081	0.105
Sm-Ox0.1-8-5	183.2	7.76	0.0228	4.46	-	0.071	0.105
Sm-Ox0.1-8-6	208.4	7.75	0.0281	3.79	-	0.064	0.103
Sm-Ox0.1-8-7	231.2	7.68	0.0286	4.41	-	0.050	0.100
Sm-Ox0.1-8-8	259.5	7.48	0.0262	4.02	-	0.053	0.097
Sm-Ox0.1-8-9	327.0	7.76	0.0247	3.91	-	-	-
Sm-Ox0.1-8-10	351.2	7.80	0.0244	5.07	-	0.064	0.099
Sm-Ox0.1-8-11	375.2	7.68	0.0238	4.46	-	0.060	0.103
Sm-Ox0.1-8-12	399.5	7.61	0.0236	4.29	-	0.060	0.101
Sm-Ox0.1-8-13	428.2	7.58	0.0228	3.78	-	0.059	0.102
Sm-Ox0.1-8-14	495.3	7.73	0.0221	3.09	-	0.055	0.100
Sm-Ox0.1-8-15	519.1	4.74	0.0217	2.76	-	0.055	0.101
Sm-Ox0.1-8-16	543.2	7.78	0.0210	3.13	-	0.068	0.103
Sm-Ox0.1-8-17	567.2	7.80	0.0213	3.73	-	0.048	0.100
Sm-Ox0.1-8-18	591.3	7.84	0.0211	2.84	-	0.045	-
Sm-Ox0.1-8-19	617.8	7.85	0.0206	2.32	-	0.050	0.098
Sm-Ox0.1-8-20	663.2	7.92	0.0204	2.56	-	0.047	0.101
Sm-Ox0.1-8-21	687.2	7.83	0.0207	2.63	1.12	0.043	0.097
Sm-Ox0.1-8-22	711.2	7.82	0.0205	2.75	1.10	0.043	0.102

Run	Time (h)	pH	Flow (mL min^{-1})	Si (µM)	Al (µM)	Oxalate output (mM)	Oxalate input (mM)
Sm-Ox0.1-8-23	735.3	7.75	0.0205	2.57	1.00	0.030	0.097
Sm-Ox0.1-8-24	759.5	7.82	0.0206	2.48	1.12	0.041	0.099
Sm-Ox0.1-8-25	785.2	7.80	0.0226	2.54	-	-	-

Sm-Ox1-3a	**Temperature 25ºC**					**Initial pH 3.09**	
Mass 0.0900 g	**Solution 0.63 mM HNO_3 + 10 mM KNO_3 + 1 mM Oxalate**						
Run	Time (h)	pH	Flow (mL min^{-1})	Si (µM)	Al (µM)	Oxalate output (mM)	Oxalate input (mM)
Sm-Ox1-3a-1	17.8	3.77	0.0518	-	-	0.922	0.957
Sm-Ox1-3a-2	41.9	3.21	0.0221	69.35	-	-	-
Sm-Ox1-3a-3	112.5	3.09	0.0210	38.67	-	0.868	0.956
Sm-Ox1-3a-4	137.2	3.07	0.0214	28.27	-	0.947	0.967
Sm-Ox1-3a-5	161.3	3.06	0.0211	21.20	-	-	-
Sm-Ox1-3a-6	185.2	3.08	0.0220	26.81	-	-	0.929
Sm-Ox1-3a-7	213.2	3.10	0.0211	24.23	-	0.943	0.959
Sm-Ox1-3a-8	281.3	3.04	0.0205	23.51	-	0.985	-
Sm-Ox1-3a-9	305.2	3.05	0.0211	19.91	-	0.916	0.931
Sm-Ox1-3a-10	329.2	3.06	0.0209	18.85	-	-	-
Sm-Ox1-3a-11	353.2	3.08	0.0211	17.57	-	0.898	0.953
Sm-Ox1-3a-12	381.0	3.07	0.0210	17.52	-	-	-
Sm-Ox1-3a-13	429.0	3.13	0.0206	15.98	-	0.901	0.886
Sm-Ox1-3a-14	473.5	6.75	0.0206	15.02	-	-	-
Sm-Ox1-3a-15	497.2	3.04	0.0209	14.21	-	0.916	-
Sm-Ox1-3a-16	521.1	3.05	0.0210	14.55	-	-	0.912
Sm-Ox1-3a-17	545.2	3.06	0.0210	14.28	-	-	-
Sm-Ox1-3a-18	573.2	3.15	0.0210	11.91	-	0.843	0.919
Sm-Ox1-3a-19	617.0	3.14	0.0204	13.96	-	-	-
Sm-Ox1-3a-20	641.0	3.07	0.0208	12.33	-	0.875	0.921
Sm-Ox1-3a-21	665.2	3.06	0.0208	12.17	-	0.837	-
Sm-Ox1-3a-22	689.3	3.07	0.0208	12.51	-	-	1.017
Sm-Ox1-3a-23	713.3	3.07	0.0208	12.28	-	0.854	-
Sm-Ox1-3a-24	741.3	3.08	0.0209	11.98	-	-	0.935
Sm-Ox1-3a-25	785.7	3.07	0.0207	11.61	-	0.941	-
Sm-Ox1-3a-26	809.3	3.07	0.0208	11.67	-	-	0.900
Sm-Ox1-3a-27	833.3	3.07	0.0209	10.92	-	0.910	-
Sm-Ox1-3a-28	857.3	3.06	0.0209	10.31	-	-	0.870
Sm-Ox1-3a-29	881.2	3.05	0.0209	11.38	-	0.883	-
Sm-Ox1-3a-30	905.6	3.12	0.0208	10.64	-	-	0.891
Sm-Ox1-3a-31	953.4	3.09	0.0203	10.74	6.03	0.966	-
Sm-Ox1-3a-32	977.5	3.06	0.0209	9.99	6.24	-	-
Sm-Ox1-3a-33	1001.3	3.07	0.0208	10.34	6.50	0.897	0.911
Sm-Ox1-3a-34	1025.4	3.06	0.0208	10.41	6.01	0.942	0.901
Sm-Ox1-3a-35	1051.2	3.06	0.0206	10.01	-	0.945	0.925

Sm-Ox1-3b		**Temperature 25ºC**				**Initial pH 3.08**	
Mass 0.0912 g		**Solution 0.63 mM HNO_3 + 10 mM KNO_3 + 1 mM Oxalate**					
Run	Time (h)	pH	Flow (mL min^{-1})	Si (µM)	Al (µM)	Oxalate output (mM)	Oxalate input (mM)
Sm-Ox1-3b-1	20.8	3.21	0.0217	76.64	-	0.945	0.957
Sm-Ox1-3b-2	91.3	0.00	0.0222	30.23	-	0.917	-
Sm-Ox1-3b-3	116.0	3.08	0.0213	24.76	-	1.004	0.956
Sm-Ox1-3b-4	140.1	3.06	0.0211	23.94	-	-	0.967
Sm-Ox1-3b-5	164.0	3.07	0.0213	23.94	-	0.990	-
Sm-Ox1-3b-6	192.0	3.10	0.0213	27.93	-	-	0.929
Sm-Ox1-3b-7	260.1	3.03	0.0209	27.82	-	0.932	0.959
Sm-Ox1-3b-8	284.1	3.04	0.0210	23.60	-	0.936	-
Sm-Ox1-3b-9	308.1	3.05	0.0208	23.56	-	0.913	0.931
Sm-Ox1-3b-10	332.1	3.05	0.0209	19.64	-	-	-
Sm-Ox1-3b-11	359.8	3.06	0.0212	19.46	-	0.931	0.953
Sm-Ox1-3b-12	407.8	3.16	0.0224	16.40	-	-	-
Sm-Ox1-3b-13	452.3	3.05	0.0210	17.06	-	0.931	0.886
Sm-Ox1-3b-14	476.0	3.03	0.0210	17.10	-	-	-
Sm-Ox1-3b-15	499.9	3.03	0.0211	15.87	-	0.899	-
Sm-Ox1-3b-16	524.0	3.07	0.0223	15.44	-	-	0.912
Sm-Ox1-3b-17	552.0	3.14	0.0211	15.43	-	-	-
Sm-Ox1-3b-18	595.8	3.06	0.0210	13.95	-	0.890	0.819
Sm-Ox1-3b-19	619.8	3.08	0.0217	14.92	-	-	-
Sm-Ox1-3b-20	644.0	3.05	0.0210	15.37	-	0.893	0.921
Sm-Ox1-3b-21	668.2	3.05	0.0209	14.03	-	0.947	-
Sm-Ox1-3b-22	692.2	3.07	0.0210	13.31	-	-	1.017
Sm-Ox1-3b-23	720.2	3.06	0.0211	13.59	-	0.924	-
Sm-Ox1-3b-24	764.5	3.05	0.0209	13.16	-	-	0.935
Sm-Ox1-3b-25	788.2	3.06	0.0209	13.01	-	0.909	-
Sm-Ox1-3b-26	812.1	3.06	0.0209	12.53	-	-	1.000
Sm-Ox1-3b-27	836.2	3.06	0.0210	11.64	4.01	0.910	-
Sm-Ox1-3b-28	860.0	3.04	0.0210	11.34	3.92	-	0.957
Sm-Ox1-3b-29	884.4	3.11	0.0208	12.45	4.14	0.897	-
Sm-Ox1-3b-30	932.3	3.06	0.0209	11.92	3.87	-	1.003
Sm-Ox1-3b-31	956.3	3.05	0.0209	12.07	3.98	0.915	-

Sm-Ox1-4a		**Temperature 25ºC**			**Initial pH 4.07**	
Mass 0.0934 g		**Solution 0.13 mM HNO_3 + 10 mM KNO_3 + 1 mM Oxalate**				
Run	Time (h)	pH	Flow (mL min^{-1})	Si (µM)	Oxalate output (mM)	Oxalate input (mM)
Sm-Ox1-4a-1	24.9	4.49	0.0289	54.21	0.993	0.930
Sm-Ox1-4a-2	72.9	4.24	0.0236	26.63	-	0.909
Sm-Ox1-4a-3	117.4	4.07	0.0233	26.46	0.998	-
Sm-Ox1-4a-4	141.1	4.06	0.0234	17.05	-	-
Sm-Ox1-4a-5	165.0	4.07	0.0236	15.35	1.056	0.912
Sm-Ox1-4a-6	189.1	4.07	0.0235	14.03	0.926	0.785
Sm-Ox1-4a-7	217.1	4.12	0.0236	13.01	0.893	0.926
Sm-Ox1-4a-8	260.9	4.07	0.0232	11.70	0.948	-
Sm-Ox1-4a-9	284.9	4.08	0.0234	10.90	0.842	0.911
Sm-Ox1-4a-10	309.1	4.06	0.0234	10.72	-	-

Run	Time (h)	pH	Flow (mL min^{-1})	Si (µM)	Oxalate output (mM)	Oxalate input (mM)
Sm-Ox1-4a-11	309.1	4.09	0.0233	10.48	0.824	0.897
Sm-Ox1-4a-12	333.3	4.07	0.0236	12.04	-	0.915
Sm-Ox1-4a-13	357.3	4.05	0.0234	9.10	0.935	-
Sm-Ox1-4a-14	385.3	4.04	0.0232	8.85	-	0.930
Sm-Ox1-4a-15	429.6	4.08	0.0233	8.76	0.910	0.902
Sm-Ox1-4a-16	453.3	4.08	0.0234	8.10	-	-
Sm-Ox1-4a-17	477.2	4.06	0.0234	7.97	0.905	0.909
Sm-Ox1-4a-18	501.3	4.05	0.0234	7.80	-	-
Sm-Ox1-4a-19	549.5	4.11	0.0234	6.48	0.891	0.913
Sm-Ox1-4a-20	597.3	4.05	0.0234	6.28	-	-
Sm-Ox1-4a-21	621.4	4.07	0.0234	5.82	0.822	0.920
Sm-Ox1-4a-22	645.3	4.08	0.0227	5.81	-	-
Sm-Ox1-4a-23	669.3	4.07	0.0234	5.45	0.814	0.903
Sm-Ox1-4a-24	699.2	4.08	0.0234	5.30	0.851	-
Sm-Ox1-4a-25	765.8	4.05	0.0231	5.93	0.731	0.900
Sm-Ox1-4a-26	789.4	4.02	0.0236	5.60	-	-
Sm-Ox1-4a-27	813.2	4.07	0.0236	5.54	0.903	0.910
Sm-Ox1-4a-28	866.1	4.08	0.0229	4.99	-	-
Sm-Ox1-4a-29	933.3	4.05	0.0231	4.88	0.899	0.912
Sm-Ox1-4a-30	957.2	4.05	0.0234	4.78	-	-
Sm-Ox1-4a-31	981.2	4.01	0.0235	4.63	0.900	0.905
Sm-Ox1-4a-32	1005.4	4.01	0.0234	4.42	-	-

Sm-Ox1-4b	**Temperature 25ºC**	**Initial pH 4.07**
Mass 0.0909 g	**Solution 0.13 mM HNO_3 + 10 mM KNO_3 + 1 mM Oxalate**	

Run	Time (h)	pH	Flow (mL min^{-1})	Si (µM)	Al (µM)	Oxalate output (mM)	Oxalate input (mM)
Sm-Ox1-4b-1	18.8	4.75	0.0222	79.94	-	0.884	0.933
Sm-Ox1-4b-2	42.9	4.28	0.0210	54.27	-	-	-
Sm-Ox1-4b-3	113.5	4.13	0.0210	28.48	-	0.937	0.950
Sm-Ox1-4b-4	138.2	4.07	0.0210	21.18	-	0.944	0.947
Sm-Ox1-4b-5	162.2	4.06	0.0208	18.89	-	-	0.932
Sm-Ox1-4b-6	186.2	4.08	0.0209	17.36	-	-	-
Sm-Ox1-4b-7	214.2	4.07	0.0209	14.95	-	0.942	0.921
Sm-Ox1-4b-8	282.2	4.05	0.0206	13.59	-	0.972	0.940
Sm-Ox1-4b-9	306.2	4.06	0.0206	13.16	-	0.901	-
Sm-Ox1-4b-10	330.2	4.06	0.0205	13.16	-	-	-
Sm-Ox1-4b-11	354.2	4.08	0.0207	12.44	-	0.959	0.921
Sm-Ox1-4b-12	382.0	4.05	0.0204	11.35	-	-	-
Sm-Ox1-4b-13	430.0	4.08	0.0205	10.07	-	0.963	0.930
Sm-Ox1-4b-14	474.5	4.02	0.0205	10.08	-	-	0.909
Sm-Ox1-4b-15	498.2	4.04	0.0203	9.74	-	-	-
Sm-Ox1-4b-16	522.1	4.05	0.0198	9.36	-	0.962	0.912
Sm-Ox1-4b-17	546.2	4.04	0.0203	9.93	-	0.928	0.885
Sm-Ox1-4b-18	574.2	4.09	0.0204	7.90	-	0.922	0.926
Sm-Ox1-4b-19	618.0	4.05	0.0202	5.50	-	0.813	-
Sm-Ox1-4b-20	642.0	4.04	0.0203	5.51	-	0.923	0.911
Sm-Ox1-4b-21	666.2	4.04	0.0203	4.99	-	-	-
Sm-Ox1-4b-22	690.3	4.04	0.0202	5.00	-	0.919	0.897

Run	Time (h)	pH	Flow (mL min^{-1})	Si (µM)	Al (µM)	Oxalate output (mM)	Oxalate input (mM)
Sm-Ox1-4b-23	714.3	4.05	0.0204	5.40	-	-	-
Sm-Ox1-4b-24	742.3	4.05	0.0203	4.73	-	0.916	0.915
Sm-Ox1-4b-25	786.7	4.03	0.0202	4.79	-	-	-
Sm-Ox1-4b-26	810.3	4.05	0.0203	4.70	-	0.910	0.930
Sm-Ox1-4b-27	834.2	4.05	0.0203	4.41	-	-	0.902
Sm-Ox1-4b-28	858.3	4.05	0.0202	4.67	-	0.906	-
Sm-Ox1-4b-29	882.2	4.03	0.0203	4.27	5.22	-	0.909
Sm-Ox1-4b-30	906.6	4.09	0.0203	4.31	5.49	0.932	-
Sm-Ox1-4b-31	954.4	4.04	0.0202	4.60	5.49	-	0.910
Sm-Ox1-4b-32	978.5	4.05	0.0201	4.13	5.60	0.915	0.915

Sm-Ox1-5a	**Temperature 25ºC**					**Initial pH 5.29**	
Mass 0.0905 g	**Solution 0.10 mM HNO_3 + 10 mM KNO_3 + 1 mM Oxalate**						
Run	Time (h)	pH	Flow (mL min^{-1})	Si (µM)	Al (µM)	Oxalate output (mM)	Oxalate input (mM)
Sm-Ox1-5a-1	25.3	6.24	0.0253	51.55	-	0.948	0.914
Sm-Ox1-5a-2	45.1	5.80	0.0244	36.33	-	-	0.924
Sm-Ox1-5a-3	69.2	5.59	0.0233	26.95	-	0.974	-
Sm-Ox1-5a-4	139.8	5.29	0.0233	18.71	-	0.986	0.930
Sm-Ox1-5a-5	164.5	5.14	0.0235	14.44	-	0.944	0.906
Sm-Ox1-5a-6	188.6	5.15	0.0233	12.65	-	0.913	-
Sm-Ox1-5a-7	212.5	5.14	0.0234	11.71	-	-	-
Sm-Ox1-5a-8	240.5	5.14	0.0231	10.61	-	0.973	0.890
Sm-Ox1-5a-9	308.6	5.15	0.0229	9.61	-	0.931	0.901
Sm-Ox1-5a-10	332.5	5.16	0.0233	8.93	-	0.963	0.910
Sm-Ox1-5a-11	356.6	5.12	0.0232	8.80	-	0.971	-
Sm-Ox1-5a-12	380.6	5.14	0.0230	7.96	-	-	0.920
Sm-Ox1-5a-13	408.3	5.12	0.0230	7.55	-	0.935	-
Sm-Ox1-5a-14	456.3	5.13	0.0230	7.30	-	0.950	0.915
Sm-Ox1-5a-15	500.8	5.13	0.0228	6.95	-	0.981	0.992
Sm-Ox1-5a-16	524.5	5.10	0.0231	6.31	-	-	-
Sm-Ox1-5a-17	548.4	5.09	0.0231	5.71	-	0.869	0.915
Sm-Ox1-5a-18	572.5	5.12	0.0229	5.78	-	0.864	0.921
Sm-Ox1-5a-19	600.5	5.13	0.0230	5.72	-	0.843	0.870
Sm-Ox1-5a-20	644.3	5.10	0.0228	6.33	-	0.900	0.858
Sm-Ox1-5a-21	668.3	5.11	0.0230	5.63	-	0.823	-
Sm-Ox1-5a-22	692.5	5.20	0.0228	5.10	-	-	0.893
Sm-Ox1-5a-23	716.5	5.14	0.0230	6.19	-	0.923	-
Sm-Ox1-5a-24	740.7	5.17	0.0229	4.90	-	-	0.911
Sm-Ox1-5a-25	768.7	5.10	0.0229	4.49	-	0.892	-
Sm-Ox1-5a-26	813.0	5.11	0.0228	4.87	-	-	0.960
Sm-Ox1-5a-27	836.7	5.19	0.0227	4.93	-	0.902	-
Sm-Ox1-5a-28	860.7	5.22	0.0225	4.49	-	-	0.954
Sm-Ox1-5a-29	884.7	5.17	0.0230	4.21	1.43	0.906	-
Sm-Ox1-5a-30	908.5	5.12	0.0229	4.18	1.17	-	0.917
Sm-Ox1-5a-31	932.9	5.20	0.0229	4.03	0.96	0.924	-
Sm-Ox1-5a-32	980.7	5.15	0.0224	4.20	1.13	-	0.919
Sm-Ox1-5a-33	1004.8	5.19	0.0228	3.90	1.03	0.913	0.915

Sm-Ox1-5b		**Temperature 25ºC**					**Initial pH 5.32**
Mass 0.0913 g		**Solution 0.098 mM HNO_3 + 10 mM KNO_3 + 1 mM Oxalate**					
Run	Time (h)	pH	Flow (mL min^{-1})	Si (µM)	Al (µM)	Oxalate output (mM)	Oxalate input (mM)
Sm-Ox1-5b-1	51.0	5.83	0.0234	40.89	-	0.878	0.910
Sm-Ox1-5b-2	118.2	5.60	0.0242	22.58	-	-	-
Sm-Ox1-5b-3	142.1	5.32	0.0233	17.97	-	0.890	0.931
Sm-Ox1-5b-4	166.1	5.28	0.0235	15.77	-	-	-
Sm-Ox1-5b-5	190.3	5.26	0.0234	14.60	-	0.883	0.899
Sm-Ox1-5b-6	218.3	5.24	0.0236	12.56	-	-	-
Sm-Ox1-5b-7	286.3	5.23	0.0234	12.42	-	0.900	0.910
Sm-Ox1-5b-8	310.2	5.19	0.0235	9.42	-	-	-
Sm-Ox1-5b-9	334.4	5.18	0.0236	7.96	-	0.900	0.915
Sm-Ox1-5b-10	358.8	5.19	0.0236	7.00	-	-	-
Sm-Ox1-5b-11	386.5	5.17	0.0235	6.86	-	0.887	0.898
Sm-Ox1-5b-12	454.5	5.25	0.0223	6.53	-	-	-
Sm-Ox1-5b-13	478.3	5.17	0.0235	6.45	-	0.915	0.825
Sm-Ox1-5b-14	502.3	5.20	0.0235	6.49	-	-	-
Sm-Ox1-5b-15	526.3	5.17	0.0234	5.44	-	0.894	0.920
Sm-Ox1-5b-16	552.8	5.17	0.0235	3.62	-	0.923	0.902
Sm-Ox1-5b-17	622.3	5.19	0.0234	3.02	-	-	-
Sm-Ox1-5b-18	649.7	5.06	0.0234	2.17	-	0.881	0.927
Sm-Ox1-5b-19	694.3	5.13	0.0235	3.51	-	0.913	-
Sm-Ox1-5b-20	722.3	5.13	0.0230	3.78	-	0.909	0.901
Sm-Ox1-5b-21	790.4	5.16	0.0231	3.16	-	-	0.906
Sm-Ox1-5b-22	814.3	5.12	0.0239	3.77	-	0.855	0.903
Sm-Ox1-5b-23	838.4	5.12	0.0236	4.00	-	-	-
Sm-Ox1-5b-24	862.3	5.09	0.0234	4.05	-	0.822	0.898
Sm-Ox1-5b-25	886.0	5.07	0.0236	3.82	-	-	-
Sm-Ox1-5b-26	958.2	5.17	0.0235	3.40	5.58	0.911	0.900
Sm-Ox1-5b-27	982.5	5.18	0.0235	3.50	10.95	-	-
Sm-Ox1-5b-28	1006.0	5.19	0.0235	3.31	10.42	0.891	0.904
Sm-Ox1-5b-29	1030.1	5.17	0.0238	3.12	3.98	0.895	0.901
Sm-Ox1-5b-30	1059.2	5.21	0.0235	3.24	10.65	0.898	0.901

Sm-Ox1-5c		**Temperature 25ºC**					**Initial pH 5.32**
Mass 0.0909 g		**Solution 0.098 mM HNO_3 + 10 mM KNO_3 + 1 mM Oxalate**					
Run	Time (h)	pH	Flow (mL min^{-1})	Si (µM)	Al (µM)	Oxalate output (mM)	Oxalate input (mM)
Sm-Ox1-5c-1	20.3	6.04	0.0193	59.54	-	0.90	0.91
Sm-Ox1-5c-2	73.2	5.84	0.0233	28.50	-	-	0.92
Sm-Ox1-5c-3	140.3	5.71	0.0230	16.64	-	0.88	0.93
Sm-Ox1-5c-4	164.3	5.32	0.0233	16.99	-	-	-
Sm-Ox1-5c-5	188.3	5.33	0.0234	13.51	-	0.90	0.90
Sm-Ox1-5c-6	212.5	5.33	0.0233	12.92	-	-	-
Sm-Ox1-5c-7	240.5	5.24	0.0234	11.01	-	0.90	0.91
Sm-Ox1-5c-8	308.5	5.31	0.0230	9.78	-	-	-
Sm-Ox1-5c-9	332.3	5.22	0.0234	7.62	-	0.90	0.92
Sm-Ox1-5c-10	356.6	5.25	0.0234	7.75	-	-	-

Run	Time (h)	pH	Flow (mL min^{-1})	Si (µM)	Al (µM)	Oxalate output (mM)	Oxalate input (mM)
Sm-Ox1-5c-11	381.0	5.25	0.0234	8.36	-	0.91	0.93
Sm-Ox1-5c-12	408.7	5.20	0.0233	7.42	-	-	-
Sm-Ox1-5c-13	476.7	5.27	0.0219	9.44	-	-	0.92
Sm-Ox1-5c-14	500.5	5.27	0.0233	5.10	-	0.89	-
Sm-Ox1-5c-15	524.5	5.26	0.0231	5.45	-	0.90	0.92
Sm-Ox1-5c-16	548.5	5.27	0.0232	4.61	-	0.84	0.90
Sm-Ox1-5c-17	575.0	5.19	0.0231	4.38	-	-	-
Sm-Ox1-5c-18	644.5	5.22	0.0231	4.00	-	0.90	0.92
Sm-Ox1-5c-19	671.8	5.07	0.0228	1.73	-	0.90	-
Sm-Ox1-5c-20	716.5	5.16	0.0229	4.51	-	0.91	0.90
Sm-Ox1-5c-21	744.5	5.16	0.0223	3.64	-	-	0.90
Sm-Ox1-5c-22	812.6	5.16	0.0218	4.52	-	0.92	0.90
Sm-Ox1-5c-23	836.5	5.14	0.0229	3.92	-	-	-
Sm-Ox1-5c-24	860.6	5.12	0.0229	4.20	-	0.87	0.90
Sm-Ox1-5c-25	884.5	5.14	0.0228	3.69	-	-	-
Sm-Ox1-5c-26	908.2	5.14	0.0229	3.71	-	0.85	0.90
Sm-Ox1-5c-27	980.3	5.24	0.0228	3.95	-	-	-
Sm-Ox1-5c-28	1004.7	5.26	0.0227	2.86	23.90	0.91	0.90
Sm-Ox1-5c-29	1028.2	5.22	0.0228	2.97	30.66	-	0.90
Sm-Ox1-5c-30	1052.3	5.20	0.0228	3.04	31.18	0.84	0.90
Sm-Ox1-5c-31	1081.4	5.34	0.0228	2.81	31.33	0.89	0.91
Sm-Ox1-5c-32	1148.3	5.25	0.0231	2.89	25.96	0.89	0.91

Sm-Ox1-6	**Temperature 25ºC**	**Initial pH 5.96**
Mass 0.0912 g	**Solution 0.005 mM HNO_3 + 10 mM KNO_3 + 1 mM Oxalate**	

Run	Time (h)	pH	Flow (mL min^{-1})	Si (µM)	Oxalate output (mM)	Oxalate input (mM)
Sm-Ox1-6-1	21.1	6.03	0.0026	73.59	0.979	1.001
Sm-Ox1-6-2	45.1	6.06	0.0212	40.84	0.929	0.973
Sm-Ox1-6-3	71.6	5.96	0.0238	30.34	-	0.944
Sm-Ox1-6-4	141.1	5.99	0.0237	12.87	0.913	-
Sm-Ox1-6-5	168.4	5.46	0.0129	9.62	0.922	0.908
Sm-Ox1-6-6	213.1	5.51	0.0236	10.29	-	-
Sm-Ox1-6-7	241.1	5.47	0.0229	9.85	0.885	0.896
Sm-Ox1-6-8	309.2	5.56	0.0233	9.88	-	-
Sm-Ox1-6-9	333.1	5.83	0.0235	9.97	0.902	0.898
Sm-Ox1-6-10	357.2	5.88	0.0234	7.00	-	-
Sm-Ox1-6-11	381.1	6.07	0.0235	6.82	0.876	0.886
Sm-Ox1-6-12	404.8	6.02	0.0233	5.94	-	-
Sm-Ox1-6-13	476.9	6.12	0.0233	5.97	0.855	0.875
Sm-Ox1-6-14	501.3	6.16	0.0232	6.33	-	0.901
Sm-Ox1-6-15	524.8	6.08	0.0235	4.91	0.892	0.903
Sm-Ox1-6-16	548.8	6.16	0.0232	4.69	-	-
Sm-Ox1-6-17	578.0	6.23	0.0232	4.51	0.854	0.900
Sm-Ox1-6-18	644.9	6.58	0.0232	4.62	-	-
Sm-Ox1-6-19	692.8	6.69	0.0231	3.68	0.834	0.839
Sm-Ox1-6-20	717.2	6.72	0.0233	3.12	-	-
Sm-Ox1-6-21	743.8	6.60	0.0234	3.36	0.793	0.800
Sm-Ox1-6-22	812.8	5.34	0.0233	3.07	0.790	0.805

Run	Time (h)	pH	Flow (mL min^{-1})	Si (µM)	Oxalate output (mM)	Oxalate input (mM)
Sm-Ox1-6-23	837.3	5.37	0.0232	3.21	0.766	0.813
Sm-Ox1-6-24	861.3	5.41	0.0232	3.23	-	-

Sm-Ox1-7a	**Temperature 25ºC**				**Initial pH 7.05**	
Mass 0.0904 g	**Solution 10 mM KNO_3 + 1 mM Oxalate**					
Run	Time (h)	pH	Flow (mL min^{-1})	Si (µM)	Oxalate output (mM)	Oxalate input (mM)
Sm-Ox1-7a-1	24.3	5.92	0.0378	21.52	-	0.914
Sm-Ox1-7a-2	44.1	5.84	0.0240	34.21	-	-
Sm-Ox1-7a-3	68.3	5.79	0.0228	27.45	-	-
Sm-Ox1-7a-4	138.8	5.96	0.0227	19.01	0.876	0.930
Sm-Ox1-7a-5	163.5	6.20	0.0229	14.75	0.898	0.906
Sm-Ox1-7a-6	187.6	6.45	0.0228	13.31	0.846	-
Sm-Ox1-7a-7	211.5	6.60	0.0229	12.73	-	-
Sm-Ox1-7a-8	239.5	6.70	0.0226	12.04	0.838	0.890
Sm-Ox1-7a-9	307.6	7.05	0.0223	37.92	0.722	-
Sm-Ox1-7a-10	331.5	7.10	0.0227	36.36	0.740	0.910
Sm-Ox1-7a-11	355.6	7.39	0.0226	9.11	-	-
Sm-Ox1-7a-12	379.6	7.17	0.0224	8.42	0.731	0.920
Sm-Ox1-7a-13	407.3	7.42	0.0225	7.43	-	-
Sm-Ox1-7a-14	455.3	7.05	0.0221	6.19	0.800	0.915
Sm-Ox1-7a-15	499.8	7.44	0.0222	5.61	-	0.592
Sm-Ox1-7a-16	523.5	7.47	0.0224	5.18	0.812	-
Sm-Ox1-7a-17	547.4	7.49	0.0225	4.72	0.731	-
Sm-Ox1-7a-18	571.5	7.41	0.0225	4.22	0.697	0.921
Sm-Ox1-7a-19	599.5	7.45	0.0225	4.38	0.722	0.870
Sm-Ox1-7a-20	643.3	7.41	0.0222	4.01	0.784	0.858
Sm-Ox1-7a-21	667.3	7.49	0.0223	3.97	0.744	-
Sm-Ox1-7a-22	691.5	7.28	0.0223	3.44	0.751	0.893
Sm-Ox1-7a-23	715.7	7.36	0.0221	3.28	0.714	-
Sm-Ox1-7a-24	739.7	7.27	0.0224	3.14	-	0.911
Sm-Ox1-7a-25	767.7	7.03	0.0223	2.91	0.855	-
Sm-Ox1-7a-26	812.0	7.10	0.0218	3.24	-	0.960
Sm-Ox1-7a-27	835.7	7.41	0.0221	2.85	0.800	-
Sm-Ox1-7a-28	859.6	7.37	0.0223	3.01	-	0.954
Sm-Ox1-7a-29	883.7	7.24	0.0223	2.61	0.842	0.900
Sm-Ox1-7a-30	907.5	7.15	0.0222	2.54	0.842	0.917
Sm-Ox1-7a-31	931.9	7.39	0.0222	2.53	0.769	0.953
Sm-Ox1-7a-32	979.7	7.24	0.0222	2.44	0.856	0.856

Sm-Ox1-7b		**Temperature 25ºC**				**Initial pH 6.99**
Mass 0.0915 g		**Solution 10 mM KNO_3 + 1 mM Oxalate**				
Run	Time (h)	pH	Flow (mL min^{-1})	Si (µM)	Oxalate output (mM)	Oxalate input (mM)
Sm-Ox1-7b-1	20.5	6.63	0.0229	33.31	0.968	0.993
Sm-Ox1-7b-2	47.0	7.01	0.0224	31.75	0.955	0.988
Sm-Ox1-7b-3	116.5	7.02	0.0223	19.12		0.935
Sm-Ox1-7b-4	143.8	6.99	0.0218	9.53	0.931	0.939
Sm-Ox1-7b-5	188.5	7.30	0.0221	9.95		
Sm-Ox1-7b-6	216.5	6.99	0.0215	10.54	0.925	0.946
Sm-Ox1-7b-7	284.6	6.97	0.0220	8.28		
Sm-Ox1-7b-8	308.5	7.09	0.0221	7.22	0.921	0.922
Sm-Ox1-7b-9	332.6	7.06	0.0222	8.31		
Sm-Ox1-7b-10	356.5	6.99	0.0219	8.24	0.900	0.896
Sm-Ox1-7b-11	380.2	7.00	0.0220	7.84		
Sm-Ox1-7b-12	452.3	7.01	0.0221	5.70	0.904	0.899
Sm-Ox1-7b-13	476.7	6.89	0.0219	5.55		
Sm-Ox1-7b-14	500.2	6.91	0.0219	5.79	0.923	0.865
Sm-Ox1-7b-15	524.3	6.93	0.0221	5.39		
Sm-Ox1-7b-16	553.4	6.89	0.0220	4.55	0.894	0.863
Sm-Ox1-7b-17	620.3	6.97	0.0223	4.55		
Sm-Ox1-7b-18	668.2	7.09	0.0219	4.51	0.854	0.877
Sm-Ox1-7b-19	692.6	6.88	0.0215	4.49		
Sm-Ox1-7b-20	719.3	6.80	0.0221	4.20	0.838	0.893
Sm-Ox1-7b-21	788.3	6.80	0.0221	4.99		
Sm-Ox1-7b-22	812.8	6.81	0.0221	3.95	0.828	0.852
Sm-Ox1-7b-23	836.7	6.75	0.0221	3.87		
Sm-Ox1-7b-24	860.5	6.81	0.0220	3.89	0.871	0.830
Sm-Ox1-7b-25	886.8	6.79	0.0220	3.79	0.846	0.810
Sm-Ox1-7b-26	956.7	6.87	0.0222	4.26		
Sm-Ox1-7b-27	980.6	6.83	0.0221	3.63	0.800	0.893
Sm-Ox1-7b-28	1004.8	6.87	0.0222	3.80		
Sm-Ox1-7b-29	1028.5	6.88	0.0221	3.70	0.843	0.890
Sm-Ox1-7b-30	1053.0	6.79	0.0221	3.82	0.842	0.891

Annexe I

American Mineralogist, Volume 96, pages 768–780, 2011

Effect of lactate, glycine, and citrate on the kinetics of montmorillonite dissolution

M. Elena Ramos,[1,*] Chiara Cappelli,[1] Marisa Rozalén,[1] Saverio Fiore,[2] and F. Javier Huertas[1]

[1]Instituto Andaluz de Ciencias de la Tierra, CSIC-Universidad de Granada, Avda Fuentenueva s/n, 18002 Granada, Spain
[2]IMAA–CNR, L.da S. Loja, 85000 Tito Scalo (PZ), Italy

Abstract

The montmorillonite dissolution in saline solutions that mimic synthetic lung fluids (SLF) was investigated to gain knowledge on the clearance mechanisms of inhaled clay particles. Dissolution rates were measured at pH 4 (macrophages) and 7.5 (interstitial fluids) at 37 °C in flow-through reactors. The effect of organic acids was investigated through the addition of lactate, citrate, and glycine (0.15, 1.5, and 15 mmol/L). Lactate or glycine does not markedly affect the montmorillonite dissolution rates at pH 4, but at pH 7.5 there exists a slight inhibitory effect of lactate on the dissolution, probably due to a reduction in the number of reactive surface sites caused by lactate adsorption. Citrate enhances the dissolution rate by 0.5 order of magnitude at pH 4 and more than 1 order of magnitude at pH 7.5, thus indicating the prevalence of the ligand-promoted over the proton-promoted dissolution mechanism under these experimental conditions. The kinetic data were used to estimate the reduction in size of an inhaled clay particle. At pH 7.5, a particle 500 nm in diameter could be reduced 25% in the presence of citrate, whereas the reduction in saline solution would only be 10% after 10 years.

Ligand adsorption was measured in batch experiments at pH 2–11 and EQ3NR was used to model the capacity of the ligands to form soluble species of Al. Citrate, glycine, and lactate adsorb onto montmorillonite under acidic conditions, up to 23, 26, and 60 μmol/g, respectively. However, only citrate can complex the released aqueous Al at pH 4 and 7.5, which contributes to enhance dissolution rate and prevents precipitation of gibbsite at pH 7.5.

The enhancement of the dissolution rate in acidic citrate solution very likely comes from the formation of surface complexes between the ligand and the edge surface of montmorillonite. In neutral conditions the effect may be also due to the decrease of the activity of Al^{3+} by formation of aqueous Al-citrate complexes.

Keywords: Montmorillonite, dissolution rate, organic ligands, adsorption

Introduction

After decades of research, a substantial and growing understanding of the important role played by geochemical processes on the health effects of biodurable minerals has been gained. Although the precise mechanism to induce disease in an organism has not been fully clarified yet, the initial contact between the organism and the mineral is via the mineral surface in an aqueous medium. The interaction of surface reactive groups (sites with acid-base properties, active sites for cation exchange, surface charge, hydrophilicity or hydrophobicity of the surface, production or adsorption of oxygen-free radicals, etc.) with the biological medium may induce the mineral toxicity (Fubini and Fenoglio 2007). Thus, it is important to see how the surface interaction occurs to understand the pathogenesis of minerals. This understanding requires a mineralogical and geochemical surface characterization. There are very few studies on mineral dissolution in a biologic medium and they are mainly focused on highly toxic asbestos and silica (Scholze and Conradt 1987; Hume and Rimstidt 1992; Werner et al. 1995; Gunter and Wood 2000; Oze and Solt 2010), as well as talc (Jurinski and Rimstidt 2001).

Smectite, kaolin, and illite constitute the main part of the fine and ultrafine fraction in soils and sediments. Therefore, they are the main compounds of suspended dusts formed by mechanical and chemical weathering processes. Human beings are constantly exposed to mineral dust. However, very few studies exist on the toxicity of smectite and clays in general. The World Health Organization indicated the dire need to tackle research on this matter in its report "Environmental Health Criteria on Bentonites and Kaolins" (WHO 2005).

Smectite dissolution has not been investigated using similar physical and chemical conditions to those found in the lung. However, this reaction has been extensively studied under Earth surface conditions for decades (Zysset and Schindler 1996; Bauer and Berger 1998; Cama et al. 2000; Huertas et al. 2001; Amram and Ganor 2005; Metz et al. 2005; Golubev et al. 2006; Rozalén et al. 2008, 2009b). The dissolution reaction is produced in specific active sites on the surface, and is controlled by several factors including temperature, pH, and the presence of organic ligands and inhibitors. Most studies agree that under the same pH conditions the dissolution rate is faster in the presence of organic ligands than that without organic ligand (Zutic and Stumm 1984; Furrer and Stumm 1986; Carroll-Webb and

* E-mail: elenaramos@ugr.es

Walther 1988; Chin and Mills 1991; Wieland and Stumm 1992; Ganor and Lasaga 1994; Oelkers and Schott 1998; Stillings et al. 1998), although the precise mechanisms are still being debated. The dissolution process is a sequence of elementary reactions at the mineral/solution interface, where the ions and molecules dissolved in the solution interact with the surface cations, favoring the bonds breaking on the surface. This process is the result of several mechanisms acting simultaneously: proton-promoted dissolution (pH effect) and ligand-promoted dissolution due to the formation of metal-ligand surface complexes (Zutic and Stumm 1984; Furrer and Stumm 1986; Chin and Mills 1991; Wieland and Stumm 1992; Stillings et al. 1998) or the decrease in the solution saturation with respect to the mineral due to formation of soluble chelates.

This study is focused on the effect of lactate, glycine, and citrate on the rate and mechanism of smectite dissolution under conditions that may be similar to those in the lung. In particular, we investigate the reactions at the montmorillonite/solution interface that contribute to montmorillonite dissolution in synthetic lung fluid (SLF), including surface adsorption of organic ligands (lactate, citrate, and glycine) onto montmorillonite and the modeling of the speciation of released elements in the interstitial solution. Although the experimental conditions do not reproduce exactly the complexity of the human body, they provide a benchmark to evaluate the biological degradation of inhaled clay particles.

MATERIALS AND METHODS

Montmorillonite characterization and pretreatment

The material used in this study was dioctahedral smectite extracted from the La Serrata–Cortijo de Archidona bentonite deposit located at Cabo de Gata (Almeria, SE Spain). For a detailed characterization of the sample and methods see Rozalén et al. (2008). This bentonite is ~92% montmorillonite and the rest consists of accessory minerals (quartz, feldspars, micas, calcite, and amphibole) plus volcanic glass. The experiments were performed on the <4 μm fraction saturated with K^+. The calculated structural formula of the K-smectite (based on a half-unit cell) corresponds to an Fe-rich montmorillonite (Newman and Brown 1987):

$$K_{0.44}(Al_{1.27}Fe^{3+}_{0.22}Mg_{0.56})(Si_{3.95}Al_{0.05})O_{10}(OH)_2$$

The corresponding atomic ratio Al/Si is 0.334. Only 0.38 K^+ ions per half formula unit are exchangeable, which indicates the presence of a small proportion of non-swelling layers.

X-ray diffraction (XRD) patterns recorded on powder specimens as well as on oriented and glycolated specimens showed that the sample is composed of a dioctahedral smectite with ~10–15% non-swelling layers, in agreement with the presence of non-exchangeable potassium determined by chemical analysis. No accessory phases were detected. The specific surface area after degassing the sample for two days at 110 °C under vacuum measured by BET (Brunauer et al. 1938), using 5-point N_2 adsorption isotherms, was 111 $m^2\ g^{-1}$ with an associated uncertainty of 10%. The edge surface area was estimated to be 6.5 $m^2\ g^{-1}$ (Rozalén et al. 2008).

Experimental setting

Dissolution experiments. Dissolution experiments were performed in single-pass, stirred, flow-through cells, which facilitated the measurement of the dissolution rate under fixed saturation state conditions by modifying the flow rate, initial sample mass, and input solution concentrations. The reactors were fully immersed in a thermostatic water-bath held at a constant temperature of 37 ± 1 °C. The flow rate was controlled with a peristaltic pump that injects the input solution into the bottom chamber of the cell (0.02 mL/min) where the solution is homogenized with a magnetic stirrer before reaching the upper chamber. The solid sample is confined within the upper chamber (reaction zone) by using two membrane filters: a 5 μm nylon mesh plus a 1.2 μm Durapore membrane at the bottom and a 0.45 μm Durapore membrane at the top. The total volume of the cell was 46 mL and the solid mass added to each cell was 0.1 g, to yield a solid solution ratio of ~2 g/L.

The composition of the input solutions mimics the fluids found in the human lung (synthetic lung fluids, SLF), the so-called Gamble's solution. They were prepared by using the formulation by Jurinski and Rimstidt (2001) with additional modifications. Saline solutions have the same molar composition, but all the salts were potassium salts to keep montmorillonite saturated in K^+: KCl 112.3 mmol/L, K_2SO_4 0.556 mmol/L, and the appropriate amount of HCl or $KHCO_3$ to adjust to the initial pH. Phosphate salts were avoided, because phosphate interferes in the Si analysis. Sodium azide (NaN_3, 2 ppm) was added as bactericide. Several runs with ligand-free saline solutions were carried out as control and background experiments covering the pH range between 3 and 8, to have the complete dissolution profile under our experimental conditions.

The effects of three different organic ligands, lactate, citrate, and glycine on the dissolution rate were investigated. Lactate and citrate are contained in interstitial fluids. Glycine was used as a proxy for the amino acids and proteins found in these fluids. The concentration of each organic anion in the interstitial fluid is not well documented. However, lactate has been reported to be the most abundant organic acid in the interstitial fluids, having a concentration of 164 ppm, followed by citrate with 23 ppm (Plumlee and Ziegler 2003).

To assess the ligand effect on the dissolution rate the input solutions were prepared by adding glycine, lactate, or citrate in three different concentrations (0.15, 1.5, and 15 mmol/L for each ligand) to the saline solution. The pH was adjusted with HCl or $KHCO_3$ solutions to ~4 or 7.5. No montmorillonite structural cations (Si, Al, Mg, Fe) were added to the input solutions. The compositions of the input solution in every dissolution experiment are reported in Table 1.

In each run, the flow rate and the input pH were held constant until steady-state conditions were achieved. The steady state was assumed to prevail when the Si output concentration remained fairly constant, differing by <6% between consecutive samples (Rozalén et al. 2008). Reaction times were from 1200 to 1800 h depending on the experimental conditions (pH, temperature, and ligand concentration). At steady state, dissolution is expected to proceed under far-from-equilibrium conditions. All the experiments consisted of a single stage; the cell was dismantled after the steady state was achieved.

After sampling every 24 h, the pHs of the output solutions were immediately measured at room temperature by using Crison combination electrodes standardized with pH 4.01 and 7.00 buffer solutions. The reported accuracy was ±0.02 pH units. To evaluate whether any temperature correction between room and experimental temperature was necessary, the pH of input and standard solutions covering a pH range from 4 to 9 was measured both at 20 and 37 °C. The difference in the pH value between both temperatures was less than the accuracy of the measurement, thus no temperature correction was applied. An aliquot of 3 mL was separated for organic ligand analysis. Then the output solutions were acidified to pH 3 with HCl to prevent the precipitation of Al- or Fe-bearing phases during storage for Si and Al analyses.

The Si concentration in the samples was determined by colorimetry by using the molybdate blue method (Grasshoff et al. 1983). Total Al concentration in the solutions was determined by atomic adsorption spectroscopy (AAS), inductively coupled plasma mass spectrometry (ICP-MS), and fluorimetry using lumogallion as a complexing agent at pH 4.86 (Howard et al. 1986). High salt concentration (~8 gL^{-1}) produced a high-matrix effect with AAS and ICP-MS which gives rise to a low reproducibility and a detection limit above the Al concentration in the samples (ppb). The presence of citrate affected the measurement of Al by fluorimetry at its highest concentration (15 mmol/L), since citrate can compete with lumogallion for Al, leading to a negative interference. A correction was carried out by adding the same concentration of ligand to the Al standards. Such an effect was not observed for lactate and glycine.

The concentration of lactate and citrate was measured by ion chromatography using a Metrohm 761 Compact Ion Chromatograph with a Metrosep Organic Acids column. The eluent was prepared with 0.5 mmol/L sulfuric acid/15% acetone. Glycine was analyzed colorimetrically with a UV-visible spectrometer, using the ninhydrin method (Sun et al. 2006). The detection limits are 5 ppb for Si, 0.5 ppb for Al, 0.9 ppm for lactate, 9 ppm for citrate, and 0.7 ppm for glycine. The associated errors were 5% for Si and Al, 3% for lactate and citrate, and 4% for glycine.

Adsorption experiments. Adsorption experiments were performed as a complement to dissolution results to assess whether ligands were adsorbed onto the montmorillonite surface as a function of pH and interpret the dissolution mechanism.

Adsorption experiments of lactate, citrate, and glycine onto montmorillonite were carried out at room temperature. Potassium chloride was added to the solu-

TABLE 1. Experimental conditions and results of flow-through dissolution experiments

Run	Duration (h)	Flow rate (mL/min)	Initial mass (g)	Ligand (mmol/L)	pH in	pH out	C Si,out (µmol/L)	C Al,out (µmol/L)	C Mg,out* (µmol/L)	C Fe,out* (µmol/L)	Al/Si	log R Si (mol g^{-1}s^{-1})	log R Al (mol g^{-1}s^{-1})	ΔR Si %	ΔR Al %
Ligand free															
Sm-SE-3	1334	0.0239	0.1005	–	3.21	3.06	8.09	3.60	*0.89*	*0.11*	0.446	–11.38	–11.26	5.0	5.0
Sm-SE-4	1334	0.0221	0.1013	–	4.24	4.10	3.49	1.30	*1.26*	*1.83*	0.374	–11.79	–11.74	5.1	5.1
Sm-SE-5	1191	0.0226	0.1008	–	5.52	5.19	1.38	0.060	*0.81*	*0.12*	0.043	–12.18	–13.07	5.1	5.1
Sm-SE-6	1191	0.0227	0.0999	–	6.17	5.83	1.37	0.039	*0.81*	*0.12*	0.029	–12.18	–13.24	5.1	5.1
Sm-SE-7	1533	0.0230	0.0990	–	6.91	7.02	1.55	0.131	*0.54*	*1.15*	0.084	–12.12	–12.71	5.1	5.1
Sm-SE-8	1538	0.0229	0.0993	–	7.92	7.58	1.61	0.23	*0.56*	*1.19*	0.141	–12.10	–12.47	5.0	5.0
Lactate															
Sm-SEL0.15-4	914	0.0198	0.0991	0.15	3.90	3.92	6.17	2.32	*2.22*	*3.24*	0.376	–11.58	–11.53	5.0	5.0
Sm-SEL0.15-4b	1676	0.0217	0.0998	0.15	3.95	3.93	3.83	1.54	*1.38*	*2.01*	0.401	–11.75	–11.66	5.0	5.0
Sm-SEL1.5-4	1030	0.0193	0.0994	1.5	4.51	4.52	2.82	1.07	*1.02*	*1.48*	0.379	–11.94	–11.88	5.1	5.1
Sm-SEL1.5-4b	1555	0.0215	0.0999	1.5	3.96	3.94	3.76	1.87	*1.35*	*1.97*	0.424	–11.76	–11.59	5.0	5.0
Sm-SEL15-4	1150	0.0193	0.0998	15	4.39	4.30	4.98	1.74	*1.79*	*2.61*	0.349	–11.69	–11.67	5.1	5.1
Sm-SEL15-4b	979	0.0220	0.1000	15	3.92	3.89	6.68	2.55	*2.40*	*3.51*	0.381	–11.50	–11.44	5.0	5.0
Sm-SEL0.15-7	1440	0.0223	0.0996	0.15	6.98	7.09	0.894	0.103	*0.31*	*0.66*	0.116	–12.37	–12.83	5.1	5.1
Sm-SEL0.15-7b	1744	0.0231	0.1001	0.15	7.05	7.50	1.52	0.12	*0.53*	*1.12*	0.080	–12.14	–12.77	5.2	5.3
Sm-SEL1.5-7	1440	0.0235	0.0997	1.5	7.22	7.28	0.774	0.135	*0.27*	*0.57*	0.179	–12.41	–12.69	5.1	5.1
Sm-SEL1.5-7b	1747	0.0221	0.0997	1.5	7.12	7.46	1.74	0.18	*0.61*	*1.29*	0.102	–12.09	–12.60	5.1	5.1
Sm-SEL15-7	1584	0.0229	0.1000	15	7.20	7.79	1.93	0.22	*0.68*	*1.43*	0.115	–12.03	–12.50	5.1	5.1
Sm-SEL15-7b	1604	0.0220	0.1006	15	7.07	7.46	1.37	0.34	*0.48*	*1.01*	0.248	–12.20	–12.33	5.1	5.1
Citrate															
Sm-SEC0.15-4	1119	0.0231	0.0999	0.15	4.00	3.99	7.44	2.87	*2.68*	*3.91*	0.386	–11.43	–11.37	5.0	5.0
Sm-SEC1.5-4	1119	0.0244	0.0999	1.5	4.14	4.13	8.71	2.98	*3.14*	*4.57*	0.344	–11.34	–11.26	5.0	4.3
Sm-SEC15-4	1168	0.0227	0.1006	15	4.04	4.03	12.09	4.65	*4.35*	*6.35*	0.385	–11.23	–11.17	5.0	5.0
Sm-SEC0.15-5a	1071	0.0217	0.1000	0.15	5.56	6.81	2.66	0.60	*0.93*	*1.97*	0.222	–11.91	–12.08	5.0	5.0
Sm-SEC0.15-5b	1197	0.0204	0.1018	0.15	5.36	5.65	3.93	1.48	*2.32*	*0.35*	0.375	–11.77	–11.72	5.0	5.0
Sm-SEC1.5-5	1149	0.0204	01.005	1.5	5.57	5.61	5.82	1.94	*3.43*	*0.52*	0.333	–11.58	–11.58	4.8	4.8
Sm-SEC15-5	1027	0.0210	0.1003	15	5.47	5.50	8.05	2.50	*4.75*	*0.72*	0.340	–11.44	–11.27	5.0	3.1
Sm-SEC0.15-7	1151	0.0230	0.0999	0.15	7.16	7.34	3.55	0.46	*1.24*	*2.63*	0.131	–11.76	–12.16	5.0	5.0
Sm-SEC1.5-7	1118	0.0200	0.1001	1.5	6.98	7.19	9.64	1.97	*3.37*	*7.13*	0.207	–11.39	–11.59	5.0	5.0
Sm-SEC15-7	1094	0.0229	0.1007	15	6.98	7.02	13.24	2.47	*4.63*	*9.80*	0.192	–11.20	–11.44	5.1	4.9
Glycine															
Sm-SEG0.15-4	1461	0.0235	0.0992	0.15	4.37	4.44	1.91	0.80	*0.69*	*1.00*	0.420	–12.02	–11.92	5.0	5.0
Sm-SEG1.5-4	1748	0.0233	0.0995	1.5	4.34	4.37	1.94	0.80	*0.70*	*1.02*	0.413	–12.02	–11.93	5.1	5.1
Sm-SEG15-4	1604	0.0217	0.1003	15	4.30	4.42	1.80	0.75	*0.65*	*0.95*	0.417	–12.09	–11.99	5.1	5.1
Sm-SEG15-4b	1917	0.0235	0.1001	15	4.34	4.33	1.74	0.66	*0.63*	*0.91*	0.381	–12.06	–12.00	5.0	5.0
Sm-SEG0.15-7	1384	0.0224	0.1002	0.15	7.26	7.40	1.57	0.14	*0.55*	*1.16*	0.092	–12.13	–12.69	5.0	5.0
Sm-SEG1.5-7	1290	0.0235	0.1001	1.5	7.24	7.34	2.31	0.10	*0.81*	*1.71*	0.043	–11.94	–12.82	5.1	5.1
Sm-SEG15-7	1056	0.0218	0.1000	15	7.32	7.87	1.53	–	*0.54*	*1.13*	–	–12.19	–	5.5	–
Sm-SEG15-7b	1317	0.0243	0.0993	15	7.29	7.49	1.35	0.11	*0.47*	*1.00*	0.084	–12.16	–12.75	5.1	5.0

Note: Dissolution rates were normalized to mass.
* Estimated concentrations (see text for details) to be used exclusively as proxy in EQ3NR calculations (data in italics).

tions as a background electrolyte. For lactate and glycine, individual suspensions were prepared for every point of the adsorption series. For lactate adsorption, a quantity of 0.023 g of montmorillonite was added to 20 mL of 10 mmol/L KCl in a polyethylene bottle. For glycine experiments the amount of montmorillonite in each suspension was 0.058 g. The suspensions were stirred for 3–4 min and left to equilibrate for 24 h. A volume of lactic acid or glycine stock solution was added to reach a total ligand concentration of 0.15 mmol/L. The pH was adjusted in each sample with an appropriate amount of HCl or KOH solution to cover a pH range from 2 to 10. After 5 h the pH was measured in each bottle and an aliquot of 10 mL was withdrawn and filtered through a 0.22 µm Durapore membrane. The solutions were analyzed for lactate or glycine.

For citrate adsorption 0.58 g of montmorillonite were suspended in 100 mL of 10 mmol/L KCl solution. The suspension was stirred for 3–4 min and equilibrated for 24 h. Then a volume of citrate stock solution was added to reach a total ligand concentration of 0.15 mmol/L and the pH was adjusted to 2 by adding 1 mol/L HCl solution. Every 20 min the pH was measured and a 5 mL aliquot was withdrawn while stirring. The pH was then increased in steps of ~1 unit using an appropriate amount of KOH solution. The 5 mL aliquot was immediately filtered through a 0.22 µm Durapore membrane and the solution was analyzed for citrate.

The anion exclusion volume of the montmorillonite was determined by measuring the concentration of chloride in montmorillonite slurries at increasing ionic strength (Polubesova and Borisover 2009). Chloride concentration in the extract was measured by ion chromatography using a Metrosep A Supp–250 column and a solution of 1.7 mmol/L $NaHCO_3$/1.8 mmol/L Na_2CO_3 as eluent. Under our experimental conditions (10 mmol/L KCl) the anion exclusion volume was estimated of 0.39 cm^3 g^{-1} of clay.

Kinetic calculations

In a well-mixed, flow-through reactor the dissolution rate, *Rate* (mol g^{-1} s^{-1}), can be calculated based on the mass balance of a given mineral component *j*. Under steady-state conditions this is given by the following equation (e.g., Cama et al. 2000; Rozalén et al. 2008):

$$\text{Rate}\left(\text{mol g}^{-1}\ \text{s}^{-1}\right) = -\frac{1}{\nu_j}\frac{q}{M}(C_{j,\text{out}} - C_{j,\text{in}}) \quad (1)$$

where ν_j is the stoichiometric coefficient of component *j* in the dissolution reaction, *q* stands for the volumetric fluid flow through the system, *M* is the mass of montmorillonite, and $C_{j,\text{out}}$ and $C_{j,\text{in}}$ correspond to the concentrations of component *j* in the output and input solutions, respectively. The rate is defined as negative for dissolution and positive for precipitation. The error in the calculated rate is estimated by using the Gaussian error propagation method and is <5% in all cases, which corresponds to ~0.05 logarithmic units. In this study the dissolution rate is calculated from the Si and Al concentrations (R_{Si} and R_{Al}) in the output solutions. All dissolution rates were normalized to the initial mass of montmorillonite (Rozalén et al. 2008).

Montmorillonite dissolves according to the following reaction:

$$K_{0.44}(Al_{1.27}Fe^{3+}_{0.22}Mg_{0.56})(Si_{3.95}Al_{0.05})O_{10}(OH)_2 + 6.18\ H^+ \rightarrow$$
$$0.44\ K^+ + 1.32\ Al^{3+} + 0.22\ Fe^{3+} + 0.56\ Mg^{2+} + 3.95\ SiO_2 + 4.09\ H_2O \quad (2)$$

The estimated equilibrium constant for the K-montmorillonite dissolution reac-

tion at 37 °C was log K_{eq}(K–Sm) = 4.94 (Rozalén et al. 2009b). The saturation state of the solution with respect to solid phases is calculated in terms of the free energy of reaction, ΔG_r:

$$\Delta G_r = RT \ln\left(\frac{\text{IAP}}{K_{eq}}\right) \quad (3)$$

where IAP and K_{eq}, respectively, stand for the ion activity product and the equilibrium constant for the dissolution reaction. Aqueous activities and chemical affinities are calculated here by using the EQ3NR geochemical code (Wolery 1992).

The IAP was calculated from pH, Si and Al concentration in the output solutions at steady-state conditions. The Mg concentration was estimated according to the Mg/Si ratio observed by Rozalén et al. (2009b) in ligand-free solutions. The same procedure was used to estimate the Fe concentration in ligand-free acidic solutions (pH 2–3). At pH 4–9, the Fe^{3+} concentration was assumed to be in equilibrium with amorphous $Fe(OH)_3$ (Rozalén et al. 2009b). Such concentrations were used as proxies for the estimation of the solution saturation in K montmorillonite. Additional tests were conducted to assess the variation of montmorillonite saturation with Mg and Fe concentration. The change in ΔG_r was negligible when Mg or Fe contents were diluted or concentrated by a factor of 10.

EQ3NR was used to model the capacity of the ligands to form soluble species of Al. To attain this aim, the Lawrence Livermore National Laboratory thermodynamic database (cmp) (Wolery 1992) was modified to include the ligands species and the complexation reactions of aqueous Al (Table 2). Although the dissolution experiments were performed at 37 °C, the most complete set of complexation constant was obtained at 25 °C. Several tests were run to assess the effect of the temperature, concluding that the variation of the species distribution due to the increase in temperature was negligible, if compared with the analytical errors and the scattering of the complexation constant in the literature.

RESULTS

Dissolution experiments

The variation with time of the output solution composition of several representative flow-through experiments is shown in Figure 1. The concentrations of Si and Al and the pH were monitored throughout the duration of all the experiments. The experimental conditions of all the series, the average pH and the concentrations of Si and Al at steady state are reported in Table 1. The nomenclature of the dissolution experiments follows the pattern: Sm-SEL0.15-4b, where *Sm-SE* is smectite in electrolyte solution that can be followed by *L*, *C*, or *G* that is the ligand used (lactate, citrate, or glycine), with its concentration in mmol/L (0.15, 1.5, or 15). The last number is the initial pH in the experiment (4 or 7.5) and finally, the *b* corresponds to a replicate.

TABLE 2. Stability constants of Al^{3+} with the organic ligands

Reaction	Constant	Reference
Lactate		
$HLac = Lac^- + H^+$	$pK_a = 3.86$	(1)
$Al^{3+} + Lac^- = Al(Lac)^{2+}$	$\log K_1 = 2.36$	(2)
$Al^{3+} + 2Lac^- = Al(Lac)_2^+$	$\log\beta_2 = 4.42$	(2)
$Al^{3+} + 3Lac^- = Al(Lac)_3$	$\log\beta_3 = 5.79$	(2)
Citrate		
$H_3Cit = H_2Cit^- + H^+$	$pK_{a_1} = 3.10$	(1)
$H_2Cit^- = HCit^{2-} + H^+$	$pK_{a_2} = 4.80$	(1)
$HCit^{2-} = Cit^{3-} + H^+$	$pK_{a_3} = 6.40$	(1)
$Al^{3+} + Cit^{3-} = Al(Cit)$	$\log K_1 = 7.98$	(3)
$Al(Cit) + H^+ = AlH(Cit)^+$	$\log K = 2.94$	(3)
$Al(Cit) = AlH_{-1}Cit + H^+$	$\log K = -3.31$	(3)
$AlH_{-1}Cit = Al(H_{-1}Cit)(OH) + H^+$	$\log K = -6.23$	(3)
Glycine		
$HOOC\text{-}CH_2\text{-}NH^+ = {}^-OOC\text{-}CH_2\text{-}NH_3^+ + H^+$	$pK_{a_1} = 2.35$	(4)
$^-OOC\text{-}CH_2\text{-}NH^+ = {}^-OOC\text{-}CH_2\text{-}NH_2 + H^+$	$pK_{a_2} = 9.78$	(4)
$Al^{3+} + 3(^-OOC\text{-}CH_2\text{-}NH_2) = Al(OOC\text{-}CH_2\text{-}NH_2)_3$	$\log\beta_3 = 19.40$	(5)

Notes: (1) Filius et al. (1997), (2) Marklund et al. (1986), (3) Martell et al. (1990), (4) Martell and Smith (1974), (5) Yadava et al. (1984).

Experiments without organic ligands. In the experiments without an organic ligand cation-release rates tend to decrease significantly with elapsed time until steady-state conditions are attained. The solution pH remains constant with elapsed time in all the experiments. High Al and Si concentrations were observed at the onset of most experiments. Afterward, Al and Si concentrations decrease asymptotically until a steady state is approached. The Al/Si release ratio increases up to a constant value at the steady state in all the experiments. Figure 2 shows the Al/Si ratio in solution at steady state as a function of the solution pH. The Al/Si release ratio at pH 4–4.5 is very close to stoichiometric, and the dissolution rates derived from Si and Al concentrations are consistent with each other. In circumneutral pH solutions (pH 4.5–8) the stoichiometric ratio decreases involving a deficit in aqueous aluminum.

Experiments with organic ligands. The evolution of pH and concentrations of Si, Al, and organic ligand with elapsed time in a representative experiment is illustrated in Figure 1. The tendency observed for Si and Al is the same as in experiments without an organic ligand: an initial fast release of montmorillonite structural cations to the solution and an asymptotical decrease until steady state is approached.

The pH remained constant in the experiments at pH 4 (Fig. 1). However, it was necessary to readjust the pH in the same series at pH 7, because of a drift to higher values during the first days of reaction.

The behavior of the Al/Si ratio with elapsed time is also similar to that found in organic ligand-free solutions (Fig. 1), which reach a constant value when steady state is approached. At pH 4 and 5.5, montmorillonite dissolution is stoichiometric irrespective of the ligand and its concentration. The dissolution reaction at pH 7–8 is incongruent in solutions with lactate, citrate, or glycine, regardless of their concentrations. Lactate, citrate, and glycine concentrations remain constant with elapsed time in all the experiments.

Adsorption experiments

Adsorption experiments were performed as a complement to dissolution series to assess whether ligands were adsorbed onto the montmorillonite surface as a function of pH and interpret the dissolution mechanism. The pH dependence of the adsorption of lactate, citrate, and glycine onto montmorillonite (adsorption edges) is shown in Figure 3. The amount of ligand adsorbed is small, but all three of these produced different adsorption patterns. In the case of lactate adsorption, three pH intervals exist. Up to pH ~6, the amount of adsorbed lactate is approximately constant, with a maximum adsorption of 60 μmol/g at pH 5.5–6. From pH 6 to 9, the adsorbed lactate is progressively lower. Finally, at pH > 9, lactate does not adsorb onto the montmorillonite surface. The glycine adsorption pattern is very similar to that found for lactate, with a maximum of 26 μmol/g, but the decrease in adsorption occurs at pH 5. Citrate adsorption is very close to zero at a low pH, increasing up to a maximum of 23 μmol/g at approximately pH 6 and decreasing over pH 6.

Saturation and aqueous speciation

To assess the contribution of Al speciation, the steady-state composition of the output solutions of the dissolution experiments

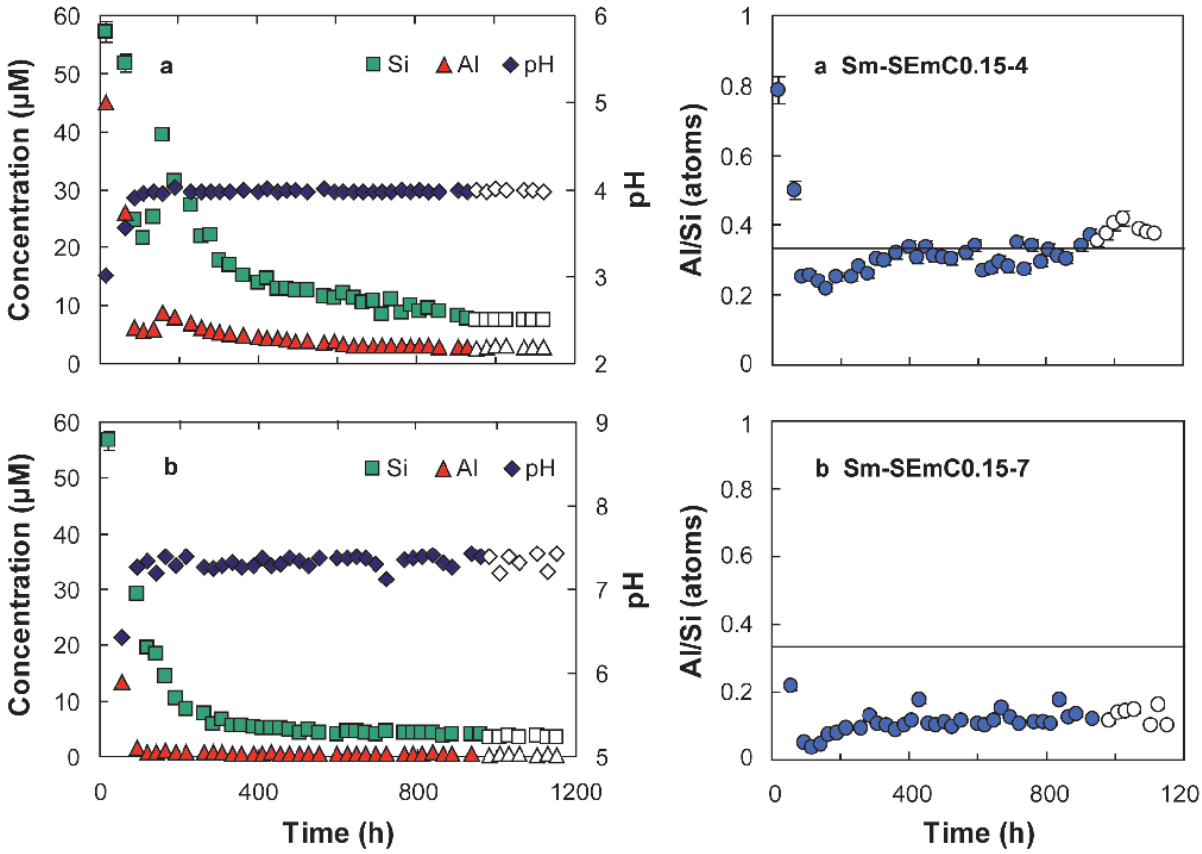

Figure 1. Evolution of the pH, Si and Al concentrations, and Al/Si atomic ratio in the output solutions of a selected group of dissolution experiments conducted in flow-through cells. Output solutions used to calculate the average steady state are denoted by open symbols. Horizontal line at Al/Si = 0.334 represents the stoichiometric ratio in the solid sample.

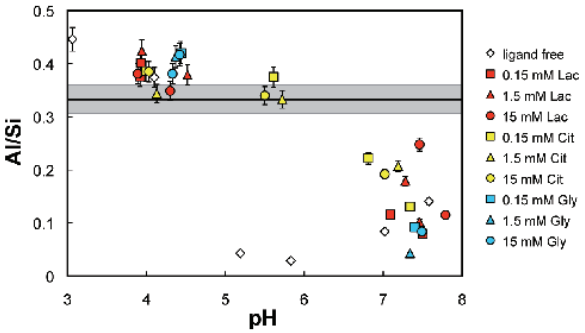

Figure 2. Variation in the Al/Si ratio with the pH in dissolution experiments. The line corresponds to stoichiometric ratio in the solid sample (Al/Si = 0.334 ± 0.027).

with no ligand, lactate, citrate, and glycine (Table 1) was modeled with EQ3NR. The saturation of the output solutions with respect to montmorillonite and secondary minerals is given in Table 3. All the solutions are undersaturated in montmorillonite, amorphous silica, quartz, and kaolinite. Ligand-free solutions are saturated in gibbsite at pH > 5.8. Solutions from the experiments at pH 7.5 with lactate or glycine are saturated in gibbsite. However, citrate solutions are undersaturated in gibbsite irrespective of the solution pH.

The aqueous speciation of the lactate, citrate, and glycine was derived from their acidity constants (Table 2) by using EQ3NR. The results are shown in Figure 4. Si-ligand speciation was not taken into account as Si forms very weak organic complexes in solution (Pokrovski and Schott 1998). The capacity of lactate, citrate, and glycine to form soluble complexes with aqueous Al^{3+} was also investigated with EQ3NR, using the corresponding constants values listed in Table 2. The concentrations of aqueous Al (0.1 to 4.7 μmol/L) and ligands (0.15, 1.5, and 15 mmol/L) in the output solutions cover a wide range of conditions. The modeling with EQ3NR reveals no substantial differences in the distribution of Al species. Thus, to facilitate the comparison the speciation results in Figure 5 were modeled for a total Al concentration of 1 μmol/L.

The Al speciation diagram was different for each ligand (Fig. 5). In the case of lactate, only the complex $Al(Lac)^{2+}$ is relevant in the range of pH between 4 and 5, representing only 10% of the total aqueous Al. For citrate, the speciation is more complex. In the pH range 3–4, three species coexist: around 10% of $AlH(Cit)^{+}$, 20% of Al(Cit), and increasing values from 1 to 80% of $Al(Cit)^{-}$. This last species reaches a maximum of 90% between pH 4 and 5, where it starts to coexist with Al(OH)

TABLE 3. Saturation state (kcal/mol) of output solutions at steady-state conditions calculated according to Equation 3 for flow-through montmorillonite dissolution experiments at 37 °C

Run	pH_{out}	K-Mont	SiO_2(am)	Qz	Gib	Kln
Sm-SE-3	3.06	−29.14	−3.25	−1.49	−6.61	−15.24
Sm-SE-4	4.10	−22.50	−3.74	−1.99	−2.99	−9.00
Sm-SE-5	5.19	−19.49	−4.29	−2.54	−0.708	−5.53
Sm-SE-6	5.83	−16.20	−4.30	−2.54	0.776	−2.57
Sm-SE-7	7.02	−12.69	−4.23	−2.47	1.40	−1.19
Sm-SE-8	7.58	−11.85	−4.21	−2.45	1.06	−1.82
Lactate series						
Sm-SEL0.15-4	3.92	−22.19	−3.41	−1.65	−3.38	−9.09
Sm-SEL0.15-4b	3.93	−23.82	−3.69	−1.93	−3.58	−10.06
Sm-SEL1.5-4	4.52	−23.27	−3.87	−2.12	−1.49	−6.26
Sm-SEL1.5-4b	3.94	−24.80	−3.70	−1.95	−3.46	−9.85
Sm-SEL15-4	4.30	−22.35	−3.53	−1.78	−2.51	−7.62
Sm-SEL15-4b	3.89	−20.54	−3.36	−1.61	−3.83	−9.90
Sm-SEL0.15-7	7.09	−14.74	−4.55	−2.80	1.18	−2.27
Sm-SEL0.15-7b	7.50	−12.55	−4.24	−2.48	0.771	−2.47
Sm-SEL1.5-7	7.28	−14.37	−4.64	−2.88	1.11	−2.58
Sm-SEL1.5-7b	7.46	−11.88	−4.16	−2.40	1.07	−1.70
Sm-SEL15-7	7.79	−12.02	−4.10	−2.35	0.758	−2.22
Sm-SEL15-7b	7.46	−11.33	−4.30	−2.55	1.45	−1.24
Citrate series						
Sm-SEC0.15-4	3.99	−22.06	−3.30	−1.54	−4.01	−10.14
Sm-SEC1.5-4	4.13	−22.89	−3.20	−1.45	−5.19	−12.30
Sm-SEC15-4	4.03	−23.13	−3.01	−1.25	−6.33	−14.20
Sm-SEC0.15-5a	6.81	−15.73	−3.91	−2.15	−1.65	−6.65
Sm-SEC0.15-5b	5.65	−18.31	−3.67	−1.92	−2.71	−8.30
Sm-SEC1.5-5	5.61	−18.63	−3.44	−1.69	−3.82	−10.06
Sm-SEC15-5	5.50	−20.17	−3.25	−1.49	−5.28	−12.59
Sm-SEC0.15-7	7.34	−13.06	−3.74	−1.98	−1.08	−5.15
Sm-SEC1.5-7	7.19	−11.64	−3.15	−1.40	−1.77	−5.36
Sm-SEC15-7	7.02	−12.95	−2.95	−1.20	−3.12	−7.68
Glycine series						
Sm-SEG0.15-4	4.44	−24.62	−4.55	−2.80	−1.93	−8.49
Sm-SEG1.5-4	4.37	−24.80	−4.54	−2.79	−2.20	−9.02
Sm-SEG15-4	4.42	−25.25	−4.59	−2.83	−2.36	−9.41
Sm-SEG15-4b	4.33	−25.93	−4.61	−2.85	−2.68	−10.09
Sm-SEG0.15-7	7.40	−13.83	−4.67	−2.92	0.963	−2.94
Sm-SEG1.5-7	7.34	−13.09	−4.44	−2.69	0.843	−2.72
Sm-SEG15-7	7.87	−13.57	−4.69	−2.93	−0.007	−4.92
Sm-SEG15-7b	7.49	−14.78	−4.76	−3.01	0.400	−4.25

Note: Positive values indicate saturation or oversaturation.
* K-Mont = K-montmorillonite; SiO_2(am) = amorphous silica; Qz = quartz; Gib = gibbsite; Kln = kaolinite.

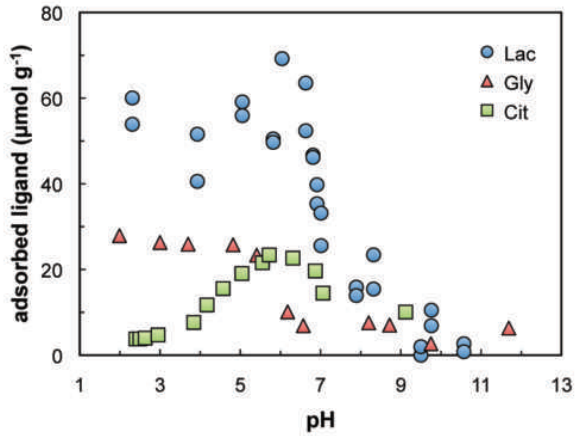

FIGURE 3. Dependence of lactate, citrate, and glycine adsorption onto smectite vs. solution pH (adsorption edge).

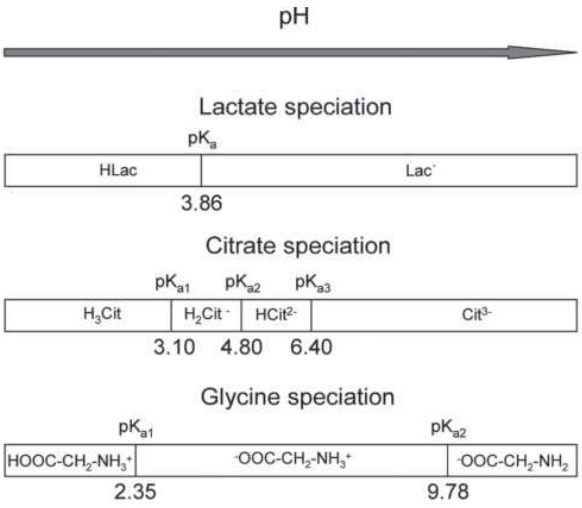

FIGURE 4. Sketch of the speciation of the lactate, citrate, and glycine with the pH.

$(Cit)^{2-}$. At pH 6, it exists 50% of $Al(Cit)^{-}$ and 50% of $Al(OH)(Cit)^{2-}$. Above pH 6, the concentration of $Al(OH)(Cit)^{2-}$ increases up to 100% at 7–8.5. Finally, for glycine no relevant amounts of Al-Gly complexes are observed under our experimental conditions. The capacity of the three ligands investigated to complex Al ions follows the trend citrate >> lactate > glycine, from strong to very weak complexants.

DISCUSSION

Dissolution experiments

Montmorillonite dissolution rates at steady state are plotted in Figure 6 as a function of the solution pH. In ligand-free solutions, the rates show the typical variation in the dissolution rate with the pH observed for Al-silicates and complex oxides: the rates decrease with increasing pH in acidic conditions, they reach a minimum at near neutral pH and increase with increasing pH at more basic conditions.

The dissolution rates derived from Si and Al concentrations are consistent with each other, indicating a stoichiometric dissolution at steady-state conditions for pH ≤ 4.5. Incongruent dissolution under circumneutral pH conditions is produced by a back-precipitation or sorption of Al and caused a decrease in the dissolution rates derived from Al concentration (Metz et al. 2005; Rozalén et al. 2008). As a consequence, the dissolution rates derived from Al under these conditions should be considered as apparent dissolution rates.

In the absence of organic ligands, the species that attack the silicate are mainly protons, water molecules, and hydroxyls, which can form surface complexes with cations at surface sites. Thus, the variation in the dissolution rate with pH can be described as the sum of the contribution of the three components associated with the concentration of protons, hydroxyls, and water molecules (Huertas et al. 1999). For acidic conditions, dissolution rate is proportional to the proton activity powers to the proton reaction order

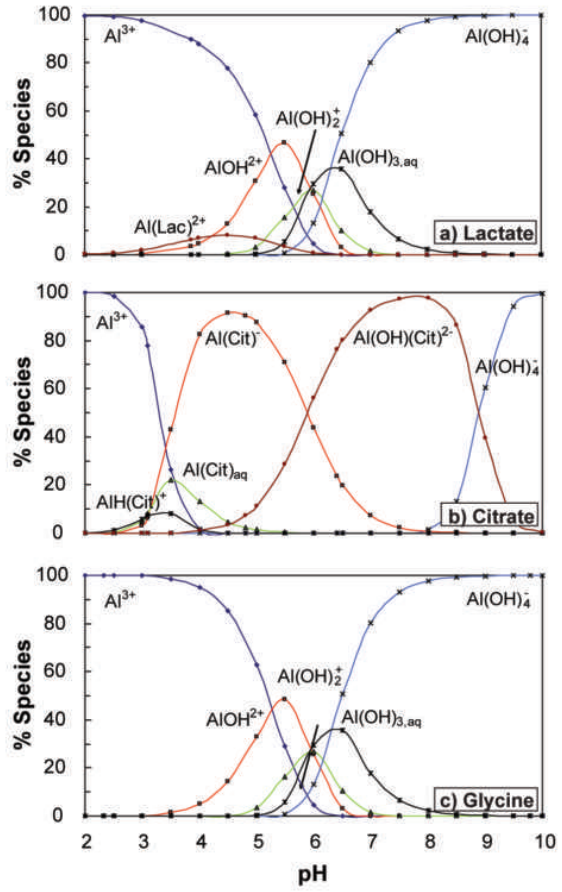

FIGURE 5. Aluminum (1 µmol/L) speciation in solutions with 1.5 mmol/L of (**a**) lactate, (**b**) citrate, and (**c**) glycine as a function of the solution pH.

$$\text{Rate (mol g}^{-1}\text{ s}^{-1}) = 10^{-10.24} a_{H+}^{0.37} \quad (4)$$

The reaction order (n_H = 0.37) is consistent with the value n_H = 0.40 obtained at 25 °C for diluted solutions of electrolytes (0.01 mol/L) (Rozalén et al. 2009b), as well as close to those from Amram and Ganor (2005) (n_H = 0.57) and Golubev et al. (2006) (n_H = 0.21) at 25 °C. Nevertheless, a similar equation cannot be derived around neutral conditions and there are not enough data on the basic branch.

Lactate and glycine solutions. The increase in the ligand concentration from 0.1 to 15 mmol/L, both at pH 4 and 7.5, does apparently not produce any relevant change in the dissolution rate (Fig. 6; Table 1). At pH ~4, the dissolution reaction is congruent with and without the lactate or glycine, since the Si- and Al-based rates are very similar in both cases. There is a slight increase in the dissolution rates by adding lactate, but the difference is within the error associated with the dissolution rate.

At pH ~7.5, the dissolution reaction is incongruent with lactate or glycine as was also observed in ligand-free solutions in this pH interval. The Si-derived dissolution rates in solution with lactate are 0.2–0.3 logarithmic units lower than those in pure electrolyte solutions except for the series with lactate 15 mmol/L, which have similar values of dissolution rate. This difference in Si-derived dissolution rates was not found in glycine experiments. The Al-based dissolution rates with lactate and glycine at pH 7.5 follow a parallel trend to the rates measured in experiments without ligands. Furthermore, Al-derived dissolution rates in lactate solutions are slightly lower than the corresponding rates in ligand-free solutions, but the differences are not significant.

Citrate. The citrate enhances the montmorillonite dissolution rate significantly at all the pH values studied and this effect strongly depends on the citrate concentration added (Figs. 6 and 7). To gain a more complete understanding of the effect of this ligand an additional set of experiments was performed at pH 5.5. The variation in the Si-derived dissolution rates (R_{Si}) with the pH is similar to that obtained in ligand-free solutions. However, a strong catalytic effect can be observed when citrate is added even at the lowest concentration. In the presence of a high concentration of citrate (15 mmol/L) the Si-release based rate is increased by 0.5 logarithmic units at pH 4 with respect to the rate calculated without organic ligand at the same pH. This increase is greater at near neutral pH, so that the rate obtained in 15 mmol/L citrate is one order of magnitude faster than that without citrate. Montmorillonite dissolution in citrate solution is stoichiometric at pH 4 and 5.5, but incongruent at pH 7.5. Nevertheless, the Al/Si ratio at the steady state increases in the experiments with citrate when compared with ligand-free solutions (Fig. 2).

The dissolution rates obtained by Golubev et al. (2006) at pH 6.7 also showed the catalytic effect of citrate, although their values were one order of magnitude lower than those obtained in the present study.

Montmorillonite biodurability. Dissolution rates are a complex function of the chemical solubility of particles in the body fluids that determine the rate at which particles dissolve (Plumlee and Ziegler 2003). The resistance to chemical dissolution in the body (particle's biodurability) controls the residence time of a particle in the lungs and it is related with the tendency to cause a disease (Jurinski and Rimstidt 2001). An estimation of biodurability of clay particles can be derived from our kinetics results by using a simple model: a disk was used as a proxy for particles shape and dissolution reaction occurs from the edge inward (Rozalén et al. 2008). Biodurability is estimated as the reduction in the diameter as time progress. Although the experimental conditions do not reproduce exactly the complexity of the human body, they provide a benchmark to evaluate the biological degradation of inhaled clay particles. The parameters used in the calculation are the following:

• Particle morphology: disks of 0.5 µm in diameter and 5 nm in thickness that correspond to 4 layers of smectite (Verburg and Baveye 1994) with a monolayer of interlayered water.

• Molar weight: 767.89 g/mol, according to the structural formula.

• Molar volume: 372.33 cm^3/mol (Robie and Hemingway 1995).

• Specific weight: 2.06.

The calculated rates allow us to estimate the dimensions of the particle as time progress, assuming that reactive surface area

corresponds to the particle edges (see discussion in Rozalén et al. 2008). The evolution of the particle radius (r) with time can be obtained by the following equation:

$$r^2 = r_0^2 - \frac{\text{Rate}_v}{\pi h} t \quad (5)$$

where r_0 is the initial radius, Rate_v the volumetric dissolution rate expressed in $\text{cm}^3\ \text{s}^{-1}$, h particle thickness, and t the elapsed time.

Simulations were performed with a concentration of 1.5 mmol/L lactate, 0.15 mmol/L glycine, and 0.15 mmol/L citrate (Fig. 8), which corresponds to the conditions most similar to biological fluids (Plumlee and Ziegler 2003). Clay particles dissolved faster at pH 4 (lysosomes) than at pH 7.5 (interstitial fluids). Considering the three ligands investigated, only citrate enhances substantially the montmorillonite dissolution. The effect of citrate is stronger at pH 4 than at pH 7.5. At pH 7.5, a particle 500 nm in diameter could be reduced 25% in the presence of citrate, whereas the reduction in saline solution would only be 10% after 10 yr. However, under both conditions, acidic and neutral, it takes several years to halve the particle diameter.

Extending the conclusions on montmorillonite to other 2:1 phyllosilicates (Rozalén et al. 2008), the chemical degradation

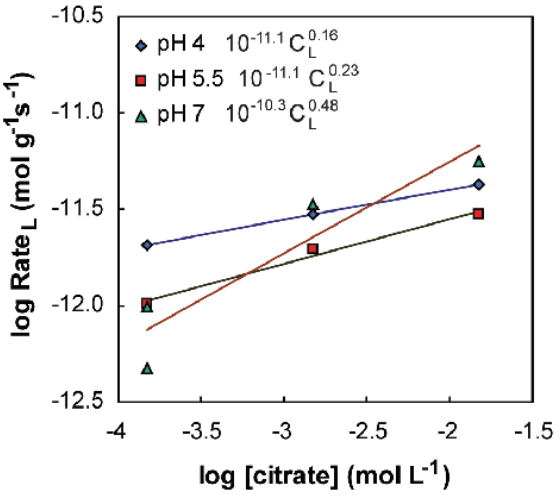

FIGURE 7. Effect of citrate on Si-derived dissolution rates. Ligand promoted dissolution rate for each pH conditions, R_L, derived from Equations 7a–7c, are included.

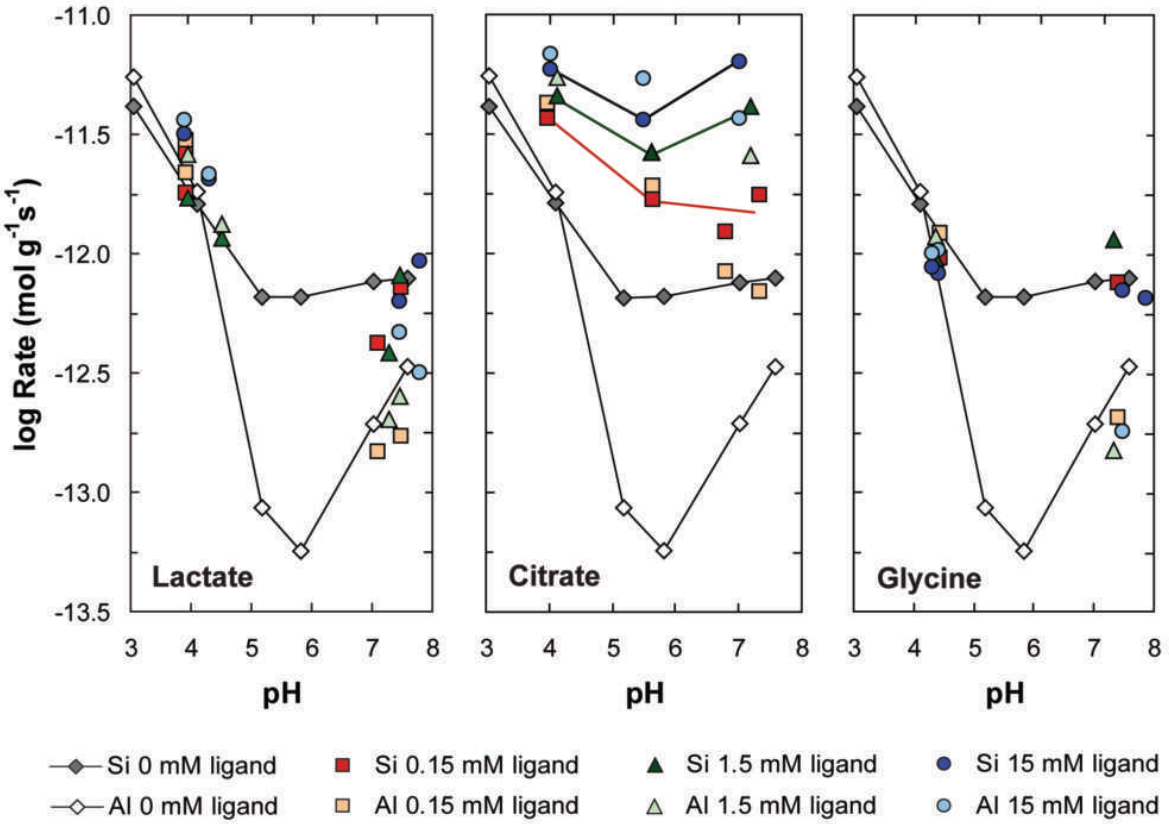

FIGURE 6. Experimental dissolution rates derived from Si and Al concentrations in outlet solution calculated with lactate, citrate, and glycine solutions. Dissolution rates in ligand-free solutions are included for comparison.

efficiency of clayey particles inhaled (smectites, illites, micas) is probably low in lung conditions. In addition, the release of elements such as Si or Al may have additional consequences for human health. Strong complexants as citrate contribute to the transport of released elements such as Al. The application of geochemical methods may help health science in the understanding of the hazard of toxic minerals as well as those considered as inert such as clay minerals.

Adsorption experiments

Ligand adsorption is the result of the interaction between ligand and montmorillonite at the mineral/solution interface. As the ligand deprotonation and montmorillonite edge surface charge are both pH dependent the adsorption reactions depend on the solution pH. The pH-dependent surface charge at the montmorillonite edge surface was modeled on the basis of three types of adsorption sites: amphoteric sites on Al cations, basic silanol sites and cation exchange sites (>ZEX) associated with the montmorillonite cation exchange capacity (Fig. 9) (Rozalén et al. 2009a). The aqueous speciation of the lactate, citrate, and glycine was derived from their acidity constant (Table 2) by using EQ3NR (Fig. 4).

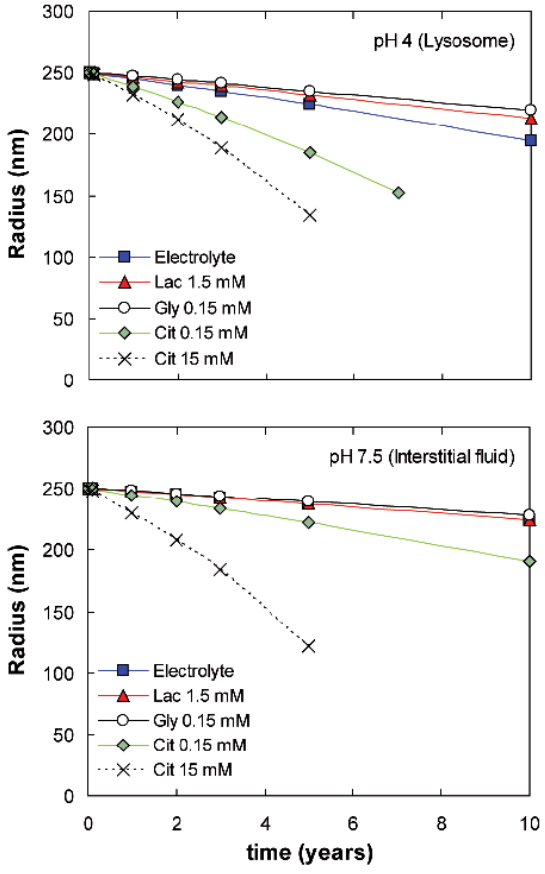

FIGURE 8. Decrease in the diameter of a smectite particle during the dissolution in lung fluids. Ligand concentrations were of 1.5 mmol/L lactate, 0.15 mmol/L glycine, and 0.15 mmol/L citrate. The curve for 15 mmol/L citrate concentration was included for comparison.

Lactate. At pH values over ~7.5, both the montmorillonite edge surface and lactate are negatively charged. There may be no interaction between the montmorillonite edge surface and lactate anion, and no lactate adsorption can be observed under alkaline conditions. Below pH 7.5, the montmorillonite edge surface is positively charged due to the relative abundance of $>AlOH_2^+$ and the positive charge increases as the solution becomes more acidic (to approximately pH <5). Negatively charged lactate adsorbs onto the montmorillonite edge surface increasing adsorption as the pH decreases from 9 to 7. Below pH 7, the amount of lactate adsorbed is approximately constant in all the experiments. This behavior indicates an electrostatic interaction between the anion and the positively charged surface, as observed for the lactate-goethite interaction (Filius et al. 1997). According to Figures 3 and 9 that correspond to the adsorption edges and the edge surface speciation of the montmorillonite, respectively, lactate adsorbed onto the montmorillonite (Lac^- or HLac) is probably bound to positively charged Al sites.

The lactate molecules in solution are predominantly uncharged below pH 3.86, while the montmorillonite edge surface is positively charged. The protonation of lactate below pH 3.86 should reduce the amount of the ligand adsorbed onto the montmorillonite edge surface. However, this behavior, found for other solids (Filius et al. 1997), is not observed in our experiments.

Citrate. The adsorption behavior of citrate also points to electrostatic binding. At approximately pH < 3.2 a very weak interaction is expected between the fully protonated citrate and positively charged montmorillonite. No clear evidence of adsorption was found. The interaction between the citrate and the montmorillonite edge surface increases from pH 3.2 up to 7 due to the partial deprotonation of citric acid. The most abundant species are H_2Cit^- (pH 3.1–4.8) and $HCit^{2-}$ (pH 4.8–6.4), which can interact with the positively charged montmorillonite edge surface, producing the adsorption maximum at pH 6. Above pH 7, the electrostatic repulsion between the fully deprotonated citrate and the negatively charged montmorillonite edge surface (both $>SiO^-$ and $>AlO^-$ sites) makes ligand adsorption difficult. This decreases progressively as the negative charge develops at the montmorillonite edge surface with an increasing pH.

Lackovic et al. (2003) found that a small amount of citric acid can be adsorbed onto kaolinite and illite, modeling the adsorption with outer-sphere complexation to the variable-charge edge groups. Their adsorption maximum (~3 µmol/g illite) is approximately one order of magnitude lower than in the present study, although the citrate solutions were also more diluted.

Glycine. The glycine molecule contains carboxylic and amino functional groups that show differential acid-base behavior with the formation of a zwitterion as a main species between pH 2.3 and 9.8 (Fig. 4). The zwitterion dominates the pH interval studied. Thus, glycine could adsorb onto smectite at the edges through carboxylate group or at the negatively charged basal plane through amino group. Due to the existence of an anion exclusion volume around the basal planes, we assume that glycine adsorption is only plausible at the montmorillonite edge surface.

The adsorption edge of glycine is very similar to that found for lactate, although shifted to more acidic conditions. The adsorption shows a plateau up to pH 5 and then a smooth decrease toward alkaline conditions, as the positive charge on montmo-

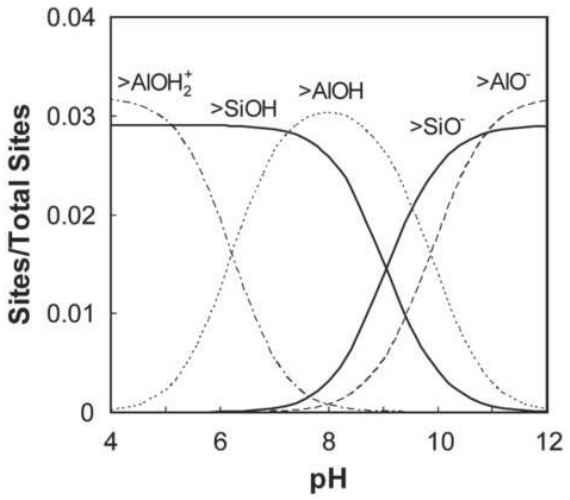

FIGURE 9. Predicted distribution of the surface species of smectite as a function of pH at 0.1 *M* ionic strength at 25 °C according to the constant capacity model, modified from Rozalén et al. (2009a). Site density is expressed in terms of the molar fraction of the total surface density for edges sites and basal plane sites (not shown).

rillonite reduces and basic sites deprotonate. A slight amount of glycine is still adsorbed above pH 7, probably through the interaction between negatively charged edge surface sites and protonated amino groups.

Hedges and Hare (1987) studied the adsorption of amino acids onto montmorillonite and kaolinite and interpreted the adsorption patterns as a result of the electrostatic interactions between the clay surface and the amino acid. These results were also found for lysine adsorbed on montmorillonite (Kitadai et al. 2009).

Dissolution mechanism

Montmorillonite dissolution in acidic and neutral solutions containing ligands may occur through contributions of proton- and ligand-promoted reactions. The effect of pH on montmorillonite dissolution (proton-promoted dissolution) has previously been studied (Rozalén et al. 2008, 2009b and references therein). The mechanism of ligand-promoted dissolution may occur through the formation of surface complexes or a reduction in the ion activity product by complexation of the released cations, in particular Al in the present case.

In the case of the formation of surface complexes, the adsorption experiments show that lactate, citrate, and glycine are adsorbed under acidic conditions (Fig. 3). The amount of ligand adsorbed onto the montmorillonite can be converted into surface density, assuming that the adsorption mainly occurs on the edge surface with an estimated edge surface area (ESA) of 6.5 $m^2 g^{-1}$. The maximum amount of ligand adsorbed per nm^2 of ESA is of 5.6 lactate, 2.4 glycine, and 2.2 citrate. These surface concentrations are in the same order of magnitude as the edge surface density of amphoteric >AlOH sites (3.55 sites nm^{-2}) and basic >SiOH sites (3.16 sites nm^{-2}) (Rozalén et al. 2009a). Nevertheless, we cannot assess if adsorption occurs by formation of inner- or outer-sphere surface complexes. However, there are some studies about the adsorption of organic ligands onto mineral surfaces by ATR-FTIR. Kubicki et al. (1999) did not observe a strong surface complexation of citrate on montmorillonite. However, Kang and Xing (2007) suggested that organic acids prefer to adsorb onto montmorillonite by outer-sphere complexation in aqueous environments, but inner-sphere complexation is favored under dry conditions.

Lactate and glycine. Soluble Al-Lac and Al-Gly complexes are not relevant at pH 4 nor pH 7.5 based on EQ3NR calculations (Fig. 5). Thus, the role of lactate or glycine in enhancing the dissolution rate through the formation of soluble Al complexes and by diminishing the activity of Al^{3+} ions is negligible. Possible effects of lactate and glycine on montmorillonite dissolution are supposed to be found in their interaction with the clay surface.

At pH ~4, there is a slight increase in the dissolution rates by adding lactate, but the difference is within the error associated with the dissolution rate. Thus, this increase is not significant enough to confirm a possible catalytic effect due to lactate. Although lactate and glycine are adsorbed onto montmorillonite (Fig. 3) at pH 4, they do not promote or inhibit the dissolution reaction. For lactate and glycine under the experimental conditions, the contribution of ligand-promoted dissolution mechanism is much less relevant than the proton-promoted mechanism.

The Al-based dissolution rates with lactate and glycine at pH 7.5 follow a parallel trend to the rates measured in experiments without ligand. Under these pH conditions and in the absence of Al ligands, montmorillonite dissolution is stoichiometric but followed by the precipitation of Al hydroxides (Rozalén et al. 2008, 2009b). Moreover, the EQ3NR calculations reveal that output solutions are almost in equilibrium with Al hydroxides (boehmite and gibbsite). Al-derived dissolution rates at pH 7.5 represent the balance between montmorillonite dissolution and Al hydroxide precipitation.

The Si-based dissolution rates indicate a slight inhibitory effect due to the addition of lactate to the solutions. Figure 3 shows that at pH 7.5 the lactate is partially adsorbed onto Al surface sites at the clay edges. At this pH value, the dissolution reaction is mainly controlled by the attack of water molecules to the reactive sites on the surface followed by the hydrolysis of the network and the release of Al and Si cations. The lactate adsorbed onto the surface at pH 7.5 could reduce the number of the reactive sites available to be attacked by water molecules, which may slightly induce a diminishing in the dissolution rate. Consequently, lactate adsorption at pH 7.5 may inhibit the dissolution reaction. This inhibitory effect was not found for glycine experiments, probably due to the small amount of glycine adsorbed at pH 7.5.

The different behavior of lactate observed at pH 4 and 7.5 is due to the effectiveness of protons and water molecules to attack the surface. The proton-promoted mechanism at pH 4 is much more efficient than the water-promoted mechanism at pH 7.5 and overwhelms the potential inhibition due to lactate adsorption in acidic solution. In neutral conditions the inhibition produced by adsorption is probably due to a reduction in available reactive sites on the montmorillonite edges.

Citrate. Comparing the dissolution rates obtained at the same concentration of citrate and at different pH (Fig. 6), a similar V-shaped trend can be observed. By increasing the citrate concentration the trend becomes smoother. At 0.15 mmol/L

citrate, the trend of the dissolution rates is similar to that found for ligand-free experiments with the Si-based dissolution rate higher at pH 4 than that found at pH 7.5 due to the efficiency of the proton-promoted mechanism at acidic pH. As citrate concentration increases up to 1.5 mmol/L the rates at pH 4 approach those at pH 7.5. At 15 mmol/L the effect of the citrate on the dissolution is so high that similar Si-derived dissolution rates were obtained for the three pH conditions, which indicates that under these conditions the ligand-promoted dissolution mechanism is much more important than the proton-promoted one. Thus, the effect of citrate is completely different from that of lactate or glycine, although citrate adsorption is more limited when compared with the other two ligands.

For a ligand there exists a rough correlation between the stability constants of aqueous and surface complexes (Kummert and Stumm 1980; Stumm et al. 1980; Sigg and Stumm 1981). Citrate forms stabler aqueous complexes with Al than lactate and glycine (Table 2). Therefore, we may suppose that citrate surface complexes are also stabler than those with lactate and glycine. Strong citrate adsorption would contribute in more extension to the detachment of Al to solution. This behavior enhances dissolution rates in citrate solutions.

The overall rate of montmorillonite dissolution can be expressed as the contribution of proton- and ligand-promoted dissolution mechanisms (e.g., Golubev and Pokrovsky 2006; Golubev et al. 2006; Olsen and Rimstidt 2008)

$$Rate_{Tot} = Rate_H + Rate_{Ligand} = k_H \cdot a_{H^+}^{n_H} + k_L \cdot a_L^{n_L}. \quad (6)$$

The first term in this equation corresponds with the proton-promoted dissolution following Equation 4 and the second term corresponds with the ligand-promoted dissolution. At each specific pH, the ligand-promoted dissolution can be estimated by subtracting the dissolution rate of ligand-free solutions from the overall dissolution rate, $R_{Tot} - R_H$ (Fig. 7), obtaining these empirical laws:

$$\text{pH 4} \quad Rate_L = 10^{-11.1} C_L^{0.16} \quad (7a)$$

$$\text{pH 5.5} \quad Rate_L = 10^{-11.1} C_L^{0.23} \quad (7b)$$

$$\text{pH 7} \quad Rate_L = 10^{-10.3} C_L^{0.48} \quad (7c)$$

Ligand-promoted dissolution rates increase with increasing citrate concentration. This effect is steeper from pH 4 to 7.5, as reveals the increase in the reaction order n_L with the solution pH, from 0.16 to 0.48. This indicates that the effect of citrate is stronger at pH 7.5 that in acidic conditions. The effect of citrate in enhancing dissolution reactions at various pH should be derived from the citrate surface adsorption and formation of aqueous Al complexes.

The stoichiometry of the reaction changes with solution pH and citrate concentration (Fig. 2). At pH 4 and 5.5, the dissolution is stoichiometric irrespective of citrate concentration, but at pH 7.5 the dissolution is incongruent even in 15 mmol/L citrate, although citrate can form stable complexes with aluminum in solution (Venturini and Berthon 1989).

Strong chelating ligands such as citrate also inhibit the hydrolytic reactions of aluminum in solution, thus retarding the crystallization of aluminum hydroxides (Jardine and Zelazny 1996). The effectiveness to hinder the hydrolysis and polymerization of aluminum increases with the affinity of organic ligands for aluminum and the concentrations of these ligands in solution. These effects may contribute to reduce saturation with respect to Al-bearing phases, including montmorillonite. EQ3NR results revealed that the aluminum in the output solutions should be completely complexed by citrate regardless of pH and citrate concentrations (Fig. 5). That is the case in the experiments with citrate at pH 4 and 5.5. Furthermore, citrate concentration should complex the total aluminum released if dissolution were stoichiometric. It is necessary to answer where the difference between stoichiometric and steady-state Al is, and why so strong a ligand as citrate cannot chelate the total Al released at pH 7 producing a stoichiometric dissolution process.

The deficit in Al may be due to precipitation of gibbsite particles (Nagy et al. 1999) or Al-citrate complexes (Cambier and Sposito 1991). Nagy et al. (1999) demonstrated that gibbsite can grow on phyllosilicate basal planes. Thus, the Al deficit can be converted into surficial gibbsite deposits. For example, the Al deficit in the experiment with 15 mmol/L citrate at pH 7.5 is 1.5 μmol. Assuming for gibbsite deposits a thickness of 4 layers (Nagy et al. 1999), a molar volume of 31.83 $cm^3\ mol^{-1}$ (Robie and Hemingway 1995), and c^* of 9.75 Å (Gaines et al. 1997), the surface covered by gibbsite is only of 0.01 m^2. That value contrasts with the total montmorillonite surface area in the experiment, which can be approximated in the following way

$$m \cdot SA_{\text{total}} \cdot \frac{1}{n} = 0.1g \cdot 750m^2 / g \cdot \frac{1}{4} = 18.75m^2 \quad (8)$$

where m is the montmorillonite mass, SA_{total} stands for the total surface area (Meunier 2003), and n corresponds to the average number of layers in smectite tactoids, which for K-montmorillonite is 4 (Verburg and Baveye 1994).

Alternative explanations consider Al adsorption at Al surface hydroxyl groups located on the broken edges of the particle surfaces at higher pH values or at permanently charged surface sites by cation exchange up to pH 3 (Charlet et al. 1993). Nevertheless, no decrease in montmorillonite swelling capacity after solvation with ethylene-glycol was observed (Moore and Reynolds 1989). An estimation of the interlayer space occupied by Al hydroxides (0.04 m^2) when compared with the total interlayer surface indicates that this effect should be difficult to detect by X-ray diffraction.

Our experimental results do not allow us to decide if one mechanism is predominant over the others. All of these could contribute to Al uptake from solution in different proportions. However, how the released Al can escape from complexation with citrate is still unclear.

One feasible hypothesis to justify the absence of Al-Cit complexation is the presence of an exclusion volume due to the high-negative surface charge of the montmorillonite. The overall surface of montmorillonite is dominated by basal planes with a permanent negative charge that develops an anion exclusion volume of 0.39 $cm^3\ g^{-1}$. The thickness of the anion exclusion volume (36 Å) can be obtained by dividing the anion exclusion volume by the external surface area, assuming that the BET surface area may be a proxy of the external surface area. Thus, a layer of solution can be found around clay particles, where

the concentration of citrate is considerably lower than the bulk concentration. Although the results of EQ3NR calculations indicate that the bulk solutions are undersaturated in gibbsite and presumably in aluminum hydroxides due to the complexation with citrate, we may hypothesize that a fraction of the detached Al precipitates or re-sorbs before diffusing through the exclusion volume and gives rise to the non-stoichiometric reaction.

ACKNOWLEDGMENTS

Financial support was obtained from projects CGL2005-00618 and CGL2008-01652 (Ministerio de Educación y Ciencia, Spain), P07-RNM-02772, and Group RNM-264 (Junta de Andalucía, Spain), with contribution of FEDER funds. M.E.R. benefited of a FPI grant (Ministerio de Educación y Ciencia), and C.C. of Erasmus (University of Naples Parthenope, Italy) and F.P.U. (Ministerio de Educación y Ciencia) grants. Carlos J. Jové-Colón helped us to include ligands in the LLNL database for EQ3NR and Ray Ferrell and two anonymous reviewers improved the manuscript with useful comments and suggestions. Paloma Sánchez and José Maceira provided technical assistance. F.J.H. a.m.d.g.

REFERENCES CITED

Amram, K. and Ganor, J. (2005) The combined effect of pH and temperature on smectite dissolution rate under acidic conditions. Geochimica et Cosmochimica Acta, 69, 2535–2546.

Bauer, A. and Berger, G. (1998) Kaolinite and smectite dissolution rate in high molar KOH solutions at 35 and 80 °C. Applied Geochemistry, 13, 905–916.

Brunauer, S., Emmett, P.H., and Teller, E. (1938) Adsorption of gases in multimolecular layers. Journal of the American Chemical Society, 60, 309–319.

Cama, J., Ganor, J., Ayora, C., and Lasaga, A.C. (2000) Smectite dissolution at 80 °C and pH 8.8. Geochimica et Cosmochimica Acta, 64, 2701–2717.

Cambier, P. and Sposito, G. (1991) Interactions of citric acid and synthetic hydroxy-aluminum montmorillonite. Clays and Clay Minerals, 39, 158–166.

Carroll-Webb, S.A. and Walther, J.V. (1988) A surface complex reaction model for the pH-dependence of corundum and kaolinite dissolution rates. Geochimica et Cosmochimica Acta, 52, 2609–2623.

Charlet, L., Schindler, P.W., Spadini, L., Furrer, G., and Zysset, M. (1993) Cation adsorption on oxides and clays: The aluminum case. Aquatic Sciences, 55, 291–303.

Chin, P.K.F. and Mills, G.L. (1991) Kinetics and mechanism of kaolinite dissolution: effects of organic ligands. Chemical Geology, 90, 307–317.

Filius, J.D., Hiemstra, T., and Van Riemsdijk, W.H. (1997) Adsorption of small weak organic acids on goethite: Modeling of mechanisms. Journal of Colloid and Interface Science, 195, 368–380.

Fubini, B. and Fenoglio, I. (2007) Toxic potential of mineral dusts. Elements, 3, 407–414.

Furrer, G. and Stumm, W. (1986) The coordination chemistry of weathering: I. Dissolution kinetics of Al_2O_3 and BeO. Geochimica et Cosmochimica Acta, 50, 1847–1860.

Gaines, R.V., Skinner, H.C.W., Foord, E.E., Mason, B., and Rosenzweig, A., Eds. (1997) Dana's New Mineralogy, 8th edition, 1819 p. Wiley, New York.

Ganor, J. and Lasaga, A.C. (1994) The effects of oxalate acid on kaolinite dissolution rate. Mineral Magazine, 58A, 315.

Golubev, S.V. and Pokrovsky, O.S. (2006) Experimental study of the effect of organic ligands on diopside dissolution kinetics. Chemical Geology, 235, 377–389.

Golubev, S.V., Bauer, A., and Pokrovsky, O.S. (2006) Effect of pH and organic ligands on the kinetics of smectite dissolution at 25 °C. Geochimica et Cosmochimica Acta, 70, 4436–4451.

Grasshoff, K., Ehrhardt, M., and Kremling, K., Eds. (1983) Methods of seawater analysis, 2nd edition. Verlag Chemie.

Gunter, M.E. and Wood, S.A. (2000) Can chrysotile alter to tremolite in the human lung? AGU Spring Meeting 2000, M51A.

Hedges, J.I. and Hare, P.E. (1987) Amino acid adsorption by clay minerals in distilled water. Geochimica et Cosmochimica Acta, 51, 255–259.

Howard, A.G., Coxhead, A.J., Potter, I.A., and Watt, A.P. (1986) Determination of dissolved aluminium by the micelle-enhanced fluorescence of its lumogallion complex. Analyst, 111, 1379–1381.

Huertas, F.J., Chou, L., and Wollast, R. (1999) Mechanism of kaolinite dissolution at room temperature and pressure. II. Kinetic study. Geochimica et Cosmochimica Acta, 63, 3261–3275.

Huertas, F.J., Caballero, E., Jiménez de Cisneros, C., Huertas, F., and Linares, J. (2001) Kinetics of montmorillonite dissolution in granitic solutions. Applied Geochemistry, 16, 397–407.

Hume, L.A. and Rimstidt, J.D. (1992) The biodurability of chrysotile asbestos. American Mineralogist, 77, 1125–1128.

Jardine, P.M. and Zelazny, L.W. (1996) Surface reactions of aqueous aluminum species. In G. Sposito, Ed., The Environmental Chemistry of Aluminum, p. 221–270. Lewis Publishers, Chelsea, Michigan.

Jurinski, J.B. and Rimstidt, J.D. (2001) Biodurability of talc. American Mineralogist, 86, 392–399.

Kang, S. and Xing, B.S. (2007) Adsorption of dicarboxylic acids by clay minerals as examined by in situ ATR-FTIR and ex situ DRIFT. Langmuir, 23, 7024–7031.

Kitadai, N., Yokoyama, T., and Nakashima, S. (2009) In situ ATR-IR investigation of L-lysine adsorption on montmorillonite. Journal of Colloid and Interface Science, 338, 395–401.

Kubicki, J.D., Schroeter, L.M., Itoh, M.J., Nguyen, B.N., and Apitz, S.E. (1999) Attenuated total reflectance Fourier-transform infrared spectroscopy of carboxylic acids adsorbed onto mineral surfaces. Geochimica et Cosmochimica Acta, 63, 2709–2725.

Kummert, R. and Stumm, W. (1980) The surface complexation of organic acid and hydrous γ-Al_2O_3. Journal of Colloid and Interface Science, 75, 373–385.

Lackovic, K., Johnson, B.B., Angove, M.J., and Wells, J.D. (2003) Modeling the adsorption of citric acid onto Muloorina illite and related clay minerals. Journal of Colloid and Interface Science, 267, 49–59.

Marklund, E., Sjoberg, S., and Ohman, L.O. (1986) Equilibrium and structural studies of silicon (IV) and aluminum (III) in aqueous-solution. 14. Speciation and equilibria in the aluminum (III)-lactic acid-OH system. Acta Chemica Scandinavica, A, 40, 367–373.

Martell, A.E. and Smith, R.M. (1974) Critical Stability Constants, Vol 1. Plenum Press, New York.

Martell, A.E., Motekaitis, R.J., and Smith, R.M. (1990) Aluminium complexes of hydroxyaliphatic and hydroxyaromatic ligands in aqueous systems—some problems and solutions. Polyhedron, 9, 171–187.

Metz, V., Amram, K., and Ganor, J. (2005) Stoichiometry of smectite dissolution. Geochimica et Cosmochimica Acta, 69, 1755–1772.

Meunier, A. (2003) Argiles, 434 p. GB Science Publisher, Paris.

Moore, D.M. and Reynolds, R.C. (1989) X-ray Diffraction and the Identification and Analysis of Clay Minerals, pp. 340. Oxford University Press, New York.

Nagy, K.L., Cygan, R.T., Hanchar, J.M., and Sturchio, N.C. (1999) Gibbsite growth kinetics on gibbsite, kaolinite, and muscovite substrates: atomic force microscopy evidence for epitaxy and an assessment of reactive surface area. Geochimica et Cosmochimica Acta, 63, 2337–2351.

Newman, A.C.D. and Brown, G. (1987) The chemical constitution of clays. In A.C.D. Newman, Ed., Chemistry of Clays and Clay Minerals, Monograph No. 6, p. 1–128. Mineralogical Society. Wiley, New York.

Oelkers, E.H. and Schott, J. (1998) Does organic acid adsorption affect alkali-feldspar dissolution rates? Chemical Geology, 151, 235–245.

Olsen, A.A. and Rimstidt, J.D. (2008) Oxalate-promoted forsterite dissolution at low pH. Geochimica et Cosmochimica Acta, 72, 1758–1766.

Oze, C. and Solt, K. (2010) Biodurability of chrysotile and tremolite asbestos in simulated lung and gastric fluids. American Mineralogist, 95, 825–831.

Plumlee, G.S. and Ziegler, T.L. (2003) The medical geochemistry of dusts, soils, and other earth materials. In H.D. Holland and K.K. Turekian, Eds., Environmental Geochemistry, vol. 9, p. 263–310. Treatise on Geochemistry, Elsevier, Amsterdam.

Pokrovski, G.S. and Schott, J. (1998) Experimental study of the complexation of silicon and germanium with aqueous organic species: Implications for germanium and silicon transport and Ge/Si ratio in natural waters. Geochimica et Cosmochimica Acta, 62, 3413–3428.

Polubesova, T. and Borisover, M. (2009) Two components of chloride anion exclusion volume in montmorillonitic soils. Colloids and Surfaces A: Physicochemical and Engineering Aspects, 347, 175–179.

Robie, R.A. and Hemingway, B.S. (1995) Thermodynamic properties of minerals and related substances at 298.15 K and 1 Bar (10^5 Pascals) pressure and at higher temperatures. U.S. Geological Survey, 2131, 461 p.

Rozalén, M.L., Huertas, F.J., Brady, P.V., Cama, J., Garcia-Palma, S., and Linares, J. (2008) Experimental study of the effect of pH on the kinetics of montmorillonite dissolution at 25 °C. Geochimica et Cosmochimica Acta, 72, 4224–4253.

Rozalén, M., Brady, P.V., and Huertas, F.J. (2009a) Surface chemistry of K-montmorillonite: Ionic strength, temperature dependence and dissolution kinetics. Journal of Colloid and Interface Science, 333, 474–484.

Rozalén, M., Huertas, F.J., and Brady, P.V. (2009b) Experimental study of the effect of pH and temperature on the kinetics of montmorillonite dissolution. Geochimica et Cosmochimica Acta, 73, 3752–3766.

Scholze, H. and Conradt, R. (1987) An in vitro study of the chemical durability of siliceous fibres. The Annals of Occupational Hygiene, 31 (4B), 683–692.

Sigg, L. and Stumm, W. (1981) The interactions of anions and weak acids with the hydrous goethite surface. Colloides and Surfaces, 2, 101–117.

Stillings, L.L., Drever, J.I., and Poulson, S.R. (1998) Oxalate adsorption at a plagioclase [An(47)] surface and models for ligand-promoted dissolution. Environmental Science and Technology, 32, 2856–2864.

Stumm, W., Kummert, R., and Sigg, L. (1980) A ligand exchange model for the adsorption of inorganic and organic ligands at hydrous oxide interfaces. Croatica Chemica Acta, 53, 291–312.

Sun, S.W., Lin, Y.C., Weng, Y.M., and Chen, M.J. (2006) Efficiency improvements on ninhydrin method for amino acid quantification. Journal of Food Composition Analysis, 19, 112–117.

Venturini, M. and Berthon, G. (1989) Aluminum speciation studies in biological fluids. Part 2. Quantitative investigation of aluminum-citrate complexes and appraisal of their potential significance in vivo. Journal of Inorganic Biochemistry, 37, 69–90.

Verburg, K. and Baveye, P. (1994) Hysteresis in binary exchange of cations on 2:1 clay minerals: A critical review. Clays and Clay Minerals, 42, 207–220.

Werner, A.J., Hochella, M.F., Guthrie, G.C., Hardy, J.A., Aust, A.E., and Rimstidt, J.D. (1995) Asbestiform riebeckite (crocidolite) dissolution in the presence of Fe chelators; implications for mineral-induced disease. American Mineralogist, 80, 1093–1103.

World Health Organization (WHO) (2005) Bentonite, kaolin and selected minerals. Environmental Health Criteria 231, pp. 1–174.

Wieland, E. and Stumm, W. (1992) Dissolution kinetics of kaolinite in acidic aqueous solutions at 25 °C. Geochimica et Cosmochimica Acta, 56, 3339–3355.

Wolery, T.J. (1992) EQ3NR, a computer program for geochemical aqueous speciation-solubility calculations: Theoretical manual, user's guide, and related documentation (Ver. 7). UCRL-MA-110662 PT III. Lawrence Livermore National Laboratory, Livermore, California.

Yadava, H.L., Singh, S., Prasad, P., Singh, R.K.P., Yadava, P.C., and Yadava, K.L. (1984) Stability constants of glycinate complexes of nickel (II), lead (II), chromium (III), aluminium (III) and thorium (IV) by paper electrophoresis. Bulletin de la Société Chimique de France, 1, 314–316.

Zutic, V. and Stumm, W. (1984) Effect of organic acids and fluoride on the dissolution kinetics of hydrous alumina. Geochimica et Cosmochimica Acta, 48, 1493–1503.

Zysset, M. and Schindler, P.W. (1996) The proton promoted dissolution kinetics of Kmontmorillonite. Geochimica et Cosmochimica Acta, 60, 921–931.

Manuscript received September 15, 2010
Manuscript accepted January 27, 2011
Manuscript handled by Barry Bickmore


IACT
INSTITUTO ANDALUZ DE CIENCIAS DE LA TIERRA


ugr
Universidad
de Granada


CSIC
Consejo Superior de Investigaciones Científicas